DOTTORATO DI RICERCA IN CHIMICA

Convenzione tra
UNIVERSITÀ DEGLI STUDI DI TRIESTE
e
UNIVERSITÀ CA' FOSCARI DI VENEZIA

CICLO XXX

SYNTHESIS, MECHANISM AND CATALYTIC APPLICATIONS OF PILLAR[n]ARENES

Settore scientifico-disciplinare: CHIM/06

DOTTORANDA
MARTA DA PIAN

COORDINATORE
PROF. MAURO STENER

SUPERVISORE DI TESI
PROF. FABRIZIO FABRIS

CO-SUPERVISORE DI TESI
PROF. ALESSANDRO SCARSO

ANNO ACCADEMICO 2016/2017

1

ACN	Acetonitrile
BmimBF$_4$	1-Butyl-3-methylimidazolium tetrafluoroborate
BmimCl	1-Butyl-3-methylimidazolium chloride
BmimPF$_6$	1-Butyl-3-methylimidazolium hexafluorophosphate
BmimTf$_2$N	1-Butyl-3-methylimidazolium bis(trifluoromethylsulfonyl)imide
BuOH	Butanol
ClCyH	Chlorocyclohexane
COCP	Cobaltocenium hexafluorophosphate
CyH	Cyclohexane
DBB	1,4-dibutoxybenzene
DCE	1,2-Dichloroethane
DCM	Dichloromethane
DEB	1,4-diethoxybenzene
DES	Deep eutectic solvent
DIEA	N,N-Diisopropylethylamine
DMSO	Dimethyl sulfoxide
FECP	(Ferrocenylmethyl)trimethylammonium hexafluorophosphate
MeOH	Methanol
P[n]	Pillar[n]arenes
P[5]	Pillar[5]arene
P[6]	Pillar[6]arene
PBu[5]	Dibutoxypillar[5]arene
PBu[6]	Dibutoxypillar[6]arene
PET	Petroleum ether

PEt[5]	Diethoxypillar[5]arene
PEt[4]Q[1]	Diethoxypillar[4]arene[1]quinone
PEt[4]HQ[1]	Diethoxypillar[4]arene[1]hydroquinone
PEt[5]d$_{10}$	Diethoxypillar[5]arene-d$_{10}$
PEt[6]	Diethoxypillar[6]arene
PEt[4]Me[1]	Diethoxypillar[4]arene[1]dimethoxybenzene
PEt[6]d$_{10}$	Diethoxypillar[6]arene-d$_{10}$
PEt[6]d$_{20}$	Diethoxypillar[6]arene-d$_{20}$
PMe[5]	Dimethoxypillar[5]arene
PMe[6]	Dimethoxypillar[6]arene
PMe[5]Et[1]	Diethoxypillar[5]arene[1]dimethoxybenzene
TMAC	Tetramethylammonium chloride

Chapter 1

Introduction

1.1. Supramolecular Receptors

The concept of supramolecular chemistry was introduced by Lehn in 1978, as: "*chemistry beyond the molecule*, bearing on the organized entities of higher complexity that result from the association of two or more chemical species held together by intermolecular forces. Its development requires the use of all resources of molecular chemistry combined with the mastering of non-covalent interactions so as to form supramolecular entities, supermolecules possessing features as well defined as those of molecules themselves."[1] Other common descriptions of supramolecular chemistry were "the chemistry of the noncovalent bond," "nonmolecular chemistry," or even "Lego chemistry" due to the "unconventional" character of the interactions at the basis of supramolecular complexes, which were mostly non-covalent forces.

Nature created complex functional materials and systems in which the functions of the whole are greater than the sum of its parts[2,3]. Taking inspiration by these natural aggregates, the first studies in the supramolecular chemistry concerned the formation of molecular assembly consisting of two main components, a host and a guest, which interacted with each other in a noncovalent manner. Generally, the host is a large molecule or aggregate such as an enzyme or synthetic macrocycle with a central cavity of tunable size. The guests may be instead, a monatomic cation, a simple inorganic anion, an ion pair, or a more sophisticated molecule such as a hormone, pheromone, or neurotransmitter.
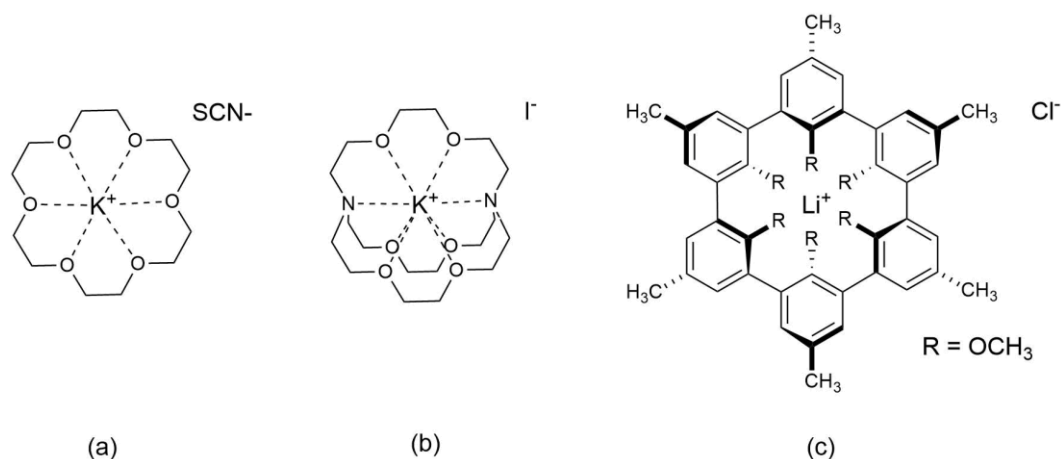
Figure 1.1 *Early supramolecular host molecules. Pedersen's crown (a) and Lehn's cryptand (b) form host-guest complexes with cations such as K^+; Cram's cavitand (c) which complexes Li^+.*

Nature inspired supramolecular chemists in using noncovalent interactions to control chemical structures and their reactivity. Pioneers in this filed were Lehn[1], Cram[4] and Pedersen[5] which examined the inclusion chemistry of simple molecular hosts such as crown ethers, cryptands, cavitands and carcerands (Figure 1.1).

In the host-guest systems the key concept leading the hosts architecture is molecular recognition, achieved by suitable receptors, the hosts, that selectively bind the desired substrates, the guests. To favor the host-guest complexation, the type and number of binding sites must be the most complementary to the guests, arranged on scaffold or framework of suitable size to accommodate the guest itself. The most stable complexes are generally obtained with hosts that are preorganized for guest binding, thus where there is no entropically and enthalpically unfavorable rearrangement on binding that reduces the overall free energy of complexation. With these leadings, scientists started developing systems in which chelate and macrocyclic effects as well as preorganization and cooperativity were key factors in the host design (Figure 1.2).[6]

Acyclic (podand)
No preorganization **Chelate effect** **Macrocyclic effect** **Cryptand effect**

○ = Donor site
○ = Acceptor site
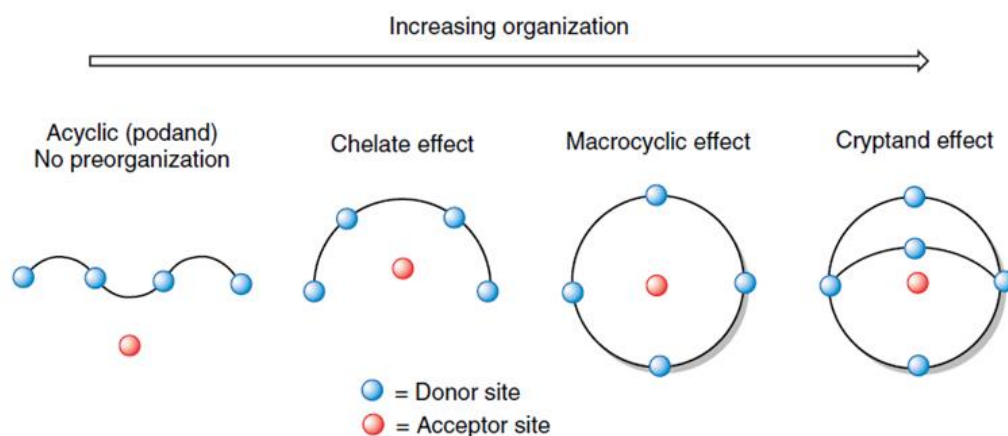
Figure 1.2 *A pictorial representation of effect of increasing host organization with increasingly restricted binding of a guest within chelate, macrocyclic, and cryptand ligands. Figure adapted from referenceerence[6]*

Nowadays, the most used molecular receptors in supramolecular chemistry are macrocycles with a hydrophobic or hydrophilic inner cavity like crown ethers, cyclophanes, catenanes, cavitands (such as cyclodextrins, calixarenes, resorcin[n]arenes and pillararenes), porphyrins, cryptophanes and carcerands.[7,8]

Anyway, the current supramolecular chemistry spans not just host-guest chemistry but also all aspects of self-assembly (Figure 1.3), which include the design and function of molecular devices and molecular assemblies, noncovalent polymers and soft matters.
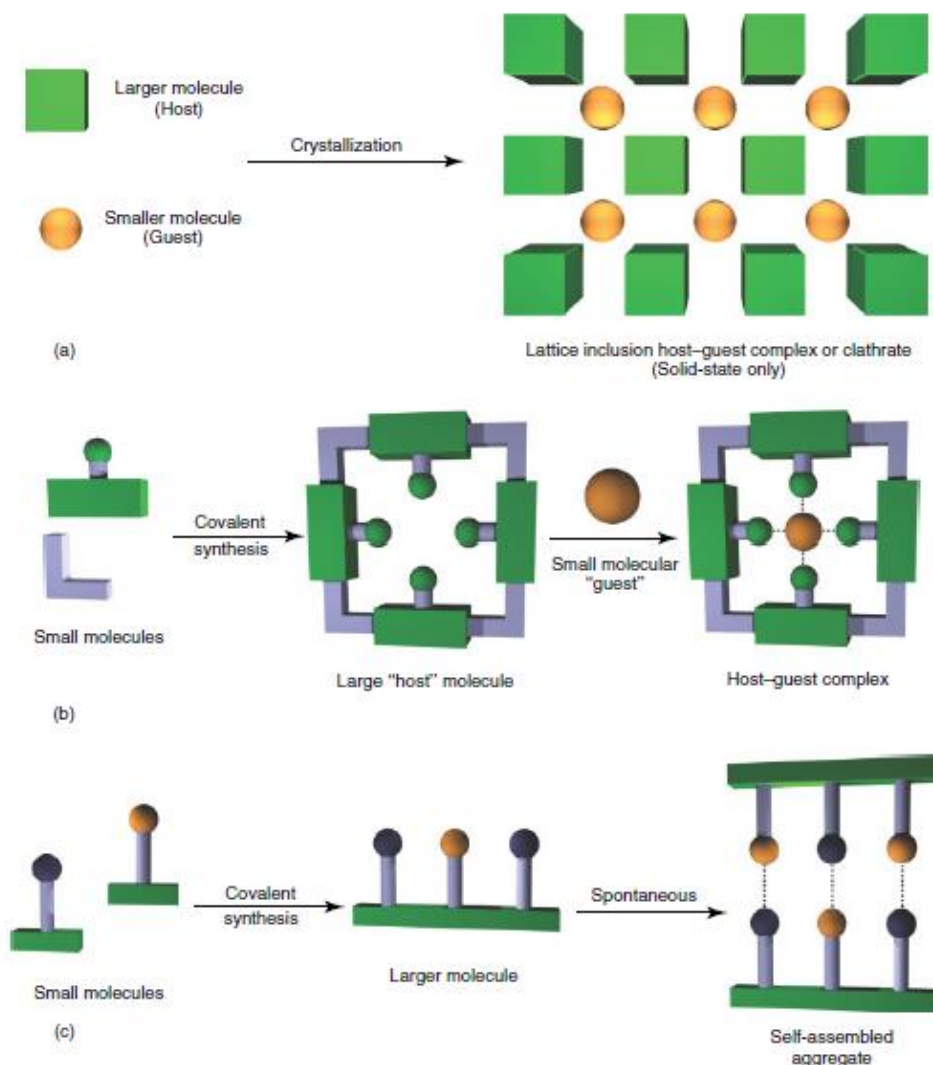
Figure 1.3 Key model in supramolecular chemistry. (a) Solid-state clathrate model, (b) molecular host–guest model, and (c) self-assembly model. Figure adapted from referenceerence[6]

1.2. Aromatic macrocycles

Among the macrocyclic host molecules used as supramolecular receptors, we concentrated our attention on aromatic macrocycles, which, due to their particular design present highly-ordered structures with various architectures showing differed size, shape, packing and flexibility features. The interesting properties displayed by these aromatic compounds, arise from the delocalized conjugated π-systems spread all over the macrocyclic network. The spatial arrangement of the constituent units is then reflected in peculiar three dimensional structures creating electron-rich cavities that show high affinity for

electron-poor guests. In principle, any aromatic unit could be used as a building block for the construction of aromatic networks[9]. In the case of aromatic molecules, differently substituted *orto-*, *meta-* and *para-*benzenes were the most frequently used, together with other polycyclic arenes, including naphthalene, anthracene, and pyrene and their derivatives[10] such as naphthalene bisimide or piromellytic bisimide.[11] Similarly, heteroaromatic units, such as pyridine, thiophene and their derivatives, were used to generate macrocycles which possessed improved coordination ability and novel electronic properties.[12,13,14] Basic factors influencing the three dimensional shape of the macrocycles are both the number of aromatic units and their topology, which, together with the linkers, whether di- or tri-topic and one- or two-atoms linkers, affect the geometry, flexibility and dynamic behavior of aromatic networks.

The formation of these receptors could be one-step or multi-steps synthesis, depending on the reactivity of the constituent units and the desired geometry, and could involve alternatively the formation of bonds between arene units and linker terminals or the formation of a bond between atoms in linker chains from substituted arene units.

1.2.1. Calixarenes, Resorcinarenes, Cyclotriveratrylenes

In the family of cyclophanes, the most commonly used macrocyclic arenes are cyclotriveratrylenes, calix[n]arenes and resorcin[n]arenes, which, due to their diverse and interesting structures and binding characteristics, have so far occupied and important role in the development of supramolecular chemistry.[15] (Figure 1.4)
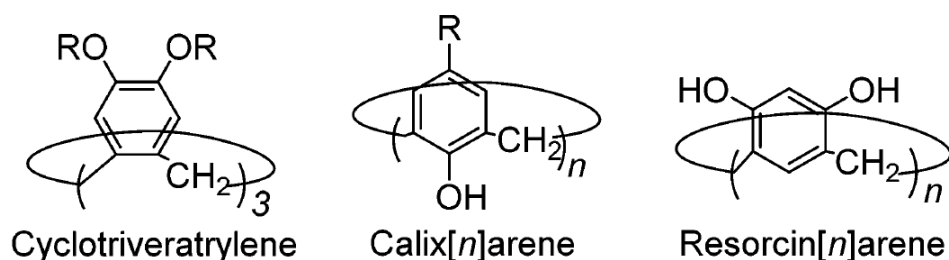
Figure 1.4 *Compact structures of calix[n]arenes, resorcin[n]arenes and cyclotriveratrylenes. Figure adapted from the reference[16]*

Among the three macrocycles reported in Figure 1.4, the first employed in supramolecular chemistry were cyclotriveratrylenes, C_3 symmetric cyclic trimers of benzene derivatives, linked in *orto*-position. Their first syntheses date back to the beginning of the century when Ewin[17] and later Robinson[18] performed an acid catalyzed condensation between veratryl alcohol and formaldehyde obtaining the cyclotriveratrylene, structurally characterized only 50 years later by Lindsey[19] and Erdtman[20].

Even though calix[n]arenes (n=4-9) were discovered before cyclotriveratrylenes in 1870s by Bayer's group,[21] they became popular only later thanks to Gutsche's work in 1978.[22,23] Calix[n]arenes are cyclic oligomers composed of phenolic units linked through methylene groups at their *meta-*positions, synthesized by electrophilic aromatic substitution catalyzed by the presence of acids or bases. A particular type of calix[n]arene are resorcin[n]arene, macrocycles based on the condensation of resorcinol with an aldehyde,[24] catalyzed by the presence of an acid and characterized, as the other members of the family, by two rims of different diameter.
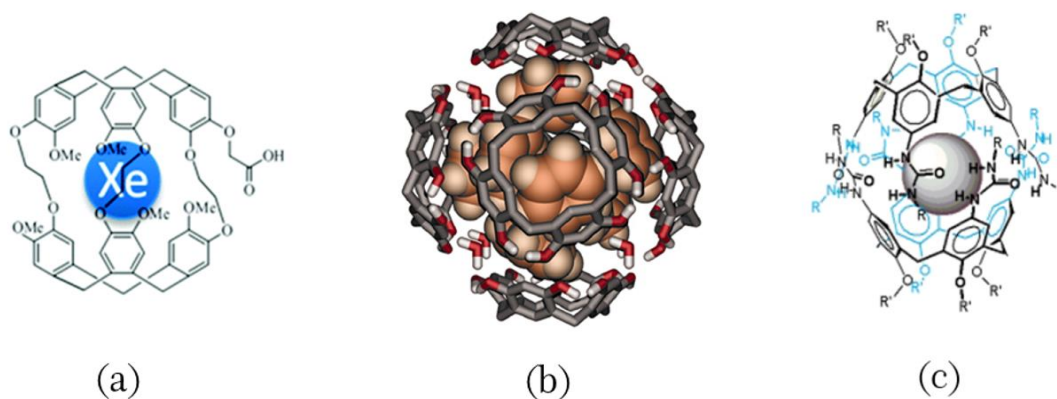
Figure 1.5 *a) A Xe complex of a cryptophane, b) hexameric capsule of resorcin[4]arene with a 8 molecules of C_6D_6 c) capsule of calix[4]arene with an appropriate guest. Figure adapted by reference*[25,26,27]

The host-guest properties of cyclotriveratrylenes are mostly determined by the nature of the substituents on the rim and several derivatizations of those macrocycles were carried out to widen the range of suitable guests. It is also worth to notice their potential use as ligand for several metals like silver, copper and palladium, resulting in chelated structure with the metal coordinated at the center of multiple cyclotriveratrylene units.[28] However, the most effective cyclotriveratrylenes-based host are cryptophanes, structures composed by two macrocycles covalently linked together by three bridges (Figure 1.5a).[29] Cryptophane have the ability to bind guests not otherwise complexed by cyclotriveratrylenes in the monomeric form, finding application as electronic devices, smart materials[30,31] and catalysts.[32,33]

Due to the well-defined conformational properties and cavities, calix[n]arene are used for the encapsulation of several ionic species such as small organic cations[34] or alkali metal cations in basic solution, and neutral molecules like organic solvents or some amines in the crystal state.[35,36] They also show enhanced host-guest properties in a self-assembled state forming a reversible capsule held by weak interactions between the functionalization on the upper rim (Figure 1.5c).[27,37] Through the structural modification of calix[n]arenes replacing the methylene groups by other units, several analogous macrocycles can be formed, such as oxacalixarenes, thiacalixarenes, and azacalixarenes, which[38] show enhanced receptor ability and selectivity toward target guests.

Similarly in aqueous media, resorcin[n]arenes can efficiently bind organic cations such as choline type guests, assuming stable cone conformations through strong intramolecular hydrogen bonds or through the derivatization of the lower rim with bulky substituents.[39] Like calix[n]arenes, they show enhanced host-guest properties by auto-assembling into capsules which, depending on the number of constituent macrocycles, display many three dimensional structures,[40] such as the hexameric capsule (Figure 1.5b) demonstrated by MacGillivray and Atwood in 1997.[41] In this particular case, due to the presence of eight hydroxyl groups in the upper rim, six molecules of resorcin[4]arene form strong hydrogen bonds with eight water molecules forming the capsule that can be observed in non-polar solvents.[26]

All the macrocycles in calix[n]arenes and resorcin[n]arenes family have been applied for the preparation of supramolecular polymers, sensors, drug/gene delivery systems, to nanodevices and catalysts.[42,43,44,45]

Other aromatic macrocycles have been developed in recent years, starting from the similar biphen[n]arenes,[16] oxatub[n]arene[46] and asar[n]arene[47] to the aromatic pyridone pentamer[48] or the ether- imide-sulfones[49], which showed good host guest abilities towards positively charged guests in virtue of their π-donating cavities (Figure 1.6). On the contrary, another macrocycle known as cyanostar, shows extraordinary binding ability with anions due to its cyanostilbene constituent units which make the cavity electronpoor.[50]

(a)

(b)

(c)

(d)

(e)

(f)
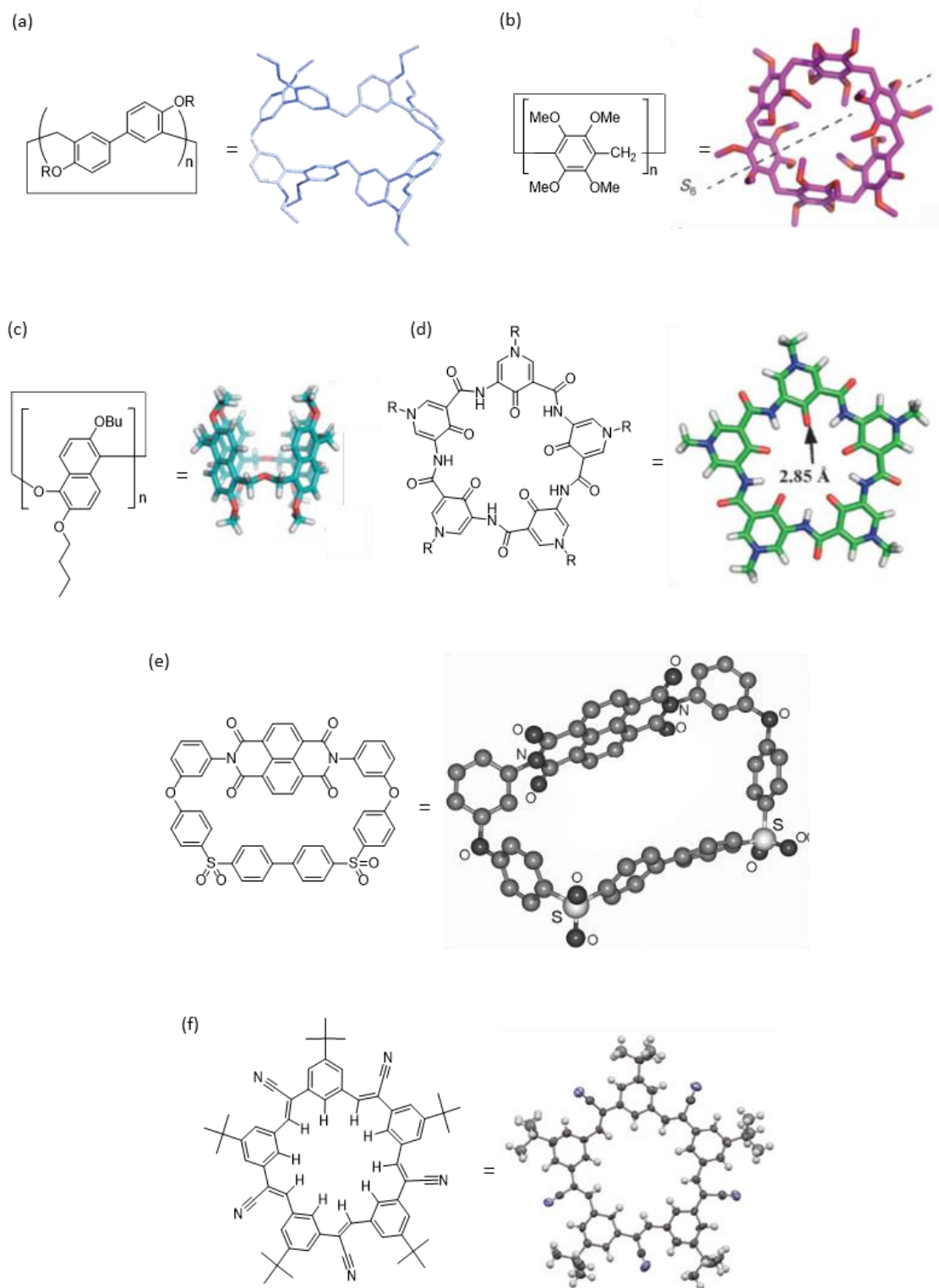
Figure 1.6 *Chemical and crystal structures of a) biphen[n]arenes, b) oxatub[n]arene, c) asar[n]arene, d) pyridone pentamer, e) ether- imide-sulfones macrocycle and f) cyanostar. Figure adapted from reference*[16,46,47, 49, 51,50]

1.2.2. Macrocyclic Arenes Applied as Biomimetic Enzymes

The need to develop artificial catalytic systems which can mime enzymatic activity derives from the drawbacks affecting natural enzymes, which make them sometimes less versatile than synthetic catalysts. In fact, although enzymes can accelerate chemical reactions up to 10^{15} folds with excellent selectivity and stereocontrol, they also present low thermal stability, low tolerance to experimental conditions and high cost of preparation and purification. Nevertheless, inspired by natural catalytic systems, several supramolecular structures were designed to mime enzymatic activity and to act as homogeneous catalysts. In this regard, several examples of cage-driven reactions, in which a supramolecular receptor or a cavitand is connected to an active site, have been developed by the scientific community.

To name a few, most of the common host macrocycles like CDs, calyx[n]arenes, resorcin[n]arenes, or curcubit[n]urils have been successfully employed to catalyze reactions with specific substrates, to afford different products depending on their affinity towards the substrates themselves.[52]

In this regard a nice example of artificial enzyme was given by Reinhoudt's group which synthesized calix[4]arenes modified with two or three Zn(II)-2,6-bis(aminomethyl)pyridyl groups. Their catalytic effect on the hydrolysis of phosphate diesters was investigated, with the aim of mimicking the dinuclear and trinuclear metallo-enzymes catalysis on dinucleotides.[53] Under neutral conditions the double Zn functionalized calix[4]arene accelerated of 23k-fold the cleavage of the phosphate ester bonds in the model substrate, while the triple Zn functionalized calix[4]arene accelerate the same reaction of 32k-fold (Figure 1.7). A mononuclear complex of the same calix[4]arene and the reference complex lacking the calix[4]arene backbone were compared with the dinuclear and trinuclear complexes, showing lower catalytic activity and proving the importance of both the cooperative effect of the metal cations and the importance of the hydrophobic effect induced by calix[4]arene cavity.

Dinucelar calix[4]arene complex   **Trinucelar calix[4]arene complex**
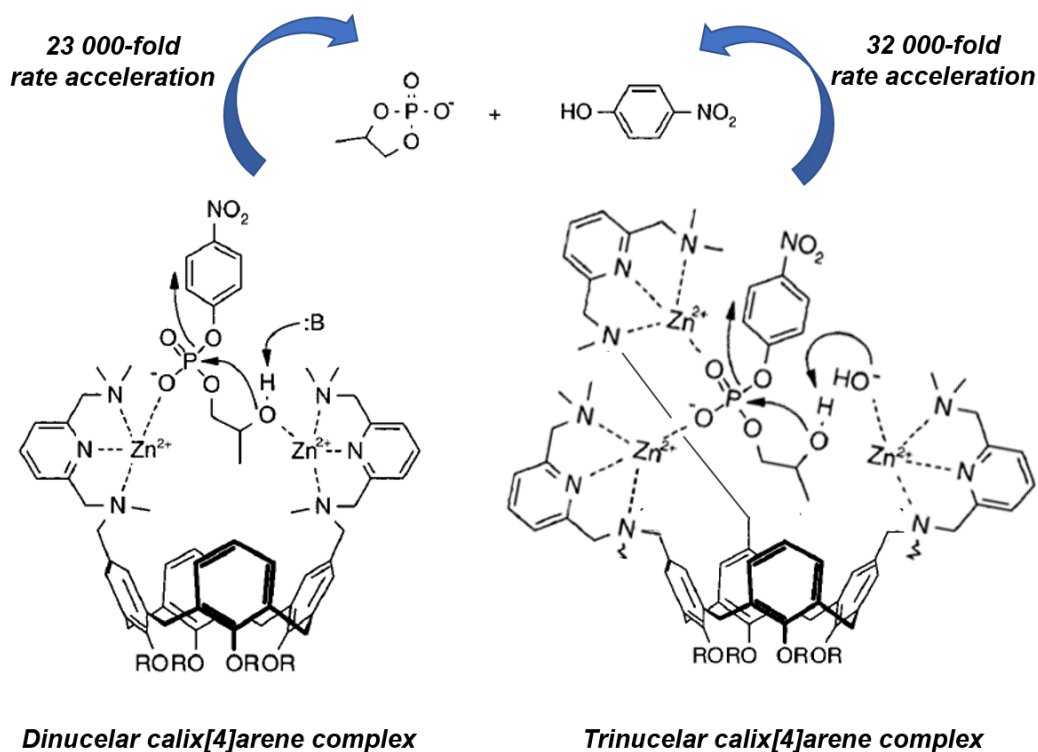
Figure 1.7 *Schematic representations of possible mechanisms for the hydrolysis of the mimic substrate phosphate diester catalyzed by the dinuclear and trinuclear Zn(II) calix[4]arene complexes displaying 23k-fold and 32k-fold rate acceleration respectively. Figure adapted from reference[53]*

Similar to calix[n]arene, the resorcinar[n]arenes scaffold functionalized with Kemp's diacid derivatives was efficiently used by Rebek's group in the epoxide ring opening cyclization reaction of epoxyalcohols (Figure 1.8).[54] This vase-like conformation of the cavitand was stabilized by intramolecular hydrogen bonds involving the cyclic array of secondary amides on the resorcin[n]arene rim. Depending on the substrate investigated the cavitand showed significant rate acceleration between 50- and 300-fold compared with a model reaction catalyzed by the same carboxylic acid present in the cavitand. These efficient catalytic performances derived from several factors, such as the high cavitand-substrate affinity, the enhanced concentration of Brønsted acid surrounding the substrate, and eventually the coiling of the substrate induced by CH-π interactions between the surface of the cavitand and the epoxyalcohol backbone. The last factor was maybe the most important since brought the reactive centers of the substrates in close proximity with a conformation similar to the reaction transition-state.
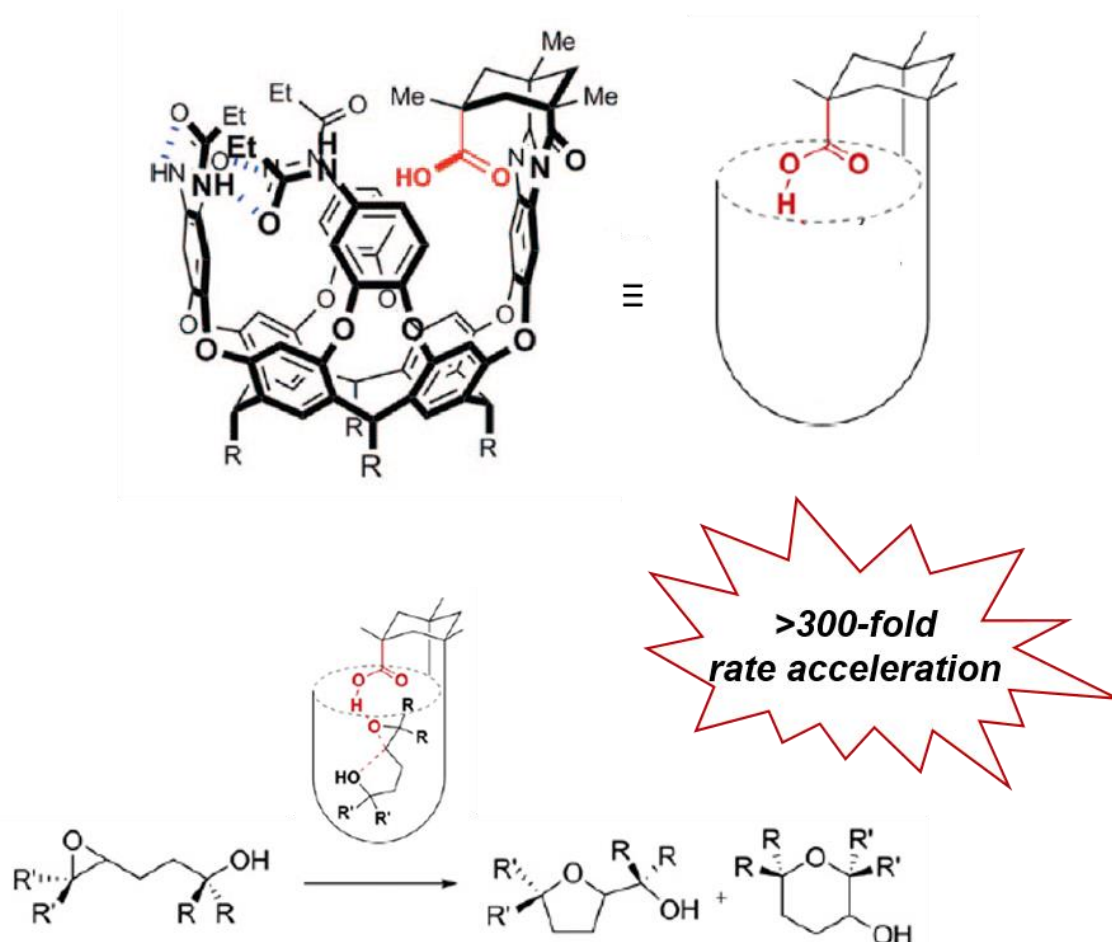
Figure 1.8 *Cavitand represented in its folded conformation which catalyzed the rearrangement of suitable 1,5-epoxyalcohols. Figure adapted from reference*[54,55]

Together with the rate acceleration enhancement an important characteristic for a good catalyst is the amount needed to accomplish its function. However, due to the effect of product inhibition, most of the supramolecular catalysts usually work only in stoichiometric amounts. Very recently, Zhang group's reported an example of photodimerization catalyzed by 1% mol of cucurbit[8]uril.[56] The reaction was performed on Brooker's merocyanine as substrates which, after dimerization, were spontaneously replaced inside the macrocycle cavity by two monomers via competitive host–guest complexation. After hours of UV irradiation the uncatalyzed photodimerization led only to 62% of product, while the reaction catalyzed by cucurbit[8]uril fully converted the substrate within 10 min, showing significant rate acceleration.
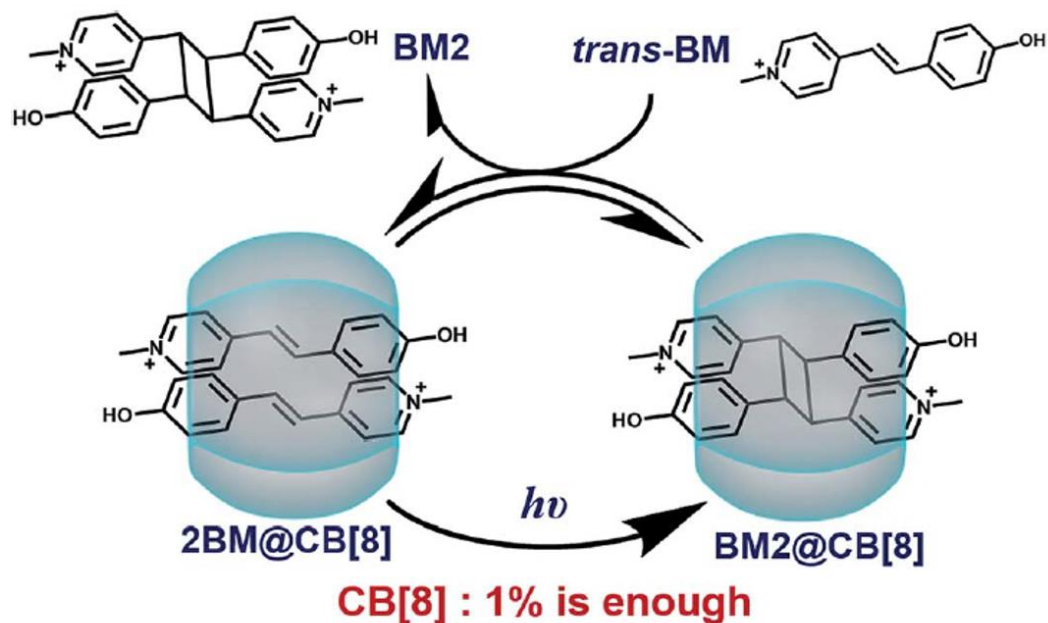
Figure 1.9 *Schematic illustration of photodimerization of the Brooker's merocyanine catalyzed by cucurbit[8]uril. Figure adapted from reference* [56]

1.3. Pillar[n]arenes: State of the Art

Almost contemporary to the other cyclic arenes, a new class of aromatic macrocycles, called pillar[n]arenes (**P[n]s**), constituted by hydroquinone units linked by methylene bridges at para positions,[57] was introduced by Ogoshi in 2008. Compared with calix[n]arenes, **P[n]s** (n = 5-15) show several advantages such as, for example, the more rigid and symmetrical structure and the ability to complex neutral species in organic solutions. With respect to other non aromatic macrocycles, like curcubiturils for example, they are easier to functionalize with different substituents, selectively on one, two, or all the aromatic units, and they are easily soluble in organic solvents. Due to these unique features, **P[n]s** have immediately attracted great attention in host-guest chemistry.[58,59,60,61] Like other macrocyclic compounds depending on the number of the constituent monomers (Figure 1.10) **P[n]s** have different cavity sizes, in a range from 5.5 Å for **P[5]** to 8.2 Å for **P[7]**. Bigger homologues **P[8-14]** present two cavities of different sizes

which can be fuse together with a final diameter in a range from 7.1 Å for **P[9]** to 14.9 Å for **P[14]**. [62]
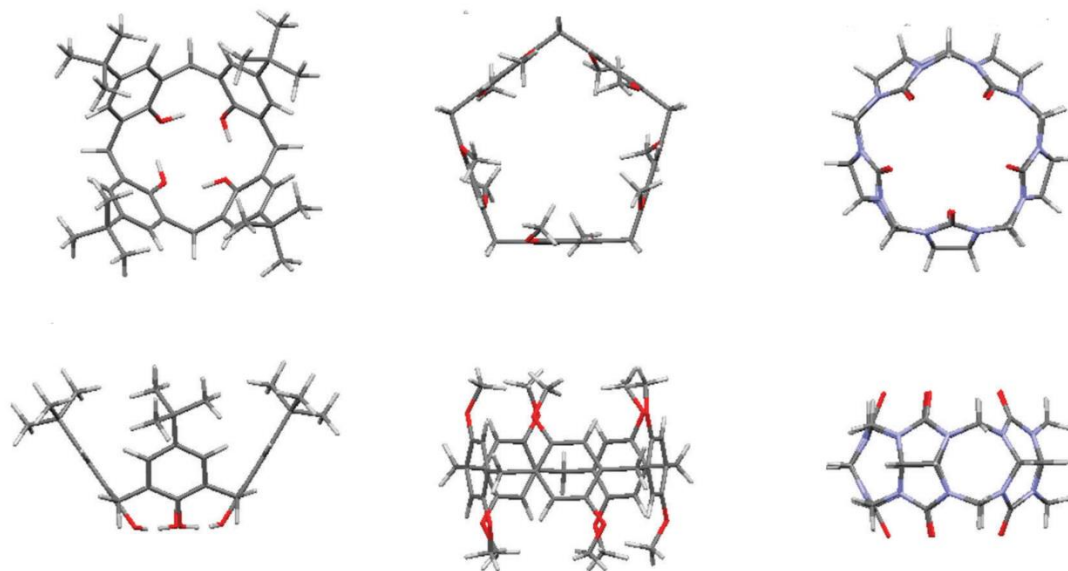
Figure 1.10 Top (up) and side (bottom) view, in order, of calix[4]arene, **P[5]** and curcubit[5]urils. Figure adapted from reference [63] and reference [61]

1.3.1. An Overview of the Most Typical Syntheses of Pillararenes

The first **P[5]** was discovered by chance investigating the reactivity of phenolic units with paraformaldehyde in phenolic resins synthesis. The acid catalyzed cyclization of different phenols derivatives led to the formation of other alkoxy-substituted macrocycles, such as cyclotriveratrylenes and resorcin[4]arenes, starting from 1,2- and 1,3- substituted aryls respectively. Depending on the position of the alkoxy substitution on the monomers, the different product structures were explained by the electron density distribution and the steric hindrance of the alkoxy substituents. In fact, the reactive sites in 1,2-dialkoxybenzene were on C4 and C5 and in 1,3-dialkoxybenzene were C4 and C6, which are far apart in both cases. Among the four electronically equivalent available positions (2, 3, 5 and 6) in 1,4-dialkoxybenzenes, the steric

hindrance of the alkoxy groups drove the second substitution in para (position 2 and 5) (Figure 1.11).
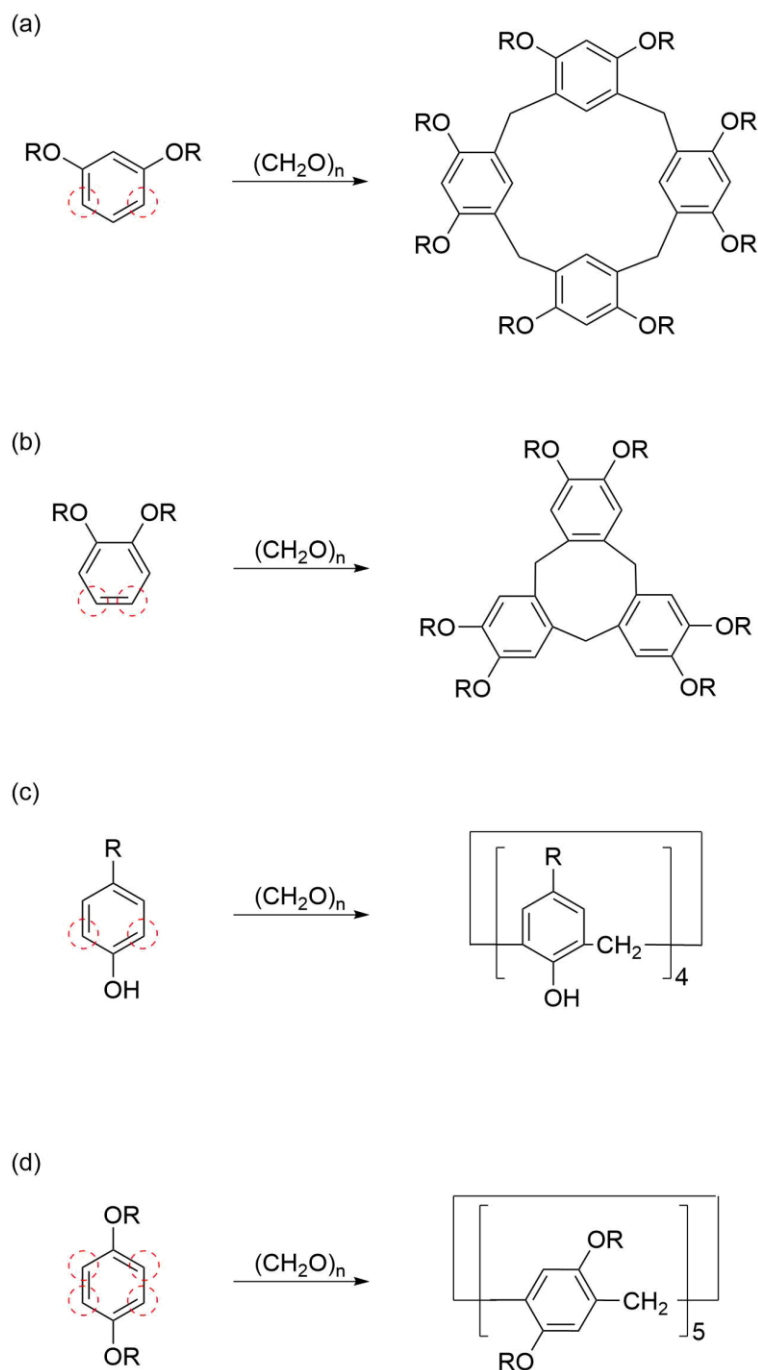
*Figure 1.11 Synthesis of (a) cyclotriveratrylenes, (b) resorcin[4]arenes, (c) calix[4]arenes, and (d) **P[5]**. Figure adapted from reference[63]*

P[5]s synthesis can be divided into two different approaches: a direct method, as published by Ogoshi, which involves the cyclisation of 1,4-dialkoxybenzenes with paraformaldehyde in the presence of a suitable catalyst,

or an indirect method, as developed by Mejier and Cao, through the cyclisation of 2,5-substituted derivatives of 1,4-dialkoxybenzene.[64]

The first **P[5]** synthesis was carried out in DCE with 1:1 molar ratio of reagents and equimolar amount of Brønsted acids, such as H_2SO_4, or Lewis acids such as $FeCl_3$, $AlCl_3$, $TiCl_4$, $SnCl_4$ and BF_3OEt_2, where the latter gave the best yields and selectivity of the desired **P[5]**. In order to widen the accessible **P[5]s** various alkoxy moieties were employed resulting in **P[5]s** with very different yields.[65]

Indirect methods were successfully tried by Cao and Meier, which reported a diethoxypillar[5]arene (**PEt[5]**) in 75% yield after referenceluxing 2,5-bis(benzyloxymethyl)-1,4-diethoxybenzene in DCM containing catalytic 4-toluenesulfonic acid. Conversely Huang reported the synthesis of a diisobutoxy substituted **P[5]** from a di(methoxymethyl) derivative obtained by the reaction of 1,4-diisobutoxybenzene with paraformaldehyde and HBr in glacial acetic acid, followed treatment with sodium methoxide. The cyclization reaction was carried out in referenceluxing DCM, with stoichiometric 4-toluenesulfonic acid hydrate to give **P[5]** in 73% yield.[66]

Huang also proposed a third possible route which involved the cyclo-oligomerization of 2,5-dialkoxybenzyl alcohols, or 2,5-dialkoxybenzyl bromides, in DCM with a catalytic amount of Lewis acid to give **P[5]** in approximately 40% yield.[67] Cao and Huang's methods were also effective for the isolation of the larger homologue **P[6]** (Figure 1.12).[67]
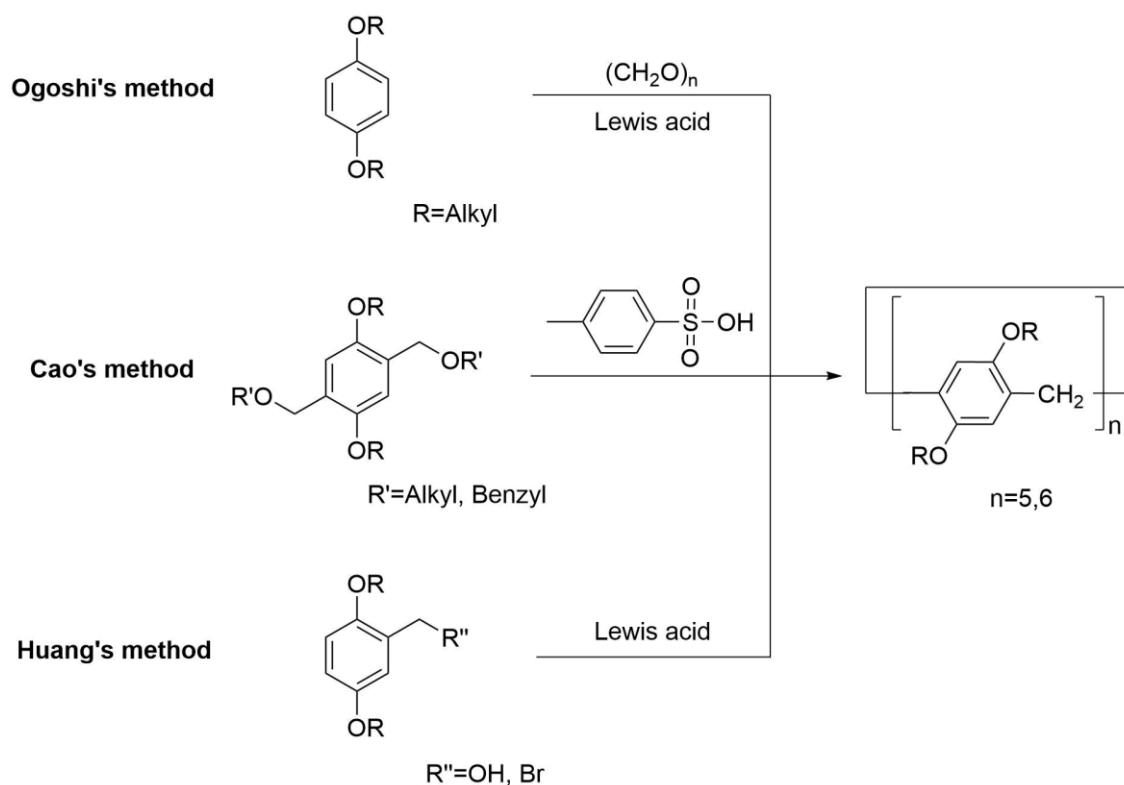
Figure 1.12 *Three synthetic strategies for* **P[n]s**.

Furthermore, the role of the catalyst in **P[n]s** synthesis was intensively studied by replacing Lewis acids with organic acids.[68,69] In particular Szumna's group proposed a moisture insensitive method using acetic *p*-toluenesulfonic acid which successfully promoted the formation of **P[5]s**, even though in lower yields compared to the Lewis acids catalyzed synthesis. Together with the role of the catalyst, several scientists investigated the effect of the solvent in the cyclization reaction, for example demonstrating a stronger binding between **P[5]** and DCE compared with chloroform, and using the solvent itself as a template.[69,70]

To broaden **P[5]s** functionalization possibilities, asymmetric substituted **P[5]s**, such as 1-butoxy-4-methoxypillar[5]arene and 1-ethoxy-4-methoxypillar[5]arene, were synthesized and whose conformational properties were extensively studied. [71,64,72]

Together with asymmetric **P[5]s**, several synthetic efforts have been made to synthesize co-pillar[5]arenes (**coP[5]s**), also known as A1/A2 **P[5]**, bearing different side groups on adjacent monomers. The first **coP[5]s** reported were

obtained in Huang's group in 10% yield from the co-cyclization of one equivalent of 1,4-dimethoxybenzene with four equivalents of 1,4-di-*n*-butoxybenzene, and in 16% yield from the co-cyclization of four equivalents of 1,4-dimethoxybenzene with one equivalent of 1,4-di-*n*-butoxybenzene.[73] In the meanwhile, Wang and Stoddart successfully obtained a bromo-functionalized **coP[5]** respectively from 1,4-bis(2-bromoethoxy)benzene and 1,4-bis(3-bromopropoxy)benzene with 1,4-dimethoxybenzene (**DMB**). [74,75] Other strategies to obtain **coP[5]s** implied selective reactions on one constituent unit of **P[5]**, such as oxidation followed by reduction on one or two constituent monomers,[76,77] or in the case of asymmetric **coP[5]s**, by deprotection of one or more substituent (Figure 1.13). [78]
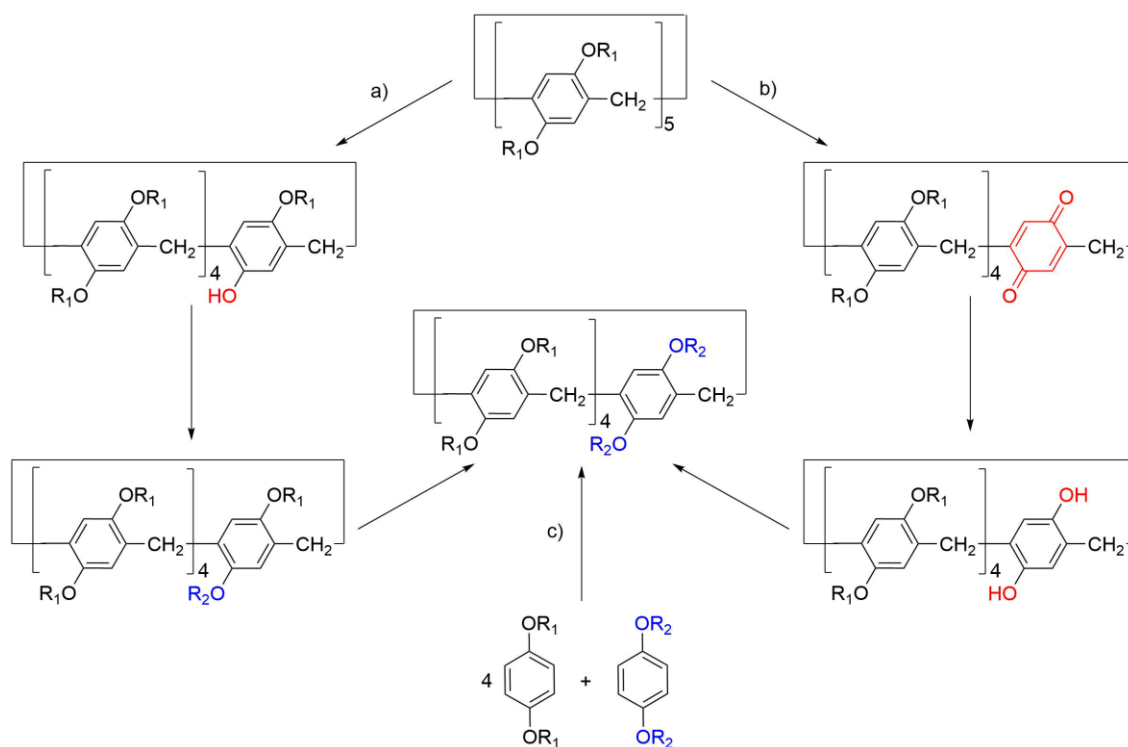
Figure 1.13 *Synthetic routes for the synthesis of* ***coP[5]s****. a) R_1, R_2= Me, nBu[74]; R_1= Me, R_2= CH_2CH_2Br[79]; R1= Me, R2= $CH_2CH_2CH_2Br$[76]; b) R_1= Me, R_2= $(CH_2)_8N(CH_3)_3$[78]; c) R_1= Me, R_2= CH_2CH_2Br[77]*

Differently from **P[5]**, **P[6]** was always isolated as secondary product. The first **P[6]** syntheses was developed by Meier and co-workers, which provided only 8% yield of diethoxy-pillar[6]arene (**PEt[6]**) and 11% yield of dibutoxy-pillar[6]arene (**PBu[6]**) respectively. Contextually the same syntheses gave 89% yield of **PEt[5]** and 86% yield of **PBu[5]**, using DCM and *p*-toluensulfonic acid as catalyst. However, few years later, the same group obtained a mixture of **P[n]s**

enriched in **P[6]**, using $FeCl_3$ as catalyst and $CHCl_3$ as solvent, isolating **PEt[6]** in 34% and **PBu[6]** in 43% yields and their homologues **P[5]s** in 30% and 31% yields respectively.[67,64] Contextually, a similar approach carried out by Hou's group, but with BF_3OEt_2 as catalyst, led to the formation of 15% yield of **PEt[6]**.[80]

Similarly to **P[5]s** synthesis, a template approach was developed for **P[6]** by Lin and Chen which synthesized di-isobutoxypillar[6]arene in 30% yield starting from 1,4-diisobutoxy-2,5-bis-(methoxymethyl) benzene in the presence of *N*-substituted naphtalendiimide.[81] Worth to mention is the method developed by Zhang, which led to the formation of **P[6]** in 53% yield by using the deep eutectic solvent choline chloride/$FeCl_3$ as a catalyst in dichloromethane.[82]

Ogoshi further improved **P[6]** synthesis working with 1,4-bis(methylcyclohexyl ether)benzene and paraformaldehyde in chlorocyclohexane in the presence of BF_3OEt_2, obtaining **P[6]** as major product in 87% yield and **P[5]** as minor product in 3% yield. [83]

Likewise **coP[5]s**, **coP[6]s** can be synthesized by oxidation-reduction method,[84] by selective mono- and bis-deprotection of the constituent monomers[85] and by co-cyclization of different monomers in the presence of suitable templates such as chlorocyclohexane.[83]

In the same time, pillar[7–10]arenes were obtained and finally characterized by Hou and coworkers using **DEB** as a monomer and chloroform as a solvent in yields between 3% and 1%.[80] Larger homologues such as pillar[11-13]arenes were isolated in Ogoshi's group in yields between 3% and 0.3% after the conversion of **PEt[5]** in chloroform for 1h in the presence of BF_3OEt_2, at 50 ℃ to overcome the energy barrier required to the ring opening and isomerization.[62]
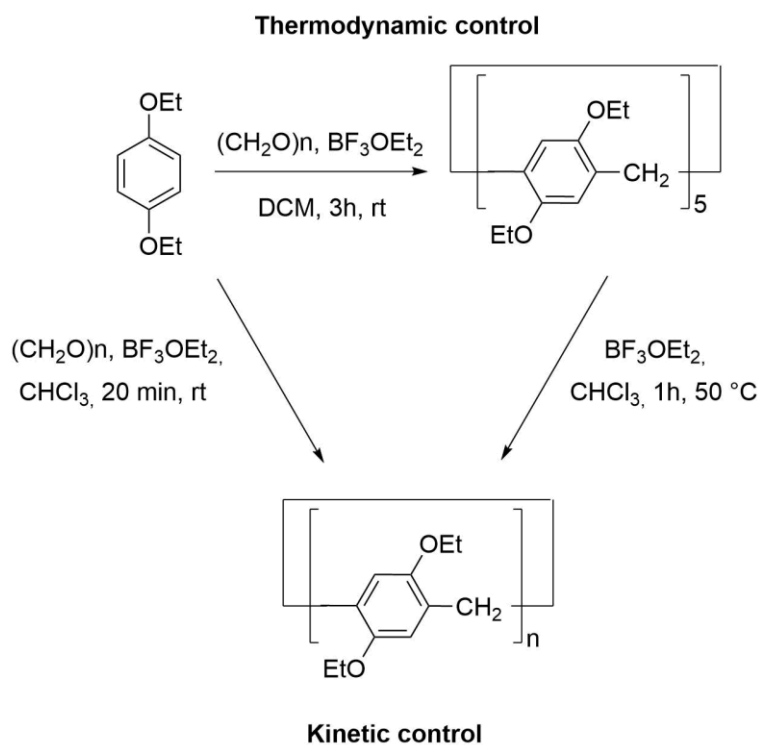
1.3.2. Thermodynamic and kinetic control

Likewise other macrocyclic compounds, where one member of the family presents much more rewarding syntheses compared to the others, **P[5]** appeared to be the preferred product. As previously stated, the catalyst, the solvent and the reaction temperature, as well as the ratio between the monomer and paraformaldehyde, play an important role in **P[5]** and **P[6]** ratio and yield. In order to understand the reasons behind the preferential formation of **P[5]** over **P[6]** several chemists investigated the cyclization mechanism. In this regard, Nierengarten's work was an important milestone, indicating that the synthesis of **P[5]** occurred through dynamic covalent bond formation and sequential methylene exchange reactions, under Friedel–Crafts reaction conditions.[86] In this work, in virtue of conformational considerations on the favored angular strain of the cyclic pentamer over the cyclic hexamer, **P[5]** is depicted as the thermodynamic product while **P[6-15]** are considered the kinetic products. In fact, in most of the syntheses **P[5]** was experimentally observed as the major product, while bigger homologues were barely formed. Finally, by changing the reaction conditions and therefore working under kinetic control, **P[n]s** were formed as important secondary products (Figure 1.14). However, by shifting the reaction from kinetic to thermodynamic control favoring the bigger pillar[n]arenes homologues instead of **P[5]s,** through **P[n]s** stabilization with template molecules or solvents, pillar[6-10]arenes could be isolated as major products, as demonstrated in Ogoshi's work of 2014.[83]

On the basis of these experimental evidences, all the next studies on pillar[n]arenes referred to **P[5]s** as the thermodynamic products and to pillar[6-10]arenes as the kinetic ones.

Figure 1.14 *Thermodynamic vs kinetic control in P[n]s synthesis. Figure adapted from reference* [62]

1.3.3. Host-Guest Properties

P[n]s can be derivatized with several functional groups which can impart good solubility both in organic as well as aqueous media and, hence, widening the number of available guests. In general, their inner cavity is strongly electron-rich and can easily accommodate small electron-poor molecules such as cations or neutral molecules with a strong dipole. [83] Host-guest properties of **P[n]s** can be classified according to the type of guest and the solvent in which **P[n]s** interactions are studied. In Figure 1.15 and Table 1.1 are summarized some examples of host-guest complexation concerning various **P[5]** and **P[6]** in different environments.

Table 1.1 *Association constants between **P[n]s** and various guests*

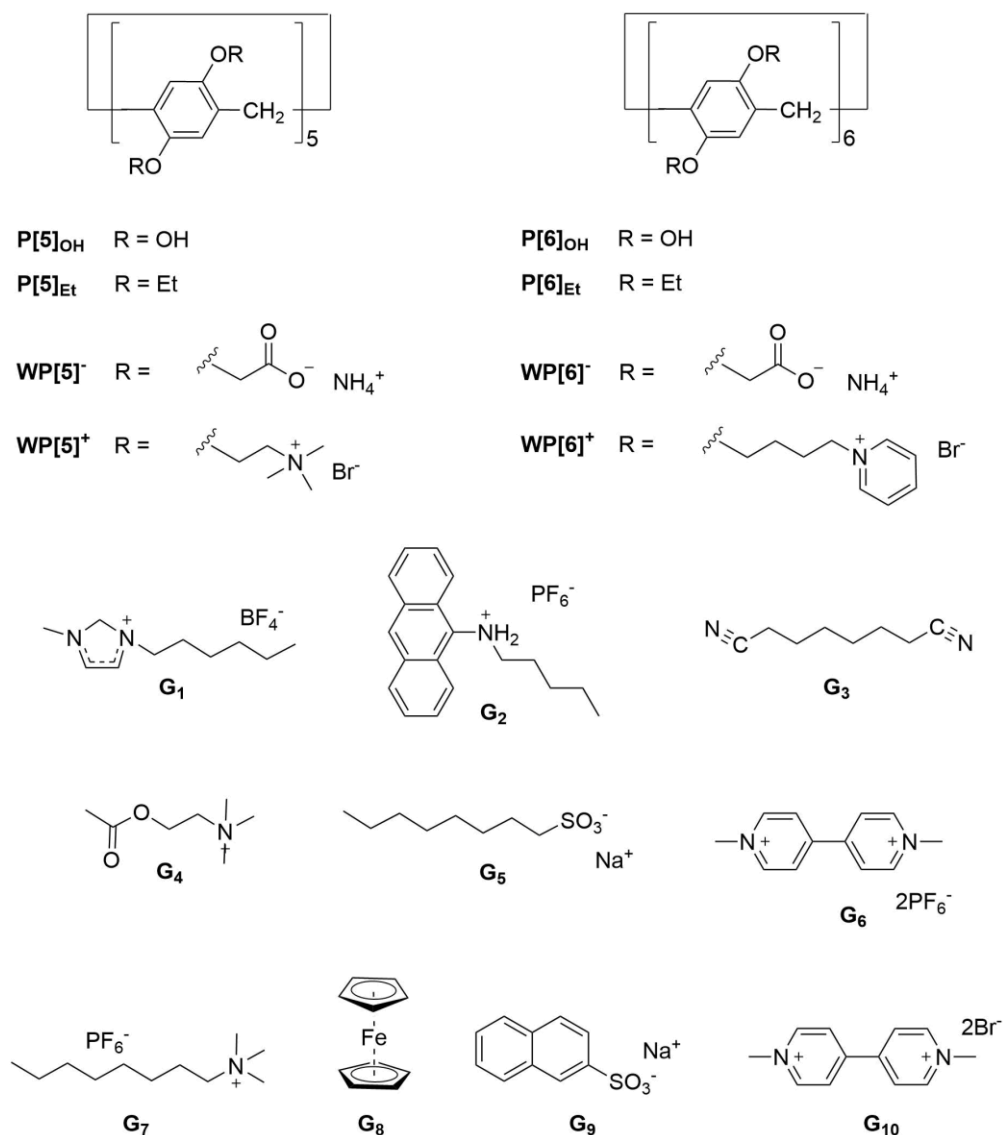| Record	P[n]	Guest	Solvent	K_{ass} M^{-1}	Method	Reference
1	$P[5]_{OH}$	G_1	Me_2CO-d_6	$K_1 = 700$ $K_2 = 1.7$	NMR	[87]
2	$P[5]_{Et}$	G_2	$CDCl_3$	6.1 ± 0.8 x 10	NMR	[88]
3	$P[5]_{Et}$	G_3	$DMSO$-d_6: $CDCl_3$ (1:9)	6.5 ± 0.5 x 10^2	NMR	[89]
4	$WP[5]^-$	G_4	H_2O	5.05 ± 0.13 x 10^4	ITC	[90]
5	$WP[5]^+$	G_5	D_2O	1.33 ± 0.44 x 10^4	NMR	[91]
6	$P[6]_{OH}$	G_6	Me_2CO-d_6	2.2 ± 0.3 x 10^2	NMR	[92]
7	$P[6]_{Et}$	G_7	$CDCl_3$	1.2 ± 0.1 x 10^3	NMR	[80]
8	$P[6]_{Et}$	G_8	CD_3CN: $CDCl_3$ (1:5)	1.8 ± 0.05 x 10	NMR	[93]
9	$WP[6]^+$	G_9	H_2O	3.8 ± 0.2 x 10^4	Fl	[94]
10	$WP[6]^-$	G_{10}	H_2O	1.02 ± 0.1 x 10^8	Fl	[95]

Figure 1.15 P[n]s Hosts and guests

Due to the electron density spread over the aromatic rings, per-alkylated **P[n]s** showed strong affinity with cationic guests (entries 2 and 7) with an average association constant of 10^2 M^{-1}. The same behavior was shown by anionic water soluble **P[n]s**, in which electrostatic interactions further increased the strength of the binding (entries 4 and 10) of three order of magnitude in the case of **P[5]** and on five order in the case of **P[6]**. In addition, because of electronic interactions, cationic water soluble **P[n]s** effectively bound small anions such as linear or aromatic sulfonates (entries 5 and 9) with an average association constant of 10^4 M^{-1}. The pronounced binding properties towards ionic guests showed by pillar[n]arenes is similar to the complexation behavior of other cyclic

arenes, and it was for some extent predictable in virtue of the studies conducted on calixarenes, resorcinarenes, crown ethers and cucurbiturils.

The real novelty is the complexation ability displayed by **P[n]s** towards neutral guest in solution, which occurs in virtue of dipole-dipole interactions and it is stronger in the presence of a permanent dipole such in the cases of in nitriles and metallocenes (entries 3 and 8) with an average association constant of 10 M^{-1}. This unique binding property takes pillar[n]arenes apart from other common macrocycles such as curcubit[n]urils[96] or calix[n]arenes[23] where the binding of neutral molecules occur only in water because of the hydrophobic effect. Pillar[n]arenes instead, due to their electron rich cavity combined with the alkoxy portal can strongly bind electron-poor neutral molecules in common organic solvents in virtue of the dipole-dipole interactions. [97]

1.3.4. Supramolecular Assemblies

Host-guest interactions of **P[n]s** have been used as driving force in supramolecular assemblies such as rotaxanes, catenanes, and supramolecular polymers, or self-assembled structure in the solid state, finding several applications in drug delivery, biosensing and smart materials. [98,99,100, 101]

After evaporation from suitable solvents, **P[5]s** auto-assemble to herringbones[77], one-dimensional channels[102] and slipped-stacked[103] crystalline structures. Example of herringbone structures were observed when per-alkylated **P[5]s** were crystallized from slow evaporation of chloroform under *n*-hexane vapors, forming pseudo-rotaxanes with the hexane encapsulated in the cavity.[104] In comparison, monodimensional infinite channels were obtained by Hou and co-workers upon evaporation of chloroform and chloroform-ethylene glycol of an ethyl acetate substituted **P[5]**.[105] In this case two different assemblies were obtained, a close-packed arranged with the adjacent molecules overlapped with a rotation angle of 36° (Figure 1.16a), and a second one also stacked in the face-to-face manner, but with no rotation of the neighboring molecules (Figure 1.16b). Per-hydroxylated **P[5]**, in which intra- and inter-molecular hydrogen

bonds are possible, crystallizes in a slipped-stacked manner instead of a monodimensional channel because of the odd number of benzene units.[106]

Also **P[6]s** including A1/A2 **P[6]s** and per-alkylated **P[6]s** in the solid state crystallize in channel-like[107] and slipped-stacked[107] structures, showing differences in the packing mode, depending on the guest, the solvent and the functional groups present in the rims. However, the intrinsic hexagonal structures of **P[6]s** causes a more regular assembly in aggregates, compared with crystals obtained from **P[5]s**. This behavior is emphasized in the case per-hydroxylated **P[6]**, which assembles in rigid and stable monodimensional channels, because of the strong intra- and inter-molecular hydrogen bonds between the OHs and the even number of units.[92]
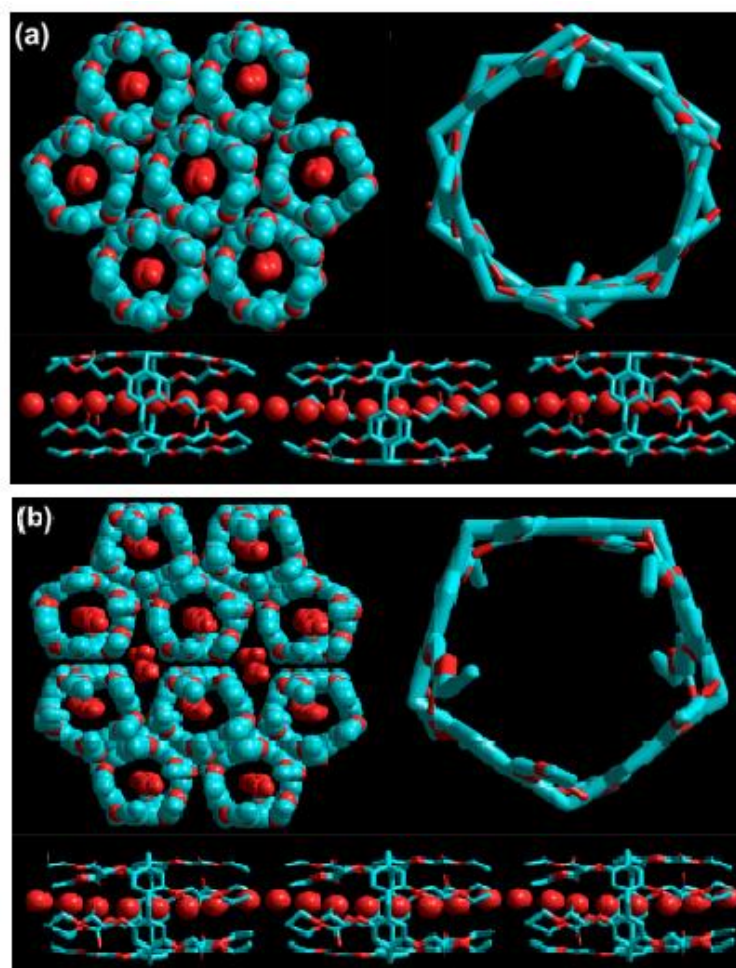
Figure 1.16 *Channel-like crystal structure of water filled* ***P[5]*** *(a) the stacking mode along the channel axis, indicating that two* ***P[5]s*** *overlapped with a rotation angle of 36°. (b) the packing mode shows that molecules well overlapped to give uniform channels. Figure arranged from reference* [105]

Rotaxanes represent one of the most important family among the mechanically interlocked molecules, attracting more and more attention because of their applications as molecular machines, as logic gates and as molecular actuators.[108,109] The first example of **P[5]**-based [2]rotaxane was synthesized in 2011 by Stoddart through the fromation of imide inside the cavity.[79] However, because of the weak binding constant between **PMe[5]** and 1,8-diaminobutane, the rotaxane yield was only 7%. One year later, Ogoshi's group reported the first **P[6]**-based [2]rotaxane (14% yield) formed by copper(I)-catalyzed azide-alkyne cycloaddition (CuAAC) between the alkyne moiety present on the axle and the azido moiety on the trityl stopper in the presence of **P[6]** (Figure 1.17).[110]

The combination of **P[n]s** with stronger interacting axes led to the formation of several [n]rotaxanes in higher yields, including [n]rotaxanes with more than one binding sites, hetero[n]rotaxanes[111,112] and stimuli responsive [n]rotaxanes[113].
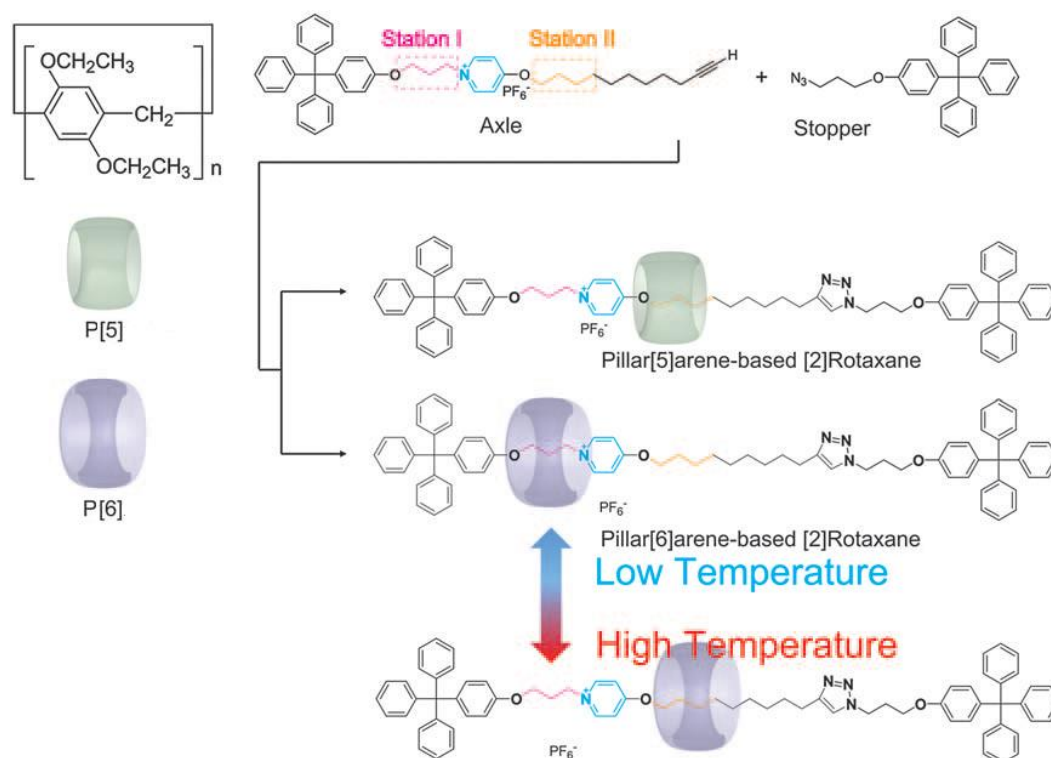
Figure 1.17 *(a)* *[2]rotaxane constructed from a* ***P[5]*** *wheel. (b) Thermo-responsive* *[2]rotaxane constructed from a* ***P[6]*** *wheel. Figure adapted from reference.[110]*

The host-guest properties of **P[n]s** also promoted the development of supramolecular aggregates such as self-inclusion complexes, cyclic dimers and

daisy chains. This behavior has mainly been showed by mono-functionalized **P[n]s** with electron poor moieties at the edge of the side group, which provided intra or inter-molecular host-guest interactions. A nice example of supramolecular aggregates was shown by Wang and co-workers which synthesized a mono-urea-functionalized **P[5]**, that in chloroform formed a pseudo[2]rotaxane and in the crystal state aggregated in the form of a [c2]daisy chain (Figure 1.18).[114] The formation of those interlocked molecules was driven by host-guest interactions between a neutral guest, such as the urea derivative, and the cavity of **P[5]**, which are strong enough to form stable pseudo[1]rotaxane. Such complexation behavior was observed also for imidazole functionalized **P[5]**, which at low concentrations led to the formation of the pseudo[1]rotaxane, while at high concentrations allowed the observation of supramolecular. Once again, the complexation driving force was the dipole-dipole interaction between the terminal imidazole in the electron-rich **P[5]** cavity.
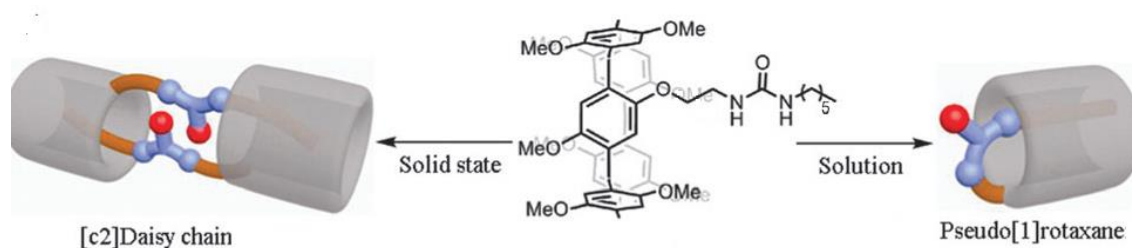

Figure 1.18 *Self-complexed aggregate (right) and cyclic dimer of the mono-urea-functionalized P[5]. Figure adapted from reference [114]*

Supramolecular polymers constructed with **P[n]s** are based on monomers held together by non-covalent interactions, which can endow the polymers with stimuli responsive properties.

An example of supramolecular polymer based on host-guest interactions was obtained by Ogoshi and co-workers as an alternating pseudo[2]rotaxane in which 1,4-diazabicyclo[2.2.2]octane (DABCO) and pyridinium mono-functionalized **P[5]** and **P[6]** respectively were interacting with each other (Figure 1.19a).[85] Conversely, an hydrogen bonded aggregate was synthesized by Wang, starting from a A1/A2 ureidopyrimidinone (UPy) functionalized **P[5]**, which self-

assembled into a poly-pseudo[2]rotaxane that was additionally cross-linked via host-guest complexation (Figure 1.19b).[115]
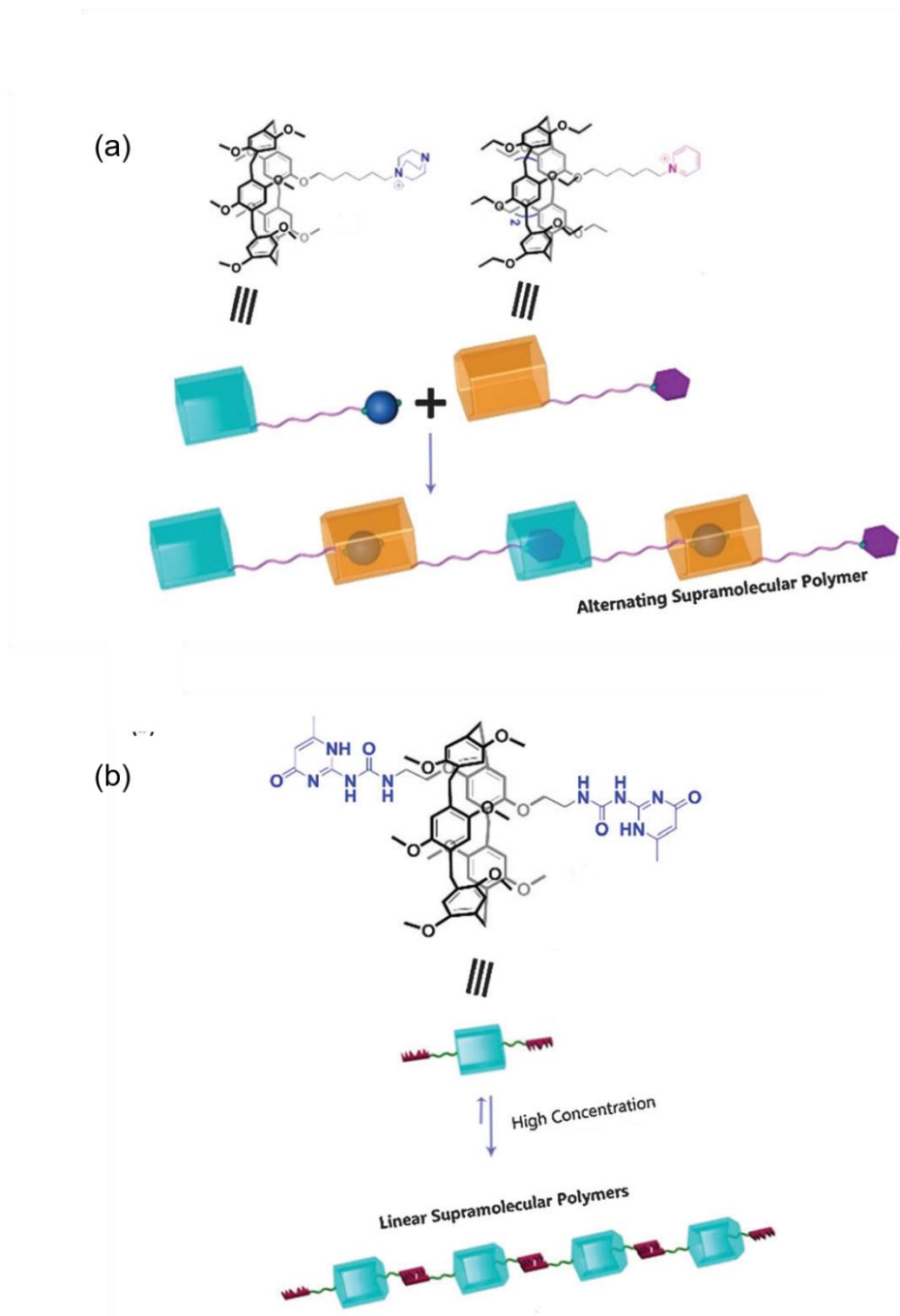

Figure 1.19 (a) Chemical structures of DABCO functionalized **P[5]** pyridinium functionalized **P[6]** and schematic illustration of the poly-pseudo[2]rotaxane network (b) Chemical structures of A1/A2 UPy functionalized **P[5]** and schematic illustration of the poly-pseudo[2]rotaxane. Figures adapted from reference[116]

P[n]s can further assemble in multidimensional aggregates, such as micelles, vesicular and tubular structures, with applications in material and biomedical science. [117,118,119,120]

Due to their rigid and symmetric structures, native **P[5]s** do not aggregate in spherical morphologies and micelles can be obtained only after **P[5]** derivatization or trough host-guest complexation with suitable molecules. Following the second strategy a very complex system based on a water soluble **P[5]** was developed by Jin and co-workers, which prepared a micelle upon complexation with methyl viologen functioned doxorubicin. The resultant micelles, due to the functionalization on **P[5]** rims, represent a pH-responsive system which further assemble at specific pH value. In fact, the aggregation occurred when the pH dropped from 7.4 to 6.5 miming the pH of a tumor extracellular environment. The aggregation led to an enhanced accumulation and better therapy effect without interfering with the cell uptake.

Host-Guest interaction

Self-assembly in water

pH-driven aggregation
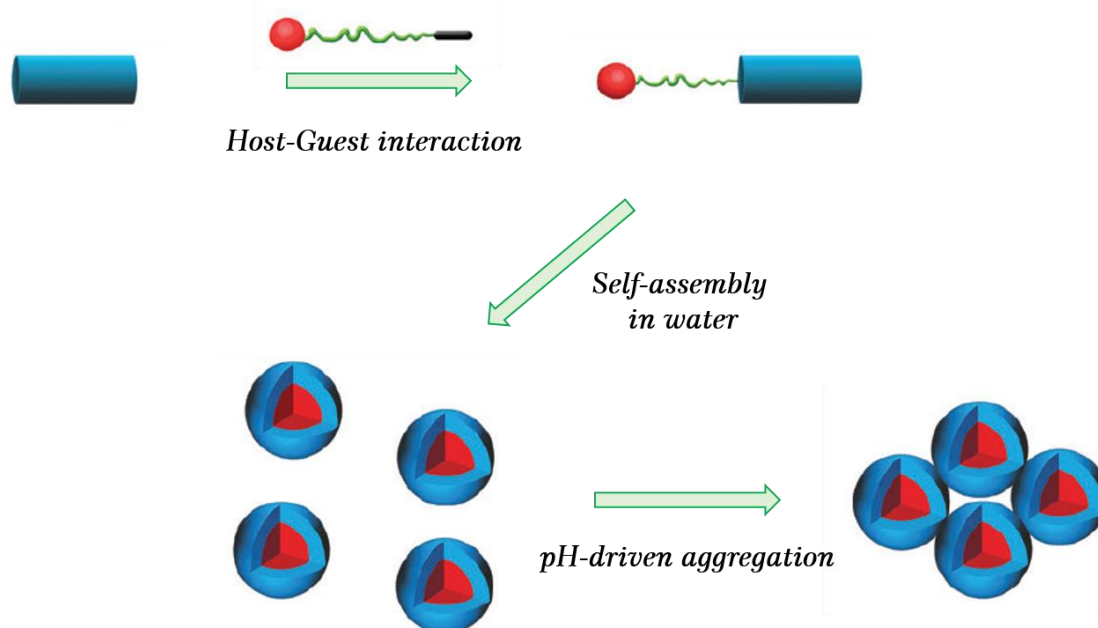
Figure 1.20 Schematic illustration of the preparation of supramolecular prodrug micelles and their pH responsive aggregate behaviour upon external pH stimulus. Figure adapted from reference [121]

Similarly, a nice example of a tubular structure was proposed by Hou's group, where the infinite face-to-face packing of **P[5]** in the crystal state, induced the formation of a water wire which served as a pathway for proton transport.[105]

After placing the **P[5]**-based structure inside a lipid bilayer, the nanotube was applied as an artificial proton channel.[122] Further stabilization to the tubular structure was given by covalent modification of **P[5]** connecting two units through a linker of a suitable length, in order to overcome the switching of the channel from a close to an open state after the potential water wire disassembly.
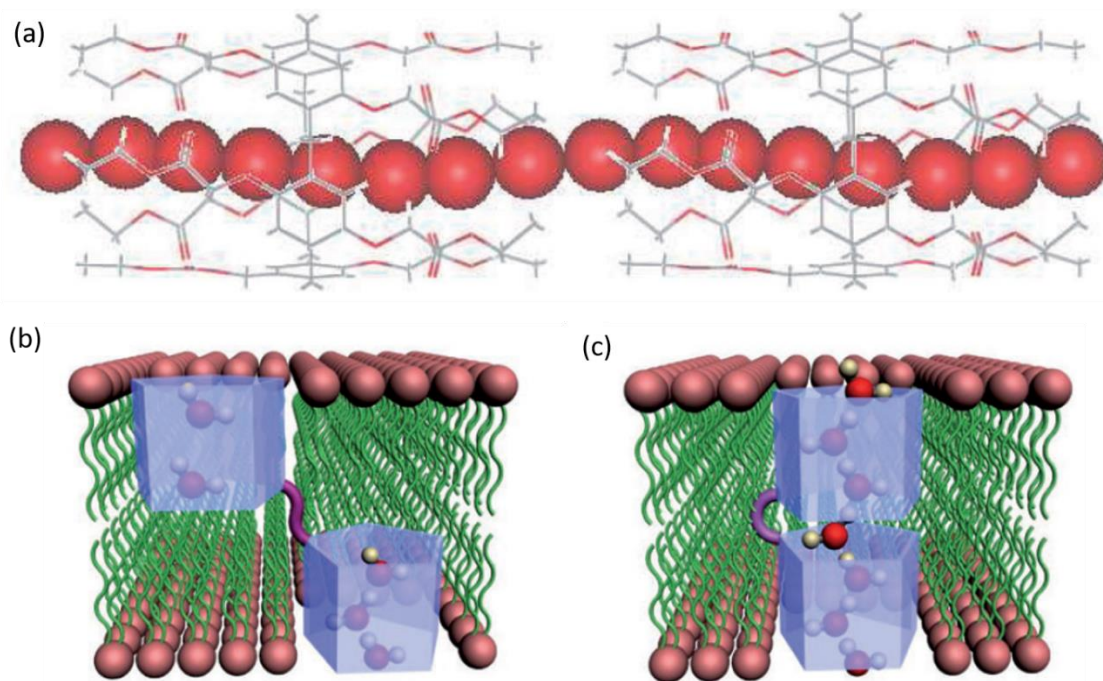

Figure 1.21 a) Partial X-ray crystal structure of P[5] derivative forming a nanotube with linear water wires encapsulated inside. b) Two molecules of P[5] derivative randomly distributed in lipid bilayer c) undergo self-assembly to form a water wire-based proton channel. Figure adapted from reference [122]

1.3.5. Applications of Pillar[n]arenes in Catalysis

Although **P[n]s** have been studied for all sort of applications, due to their recent history, they have been rarely exploited in supramolecular catalysis and so far only six example were published.

Ogoshi and co-workers showed an amphiphilic **P[5]** used as phase transfer catalyst in the biphasic oxidation of alkene to the corresponding aldehyde by KMnO$_4$, with higher selectivity towards linear substrates (Figure 1.22).[123] The starting **P[5]** was fully functionalized with phosphonium cations which made it soluble both in organic and aqueous solvents leaving unaltered its host-guest

abilities towards linear alkenes. Due to the positive charges on the rims the amphiphilic **P[5]** was able to encapsulate MnO_4^- and transferred it from the aqueous phase to the organic phase in order to ensure an efficient oxidation of the substrate. The catalytic efficiency of **P[5]** was ensured both by its complexation ability towards the substrate and to its amphiphilic nature which allowed the phase transfer of the oxidant. Furthermore, the success of the reaction was ensured by the selective higher complexation between **P[5]** and the starting alkene with respect to the resulting aldehyde.
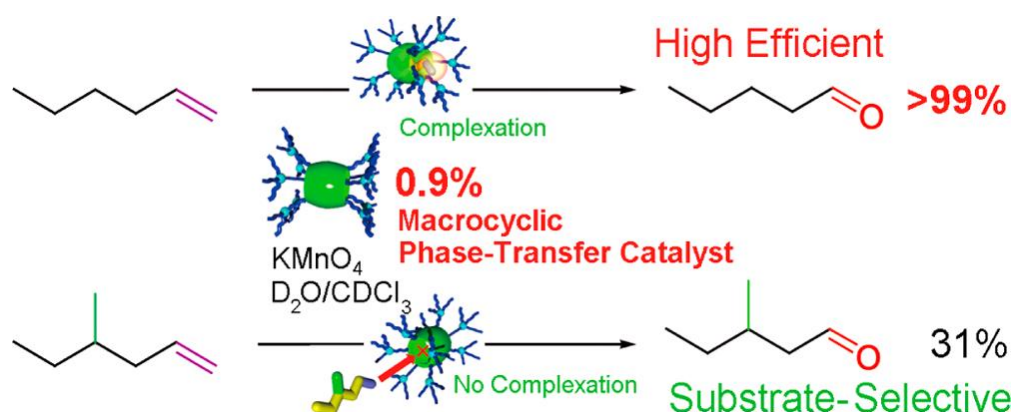
***Figure 1.22*** *Oxidation of terminal alkenes mediated by the presence of an amphiphilic* **P[5]**. *Figure adapted from reference* [123]

Similarly Nome and co-workers used a cationic water soluble **P[5]** as phosphate transfer catalyst to promote the hydrolysis of phosphate monoesters.[124] A quaternary ammonium **P[5]** was coupled with the dianion 2,4-dinitrophenylphosphate forming a stable 1:2 complex after 1500 ps. The water soluble **P[5]** acted as a mimic for the enzyme phosphatase by accelerating the spontaneous hydrolysis of the dianion at pH=7 of ten-fold and of four fold for the monoanion. Also in this case the cavity had a phase transfer role. The catalytic activity was strongly dependent from the host-guest complex strength, where **P[5]** showed much more affinity for the dianion than the monoanion, relying on the existent equilibrium between the complexed and the free species (Figure 1.23).
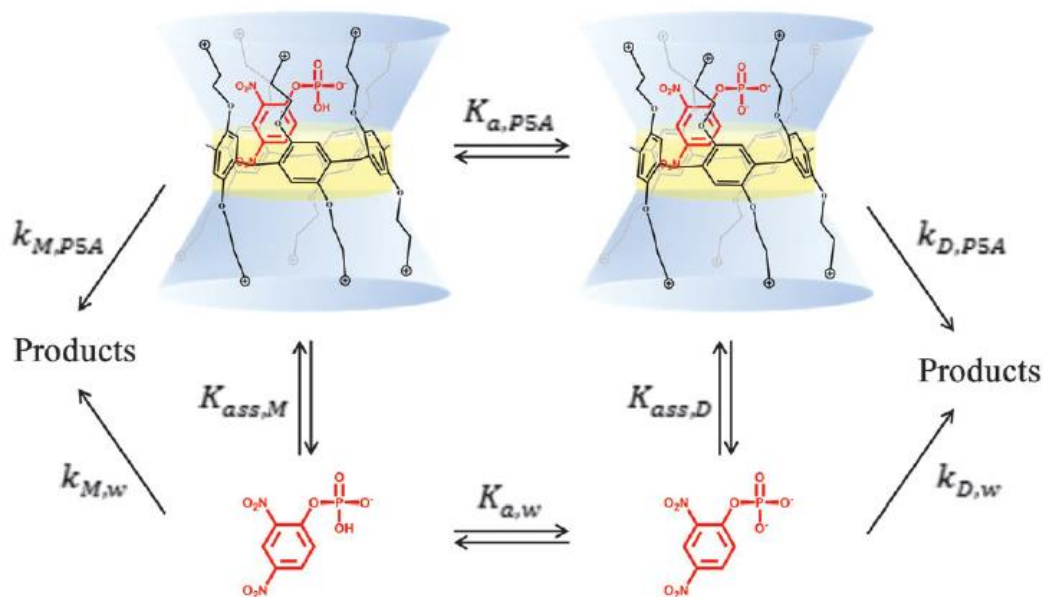
Figure 1.23 *Schematic representation of the four simultaneous pathways: (i) monoanion in water, kM,w, (ii) monoanion bound to the pillararene, kM,P5A, (iii) dianion in water, kD,w, and (iv) dianion bound in the pillararene cavity, kD,P5A. Figure adapted from reference [124]*

Yu's group showed how an anionic water soluble **P[5]** could efficiently inhibit the hydrolysis of acetylcholine in the presence of acetylcholinesterase.[125] The acetate derivative of **P[5]** efficiently hosted several trimethylammonium derivatives with increasing association constants according to the length of the alkyl chain of the guests. This suggested that alkyl chain was deeply penetrated inside the cavity exposing the ammonium group to the **P[5]** rim. Due to the hydrophobicity of the cavity and the anionic groups on the rims, the water soluble **P[5]** represented the perfect host for acetylcholine (Figure 1.24) and was efficiently employed as inhibitor of acetylcholine hydrolysis.
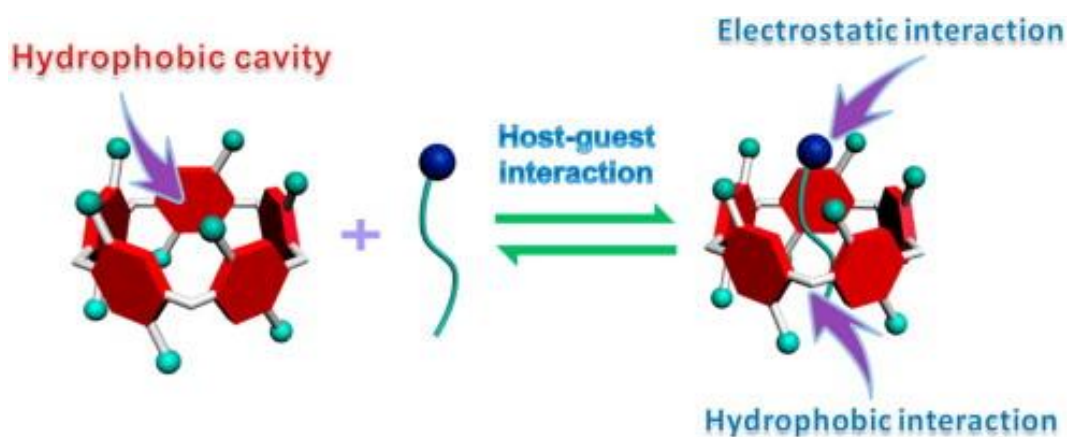
Figure 1.24 *Host-guest complexation between acetylcholine and the water soluble P[5] due to hydrophobic and electrostatic interactions. Figure adapted from reference [125]*

A more complex system was developed by Huang and co-workers that proposed a self-assembling composite micro-tubes based on amphiphilic P[5] and decorated it with gold nanoparticles able to catalyze the reduction of *p*-nitroaniline with NaBH$_4$.[126] Due to the presence of terminal amines, the amphiphilic P[5]s were able to interact with the gold nanoparticles. covering the nanoparticles surface in a bilayer arrangement with the exposition of the amine moieties. Contextually the same water soluble P[5] underwent a monolayer self-assembly into nanotubes which were decorated by the P[5] coated nanoparticles (Figure 1.25) through hydrogen bonding. These Au-decorated tubular structures were efficient catalysts in the aqueous reduction of *p*-nitroaniline. The stability of the tubular system (loss of 3% after 20 cycles) was the key factor to ensure the efficient catalysis.
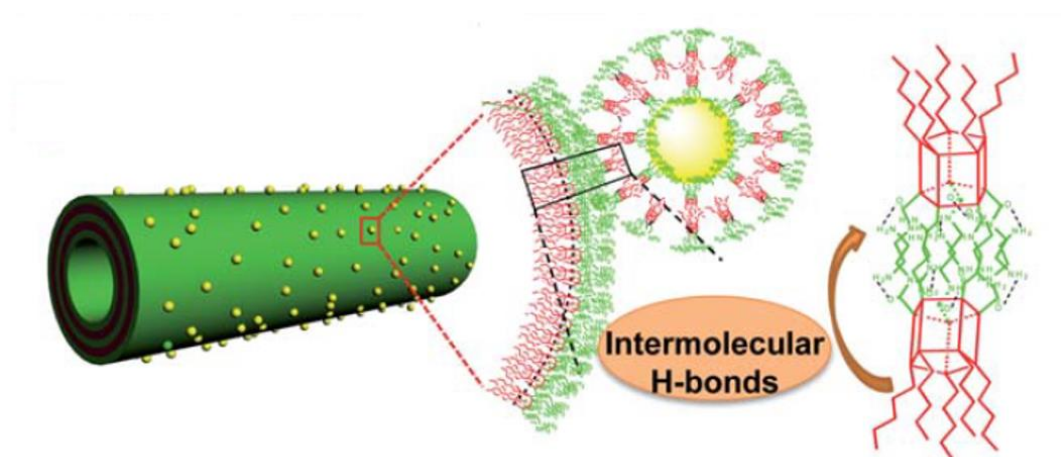
Figure 1.25 *Schematic illustration of a single AP5-microtube decorated with gold nanoparticles. Figure adapted from reference [126]*

Wang's group synthesized a **P[5]**-based imidazolium salts to be used as ligand for $PdCl_2(CH_3CN)_2$, to catalyze the Heck coupling reaction of styrene and aryl halides (Figure 1.26).[127] For this purpose **P[5]** was functionalized with the *N*-heterocyclic carbene group in order to act as macrocycle-based ligand for the Pd catalyst. The reactivity of the system was studied on different substrates an compared with a model reaction without **P[5]**, showing enhanced products yields due to the steric bulk of the **P[5]**-based ligand itself.

Figure 1.26 Heck coupling reaction mediated by the presence of a P[5]-N-heterocyclic carbene ligand. Figure adapted from reference [127]

The last example, developed by Yang and co-workers, concerned a **P[5]**-based [1]rotaxane used as catalyst in a Knovenagel condensation between malonitrile and acetone (Figure 1.27).[128] The same reaction in the presence of the monomer of the rotaxane was found to be two times faster than the reaction catalyzed by the rotaxane itself, displaying the essential role played by the tertiary amine on the rotaxane stopper. Even though partially occupied by the rotaxane axe, the cavity of **P[5]** slightly inhibited the reactive malonitrile through host-guest interaction, inhibiting the reaction if compared to the same condensation in the presence of the rotaxane monomer.
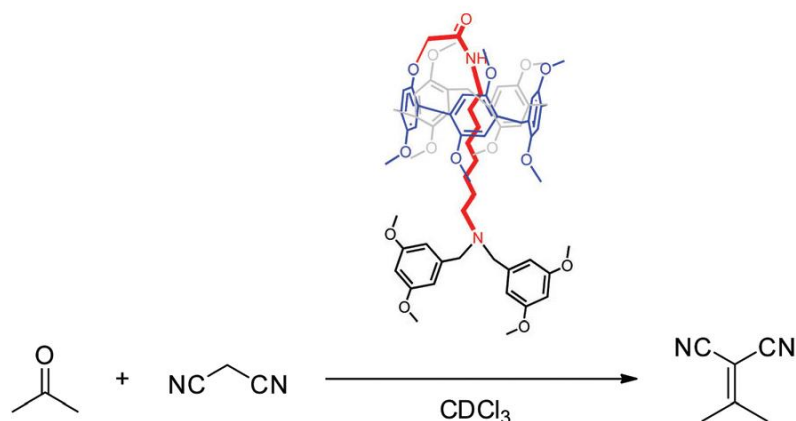
Figure 1.27 *Knovenagel reaction catalyzed by **P[5]**-based [1]rotaxane. Figure adapted from reference [128]*

However, none of the above described systems presented a catalytic effect strictly dependent on the cavity of **P[5]**, rather showing reactions accelerated in virtue of the cyclic pentamer functionalization or self-assembled structures. The lack of **P[n]s** used as true organocatalysts where the catalytic activity is directly connected to the binding of the substrates within the cavity of the **P[n]** inspired our work for the design of an efficient reaction where **P[n]** truly acts as a supramolecular catalyst.

1.4. References

1. J.-M. Lehn, *Angewandte Chemie International Edition in English*, 1988, **27**, 89-112.

2. M. G. L. van den Heuvel and C. Dekker, *Science*, 2007, **317**, 333-336.

3. S. Biswas, K. Kinbara, T. Niwa, H. Taguchi, N. Ishii, S. Watanabe, K. Miyata, K. Kataoka and T. Aida, *Nat Chem*, 2013, **5**, 613-620.

4. D. J. Cram, *Angewandte Chemie International Edition in English*, 1988, **27**, 1009-1020.

5. C. J. Pedersen, *Angewandte Chemie International Edition in English*, 1988, **27**, 1021-1027.

6. P. A. Gale and J. W. Steed, *Supramolecular chemistry : from molecules to nanomaterials*, Wiley-Blackwell, [Oxford], 2012.

7. X. J. Loh, *Materials Horizons*, 2014, **1**, 185-195.

8. G. Yu, K. Jie and F. Huang, *Chemical Reviews*, 2015, **115**, 7240-7303.

9. D. Astruc, *Modern Arene Chemistry*, Wiley-VCH Verlag GmbH & Co. KGaA, 2004.

10. P. P. Fu, *Journal of the American Chemical Society*, 1998, **120**, 8901-8902.

11. P. Spenst and F. Würthner, *Journal of Photochemistry and Photobiology C: Photochemistry Reviews*, 2017, **31**, 114-138.

12. K. E. Krakowiak, R. M. Izatt and J. S. Bradshaw, *Journal of Heterocyclic Chemistry*, 2001, **38**, 1239-1248.

13. H. Zhongying and C. P. Michael, *Tetrahedron Letters*, 1994, **35**, 3493-3496.

14. I. T. Ho, Z. Zhang, M. Ishida, V. M. Lynch, W.-Y. Cha, Y. M. Sung, D. Kim and J. L. Sessler, *Journal of the American Chemical Society*, 2014, **136**, 4281-4286.

15. T. J. J. Müller and U. H. F. Bunz, *Functional Organic Materials: Syntheses, Strategies and Applications*, Wiley-VCH Verlag GmbH & Co. KGaA, 2007.

16. L. Dai, Z.-J. Ding, L. Cui, J. Li, X. Jia and C. Li, *Chemical Communications*, 2017, DOI: 10.1039/C7CC06767D.

17. G. Barger and A. J. Ewins, *Journal of the Chemical Society, Transactions*, 1909, **95**, 552-560.

18. G. M. Robinson, *Journal of the Chemical Society, Transactions*, 1915, **107**, 267-276.

19. A. S. Lindsey, *Journal of the Chemical Society (Resumed)*, 1965, DOI: 10.1039/JR9650001685, 1685-1692.

20. H. Erdtman, F. Haglid and R. Ryhage, *Acta Chemica Scandinavica*, 1964, DOI: 10.3891/acta.chem.scand.18-1249, 1249-1254.

21. A. Baeyer, *Berichte der deutschen chemischen Gesellschaft*, 1872, **5**, 1094-1100.

22. R. Muthukrishnan and C. D. Gutsche, *The Journal of Organic Chemistry*, 1979, **44**, 3962-3964.

23. C. D. Gutsche, *Calixarenes*, Royal Society of chemistry, Cambridge, 1989.

24. A. G. S. Hoegberg, *The Journal of Organic Chemistry*, 1980, **45**, 4498-4500.

25. S. Korchak, W. Kilian and L. Mitschang, *Chemical Communications*, 2015, **51**, 1721-1724.

26. T. Evan-Salem, I. Baruch, L. Avram, Y. Cohen, L. C. Palmer and J. Rebek, *Proceedings of the National Academy of Sciences*, 2006, **103**, 12296-12300.

27. J. J. Rebek, *Chemical Communications*, 2000, DOI: 10.1039/A910339M, 637-643.

28. C. J. Sumby, K. C. Gordon, T. J. Walsh and M. J. Hardie, *Chemistry – A European Journal*, 2008, **14**, 4415-4425.

29. A. Collet, *Tetrahedron*, 1987, **43**, 5725-5759.

30. P. Sun, Y. Jiang, G. Xie and X. Du, 2010.

31. S.-C. Lo and P. L. Burn, *Chemical Reviews*, 2007, **107**, 1097-1116.

32. J. A. Aaron, J. M. Chambers, K. M. Jude, L. Di Costanzo, I. J. Dmochowski and D. W. Christianson, *Journal of the American Chemical Society*, 2008, **130**, 6942-6943.

33. K. T. Holman, J. W. Steed and J. L. Atwood, *Angewandte Chemie*, 1997, **109**, 1840-1842.

34. W. Abraham, *Journal of inclusion phenomena and macrocyclic chemistry*, 2002, **43**, 159-174.

35. R. Kumar, Y. O. Lee, V. Bhalla, M. Kumar and J. S. Kim, *Chemical Society Reviews*, 2014, **43**, 4824-4870.

36. M. C. Calama, P. Timmerman and D. N. Reinhoudt, *Angewandte Chemie International Edition*, 2000, **39**, 755-758.

37. M. M. Conn and J. Rebek, *Chemical Reviews*, 1997, **97**, 1647-1668.

38. F. Davis and S. Higson, *Macrocycles : construction, chemistry, and nanotechnology applications*, Wiley, Hoboken, 2011.

39. H.-J. Schneider and U. Schneider, *Journal of inclusion phenomena and molecular recognition in chemistry*, 1994, **19**, 67-83.

40. K. Kobayashi and M. Yamanaka, *Chemical Society Reviews*, 2015, **44**, 449-466.

41. L. R. MacGillivray and J. L. Atwood, *Journal of the American Chemical Society*, 1997, **119**, 6931-6932.

42. S. Ibach, V. Prautzsch, F. Vögtle, C. Chartroux and K. Gloe, *Accounts of Chemical Research*, 1999, **32**, 729-740.

43. D.-S. Guo and Y. Liu, *Chemical Society Reviews*, 2012, **41**, 5907-5921.

44. H. J. Kim, M. H. Lee, L. Mutihac, J. Vicens and J. S. Kim, *Chemical Society Reviews*, 2012, **41**, 1173-1190.

45. J. Atwood, *Comprehensive Supramolecular Chemistry II*, Elselvier, 2017.

46. F. Jia, Z. He, L.-P. Yang, Z.-S. Pan, M. Yi, R.-W. Jiang and W. Jiang, *Chemical Science*, 2015, **6**, 6731-6738.

47. S. T. Schneebeli, C. Cheng, K. J. Hartlieb, N. L. Strutt, A. A. Sarjeant, C. L. Stern and J. F. Stoddart, *Chemistry – A European Journal*, 2013, **19**, 3860-3868.

48. C. Ren, V. Maurizot, H. Zhao, J. Shen, F. Zhou, W. Q. Ong, Z. Du, K. Zhang, H. Su and H. Zeng, *Journal of the American Chemical Society*, 2011, **133**, 13930-13933.

49. H. M. Colquhoun, D. J. Williams and Z. Zhu, *Journal of the American Chemical Society*, 2002, **124**, 13346-13347.

50. Z. Du, C. Ren, R. Ye, J. Shen, V. Maurizot, Y. Lu, J. Wang and H. Zeng, *Chemical Communications*, 2011, **47**, 12488-12490.

51. T. Ogoshi, S. Kanai, S. Fujinami, T.-a. Yamagishi and Y. Nakamoto, *Journal of the American Chemical Society*, 2008, **130**, 5022-5023.

52. M. Xue, Y. Yang, X. Chi, Z. Zhang and F. Huang, *Accounts of Chemical Research*, 2012, **45**, 1294-1308.

53. H. Zhang and Y. Zhao, *Chemistry – A European Journal*, 2013, **19**, 16862-16879.

54. T. Ogoshi and T. Yamagishi, *Chemical Communications*, 2014, **50**, 4776-4787.

55. P. J. Cragg and K. Sharma, *Chemical Society Reviews*, 2012, **41**, 597-607.

56. T. Ogoshi, N. Ueshima, F. Sakakibara, T.-a. Yamagishi and T. Haino, *Organic Letters*, 2014, **16**, 2896-2899.

57. T. Ogoshi, *Pillararenes*, The Royal Society of Chemistry, Cambridge, UK, 1st edn., 2016.

58. Y. Kou, H. Tao, D. Cao, Z. Fu, D. Schollmeyer and H. Meier, *European Journal of Organic Chemistry*, 2010, **2010**, 6464-6470.

59. T. Ogoshi, K. Kitajima, T. Aoki, S. Fujinami, T.-a. Yamagishi and Y. Nakamoto, *The Journal of Organic Chemistry*, 2010, **75**, 3268-3273.

60. C. Han, F. Ma, Z. Zhang, B. Xia, Y. Yu and F. Huang, *Organic Letters*, 2010, **12**, 4360-4363.

61. D. Cao, Y. Kou, J. Liang, Z. Chen, L. Wang and H. Meier, *Angewandte Chemie International Edition*, 2009, **48**, 9721-9723.

62. K. Wang, L.-L. Tan, D.-X. Chen, N. Song, G. Xi, S. X.-A. Zhang, C. Li and Y.-W. Yang, *Organic & Biomolecular Chemistry*, 2012, **10**, 9405-9409.

63. T. Boinski and A. Szumna, *Tetrahedron*, 2012, **68**, 9419-9422.

64. S. Santra, I. S. Kovalev, D. S. Kopchuk, G. V. Zyryanov, A. Majee, V. N. Charushin and O. N. Chupakhin, *RSC Advances*, 2015, **5**, 104284-104288.

65. Z. Zhang, Y. Luo, B. Xia, C. Han, Y. Yu, X. Chen and F. Huang, *Chemical Communications*, 2011, **47**, 2417-2419.

66. T. Ogoshi, K. Kitajima, T.-a. Yamagishi and Y. Nakamoto, *Organic Letters*, 2010, **12**, 636-638.

67. Z. Zhang, B. Xia, C. Han, Y. Yu and F. Huang, *Organic Letters*, 2010, **12**, 3285-3287.

68. Q. Duan, W. Xia, X. Hu, M. Ni, J. Jiang, C. Lin, Y. Pan and L. Wang, *Chemical Communications*, 2012, **48**, 8532-8534.

69. N. L. Strutt, D. Fairen-Jimenez, J. Iehl, M. B. Lalonde, R. Q. Snurr, O. K. Farha, J. T. Hupp and J. F. Stoddart, *Journal of the American Chemical Society*, 2012, **134**, 17436-17439.

70. C. Han, Z. Zhang, G. Yu and F. Huang, *Chemical Communications*, 2012, **48**, 9876-9878.

71. T. Ogoshi, D. Yamafuji, D. Kotera, T. Aoki, S. Fujinami and T.-a. Yamagishi, *The Journal of Organic Chemistry*, 2012, **77**, 11146-11152.

72. T. Ogoshi, K. Demachi, K. Kitajima and T.-a. Yamagishi, *Chemical Communications*, 2011, **47**, 7164-7166.

73. N. L. Strutt, R. S. Forgan, J. M. Spruell, Y. Y. Botros and J. F. Stoddart, *Journal of the American Chemical Society*, 2011, **133**, 5668-5671.

74. X.-B. Hu, Z. Chen, L. Chen, L. Zhang, J.-L. Hou and Z.-T. Li, *Chemical Communications*, 2012, **48**, 10999-11001.

75. H. Ke, C. Jiao, Y.-H. Qian, M.-J. Lin and J.-Z. Chen, *Chinese Journal of Chemistry*, 2015, **33**, 339-342.

76. J. Cao, Y. Shang, B. Qi, X. Sun, L. Zhang, H. Liu, H. Zhang and X. Zhou, *RSC Advances*, 2015, **5**, 9993-9996.

77. T. Ogoshi, N. Ueshima, T. Akutsu, D. Yamafuji, T. Furuta, F. Sakakibara and T.-a. Yamagishi, *Chemical Communications*, 2014, **50**, 5774-5777.

78. G. Yu, G. Tang and F. Huang, *Journal of Materials Chemistry C*, 2014, **2**, 6609-6617.

79. T. Ogoshi, H. Kayama, D. Yamafuji, T. Aoki and T.-a. Yamagishi, *Chemical Science*, 2012, **3**, 3221-3226.

80. M. Holler, N. Allenbach, J. Sonet and J.-F. Nierengarten, *Chemical Communications*, 2012, **48**, 2576-2578.

47

81. T. Ogoshi, S. Tanaka, T.-a. Yamagishi and Y. Nakamoto, *Chemistry Letters*, 2011, **40**, 96-98.

82. C. Li, X. Shu, J. Li, J. Fan, Z. Chen, L. Weng and X. Jia, *Organic Letters*, 2012, **14**, 4126-4129.

83. X. Shu, S. Chen, J. Li, Z. Chen, L. Weng, X. Jia and C. Li, *Chemical Communications*, 2012, **48**, 2967-2969.

84. G. Yu, J. Yang, D. Xia and Y. Yao, *RSC Advances*, 2014, **4**, 18763-18771.

85. Y. Ma, X. Ji, F. Xiang, X. Chi, C. Han, J. He, Z. Abliz, W. Chen and F. Huang, *Chemical Communications*, 2011, **47**, 12340-12342.

86. Y. Ma, X. Chi, X. Yan, J. Liu, Y. Yao, W. Chen, F. Huang and J.-L. Hou, *Organic Letters*, 2012, **14**, 1532-1535.

87. W. Xia, X.-Y. Hu, Y. Chen, C. Lin and L. Wang, *Chemical Communications*, 2013, **49**, 5085-5087.

88. W. Chen, Y. Zhang, J. Li, X. Lou, Y. Yu, X. Jia and C. Li, *Chemical Communications*, 2013, **49**, 7956-7958.

89. G. Yu, X. Zhou, Z. Zhang, C. Han, Z. Mao, C. Gao and F. Huang, *Journal of the American Chemical Society*, 2012, **134**, 19489-19497.

90. J. W. Lee, S. Samal, N. Selvapalam, H.-J. Kim and K. Kim, *Accounts of Chemical Research*, 2003, **36**, 621-630.

91. Y. Wang, G. Ping and C. Li, *Chemical Communications*, 2016, **52**, 9858-9872.

92. G. Yu, W. Yu, Z. Mao, C. Gao and F. Huang, *Small*, 2015, **11**, 919-925.

93. T. Adiri, D. Marciano and Y. Cohen, *Chemical Communications*, 2013, **49**, 7082-7084.

94. B. Shi, K. Jie, Y. Zhou, J. Zhou, D. Xia and F. Huang, *Journal of the American Chemical Society*, 2016, **138**, 80-83.

95. Q. Lin, X.-M. Jiang, L. Liu, J.-F. Chen, Y.-M. Zhang, H. Yao and T.-B. Wei, *Soft Matter*, 2017, **13**, 7222-7226.

96. O. Danylyuk and V. Sashuk, *CrystEngComm*, 2015, **17**, 719-722.

97. X. Chi, M. Xue, Y. Yao and F. Huang, *Organic Letters*, 2013, **15**, 4722-4725.

98. T. Ogoshi, R. Sueto, K. Yoshikoshi, Y. Sakata, S. Akine and T.-a. Yamagishi, *Angewandte Chemie International Edition*, 2015, **54**, 9849-9852.

99. W. Si, X.-B. Hu, X.-H. Liu, R. Fan, Z. Chen, L. Weng and J.-L. Hou, *Tetrahedron Letters*, 2011, **52**, 2484-2487.

100. T. Ogoshi, T. Aoki, K. Kitajima, S. Fujinami, T.-a. Yamagishi and Y. Nakamoto, *The Journal of Organic Chemistry*, 2011, **76**, 328-331.

101. C. Han, L. Gao, G. Yu, Z. Zhang, S. Dong and F. Huang, *European Journal of Organic Chemistry*, 2013, **2013**, 2529-2532.

102. D. A. Leigh, M. Á. F. Morales, E. M. Pérez, J. K. Y. Wong, C. G. Saiz, A. M. Z. Slawin, A. J. Carmichael, D. M. Haddleton, A. M. Brouwer, W. J. Buma, G. W. H. Wurpel, S. León and F. Zerbetto, *Angewandte Chemie International Edition*, 2005, **44**, 3062-3067.

103. L. Gao, Z. Zhang, B. Zheng and F. Huang, *Polymer Chemistry*, 2014, **5**, 5734-5739.

104. T. Ogoshi, D. Yamafuji, T. Aoki and T.-a. Yamagishi, *Chemical Communications*, 2012, **48**, 6842-6844.

105. C. Ke, N. L. Strutt, H. Li, X. Hou, K. J. Hartlieb, P. R. McGonigal, Z. Ma, J. Iehl, C. L. Stern, C. Cheng, Z. Zhu, N. A. Vermeulen, T. J. Meade, Y. Y. Botros and J. F. Stoddart, *Journal of the American Chemical Society*, 2013, **135**, 17019-17030.

106. X. Hou, C. Ke, C. Cheng, N. Song, A. K. Blackburn, A. A. Sarjeant, Y. Y. Botros, Y.-W. Yang and J. F. Stoddart, *Chemical Communications*, 2014, **50**, 6196-6199.

107. S. Dong, J. Yuan and F. Huang, *Chemical Science*, 2014, **5**, 247-252.

108. M. Ni, X.-Y. Hu, J. Jiang and L. Wang, *Chemical Communications*, 2014, **50**, 1317-1319.

109. X.-Y. Hu, P. Zhang, X. Wu, W. Xia, T. Xiao, J. Jiang, C. Lin and L. Wang, *Polymer Chemistry*, 2012, **3**, 3060-3063.

110. C. Li, *Chemical Communications*, 2014, **50**, 12420-12433.

111. H. Zhang, K. T. Nguyen, X. Ma, H. Yan, J. Guo, L. Zhu and Y. Zhao, *Organic & Biomolecular Chemistry*, 2013, **11**, 2070-2074.

112. H. Zhang, N. L. Strutt, R. S. Stoll, H. Li, Z. Zhu and J. F. Stoddart, *Chemical Communications*, 2011, **47**, 11420-11422.

113. D. Xia, G. Yu, J. Li and F. Huang, *Chemical Communications*, 2014, **50**, 3606-3608.

114. H. Zhang, X. Ma, K. T. Nguyen and Y. Zhao, *ACS Nano*, 2013, **7**, 7853-7863.

115. Y. Wang, J. Du, Y. Wang, Q. Jin and J. Ji, *Chemical Communications*, 2015, **51**, 2999-3002.

116. W. Si, L. Chen, X.-B. Hu, G. Tang, Z. Chen, J.-L. Hou and Z.-T. Li, *Angewandte Chemie*, 2011, **123**, 12772-12776.

117. M. Raynal, P. Ballester, A. Vidal-Ferran and P. W. N. M. van Leeuwen, *Chemical Society Reviews*, 2014, **43**, 1734-1787.

118. P. Molenveld, W. M. G. Stikvoort, H. Kooijman, A. L. Spek, J. F. J. Engbersen and D. N. Reinhoudt, *The Journal of Organic Chemistry*, 1999, **64**, 3896-3906.

119. S. R. Shenoy, F. R. Pinacho Crisóstomo, T. Iwasawa and J. Rebek, *Journal of the American Chemical Society*, 2008, **130**, 5658-5659.

120. R. J. Hooley and J. Rebek, *Chemistry & Biology*, 2009, **16**, 255-264.

121. Y. Kang, X. Tang, H. Yu, Z. Cai, Z. Huang, D. Wang, J.-F. Xu and X. Zhang, *Chemical Science*, 2017, DOI: 10.1039/C7SC04125J.

122. T. Ogoshi, N. Ueshima and T.-a. Yamagishi, *Organic Letters*, 2013, **15**, 3742-3745.

123. D. G. Liz, A. M. Manfredi, M. Medeiros, R. Montecinos, B. Gomez-Gonzalez, L. Garcia-Rio and F. Nome, *Chemical Communications*, 2016, **52**, 3167-3170.

124. B. Hua, J. Zhou and G. Yu, *Tetrahedron Letters*, 2015, **56**, 986-989.

125. Y. Yao, M. Xue, Z. Zhang, M. Zhang, Y. Wang and F. Huang, *Chemical Science*, 2013, **4**, 3667-3672.

126. X.-D. Xiao, Y.-L. Bai, J.-Q. Liu and J.-W. Wang, *Tetrahedron Letters*, 2016, **57**, 3385-3388.

127. X.-S. Du, C.-Y. Wang, Q. Jia, R. Deng, H.-S. Tian, H.-Y. Zhang, K. Meguellati and Y.-W. Yang, *Chemical Communications*, 2017, **53**, 5326-5329.

Chapter 2

Aim of the Thesis

The main objective of this PhD thesis was to study the synthesis of pillar[n]arenes and to exploit their potential applications as supramolecular catalysts.

This class of aromatic macrocycles became popular for their one-step high yielding syntheses, which most of the time favored the smaller member of the family pillar[5]arene. Due to the lack of selective strategies which could lead to pillar[6]arenes formation in high yields, the first target of this thesis was to optimize the synthesis of the cyclic hexamer through a template approach. The idea was developed from an initial investigation on the binding abilities of pillar[n]arenes for small electron poor molecules, which led us to consider different cationic guests as a template.

Although selective for the cyclic pentamer or the cyclic hexamer, the synthesis of pillar[n]arenes always led to multiple products in equilibrium with one another. The second goal of this thesis was the comprehension of the factors affecting this equilibrium with a close attention to the mechanism responsible for the products interconversion. The role of all the chemical species involved in the reactions was evaluated through MS studies during the eight-months stay in Prof. Christoph Schalley's group at Freie Universität Berlin of Berlin. The last part of the project aimed to disclose the reaction mechanism, involved the synthesis of the first isotopically labelled pillar[5]arene.

Together with their easy and convenient synthesis, pillar[n]arenes chemistry found application in supramolecular chemistry for their unique ability in binding neutral guests. From this lead, we developed the third goal of this thesis aimed at the application of these macrocycles in homogeneous catalysis. Since no example of pillar[n]arenes as true organocatalysts were so far reported, we focused our attention on the electron rich confined space ensured by pillar[5]arene cavity, expecting a positive catalytic effect in reactions between neutral substrates presenting cationic transition states.

Chapter 3

Cation templated Improved Synthesis of Pillar[6]arenes
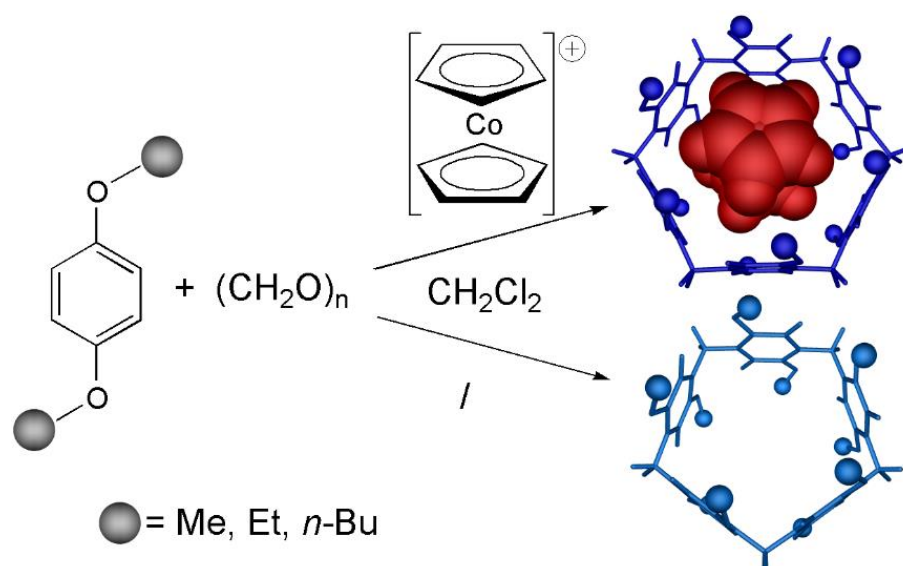
3.1. Templated Synthesis: a Short Introduction

Since their discovery, **P[n]s** showed impressive host–guest properties due to their semi-rigid, symmetric and electron-donating cavity that promotes selective binding of unusual neutral molecules.[129] Therefore, great attention has been focused on the optimization of the syntheses of the two most promising members of the family, **P[5]** and **P[6]**, which usually proceeded through the condensation reaction between *para*-bis-alkoxy benzene derivatives and paraformaldehyde,[67] or, alternatively, through the self-condensation reaction of 2,5-substituted derivatives of 1,4-dialkoxy benzene.[66]

In order to improve the efficiency of **P[5]** and **P[6]** syntheses, different catalysts, such as the most common Lewis acids[65] or some organic Brønsted acids,[68] have been successfully employed in various concentration and molar ratio with respect to the reacting monomers. In one contribution the key factor to ensure a high yielding **P[5]** and **P[6]** synthesis was the physical state of the catalysts, and in particular, the combination of $FeCl_3$ with choline chloride to form a deep eutectic solvent (**DES**) was investigated.[82]

However, most of the procedures reported higher yields for the cyclic pentamer, with ratios **P[5]/P[6]** ranging from 30 to 1.5.[130] Only some few very recent examples in the literature reported an inversion of this trend, with the formation of higher amounts of **P[6]** derivatives, using mainly a templating approach promoted by the presence of strategic solvents or electron-poor guests, such as chloro-cyclohexane[83] or naphthalene diimide.[81]
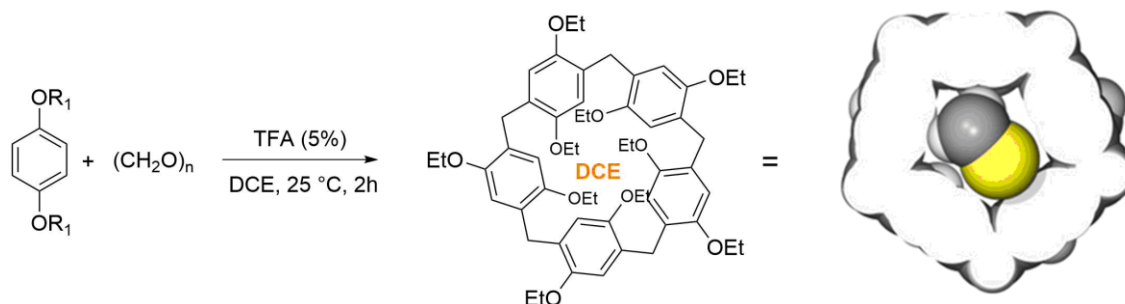
Figure 3.1 *Szumna solvent templated synthesis of **PEt[5]**. Figure adapted from reference[69]*

The efficient use of templates to steer the reaction towards less favorite products is a well-known strategy employed since the sixties, which some decades later found application in the synthesis of supramolecular species. Examples of this strategy are the synthesis of crown ethers[131] or phtalocyanines[132] based on metal ion guests, catenanes[133] based on electrostatic and dispersive forces and paracyclophanes[134] based on covalently bound templates. Similarly, cyclotrimers[135] are templated by a porous coordination framework, as well as mesoporous nanostructure which are based on sacrificial molecular organic framework templates[136] and polymers or nanoparticles templated by surfactants.[137]

Almost coinciding with our work, a new efficient and scalable method for the selective synthesis of **P[6]** derivatives was developed by Zyryanov using sulfuric acid as catalyst in solvent free condition, in which the *para*-dialkoxybenzene and paraformaldehyde melt together to form **P[6]** in 85% within 10 minutes.[138] However, the difficult removal of the residual catalyst and the difficult purification of the crude **P[6]**-represent important drawbacks of this procedure.
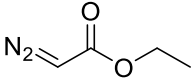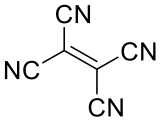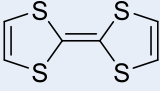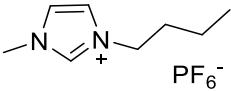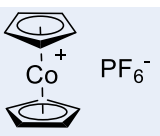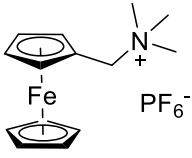
In the present Chapter we report our approach for an improved synthesis of **P[6]** conducted in the presence of different cationic guests as templates to evaluate their effect on the synthesis of the desired product (Scheme 3.1). We used a direct condensation of *para*-dialkoxybenzene and paraformaldehyde catalyzed by the presence of 0.3% mol of $FeCl_3$ in DCM at room temperature. Where applicable, the catalyst and the template were melt together in a **DES** form and the amount of the template was carefully evaluated to enhance the catalyst efficiency.

3.2. *Results and Discussion*

3.2.1. *Suitable Templates Investigation*

In order to find suitable guests to be used to steer the selectivity towards the **P[6]** rather than the **P[5]**, complexation experiments of several electron poor molecules with ethoxy substituted **P[5]** and **P[6]** as model hosts were evaluated through ^{1}H NMR spectroscopy (Table 3.1), showing once more the **P[n]** preferential binding towards cationic species (Table 3.1, entries 5, 6, 7). The binding ability was calculated in terms of downfield shift of the pillararenes aromatic peak in the presence of the guest compared with the same peak in the absence of the guest. In all the experiments, the host-guest complexation equilibrium showed fast exchange rate compared to the NMR time scale, showing resonances at chemical shift values that are the average balance between the resonances of the free and the complexed species.

Table 3.1 Evaluation of the preferential binding of different electron poor molecules towards **PEt[5]** *and* **PEt[6]***. The [Host]/[Guest] ratio was set to 1/6 and all experiments were performed in CDCl₃ at 298K.*

#	Guest	PEt[5]	PEt[6]
		Δδ (ppm)	Δδ (ppm)
1		0	0
2		0	0
3		0	0
4		0	0
5		-0.12	0
6		0	-0.2
7		0	-0.1

From these experiments we decided to investigate in detail the selective binding between **PEt[5]** and 1-butyl-3-methylimidazolium hexafluorophosphate (**BmimPF₆**) and between **PEt[6]** and cobaltocenium hexafluorophosphate (**COCP**) or (ferrocenylmethyl)trimethylammonium hexafluorophosphate (**FECP**).

Due to the deshielding effect induced by the inclusion of the guest inside the host cavity, **PEt[5]** presented downfield shifted peaks both in the aromatic

and in the aliphatic regions (Figure 3.2), where the latter referred to the interaction of the ethoxy chains on the rims with the guest. Due to the poor solubility of the **BmimPF₆** in CDCl₃, another complexation experiment was performed in CDCl₃/DMSO-d₆ (5:1, v/v) in order to observe the shift induced also in the guest peaks (Figure 3.2b). As expected, all **BmimPF₆** resonances exhibited an upfiled shift due the deshielding effect of **PEt[5]** cavity.
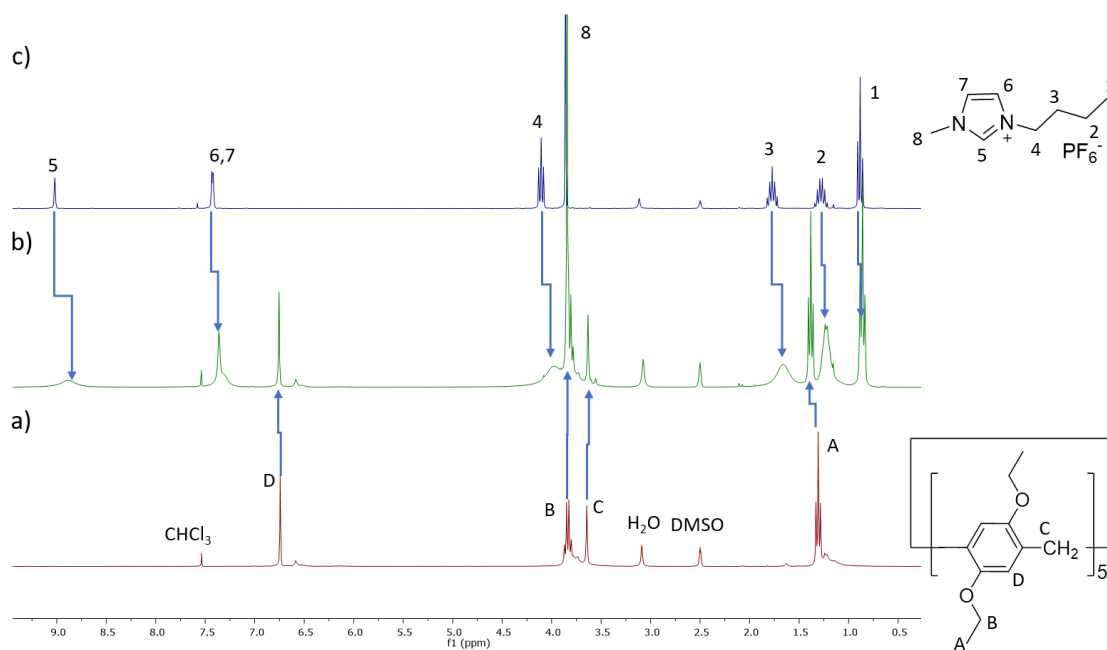
Figure 3.2 ¹H NMR spectra (300 MHz, 298 K) of a) [PEt[5]]=2mM, b) [BmimPF₆]=6[PEt[5]]=12mM, c)[BmimPF₆]=2mM in CDCl₃/DMSO-d₆ (5:1, v/v).

Due the poor solubility of **COCP** and **FECP** in CDCl₃ the next complexation experiments were performed in CDCl₃/ACN-d₃ (5:3, v/v) and CDCl₃/ACN-d₃ (5:1, v/v) respectively. Similar interpretation was applied to **PEt[6]** based complex (Figure 3.3) where the host showed the same downfield peak shift in the aromatic region, and **COCP** upfield shifted signals (Figure 3.3b). Similarly, we observed the same behavior for **PEt[6]** and **FECP** which showed a considerable upfield shift due to the guest positioning in the shielding region of the aromatic cavity (Figure 3.4).
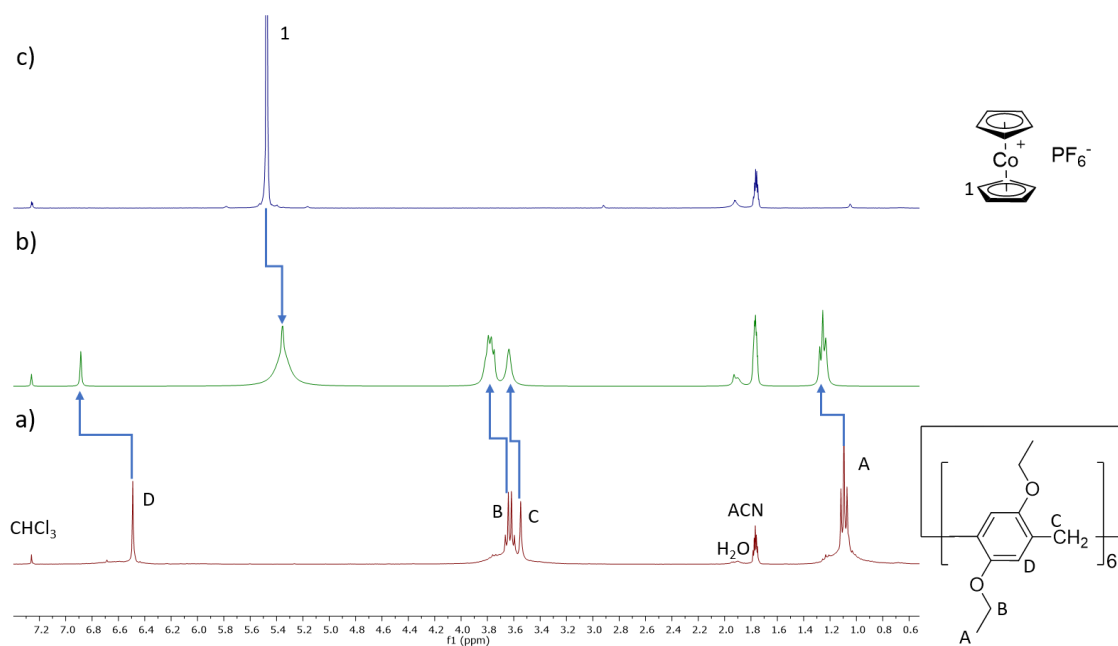
Figure 3.3 *¹H NMR spectra (300 MHz, 298 K) of a) [PEt[6]]=2mM, b) [COCP]=6[PEt[6]]=12mM, c)[COCP]=2mM in CDCl₃/ACN-d₃ (5:3, v/v).*
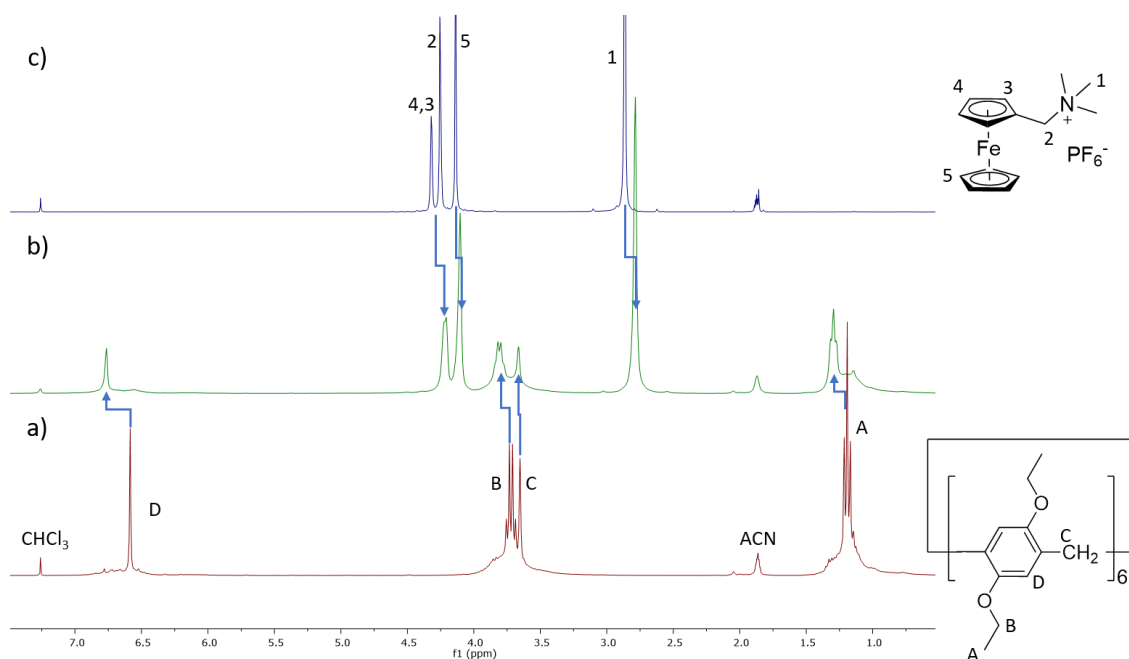
Figure 3.4 *¹H NMR spectra (300 MHz, 298 K) of a) [PEt[6]]=2mM, b) [FECP]=6[PEt[6]]=12mM, c)[FECP]=2mM in CDCl₃/ACN-d₃ (5:1, v/v).*

Since **COCP** showed the greater affinity for **PEt[6]**, the host-guest complex formation was investigated in detail by means of ¹H NMR titration, following the aromatic resonance of the host with the molar ratio between guest and host. The

plot of the $\Delta\delta$ for the host as a function of [**COCP**]/[**PEt[6]**] was fitted considering a 1:1 binding mode between host and guest and the fitting curve obtained led to a K_{ass} of 1.2×10^4 M^{-1} (Figure 3.5). The value observed was indicative of a good affinity between the cationic guest **COCP** and the larger host **PEt[6]** and it was comparable to what observed for the known interaction between similar **P[6]**s and ferrocenium salts.[93]
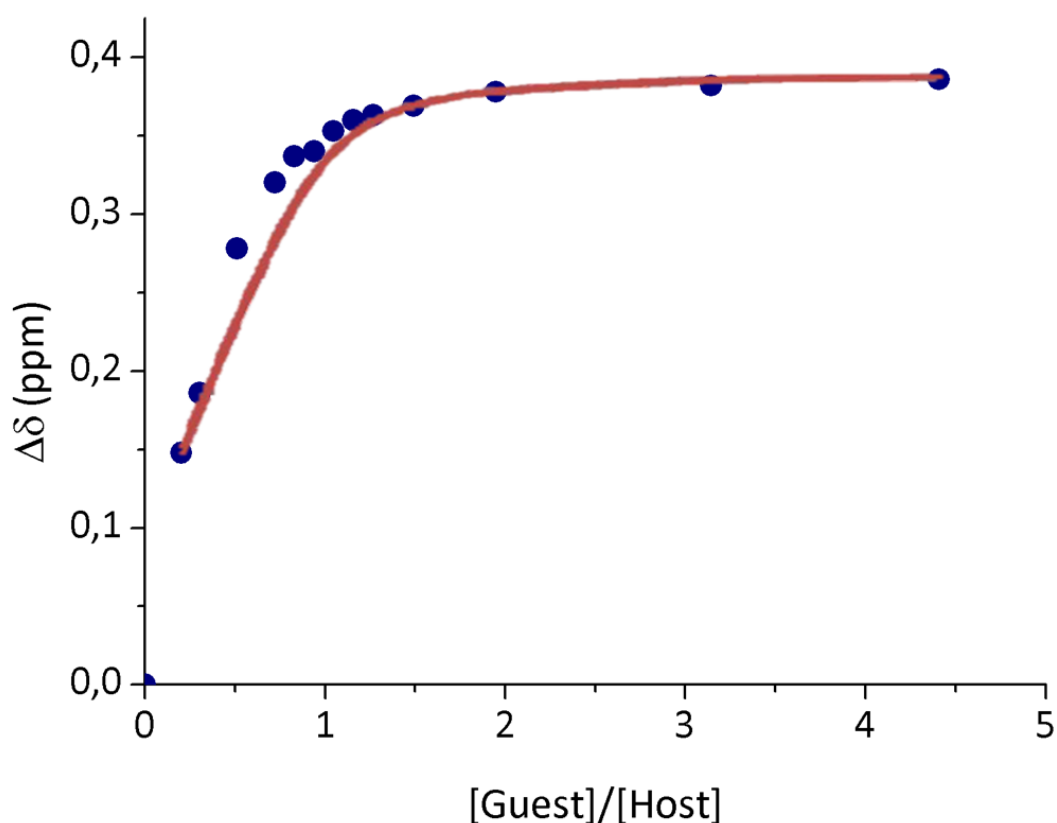
*Figure 3.5 Plot for the titration of **PEt[6]** with **COCP** and fitting of the data for the calculation of the K_{ass} (1.2 x 10^4 M^{-1})*

Nevertheless, according to structural considerations on the guest pentagonal shape, a better host-guest interaction of the cycle pentamer **PEt[5]** rather than of the cycle hexamer **PEt[6]** would be expected. Therefore, in order to better investigate the complexation behavior between **COCP** and **PEt[5]** or **PEt[6]** respectively, the two host-guest inclusion structures were modelled at a semiempirical PM3 level of **COCP@PEt[5]** (Figure 3.6) and **COCP@PEt[6]** (Figure 3.7) showed that the guest **COCP** is forced to fit into **PEt[5]** cavity arranging the cyclopentadienes in an eclipsed conformation, while, in the larger

PEt[6] cavity, **COCP** fitted in a more favored staggered conformation, avoiding in addition the contacts with the inner walls of the cavity itself.
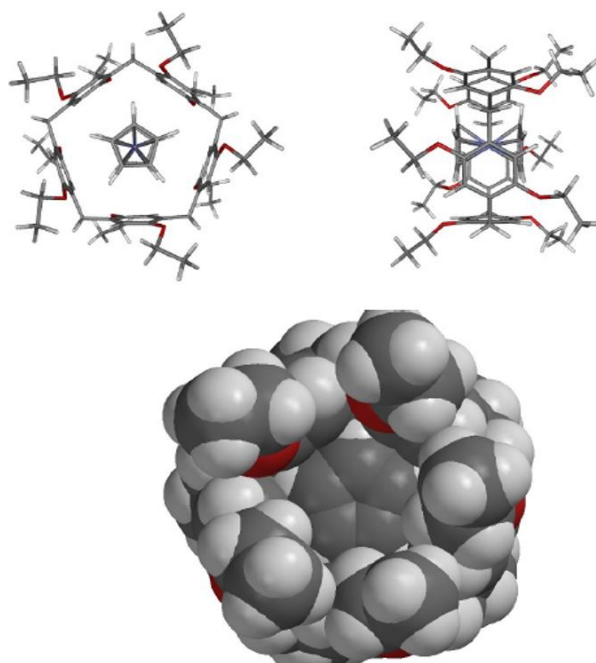
*Figure 3.6 Minimized (semiempirical PM3) structure of **COCP@PEt[5]** on top (left: front view; right: lateral view) and space filling structures bottom (front view).*
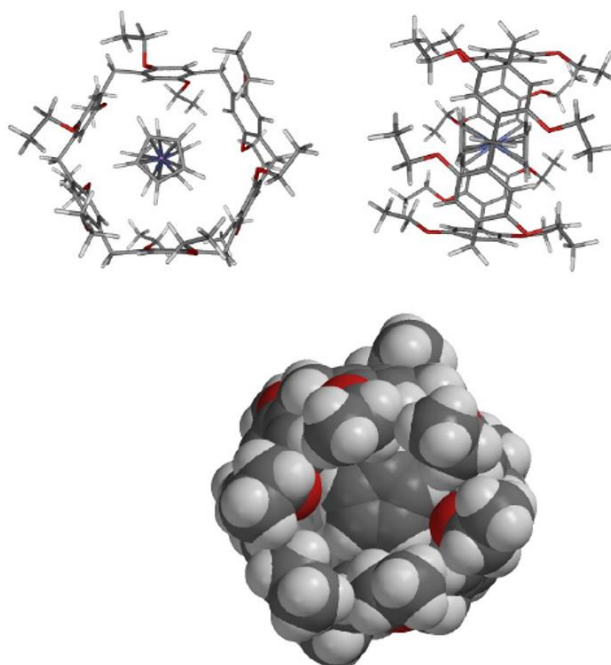
*Figure 3.7 Minimized (semiempirical PM3) structure of **COCP@PEt[6]** on top (left: front view; right: lateral view) and space filling structures bottom (front view).*

Due to the selective binding for **PEt[5]** or **PEt[6]** alternatively, we decided to use these salts as templates in our pillararenes syntheses. In fact, a favorable complexation was observed for **BmimPF₆** and the smaller **PEt[5]** while no binding evidences were observed for **BmimPF₆** with **PEt[6]**. On the opposite, metallocenium salts **COCP** and **FECP** were successfully included in **PEt[6]** showing clear binding evidences, while **PEt[5]** in the same conditions did not bind them.

Due to the known high affinity shown by quaternary ammonium compounds for both of pillar[n]arenes,[73,66] tetramethylammonium chloride (**TMAC**) was considered as further possible template together with **COCP**, **FECP** and **BmimPF₆**.

3.2.2. *Pillar[n]arenes Syntheses from Different Monomers*
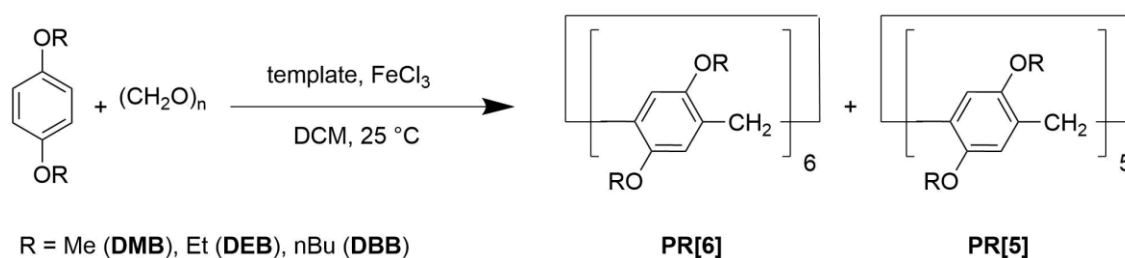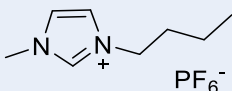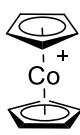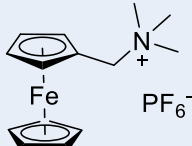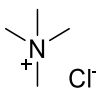
Scheme 3.1 *Cation templated synthesis of* **P[5]** *and* **P[6]** *from different dialkoxy benzene derivatives (***DMB***,* ***DEB***,* ***DBB***).*

Starting from the commercially available hydroquinone and alkyl iodides, three different *para*-disubstituted benzene alkyl derivatives were quantitatively synthesized in DMSO at room temperature. Cyclization reactions of 1,4-dimethoxybenzene (**DMB**), 1,4-diethoxybenzene (**DEB**) or 1,4-dibutoxybenzene (**DBB**) with paraformaldehyde and FeCl₃ as catalyst were conducted to obtain the corresponding **P[6]**s and **P[5]**s (**PMe[6]**, **PMe[5]**, **PEt[6]**, **PEt[5]**, **PBu[6]**, **PBu[5]** respectively) (Table 3.2, entries 1, 2 and 3).

Analogous reactions were repeated in the presence of the templates 25% mol (**TMAC**, **COCP**, **FECP** or **BmimPF₆** respectively) (Table 3.2, entries 4-15)

resulting in different **PR[6]**s/**PR[5]**s depending on the substituent and the template employed.

Table 3.2 *Synthesis of* ***PR[5]*** *and* ***PR[6]*** *with different starting monomers (****DMB****,* ***DEB****,* ***DBB****) and different templating agents:* ***TMAC*** *and* ***BmimPF6*** *15 mol%,* ***COCP*** *and* ***FECP*** *25 mol%.* [a] *isolated yields.*

#	Monomer	Template	Conversion (%)	PR[6][a]/PR[5][a] (%)
1	DMB	/	27	7/traces
2	DEB	/	29	6/3
3	DBB	/	12	5/traces
4	DMB		10	2/8
5	DEB		94	13/13
6	DBB		2	traces/traces
7	DMB		100	6/5
8	DEB		100	38/7
9	DBB		59	32/28
10	DMB		100	traces/22
11	DEB		100	6/19
12	DBB		8	7/10
13	DMB		100	13/30
14	DEB		100	19/24
15	DBB		27	15/12

It is worth to notice that all the reactions carried out without templates employed led to conversions comparable to those reported in the literature[139] but lower in terms of isolated yields. Unsoluble polymers and soluble oligomers in all the cases were observed as undesired by-products.

Starting from **DMB** as substrate and in the presence of **TMAC** the reaction led to quantitative conversion of the aromatic substrate and to the formation of **PMe[6]** and **PMe[5]** in 13% and 30% isolated yields respectively (Table 3.2, entry 13), confirming the higher selectivity towards the smaller host and displaying an overall yield increased for both products compared to the non-templated approach (Table 3.2, entry 1). Switching to the diethoxy **DEB** substrate, an increase of the overall amount of the corresponding **PEt[6]** was observed (19% yield), almost in a 1:1 ratio with its **PEt[5]** homologue (24% yield) (Table 3.2, entry 14). Although the longer butoxy **DBB** benzene derivative displayed incomplete conversion, **PBu[6]** was obtained in slightly higher isolated yield (15%) than **PBu[5]** (13% yield) (Table 3.2, entry 15). Even though apparently the template **TMAC** presented no preferential affinity towards **P[5]**s or **P[6]**s some considerations can be drawn from the comparison with the non-templated approach (Table 3.2, entry 1-3). As a matter of fact, in all the three substrates both higher yields were obtained in the presence of this salt and the selectivity in favor of **P[6]** increased concomitantly.

A similar trend was observed with the cationic species **FECP** displaying quantitative conversions with the smaller aromatic substrate **DMB** and **DEB** and a **P[6]**/**P[5]** ratio that increased along with the chain length of the substituents. Nevertheless, **PMe[5]** was isolated as the major isomer, with a maximum 22% yield (Table 3.2, entry 10), while the corresponding **PMe[6]** was obtained only in traces. With longer substituents, the main product was always the cyclic pentamer, with **PEt[5]** yield three times higher than that of **PEt[6]** (Table 3.2, entry 11) and **PBu[5]** yield almost double compared to **PBu[6]** yield (Table 3.2, entry 12). The observed **P[6]**/**P[5]** ratio seems not to be in accordance with the results obtained from the complexation experiments, where the template **FECP** preferred the inclusion into the larger **PEt[6]** cavity rather than into the smaller **PEt[5]** cavity. Therefore, the complexation ability of **FECP** was not enough to ensure an efficient templated effect.

The use of **BmimPF$_6$** as templating unit did not provide good results, since for all the monomers investigated the yield of the corresponding macrocycles were rather low, in most of the cases due also to low conversions of the substrates
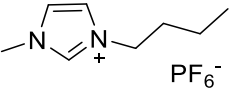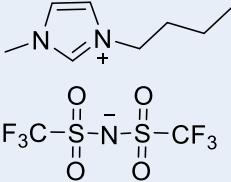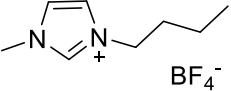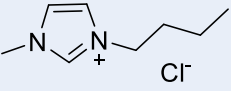
themselves (Table 3.2, entry 4 and 12). Similarly to the case of **FECP**, **BmimPF₆** did not show any preference for the smaller **PEt[5]** despite its complexation behavior observed by ¹H NMR suggested the opposite. In fact, the reaction carried out from **DEB** as a monomer gave an equal product distribution with 13% yield for both **PEt[5]** and **PEt[6]** (Table 3.2, entry 5).

In accordance with the previous complexation studies, all the syntheses in the presence of **COCP** gave the cyclic hexamer as the preferred product, even for the smaller substituted **PMe[6]** (6% yield) compared to its homologue **PMe[5]** (5% yield) (Table 3.2, entry 7). The best results were obtained employing **DEB** as monomer that reacted quantitatively to furnish 38% and 7% yields for **PEt[6]** and **PEt[5]**, respectively (Table 3.2, entry 8). With the longer **DBB** the synthesis led to **PBu[6]** in 32% yield and almost the same amount of **PBu[5]** (28% yield) (Table 3.2, entry 9), with a reduction of the template efficiency in terms of selectivity towards **PBu[6]**.

3.2.3. Different 1-Butyl-3-methylimidazolium Salts as Templating Unit

The counter anion effect was also evaluated in the synthesis of **PEt[6]** and **PEt[5]** by using different salts such as **BmimPF₆**, 1-butyl-3-methylimidazolium bis(trifluoromethylsulfonyl)imide (**BmimTf₂N**), 1-butyl-3-methylimidazolium tetrafluoroborate (**BmimBF₄**) and 1-butyl-3-methylimidazolium chloride (**BmimCl**), as reported in Table 3.3.

*Table 3.3 Synthesis of **PEt[6]** and **PEt[5]** in the presence of 1-butyl-3-methyl imidazolium with different counter anions.*

#	Template	Conversion (%)	PEt[6] [a]/PEt[5][a] (%)
1	PF$_6^-$	94	13/13
2	F$_3$C–S–N–S–CF$_3$	31	6/6
3	BF$_4^-$	20	2/3
4	Cl$^-$	2	traces/traces

While the products selectivity remained unaffected, **PEt[6]** /**PEt[5]** ratio yields decreased together with the coordination strength of the anion and nicely in accordance with the decrease of the counter anion average radius. [140]

3.2.4. Effect of the Template Concentration

We further investigated the effect of **COCP** molar amount on the cyclization reaction in the synthesis of **PEt[6]**, observing that the conversion, and even more importantly **PEt[6]** and **PEt[5]** yields, were not much affected by the amount of the templating cation. The best conditions were observed using 25 mol% of **COCP** leading to 38% isolated yield of **PEt[6]** (Table 3.4, entry 2), while in the presence of a lower (20 mol%) or higher amount (30 mol%) of template, the yields of **PEt[6]** slightly decreased.

Table 3.4 *Synthesis of **PEt[6]** and **PEt[5]** with different molar amounts of **COCP**.*

#	COCP (mol%)	Conversion (%)	PEt[6] [a]/PEt[5][a] (%)
1	20	93	37/6
2	25	100	38/7
3	30	83	34/5

The scalability of the reactions was also taken into account by increasing seven times the amount of starting materials in the synthesis of **PEt[6]** with the reaction conditions described in Table 3.4, entry 2. The reaction led to quantitative conversion of the aromatic reagent and formation of the corresponding **PEt[6]** macrocycle in 38% isolated yield. We can conclude that, since the synthesis of **DEB** from hydroquinone is a quantitative reaction, the selective two steps synthesis of **PEt[6]** from hydroquinone is possible with an overall yield of 38%.

3.3. Conclusions

In conclusion, we successfully obtained a high yielding template syntheses of the hexameric pillararenes **PR[6]** from para-dialkoxy benzene derivatives (**DMB**, **DEB** and **DBB**) and paraformaldehyde, with FeCl$_3$ as Lewis acid in the presence of the templating salts **TMAC**, **COCP**, **FECP** or **BmimPF$_6$** respectively. Compared with other **P[6]** selective syntheses,[130] our approach was rather straightforward with the use of economic and environmentally friendly catalyst, requiring a templating unit only in substoichiometric amount. The non-coordinating role of the counter anion together with the amount of the required template were also evaluated. In accordance with previous studies on the complexation affinity between the guest **COCP** and the host **PEt[6]**, the

cyclization of the monomer **DEB** in the presence of 25 mol% of **COCP** as template resulted in the maximum amount of **PEt[6]** ever synthetized. After scaling seven times the reaction and considering the two steps synthesis starting from hydroquinone, **PEt[6]** was obtained in an overall 38% yield.

3.4. *Experimental Section*

3.4.1. *General Procedure*

Solvents used in the study were reagent grade and purchased from commercial national sources. Hydroquinone, iodomethane, iodoethane, bromobutane, paraformaldehyde, $FeCl_3$, tetramethylammonium chloride, bis(cyclopentadienyl)cobalt (III) hexafluorophosphate were reagent grade and purchased from Sigma-Aldrich. Deionized water was used in all experiments. ^1H and ^{13}C NMR spectra were collected on a Bruker-300 MHz NMR spectrometer. Low resolution electrospray ionization mass spectrometry LRMS (ESI-MS) experiments were carried out in positive mode with Agilent Technologies LC/MSD Trap SL AGILENT instrument (mobile phase acetonitrile). (Ferrocenylmethyl)trimethylammonium hexafluorophosphate was synthesized and characterized according to literature procedures.[141]

3.4.2. *Synthetic Procedures*

3.4.2.1. *Synthetic Rroute for P[5] and P[6] through DES*
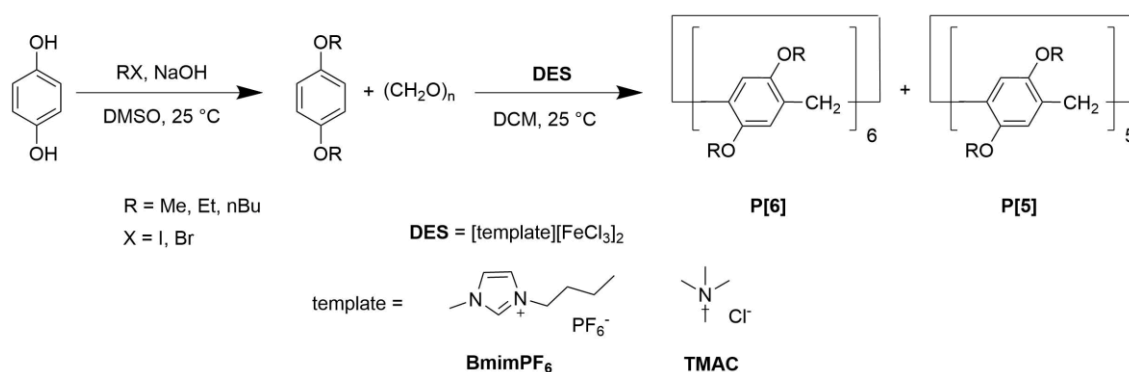
Scheme 3.2 Synthesis of the dialkoxy benzene derivatives (DMB, DEB, DBB) and templated synthesis of P[5] and P[6] through DES.

3.4.2.2. *Synthesis of DMB, DEB and DBB*

RX (44.1 mmol) (R = Me, Et, nBu) (X = I, Br) and NaOH (1.76 g, 44.1 mmol) were added to a solution of HQ (1.6 g, 14.7 mmol) in DMSO (50 ml) under air atmosphere at 25 °C. The mixture was stirred for 2 h and then was poured into ice and water (100 ml). The solid precipitate was filtered and washed with water resulting in the desired *para*-dialkoxy benzene as white crystals. Yield of **DMB** 95% (1.899 g, 13.75 mmol), Yield of **DEB** 98% (2.391 g, 14.4 mmol), Yield of **DBB** 96% (3.137 g, 14.1 mmol)

3.4.2.3. *Synthesys of P[5] and P[6]*

A mixture of $FeCl_3$ (0.048 g, 0.3 mmol) and **BmimPF$_6$** (or **TMAC**) (0.6 mmol) was heated at 110 °C with gentle stirring until a dark brown viscous liquid was obtained. A solution of 1,4-dialkoxybenzene (0.166 g, 1.0 mmol), paraformaldehyde (0.091 g, 3.0 mmol) in DCM (20 ml) was added to the mixture. After stirring at room temperature for 4 h, the reaction was quenched by addition of water. The organic phase was separated and washed with saturated aqueous $NaHCO_3$, water and brine. The crude product was purified by column chromatography (eluent: CyH/DCM in gradient from 3:7 to 1:9

3.4.2.4. *Synthesis of PR[5] and PR[6] Templated by Metallocene Derivatives*
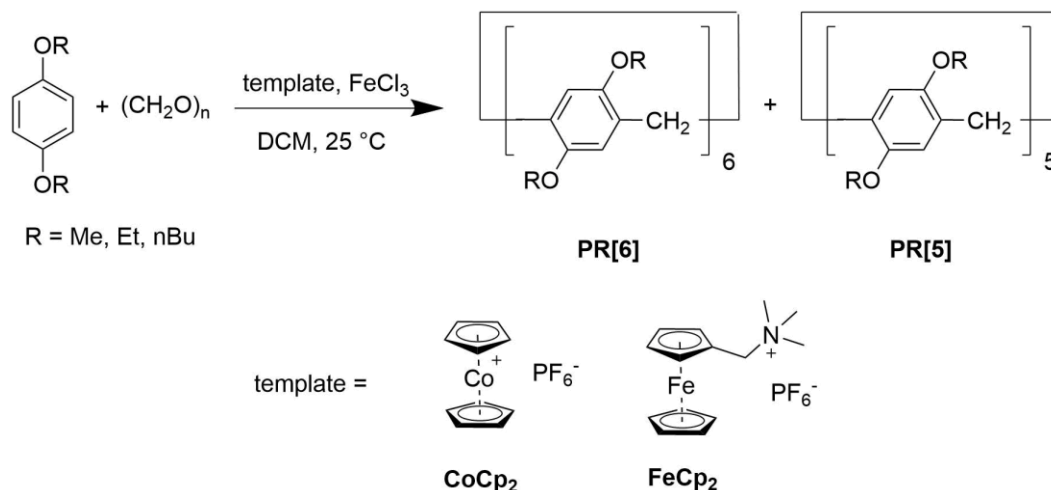
Scheme 3.3 *Metallocene derivatives templated synthesis of **P[5]** and **P[6]***.

A mixture of $FeCl_3$ (50.3 mg, 0.3 mmol), **COCP** (or **FECP**) (0.04 mmol), 1,4-dialkoxybenzene (1.0 mmol), paraformaldehyde (90 mg, 3.0 mmol) in DCM (20 ml) was stirred at room temperature for 4 h. The reaction was quenched by addition of water. The organic phase was separated and washed with saturated aqueous $NaHCO_3$, water and brine. The crude product was purified by column chromatography (eluent: CyH/DCM in gradient from 3:7 to 1:9).

3.4.3. *Compounds Characterization*

DMB: ^{1}H NMR (300 MHz, $CDCl_3$, 298 K), δ 6.84 (s, 4H), 3.77 (s, 6H).

DEB: ^{1}H NMR (400 MHz, $CDCl_3$, 298 K), δ 6.82 (s, 4H), 3.98 (q, $J = 7.0$ Hz, 4H), 1.40 (t, $J = 7.0$ Hz, 6H).

DBB: ^{1}H NMR (300 MHz, $CDCl_3$, 298 K), δ 6.82 (s, 4H), 3.90 (t, $J = 6.6$ Hz, 4H), 1.76 – 1.69 (m, 4H), 1.47 (m, 4H), 0.96 (t, $J = 7.4$ Hz, 6H).

PMe[5]: ^{1}H NMR (300 MHz, $CDCl_3$, 298 K) δ (ppm): 6.75 (s, 10H), 3.77 (s, 10H), 3.73 (s, 30H). ^{13}C NMR (300 MHz, $CDCl_3$, 298 K) δ (ppm) 150.66, 128.21,

113.90, 55.70, 29.51. MS (ESI): *m/z* 750,6 [M], 773.5 [M+Na$^+$], 789.5 [M+K$^+$], 824.6 [M+(CH$_3$)$_4$N$^+$].

PMe[6] :^{1}H NMR (300 MHz, CDCl3, 298 K) δ (ppm): 6.69 (s, 12H), 3.69 (s, 12H), 3.64 (s, 36H). ^{13}C NMR (300 MHz, CDCl$_3$, 298 K) δ (ppm): 151.40, 127.43, 113.59, 56.09, 29.67. MS (ESI): *m/z* 901,6 [M+H$^+$], 918.1 [M+NH$_4$$^+$].

PEt[5]: ^{1}H NMR (300 MHz, CDCl3, 298 K) δ (ppm): 6.72 (s, 10H), 3.81 (q, J = 6Hz, 10H), 3.77 (s, 10), 1.25 (t, *J* = 6 Hz, 30H). ^{13}C NMR (300 MHz, CDCl$_3$, 298 K) δ (ppm): 149.81, 128.48, 115.07, 63.74, 29.83, 15.03. MS (ESI): *m/z* 891.7 [M+H$^+$], 908.6 [M$^+$+ NH$_4$$^+$], 929.7.6 [M$^+$+ K$^+$], 964.7 [M$^+$+ N(CH$_3$)$_4$$^+$]

PEt[6]:^{1}H NMR (300 MHz, CDCl$_3$, 298 K) δ (ppm): 6.69 (s, 12H), 3.80 (q, *J* = 6Hz, 12H), 3.79 (s, 12H), 1.28 (t, *J* = 6 Hz, 36H). ^{13}C NMR (300 MHz, CDCl$_3$, 298 K) δ (ppm): 150.35, 127.78, 115.16, 63.93, 30.86, 15.11. MS (ESI): *m/z* 1068.9 [M+], 1091.9 [M+Na$^+$], 1107.9 [M+K$^+$], 1170.9 [M+T$_1$].

PBu[5]: ^{1}H NMR (300 MHz, CDCl3, 298 K) δ (ppm): 6.92 (s, 10H), 3.93 (t, *J* = 6Hz, 20H), 3.82 (s, 10H), 1.86 (q, *J* = 6Hz, 20H), 1.59 (s, *J* = 6Hz, 20H), 1.05 (t, 30H). ^{13}C NMR (300 MHz, CDCl$_3$, 298 K) δ (ppm): 149.74, 128.15, 114.64, 67.90, 32.03, 29.33, 19.51, 14.02. MS (ESI): *m/z* 1171.1[M+H$^+$], 1189.2 [M+NH$_4$$^+$], 1210.1 [M+K$^+$].

PBu[6]: ^{1}H NMR (300 MHz, CDCl3, 298 K) δ (ppm): 6.69 (s, 12H), 3.76 (t, *J* = 6Hz, 24H), 3.76 (s, 12H), 1.69 (q, *J* = 6Hz, 24H), 1.42 (s, *J* = 6Hz, 24H), 0.91 (t, 36H). ^{13}C NMR (300 MHz, CDCl$_3$, 298 K) δ (ppm): 150.41, 127.80, 114.93, 68.17, 31.87, 30.70, 19.39, 13.90. MS (ESI): *m/z* 1423.4[M+NH$_4$$^+$], 1477.3 [M+N(CH$_3$)$_4$$^+$].
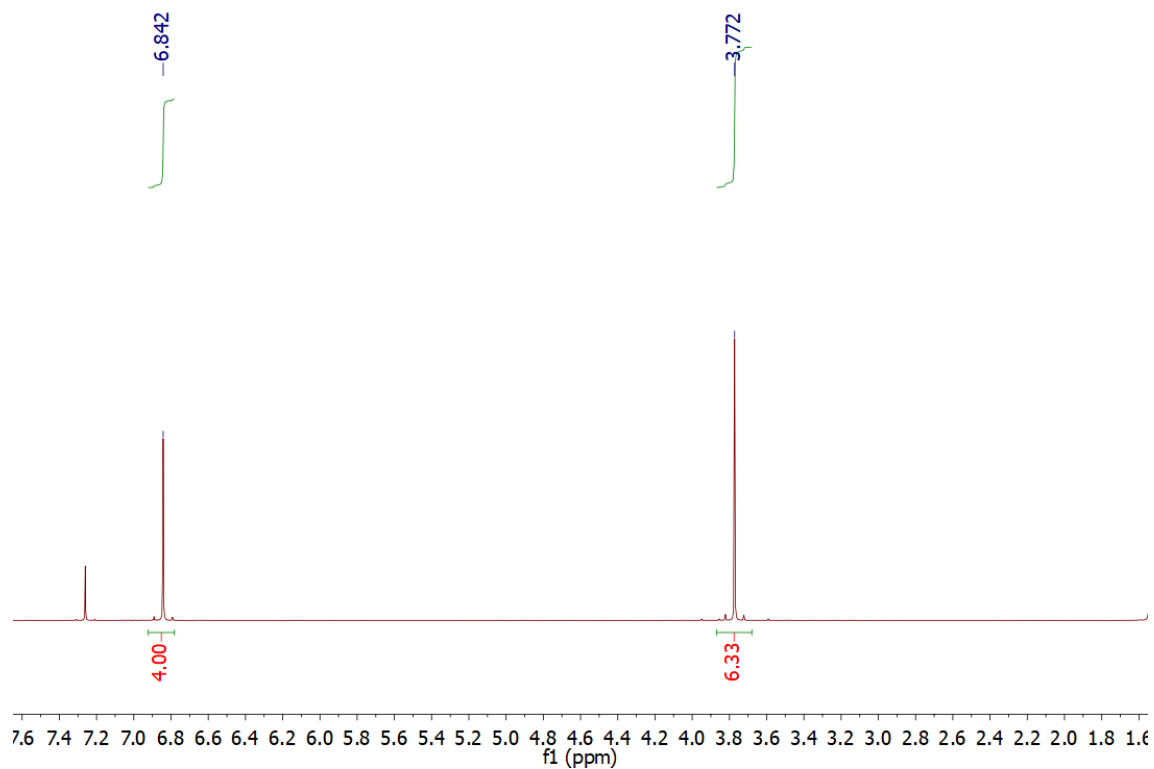
Figure 3.8 ¹H NMR (400 MHz, CDCl₃, 298 K) of **DMB**.
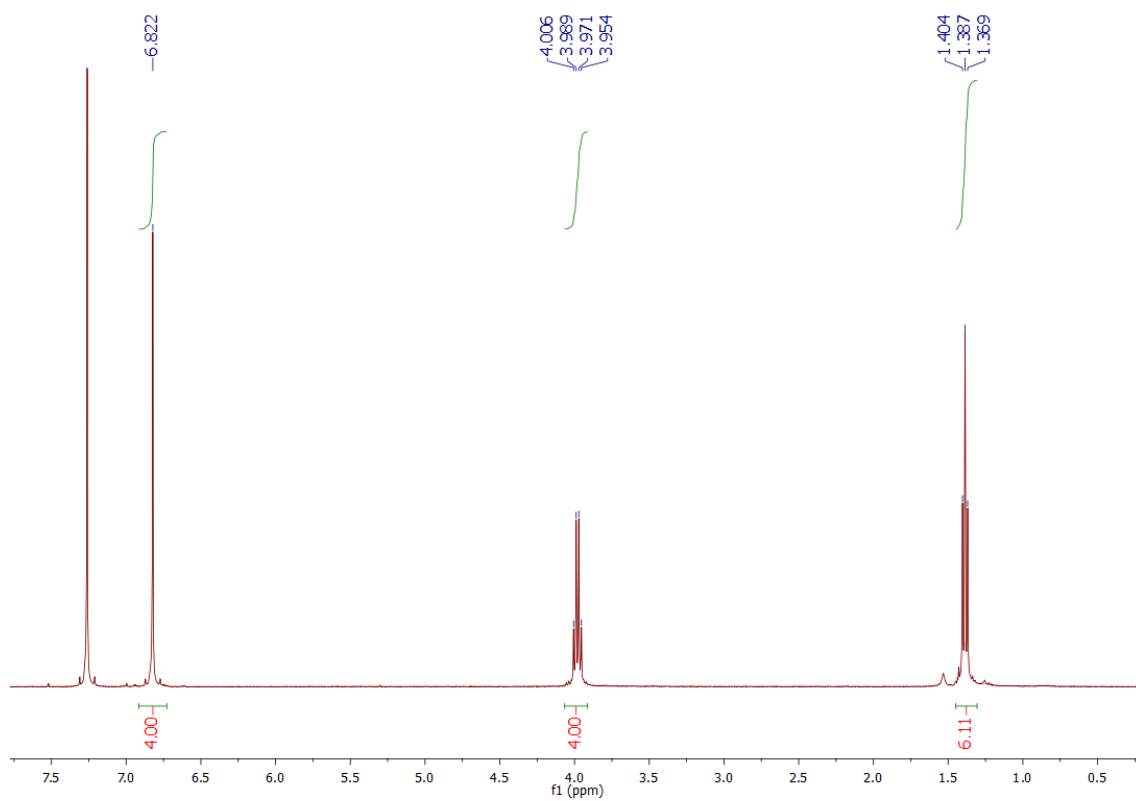
Figure 3.9 ¹H NMR (400 MHz, CDCl₃, 298 K) of **DEB**
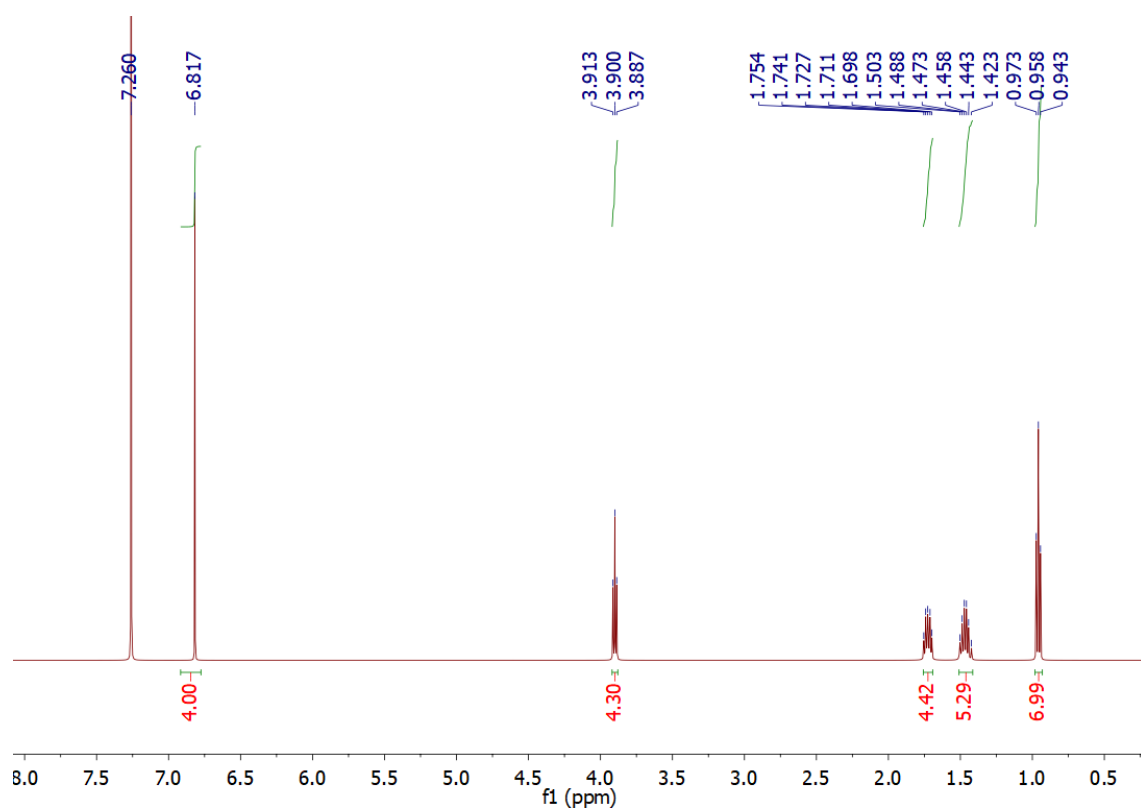
Figure 3.10 1H NMR (400 MHz, CDCl3, 298 K) of **DBB**
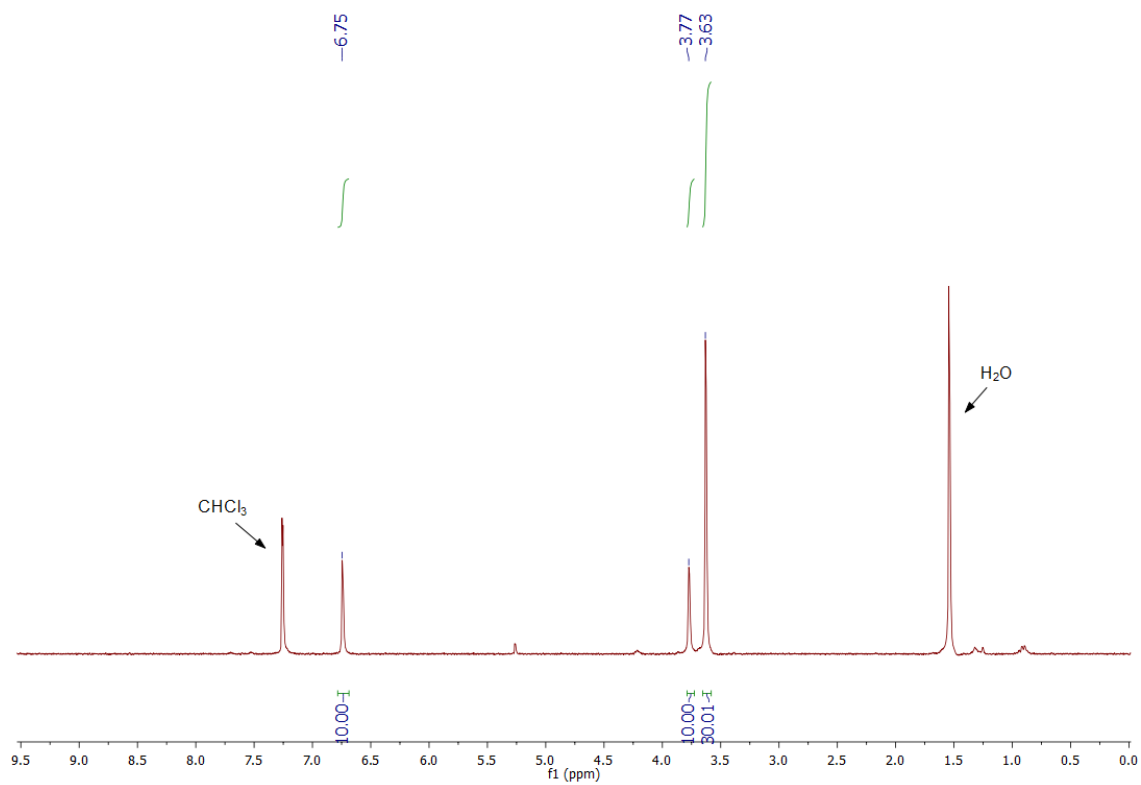
Figure 3.11 ^{1}H NMR (400 MHz, CDCl$_3$, 298 K) of **PMe[5]**.
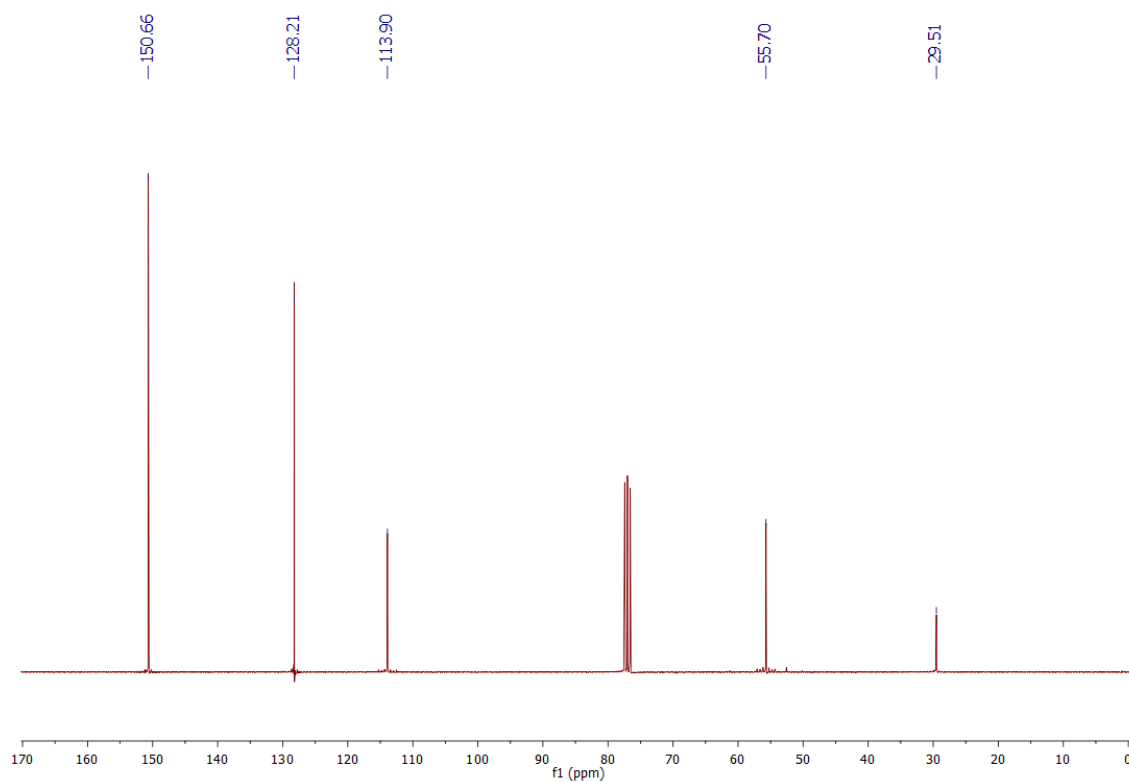
Figure 3.12 ^{13}C NMR (400 MHz, CDCl$_3$, 298 K) of **PMe[5]**.
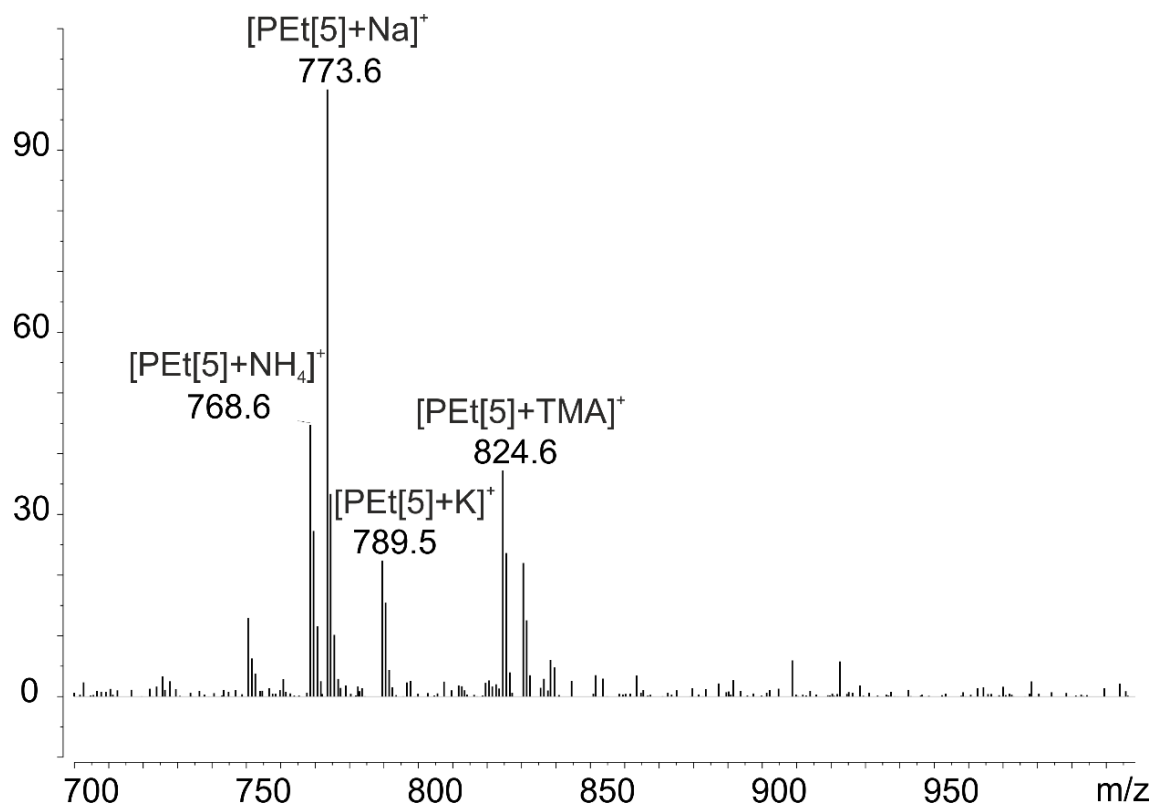
Figure 3.13 ESI-MS spectrum of **PMe[5]**.
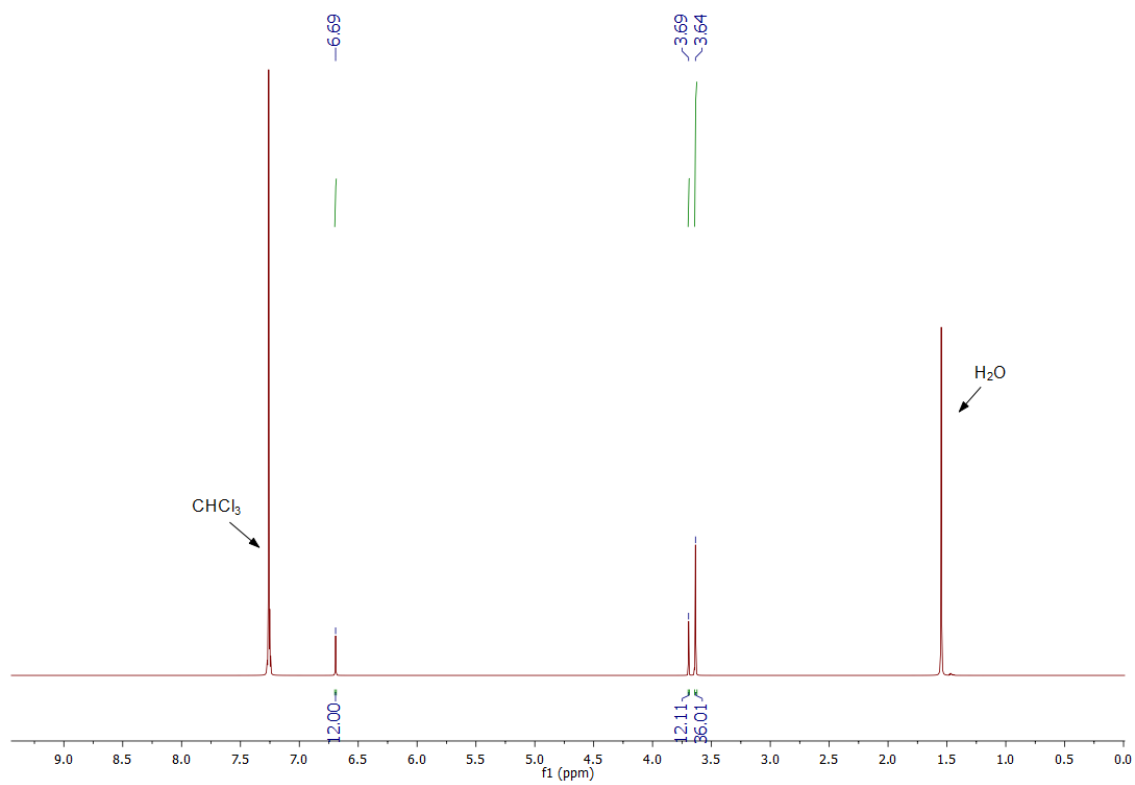
Figure 3.14 *¹H NMR (400 MHz, CDCl₃, 298 K) of PMe[6].*
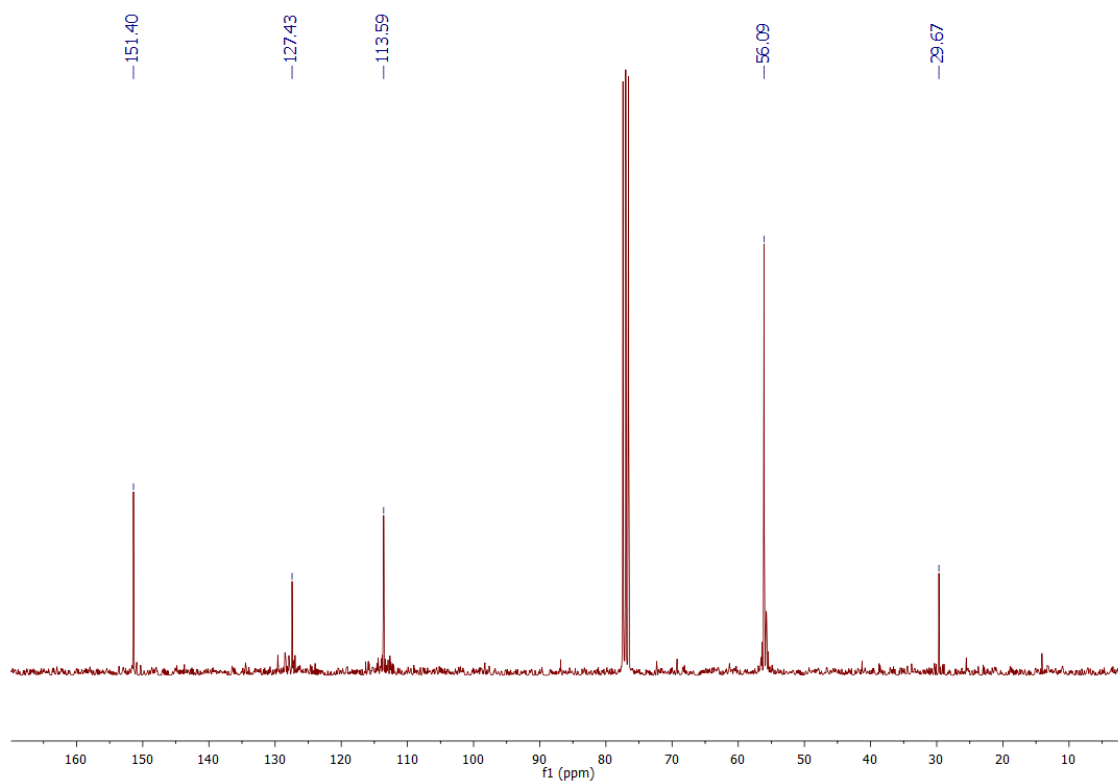
Figure 3.15 *¹³C NMR (400 MHz, CDCl₃, 298 K) of PMe[6].*
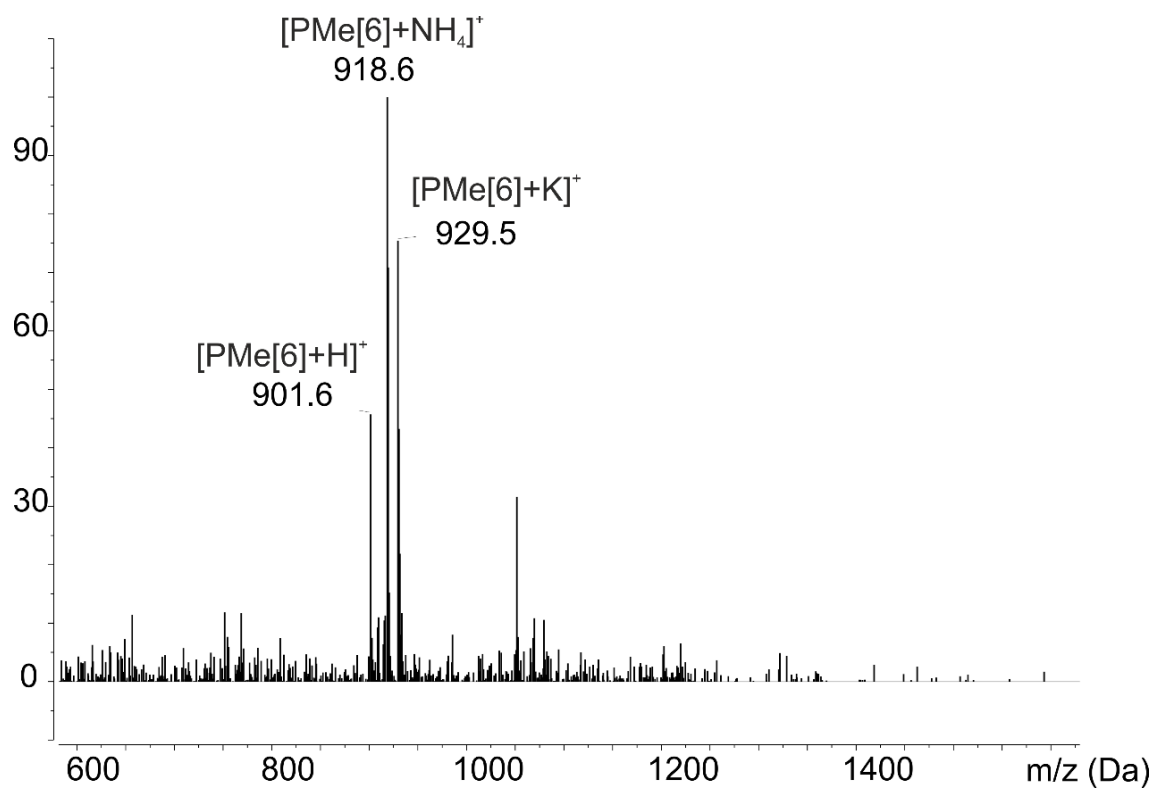
Figure 3.16 *ESI-MS spectrum of **PMe[6]**.*
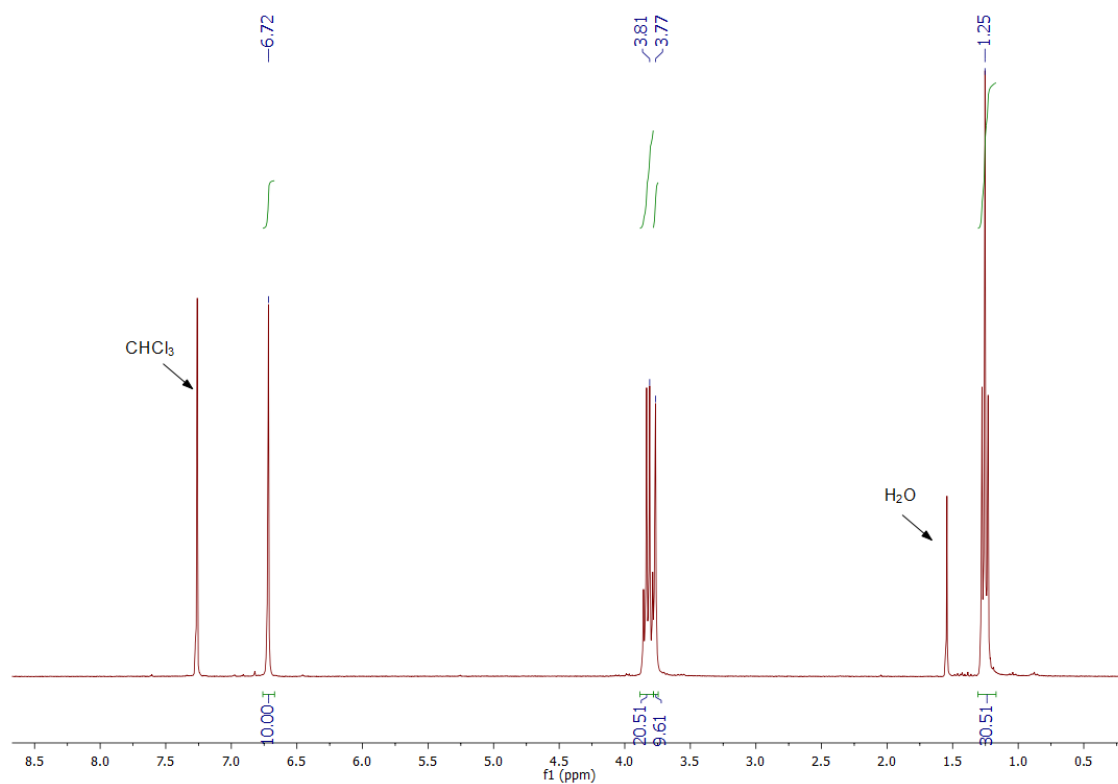
Figure 3.17 *¹H NMR (400 MHz, CDCl₃, 298 K) of **PEt[5]**.*
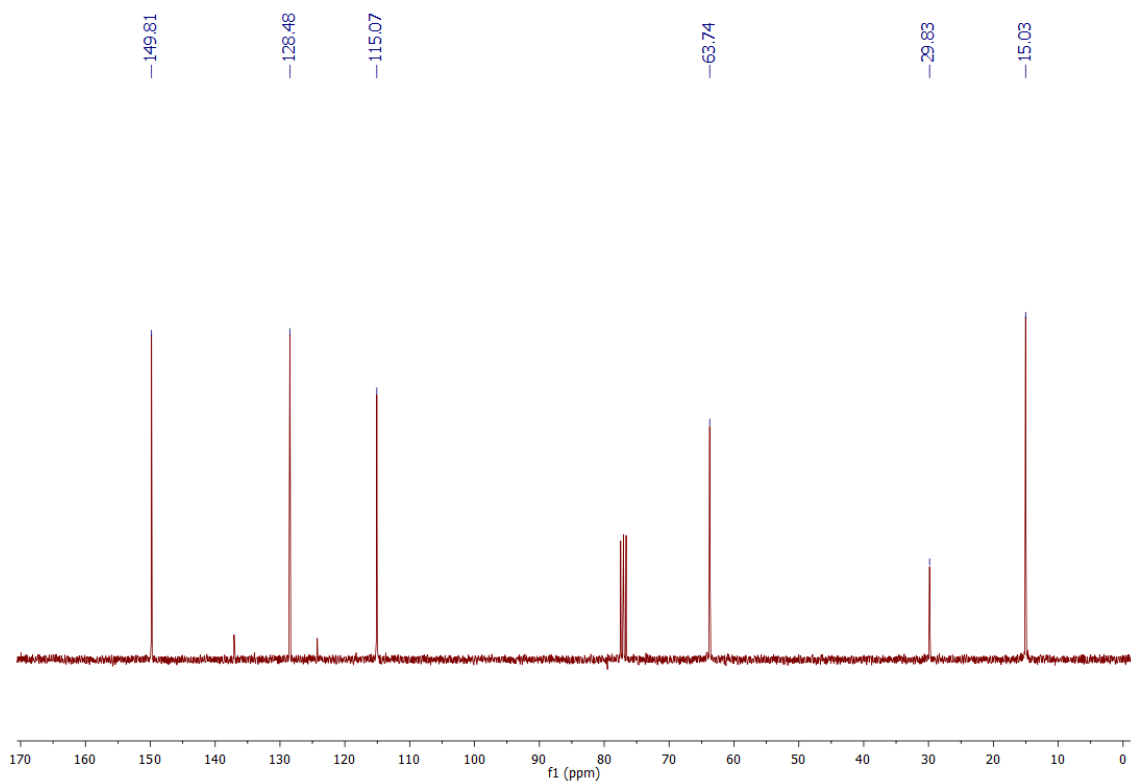
Figure 3.18 ^{13}C *NMR (400 MHz, CDCl₃, 298 K) of* **PEt[5]**.
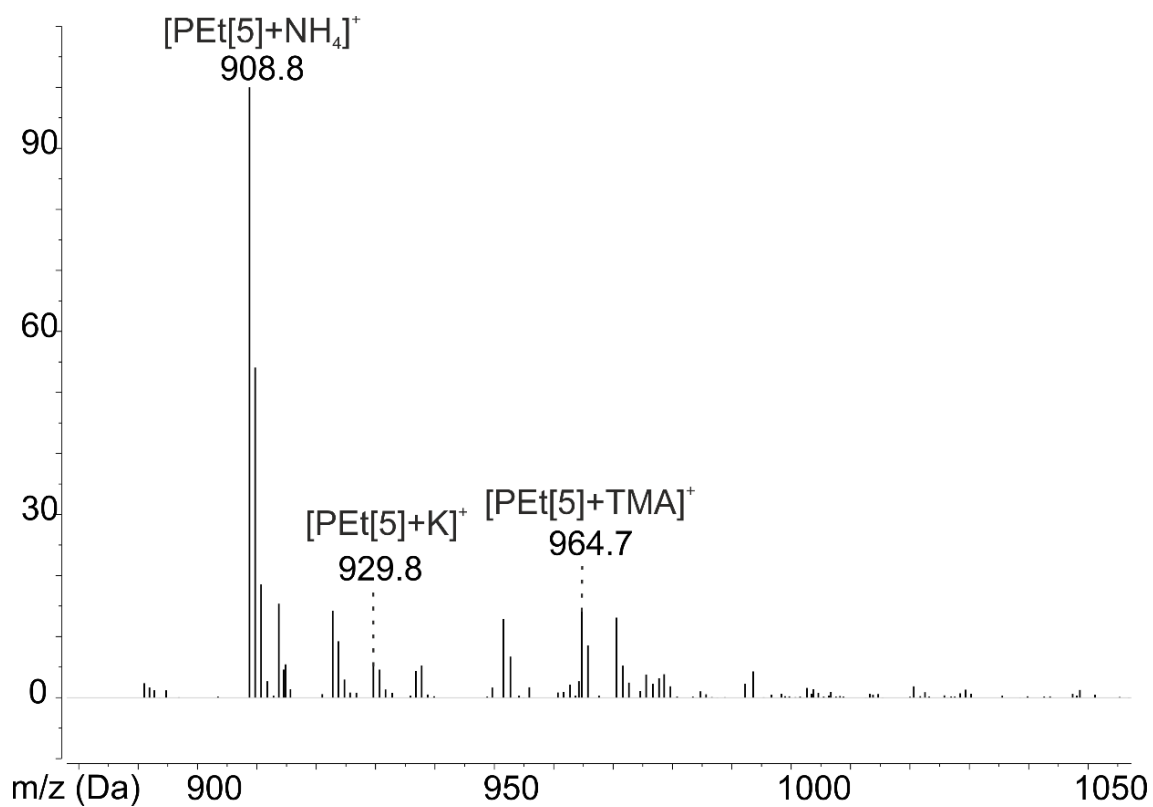
Figure 3.19 *ESI-MS spectrum of* **PEt[5]**.
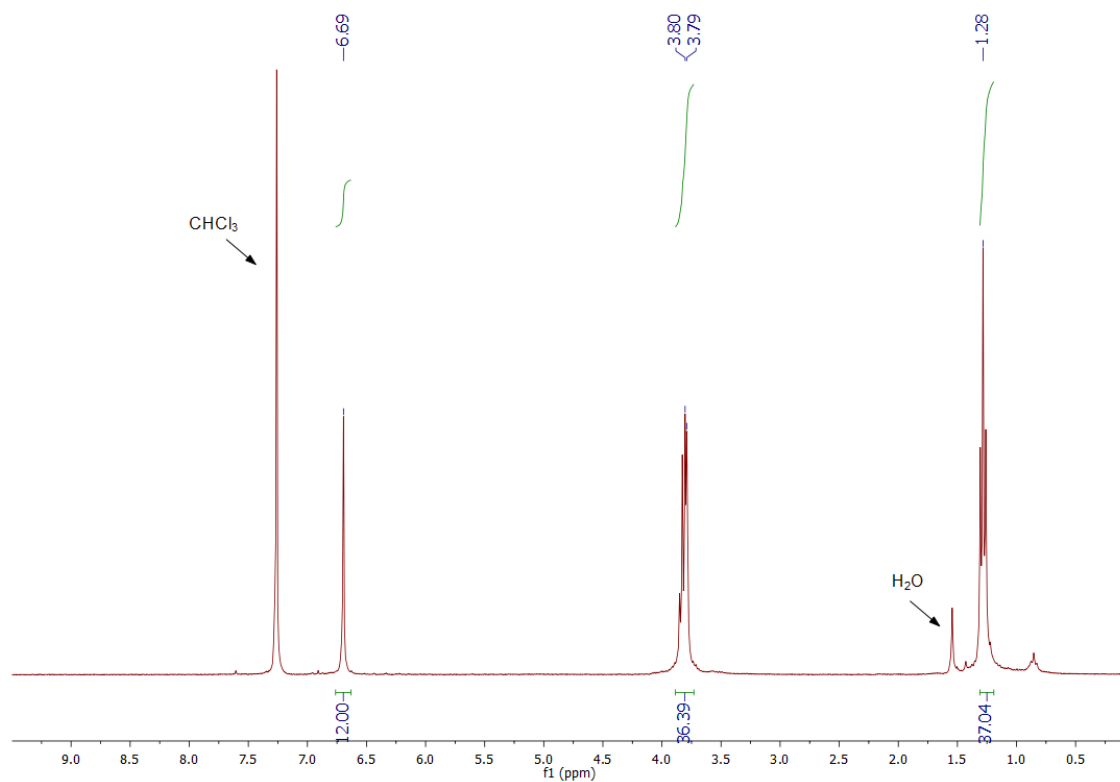
Figure 3.20 ^1H *NMR (400 MHz, CDCl$_3$, 298 K) of* **PEt[6]**.
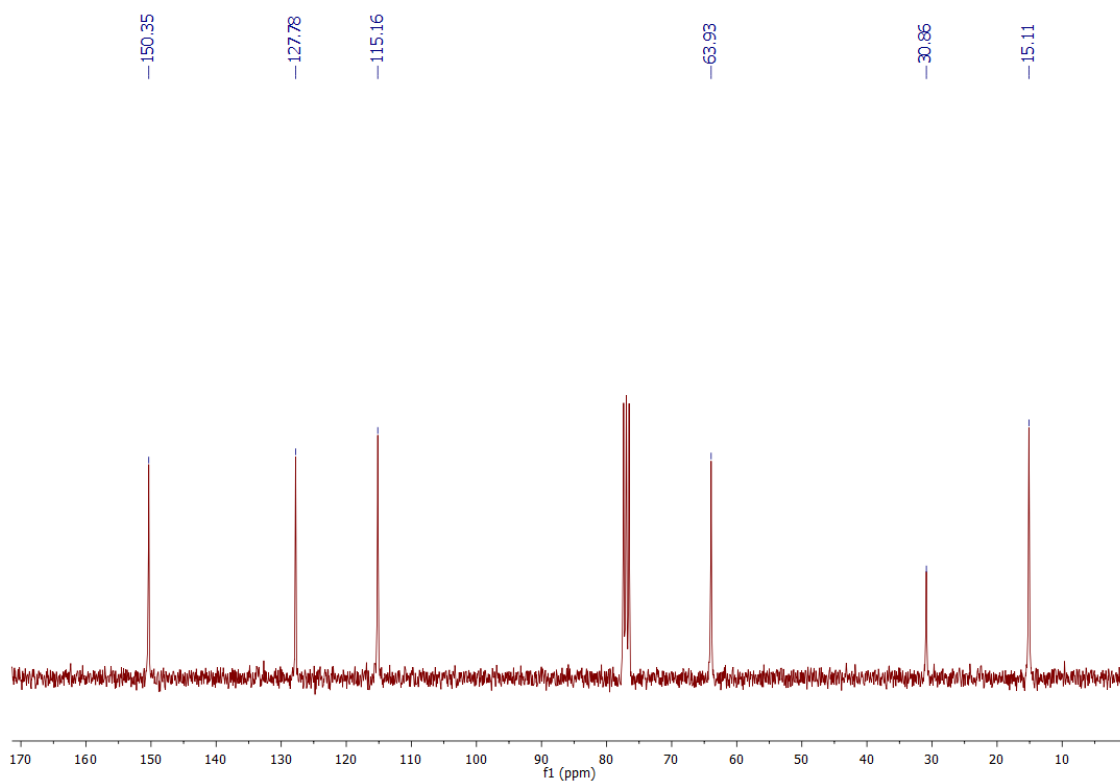
Figure 3.21 ^{13}C *NMR (400 MHz, CDCl$_3$, 298 K) of* **PEt[6]**.
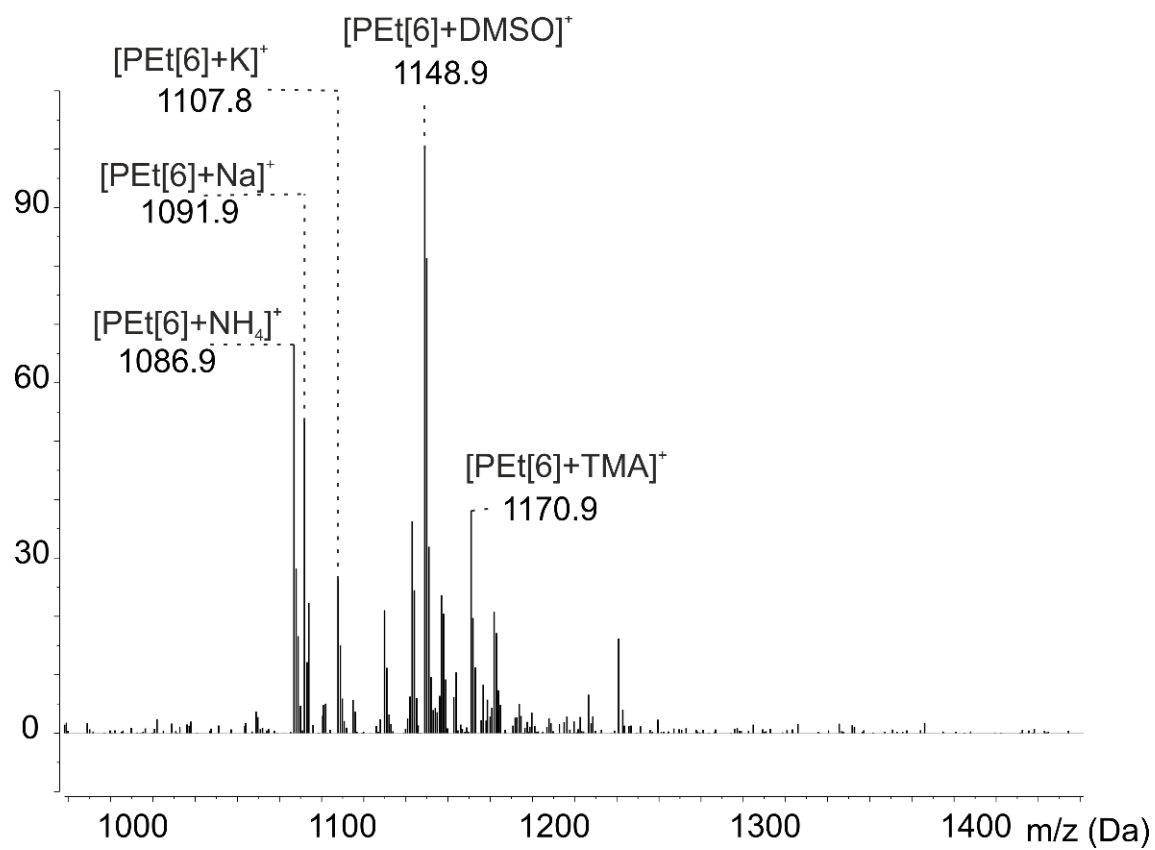
Figure 3.22 ESI-MS spectrum of **PEt[6]**.
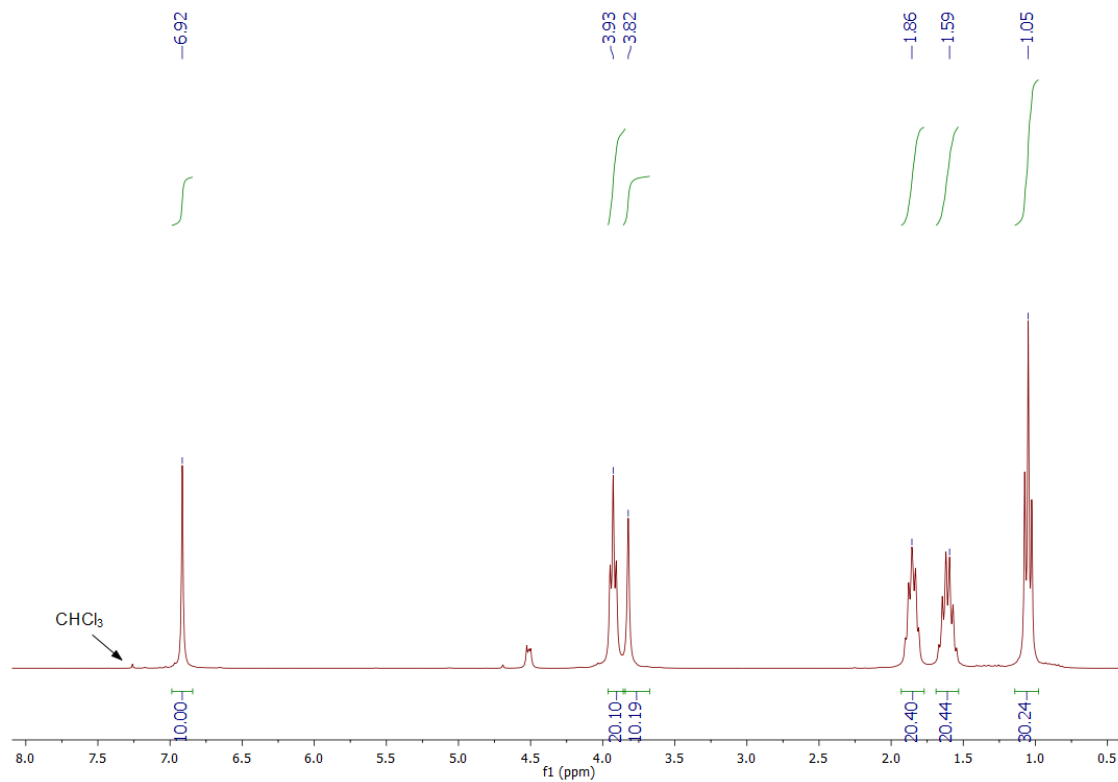
Figure 3.23 ^1H NMR (400 MHz, CDCl$_3$, 298 K) of **PBu[5]**.
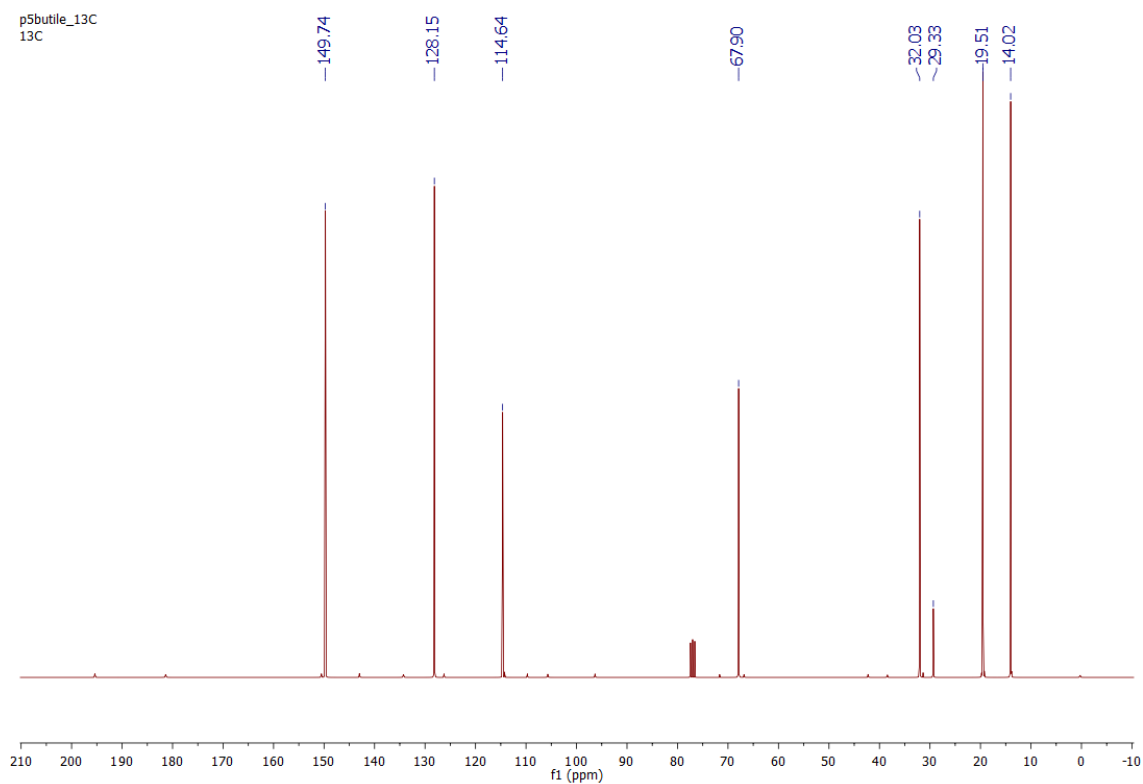
Figure 3.24 ^{13}C NMR (400 MHz, CDCl$_3$, 298 K) of **PBu[5]**.
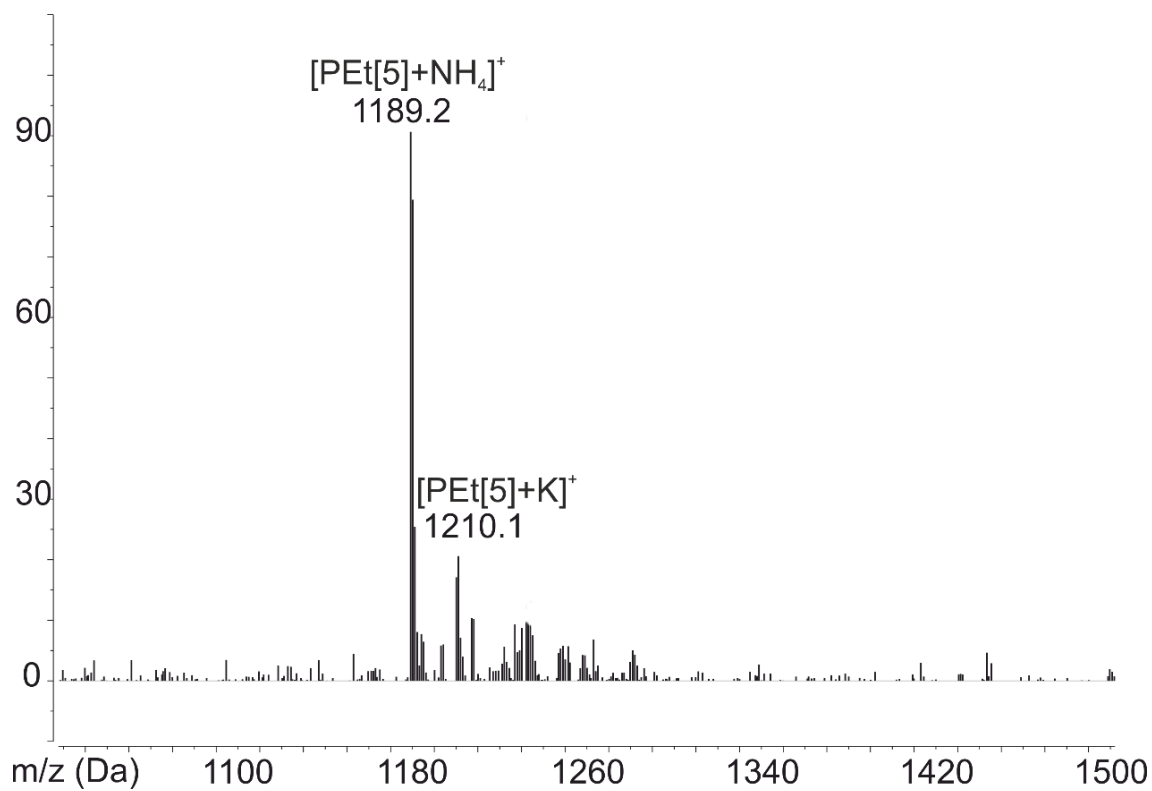
Figure 3.25 ESI-MS spectrum of **PBu[5]**.
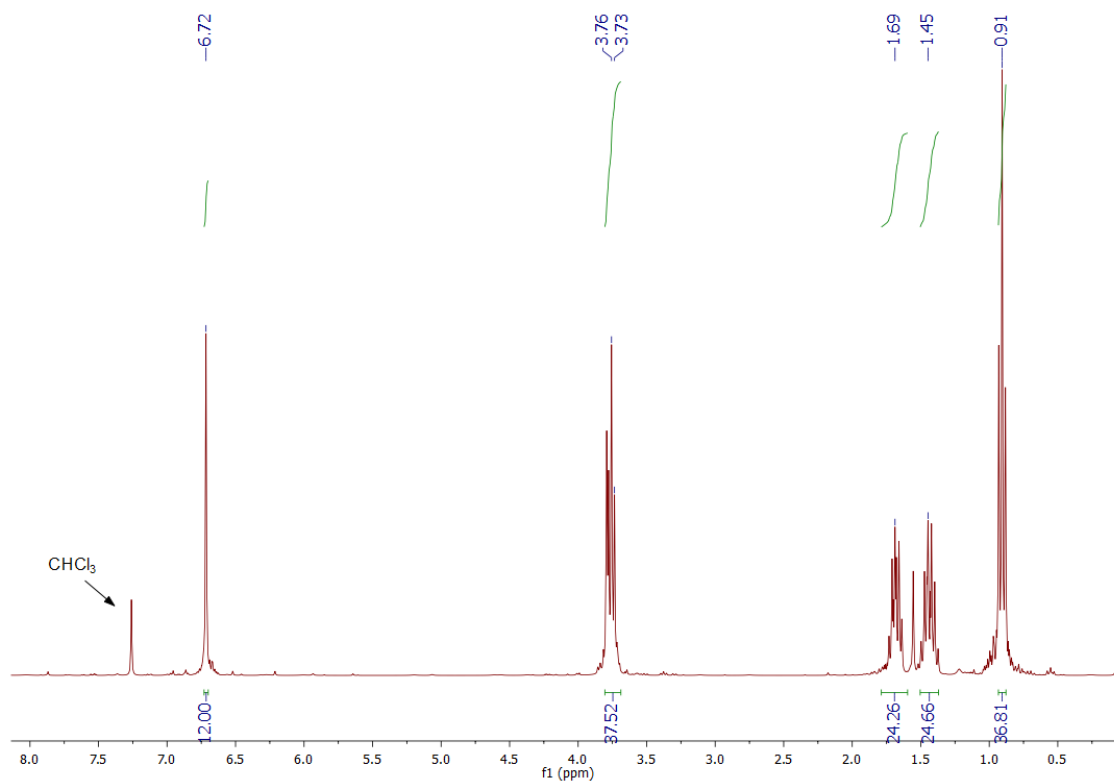
Figure 3.26 *¹H NMR (400 MHz, CDCl₃, 298 K) of **PBu[6]**.*
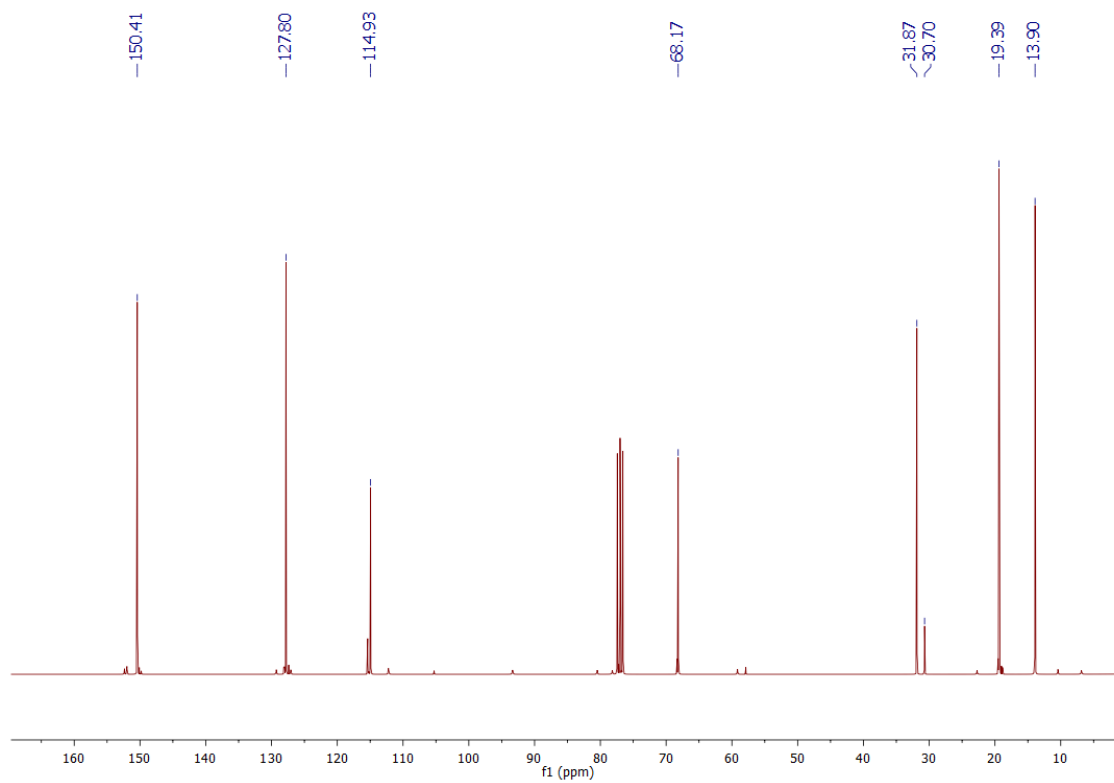
Figure 3.27 *¹³C NMR (400 MHz, CDCl₃, 298 K) of **PBu[6]**.*
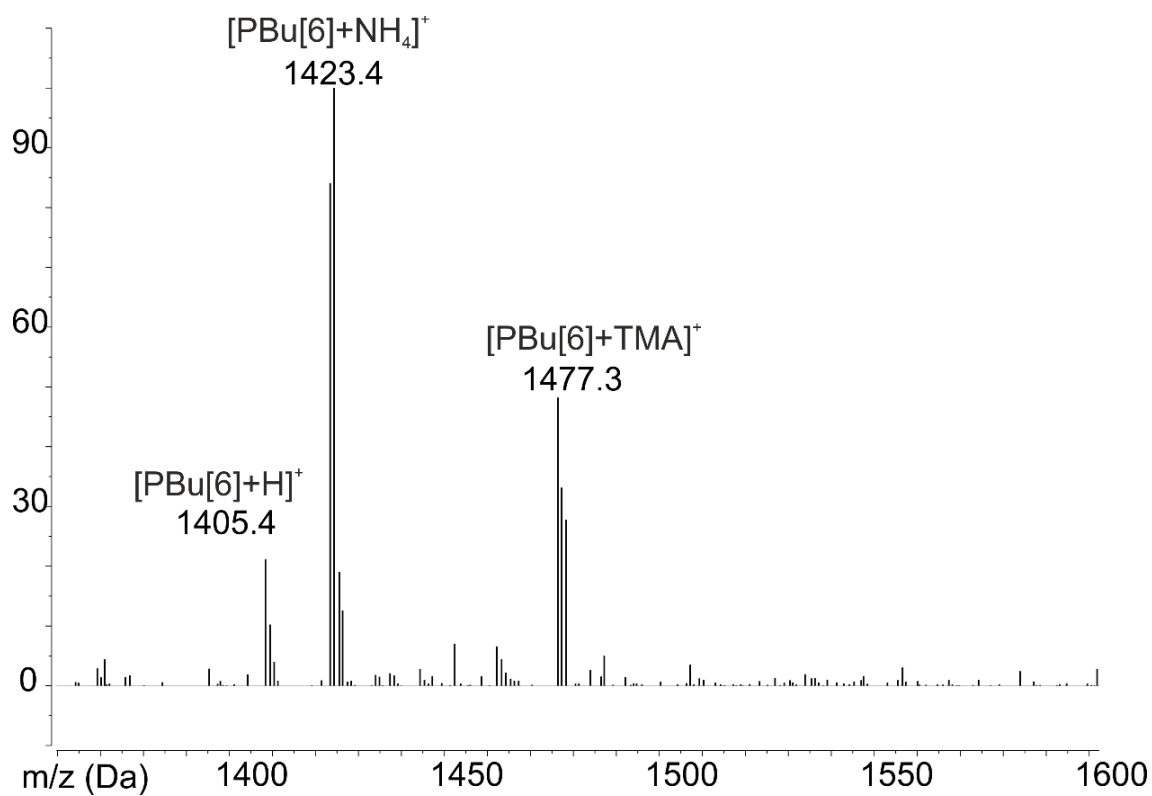
Figure 3.28 ESI-MS spectrum of **PBu[6]**.

3.4.4. Complexation Experiments

ESI-MS Spectra of Host-Guest complexes **PEt[5]@BmimPF₆**, **PEt[6]@COCP** and **PEt[6]@FECP**,
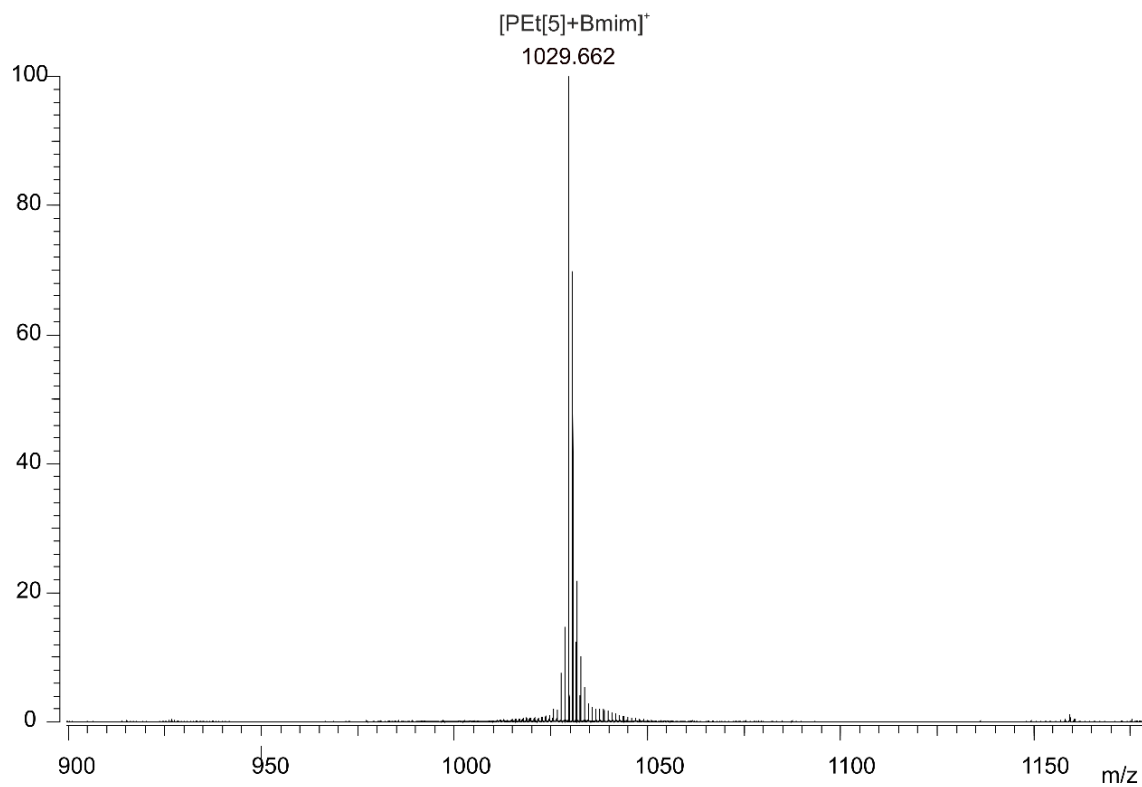
Figure 3.29 ESI-MS spectrum of **PEt[5]@BmimPF₆**, m/z 1029.7.
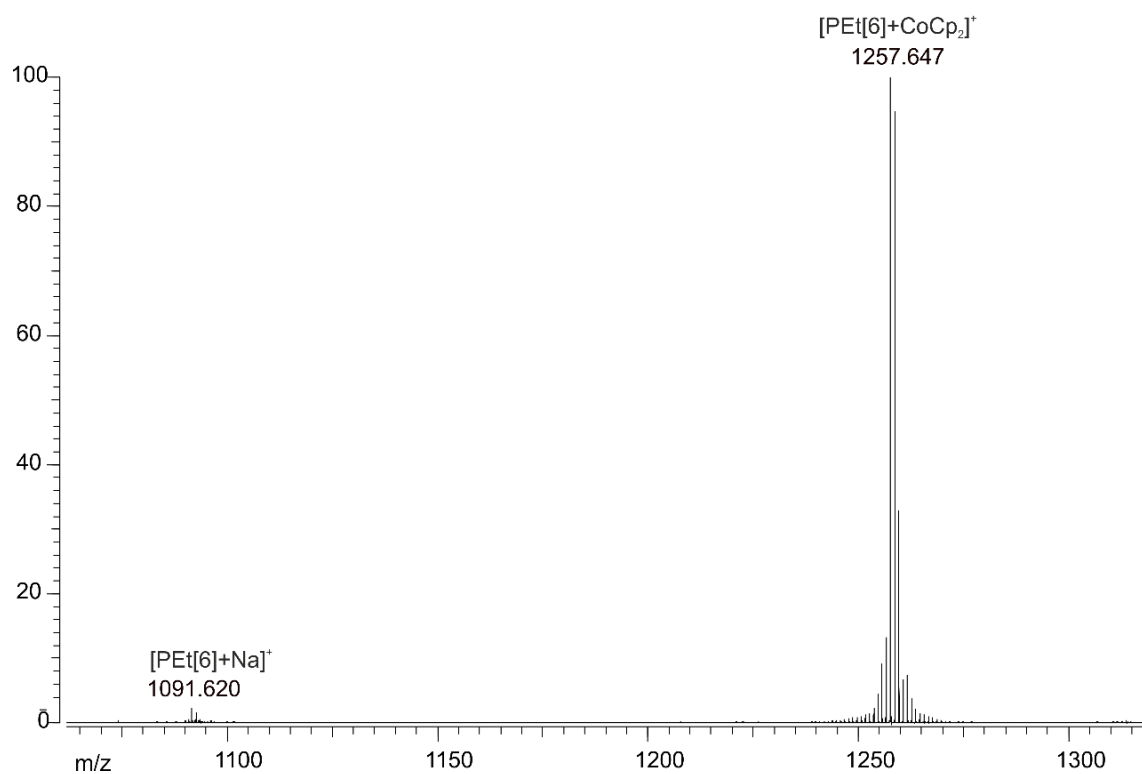
Figure 3.30 ESI-MS spectrum of **PEt[6]@COCP**, m/z 1257.6.
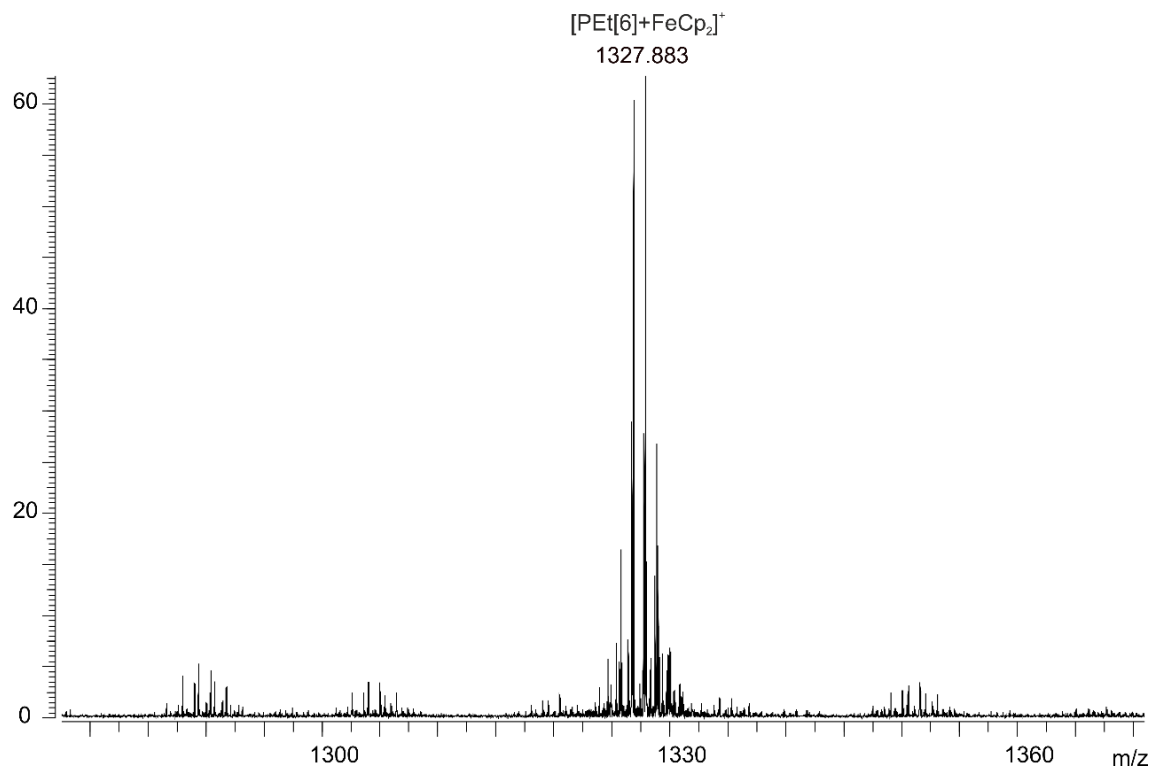
Figure 3.31 ESI-MS spectrum of *PEt[6]@FECP*, m/z 1326.9.

1H NMR Spectra of the complexation experiments *PEt[6]@BmimPF₆*, *PEt[5]@COCP and PEt[5]@FECP*,
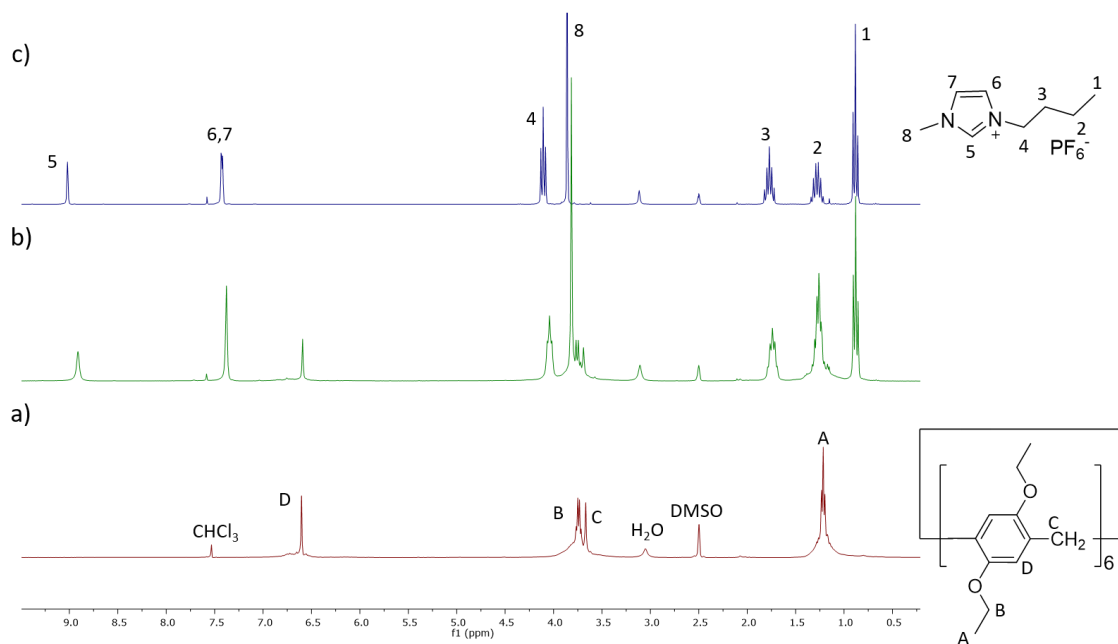
Figure 3.32 ¹H NMR spectra (300 MHz, 298 K) of a) *[PEt[6]]=2mM*, b) *[BmimPF₆]=6[PEt[6]]=12mM, c)[BmimPF₆]=2mM in CDCl₃/DMSO-d₆ (5:1, v/v)*
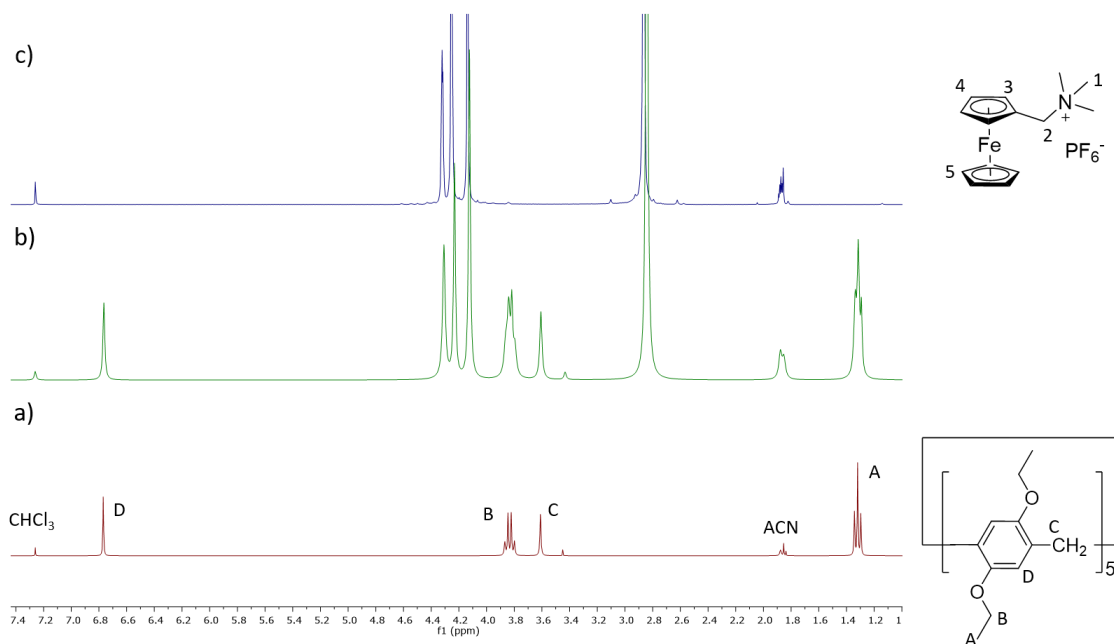
Figure 3.33 ¹H NMR spectra (300 MHz, 298 K) of a) *[PEt[5]]=2mM*, b) *[FECP]=6[PEt[5]]=12mM, c)[FECP]=2mM in CDCl₃/ACN-d₃ (5:1, v/v).*
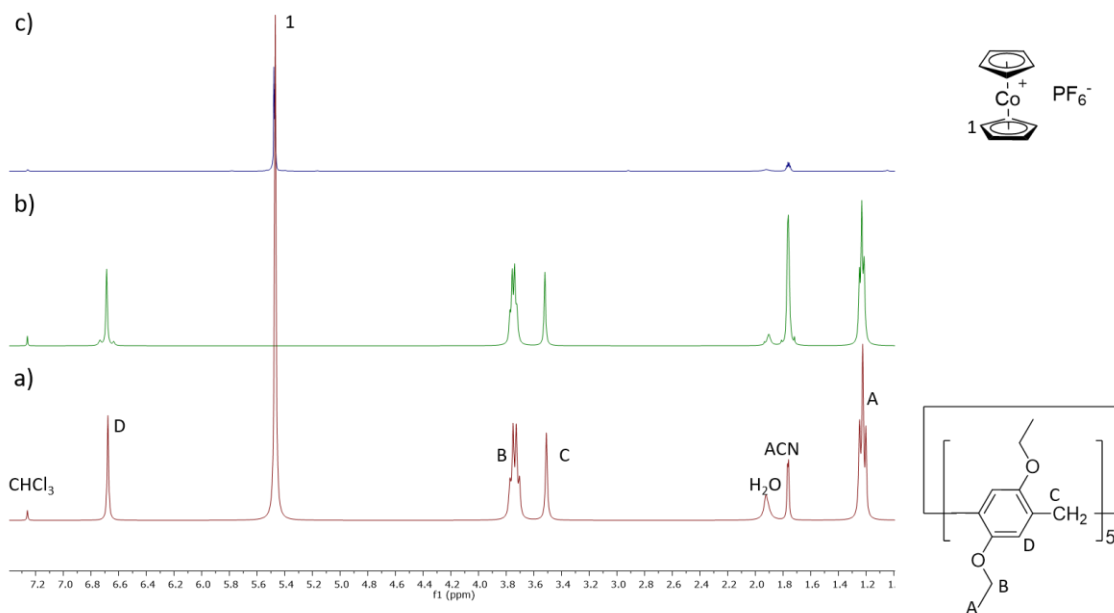
Figure 3.34 ¹H NMR spectra (300 MHz, 298 K) of a) *[PEt[5]]=2mM*, b) *[COCP]=6[PEt[5]]=12mM, c)[COCP]=2mM in CDCl₃/ACN-d₃ (5:3, v/v).*
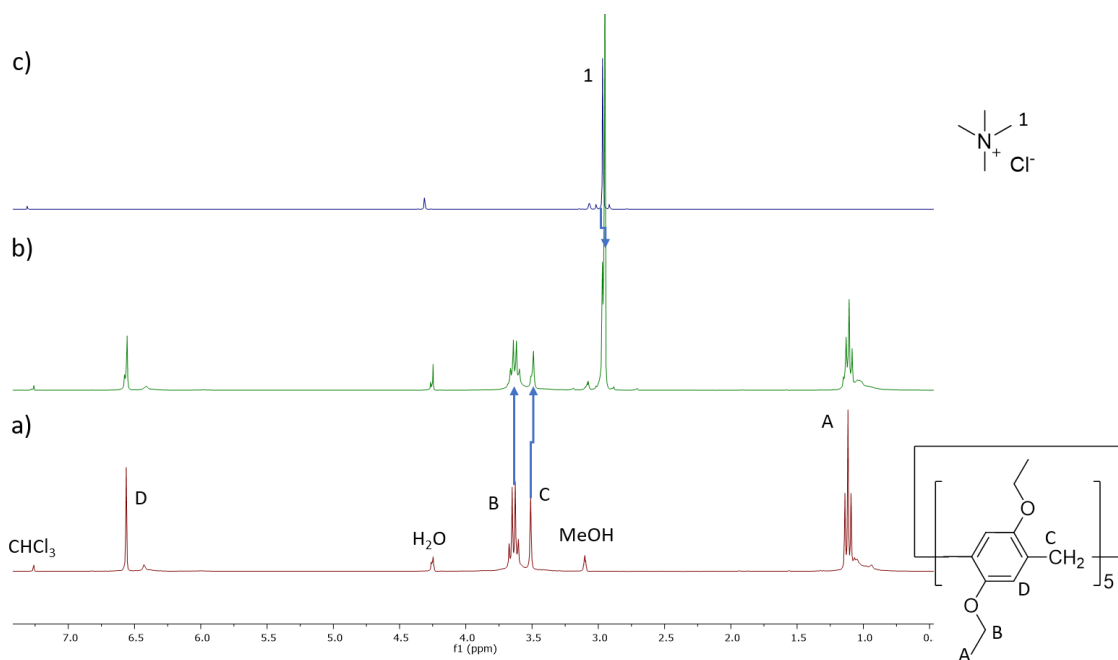
Figure 3.35 ^1H *NMR spectra (300 MHz, 298 K) of a) **[PEt[5]]**=2mM, b) **[TMAC]**=6**[PEt[5]]**=12mM, c)**[TMAC]**=2mM in CDCl₃/MeOH-d₄ (5:3, v/v).*
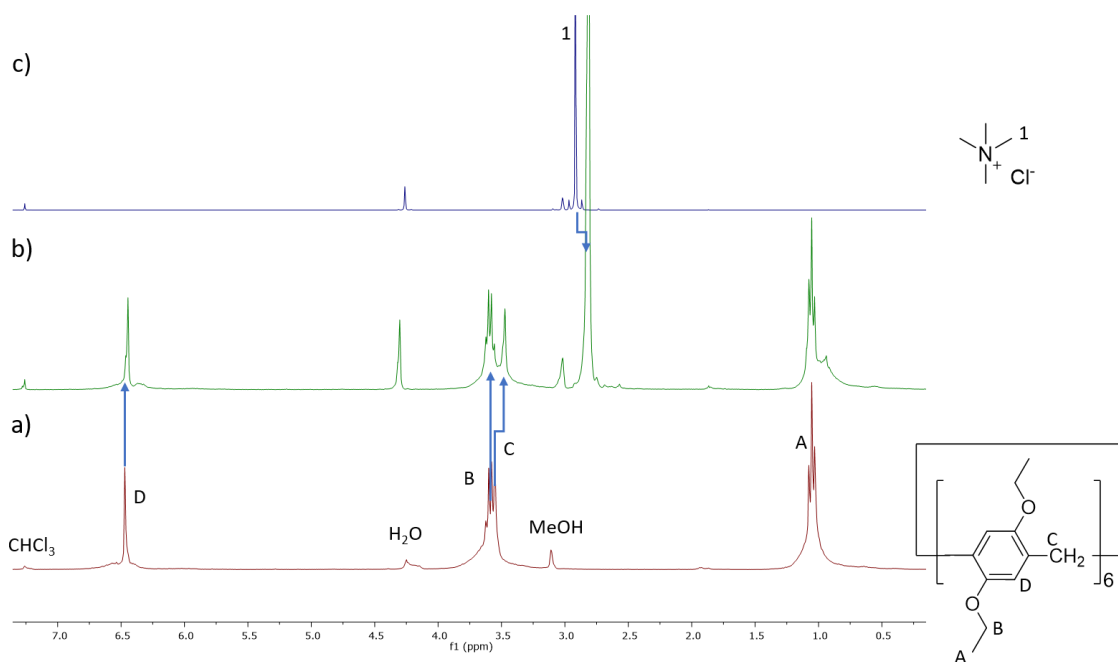
Figure 3.36 ^1H *NMR spectra (300 MHz, 298 K) of a) **[PEt[6]]**=2mM, b) **[TMAC]**=6**[PEt[6]]**=12mM, c)**[TMAC]**=2mM in CDCl₃/MeOH-d₄ (5:3, v/v).*

3.5. References

1. X. Lou, H. Chen, X. Jia and C. Li, *Chinese Journal of Chemistry*, 2015, **33**, 335-338.

2. D. Cao, Y. Kou, J. Liang, Z. Chen, L. Wang and H. Meier, *Angewandte Chemie International Edition*, 2009, **48**, 9721-9723.

3. C. Han, F. Ma, Z. Zhang, B. Xia, Y. Yu and F. Huang, *Organic Letters*, 2010, **12**, 4360-4363.

4. T. Ogoshi, K. Kitajima, T. Aoki, S. Fujinami, T.-a. Yamagishi and Y. Nakamoto, *The Journal of Organic Chemistry*, 2010, **75**, 3268-3273.

5. K. Wang, L.-L. Tan, D.-X. Chen, N. Song, G. Xi, S. X.-A. Zhang, C. Li and Y.-W. Yang, *Organic & Biomolecular Chemistry*, 2012, **10**, 9405-9409.

6. J. Cao, Y. Shang, B. Qi, X. Sun, L. Zhang, H. Liu, H. Zhang and X. Zhou, *RSC Advances*, 2015, **5**, 9993-9996.

7. D. Cao and H. Meier, *Synthesis*, 2015, **47**, 1041-1056.

8. T. Ogoshi, N. Ueshima, T. Akutsu, D. Yamafuji, T. Furuta, F. Sakakibara and T.-a. Yamagishi, *Chemical Communications*, 2014, **50**, 5774-5777.

9. H. Ke, C. Jiao, Y.-H. Qian, M.-J. Lin and J.-Z. Chen, *Chinese Journal of Chemistry*, 2015, **33**, 339-342.

10. T. Boinski and A. Szumna, *Tetrahedron*, 2012, **68**, 9419-9422.

11. G. W. Gokel, D. J. Cram, C. L. Liotta, H. P. Harris and F. L. Cook, *Organic Syntheses*, 1977, **57**, 30.

12. D. Wohrle and G. Meyer, *Kontakte (Darmstadt)*, 1985, **3**, 38.

13. D. B. Amabilino, P. R. Ashton, A. S. Reder, N. Spencer and J. F. Stoddart, *Angewandte Chemie International Edition in English*, 1994, **33**, 433-437.

14. J. Breitenbach, F. Ott and F. Vögtle, *Angewandte Chemie International Edition in English*, 1992, **31**, 307-308.

15. Y.-S. Wei, M. Zhang, P.-Q. Liao, R.-B. Lin, T.-Y. Li, G. Shao, J.-P. Zhang and X.-M. Chen, 2015, **6**, 8348.

16. M. H. Yap, K. L. Fow and G. Z. Chen, *Green Energy & Environment*, 2017, **2**, 218-245.

17. Y. Xie, D. Kocaefe, C. Chen and Y. Kocaefe, *Journal of Nanomaterials*, 2016, **2016**, 10.

18. S. Santra, D. S. Kopchuk, I. S. Kovalev, G. V. Zyryanov, A. Majee, V. N. Charushin and O. N. Chupakhin, *Green Chemistry*, 2016, **18**, 423-426.

19. W. Xia, X.-Y. Hu, Y. Chen, C. Lin and L. Wang, *Chemical Communications*, 2013, **49**, 5085-5087.

20. Z. Zhang, B. Xia, C. Han, Y. Yu and F. Huang, *Organic Letters*, 2010, **12**, 3285-3287.

21. H. Tao, D. Cao, L. Liu, Y. Kou, L. Wang and H. Meier, *Science China Chemistry*, 2012, **55**, 223-228.

22. A. M. Fernandes, M. A. A. Rocha, M. G. Freire, I. M. Marrucho, J. A. P. Coutinho and L. M. N. B. F. Santos, *The Journal of Physical Chemistry B*, 2011, **115**, 4033-4041.

23. J. K. Lindsay and C. R. Hauser, *The Journal of Organic Chemistry*, 1957, **22**, 355-358.

Insights into the Synthesis of Pillar[5]arene and its Conversion into Pillar[6]arene: Mechanistic Analysis through ESI-MS
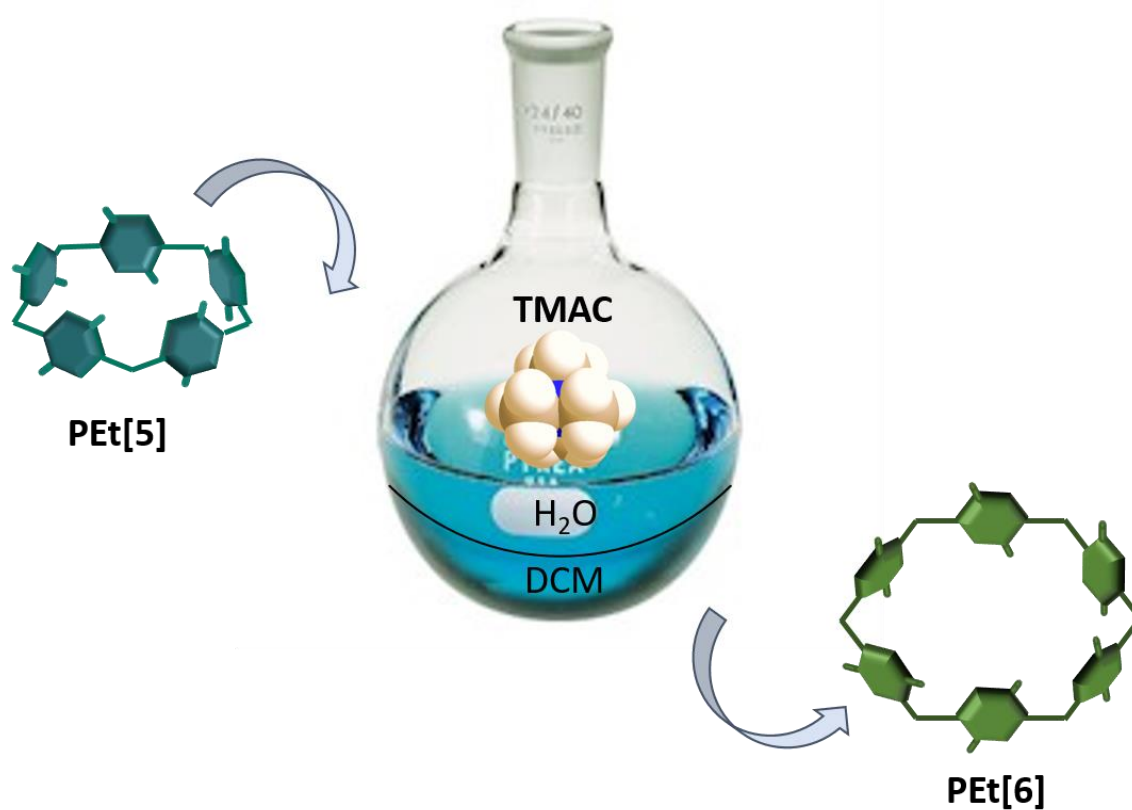
4.1. *Interconversion Between Pillar[n]arenes*

As well as in the synthesis of calix[n]arenes and cucurbit[n]urils, even in the case of pillar[n]arenes the formation of the smaller family member is particularly favored. Indeed, the cyclic pentamer **P[5]** was discovered for first by Ogoshi and collaborators, which initially introduced the symmetric **PMe[5]**[57] (22% yield) prepared in DCE with equimolar **DMB** and paraformaldehyde in the presence of the equimolar amount of BF_3OEt_2 as promoter. Using 3 equivalent of paraformaldehyde and reducing the reaction time to 3 minutes, the synthesis was further improved obtaining the same macrocycle in 71% yield.[106] Most recently, Szumna and Boinsky proposed a moisture insensitive air tolerant method, using of trifluoracetic acid as catalyst and leading to the formation of **P[5]** in 81% yield.[69]

Although **P[6]** was initially considered a secondary product in the synthesis of **P[5],** Meier and co-workers synthesized on purpose a mixture of pillar[n]arenes enriched in **PEt[6]**[67] using chlorinated dry solvents and $FeCl_3$ as a catalyst. Other synthetic procedures use other acids in stoichiometric and sub-stoichiometric amount as promoters, mimicking Meier's experimental conditions.[66,68,91] With a different approach, as previously described in Chapter 3, our group recently employed the same strategy with small cationic guests as templates to steer the synthesis toward the formation of dialkoxy substituted **P[6]**.[142]

Nierengarten and co-workers[86] described that the synthesis of pillararenes is characterized by an equilibrium between larger and smaller macrocycles demonstrating that the synthesis of **P[5]** and homologues occurs under Friedel–Crafts conditions and it is driven by dynamic covalent bond formation. In particular, it was shown that the dialkoxy **P[5]** is the thermodynamic product while the corresponding **P[6]** is the kinetic one.

Ogoshi's group described a procedure involving chlorocyclohexane (ClCyH) as a templating solvent to obtain a methylcyclohexyl substituted **P[6]** in 87% yield under thermodynamically controlled conditions. Furthermore, pillar[n]arenes

interconversion (Figure 4.1a) was carried out through the overcome of the kinetic barrier of the ring opening reaction by raising the temperature up to 80 °C, in particular employing DCE as template for the conversion of **P[6]** into **P[5]** or ClCyH as template for converting **P[5]** into **P[6]**.[83] Conversely larger ethoxy-substituted pillar[n]arenes like **PEt[n]s** (n=6-15) were obtained by the conversion of **PEt[5]** in chloroform in the presence of BF_3OEt_2 as catalysts at 50 °C, ensuring the ring-opening process under heating conditions (Figure 4.1b). Since chloroform could not act as templating solvent the reaction proceeded under kinetic control affording a mixture of enlarged homologues. [62]
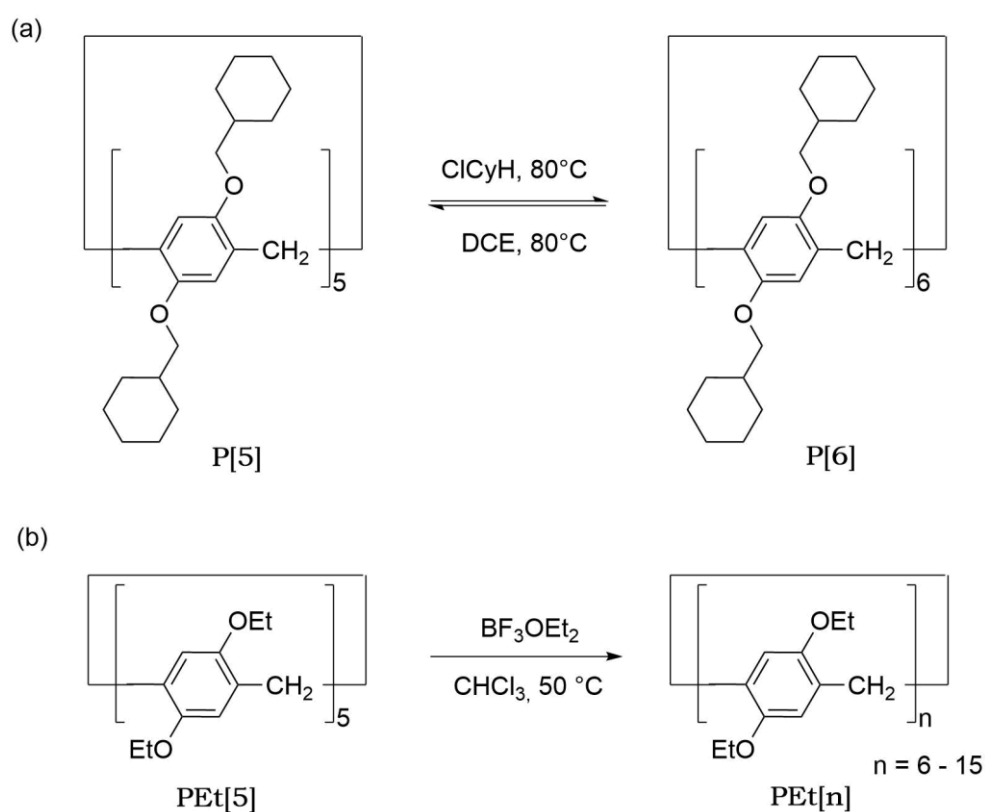
Figure 4.1 a) interconversion between *P[5]* and *P[6]* under thermodynamic control, b) conversion of *PEt[5]* into *PEt[n]* (n = 6-15) under kinetic control. Figure adapted by reference [83,62]

Taking inspiration from these works, in the present chapter we discuss **PEt[5]** and **PEt[6]** synthetic approaches mediated by $FeCl_3$ and **TMAC** in DCM by monitoring the reaction with ESI-MS analysis, and focusing also on the conversion of **P[5]** into **P[6]**, without using templating guests, at room temperature and in a aqueous-organic medium.

4.2. Results and Discussion

4.2.1. The Cyclization Reaction

In chapter 3 we reported the templated syntheses of both **P[5]** and **P[6]** with the preferential formation of the larger host in up to 38% yield in the presence of the best **P[6]** fitting guest **COCP**. Contextually in the synthesis starting from the monomer **DEB** with paraformaldehyde and FeCl$_3$, in DCM at room temperature (Scheme 4.1) templated by **TMAC**, we observed a change in the selectivity of the reaction. In fact the ratio between **PEt[6]** and **PEt[5]** yields increased from 1:1 to 2:1 according to the quenching step and the workup timing. We therefore focused our attention on the workup procedure and observed that the initial product distribution (right after addition of water, subsequent extraction of the crude product with DCM and purification by flash chromatography) was 24% for **PEt[5]** and 19% for **PEt[6]**. When the addition of water quenched the reaction and the mixture was stirred up to one week before product isolation, this distribution drastically changed, obtaining 16% for **PEt[5]** and 44% for **PEt[6]** (Figure 4.2).
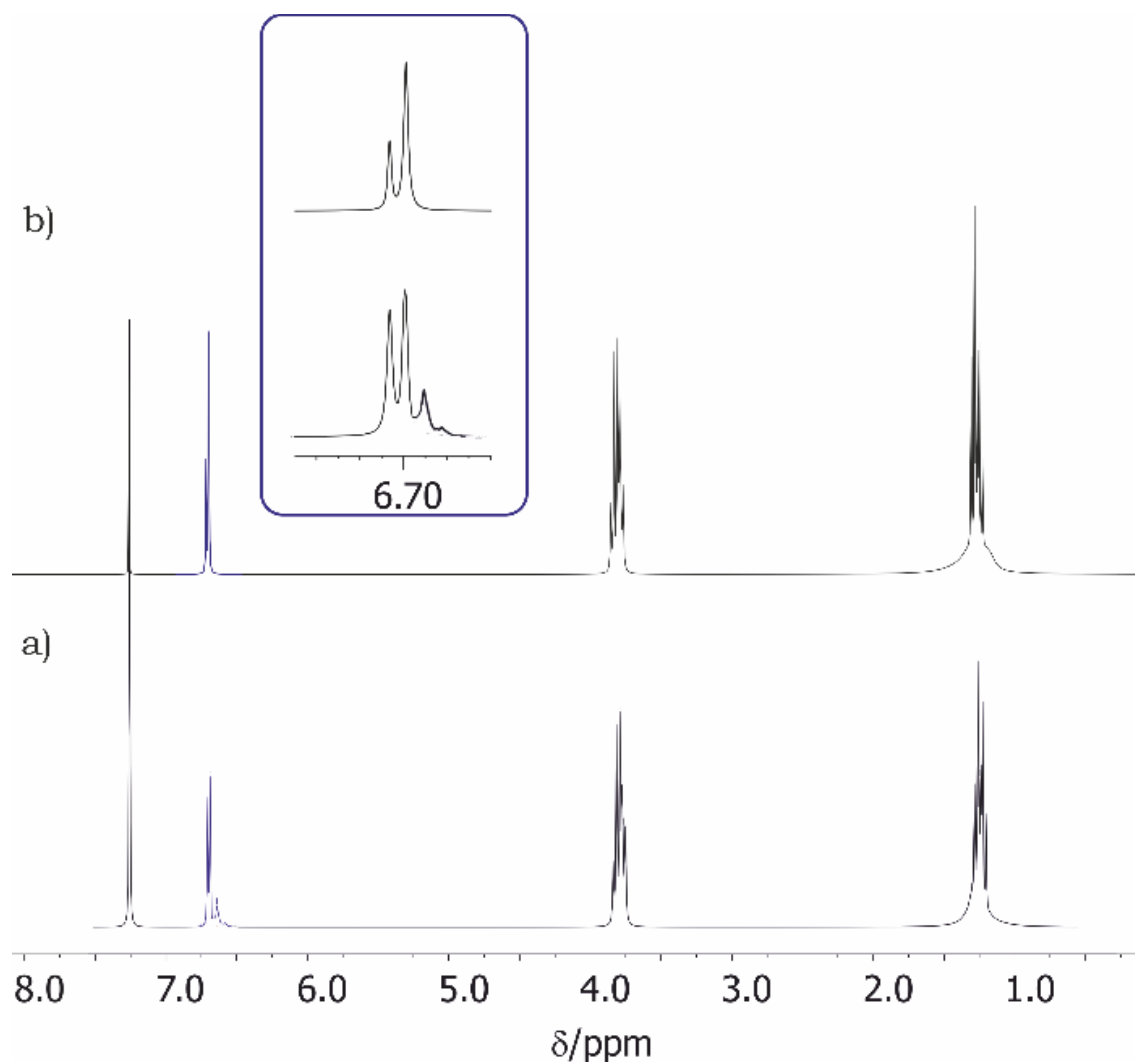
Figure 4.2 ^{1}H NMR spectra of the cyclization reaction of **DEB** in the presence of **TMAC** as template and FeCl₃ as catalysts in DCM at room temperature for 4h. a) purified right after addition of water and b) one week later.

This modification of the products distribution was clearly appreciable by the ^{1}H NMR spectra of the freshly and weekly elaborated crudes (Figure 4.2), where the intensities of **PEt[6]** aromatic peak (12 H) increased with respect to the resonance of **PEt[5]** aromatic signal (10 H). Further broad signal in the aromatic area, referred to the oligomeric side products (**OEt[n]**), visible in the ^{1}H NMR spectra of the reaction mixture before workup (Figure 4.2a), disappeared in the spectrum of the crude product after one week of stirring in the presence of water (Figure 4.2b). This behavior was ascribable to an ongoing equilibrium process occurring among the two macrocyclic species and the side oligomeric products present in the reaction mixture.

In order to better understand this unexpected change on the **PEt[6]/PEt[5]** yields ratio upon water quenching, we firstly focused our attention on the linear oligomers present in the reaction mixture. With the definition of oligomers we referred to all the species soluble in chloroform present in the reaction mixture after work-up and which were eluted as last fraction during the column chromatography. So far, they have been described in the literature as unavoidable side-products in most of **P[n]s** syntheses without any further structural investigation or characterization.
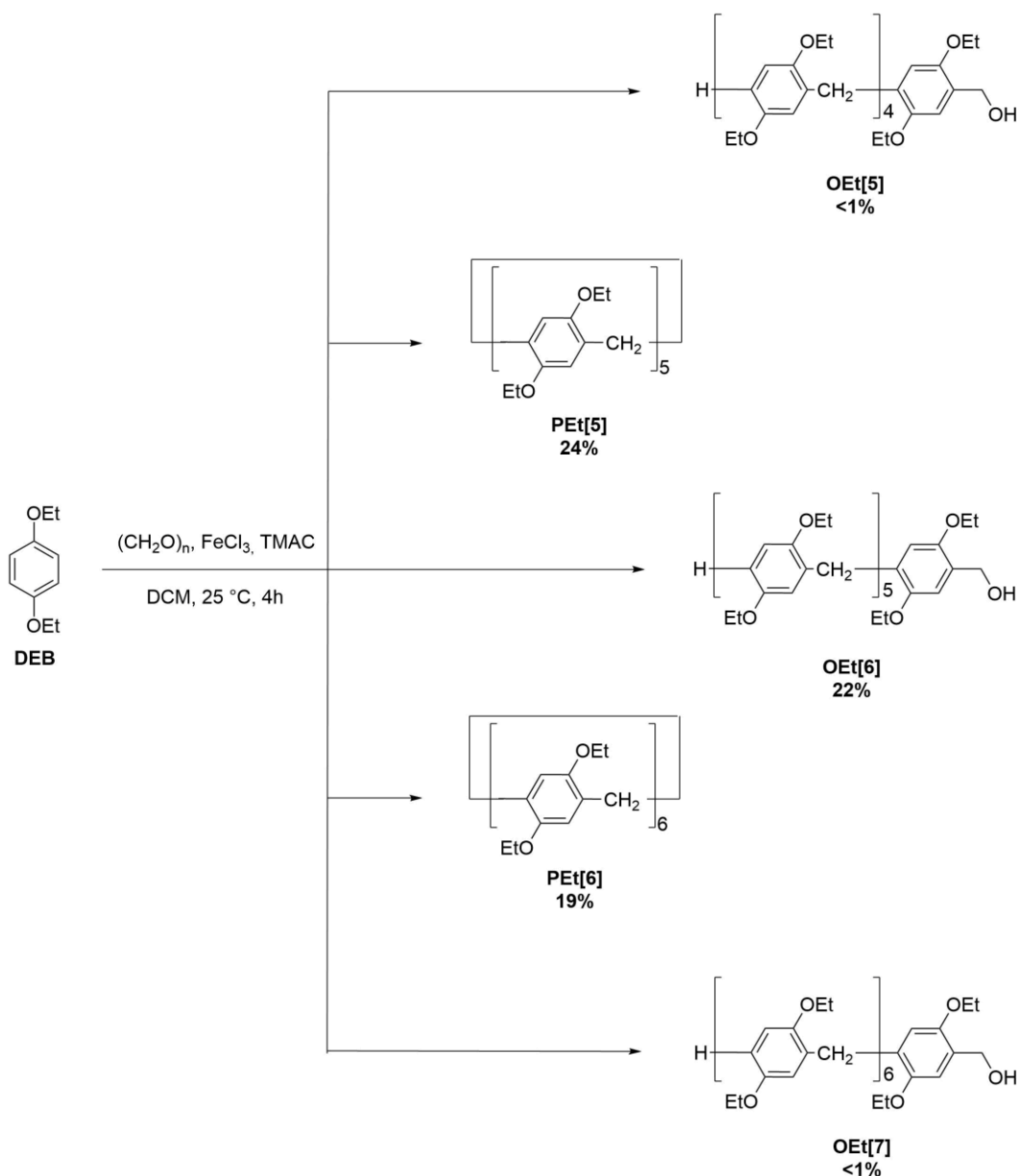
Scheme 4.1 *Synthesis of **PEt[n]** (n = 5,6) by reaction of **DEB** with paraformaldehyde in DCM, in the presence of **TMAC** and FeCl₃ and observation of the formation of the linear oligomers **OEt[n]** (n = 5,6,7) as reaction by-products.*

The ^{1}H NMR spectrum (Figure 4.3) showed one broad peak in the aromatic region concomitantly with other two resonances in the aliphatic region, almost coincident with the characteristic signals of both **PEt[5]** and **PEt[6]**. As expected, this suggested a similar structure but with lower degree of symmetry resulting in broad peaks instead of discrete multiplets. Unlike their counterparts (**P[n]s**), the oligomers were not detectable with soft ionization methods (ESI-MS), and therefore, their molecular weight and their exact composition were determined by EI-MS (Scheme 4.1). We purified by flash chromatography a freshly elaborated crude of reaction, isolating a mixture of three oligomers (23 % yield), whose most abundant component (a relative 95% of the oligomeric mixture) was the linear form of the cyclic hexamer **PEt[6]** with a terminal benzylic alcohol residue (**OEt[6]**) (Figure 4.3b).
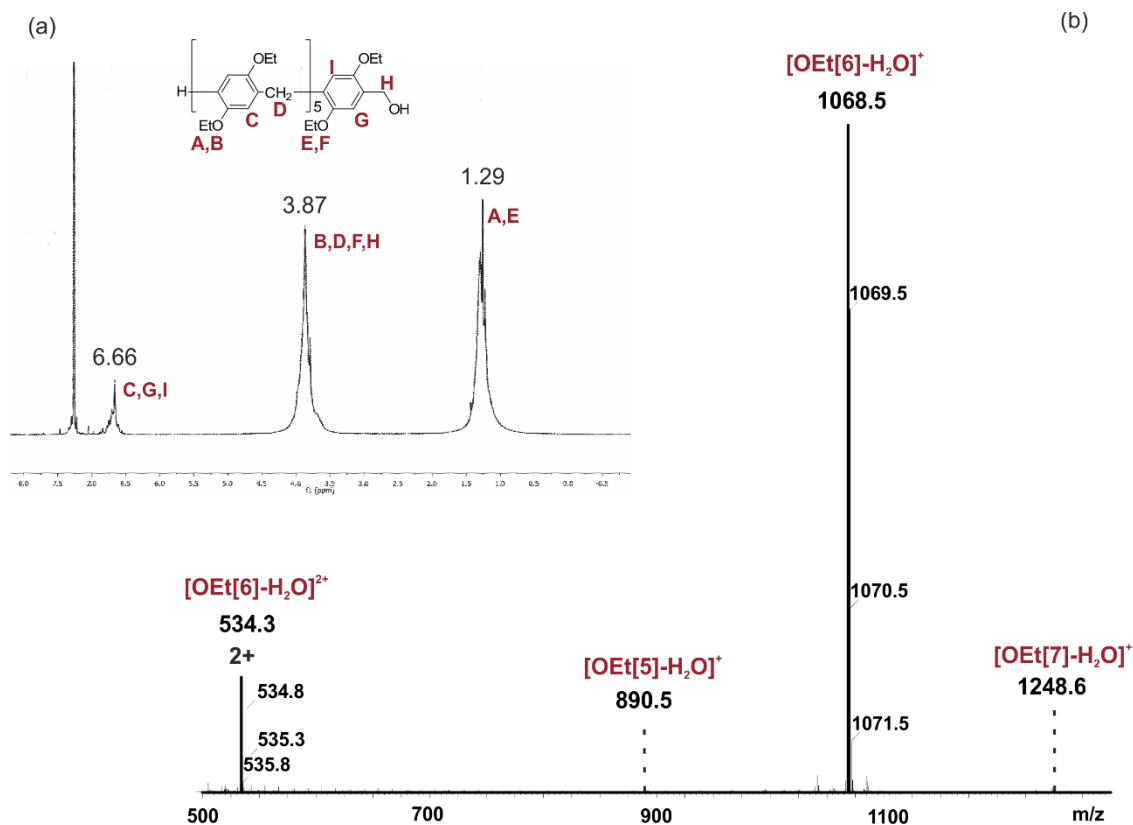
Figure 4.3 a) ^{1}H-NMR spectrum of **OEt[n]s** mixture (n = 5,6,7) and b)EI-MS spectrum of **OEt[n]s** mixture.

The identity of **OEt[6]** was confirmed by ^{1}H NMR and by EI-MS spectra. Through this ionization method **OEt[6]** produced a fragment *m/z* 1068.6, due to the loss of a water molecule, and a doubly charged peak *m/z* 534.3, resulting from

the same fragment. Although **OEt[6]** was the main oligomeric product, other less abundant oligomers were detectable and they were identified as the linear analogues of the cyclic pentamer **PEt[5]** and heptamer **PEt[7]** respectively, both with a terminal benzyl alcohol moiety (**OEt[5]** and **OEt[7]** respectively). The relative amount of the oligomers was determined comparing the intensities of the peaks in the EI-MS spectrum and calculating the equivalent value in moles from the weight of the corresponding fraction. The shorter **OEt[5]** and larger **OEt[7]** oligomers were present in amounts lower than 2% in the overall reaction mixture, allowing us not to consider them in the future studies and focusing mainly on **OEt[6]**. The oligomers reactivity was therefore studied taking into account **OEt[6]** as the starting material.
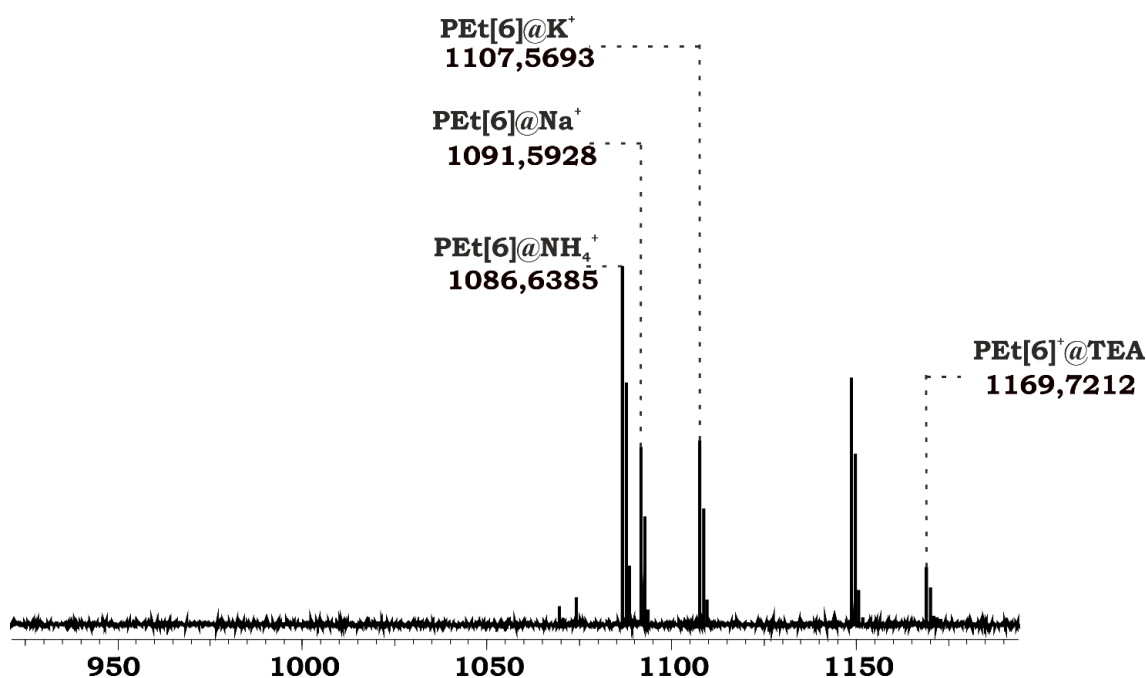
Figure 4.4 EI-MS spectrum of OEt[6] conversion into PEt[6] after 1 week, with FeCl₃ as catalysts and TMAC as template, in DCM/H₂O at 25 °C

After purification of the oligomer **OEt[6]** we studied its reactivity, again through MS spectroscopy, in the same reaction conditions used in the **TMAC** templated syntheses of **PEt[n]s**, with a close attention to its conversion into the bigger hexamer **PEt[6]**. **OEt[6]** was combined with paraformaldehyde, $FeCl_3$ and **TMAC** in a biphasic solution of dichloromethane and water at room temperature. The reaction was then stirred for four days leading to the exclusively formation of **PEt[6]** in 56% isolated yield. The reaction outcome was unambiguously

97

confirmed by the recorded ESI-MS spectrum (Figure 4.4) in which peaks at m/z 1086.64, attributed to the complex **PEt[6]@NH$_4^+$**, m/z 1091.59, attributed to the complex **PEt[6]@Na$^+$**, and m/z 1107.57, attributed to the complex **PEt[6]@K$^+$**, were detected, while peaks at m/z 891.5, 908.5, 913.5, 929.5, ascribable to the analogue **PEt[5]** complexes, were not present.
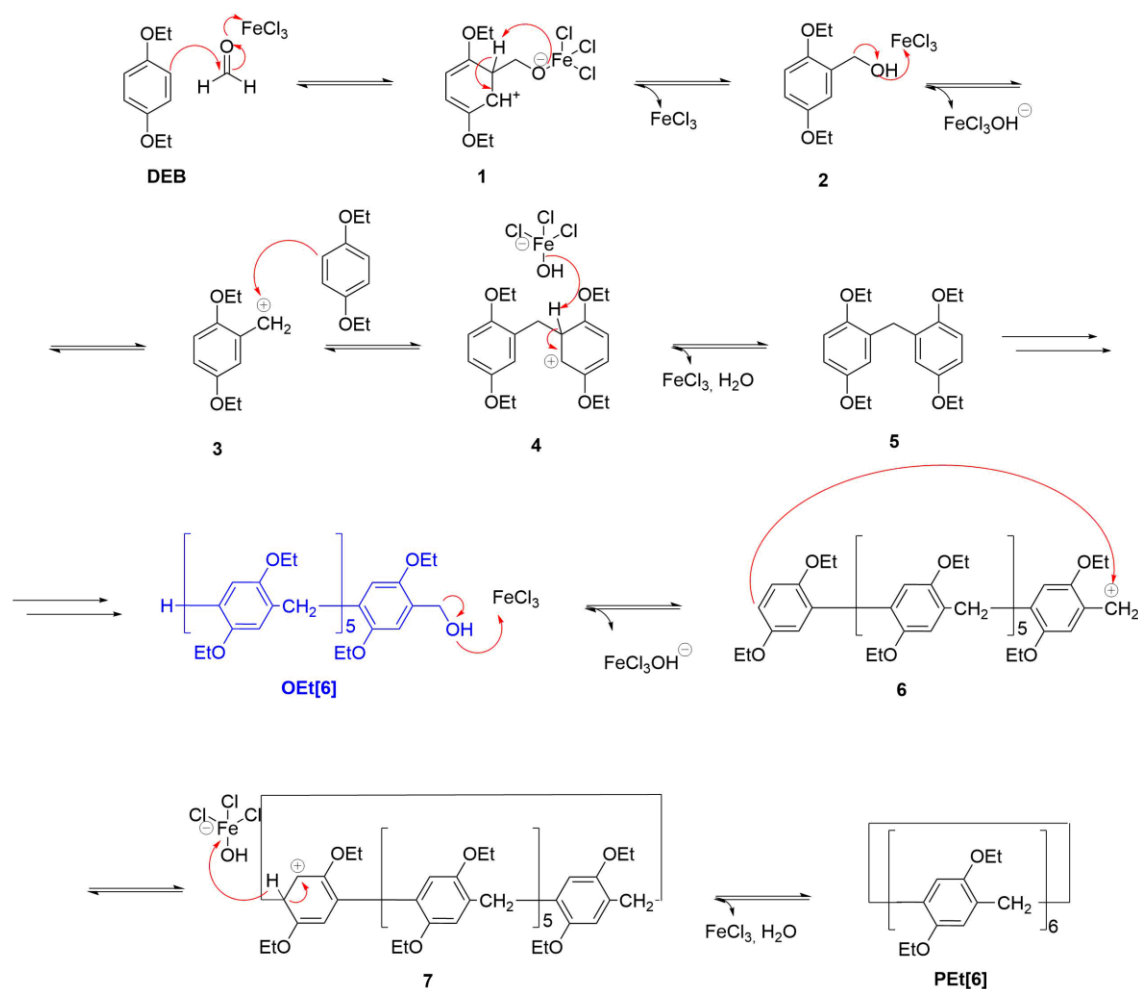
Scheme 4.2 *Cyclization mechanism under Friedel Craft conditions with* **OEt[6]** *enlightened in blue.*

On the basis of these observation and the mechanistic studies already present in the literature (Scheme 4.2), we performed some control experiments to verify the role of the template **TMAC**, the catalysts and the methylene source usually involved in the cyclization reaction under study. In order to investigate the influence of all the chemical species involved on the oligomers conversion, **OEt[6]** was either combined with all of them or just with FeCl$_3$ and **TMAC** together or separately (Table 4.1). Since **OEt[6]** had already the right number of

carbon atoms and was identical to the precursor of the benzylic intermediate **6** in **PEt[6]** synthesis (Scheme 4.2), paraformaldehyde was not necessary to complete the cyclization (Table 1, entry 1). The final yields of **PEt[6]** were strongly dependent on both **TMAC** and $FeCl_3$, and in particular the presence of the template rather than the catalyst showed a larger influence on the synthesis of **PEt[6]**. The hexameric macrocycle was obtained in 55% yield when both **TMAC** and $FeCl_3$ were present in the reaction mixture (Table 1, entry 2), while when either $FeCl_3$ (Table 1, entry 3) or **TMAC** (Table 1, entry 4) were used, **PEt[6]** was obtained in 24% and 32% isolated yield, respectively.

Table 4.1 *Synthesis of **PEt[6]** in DCM/water at 25 °C for 1 week, in the absence/presence of paraformaldehyde, $FeCl_3$ and **TMAC***

#	Paraformaldehyde	FeCl₃	TMAC	Isolated Yield (%)
1	✓	✓	✓	55
2	-	✓	✓	55
3	-	✓	-	24
4	-	-	✓	32

In the presence of the tetramethylammonium cation the reaction did not reach a conversion as high as when in the presence of $FeCl_3$ because in this case the cyclization was not acid catalyzed and occurred only by the template effect of **TMAC**. The experiment performed with $FeCl_3$ and without **TMAC**, gave a similar result with 24% isolated yield of **PEt[6]**. In this case the catalyst was sufficient to ensure the closure of the cyclic hexamer, as depicted in Scheme 4.2, promoting a sort of pre-organization through the interaction between the cation Fe^{3+} and the oxygen atoms on the oligomer. Nevertheless, the presence of an actual template (presumably acting as a very mild template itself) was more effective than just the catalyst to ensure the cyclization into **PEt[6]**..

These experiments underline a previously underestimated role of the oligomers in the formation of pillararenes, extending their role from undesired by-products to fundamental intermediate in the synthesis of **PEt[6]**.

4.2.2. *Conversion of PEt[5] into PEt[6]*

The synthesis showed in Scheme 4.1 afforded **PEt[6]** in overall 13% yield from the conversion of **OEt[6]**. This amount is not enough to fully justify the 44% yield of the cyclic hexamer obtained after prolonging the quenching procedure up to one week. As a consequence the larger amount of **PEt[6]** experimentally observed should come from other sources alternative to the direct synthesis from **DEB** and the conversion of **OEt[6]**. From this observation, we focused our attention on the other potential source of monomeric units present in the mixture, i.e. **PEt[5]** studying its reactivity in the presence of **TMAC**, $FeCl_3$ and paraformaldehyde in a biphasic solution of dichloromethane and water (Scheme 4.3). The experimental evaluation of the factors affecting the conversion of **PEt[5]** into **PEt[6]** was performed analyzing the crude reaction mixture by ESI-MS and calculating **PEt[6]/PEt[5]** ratio by sum of the intensities of the corresponding pillararene peaks. In some cases **PEt[6]** was also isolated by prep-TLC confirming the yield calculated by ESI-MS. After 24 h of stirring in the biphasic solution, we observed the formation of a detectable amount of **PEt[6]** when all the reactive chemical species were involved, that, after one week, reached a non negligible 8% yield (Figure 4.5).
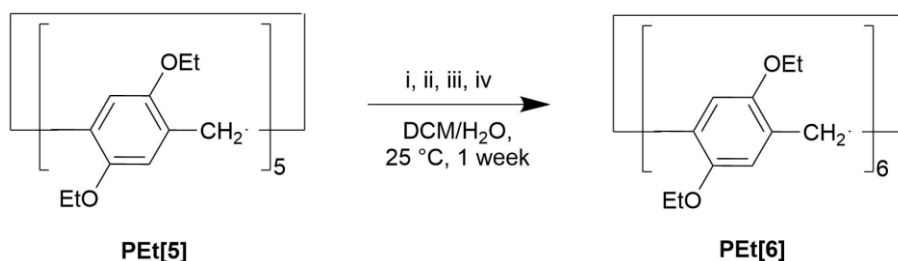
Scheme 4.3 *Conversion of* **PEt[5]** *with i) paraformaldehyde, $FeCl_3$ and* **TMAC** *leading to* **PEt[6]** *in 8% yield, ii) $FeCl_3$ and* **TMAC** *leading to* **PEt[6]** *in 8% yield, iii) $FeCl_3$ leading to* **PEt[6]** *in less than 1% yield, iv)* **TMAC** *leading to* **PEt[6]** *in less than 1% yield.*

a)

b)
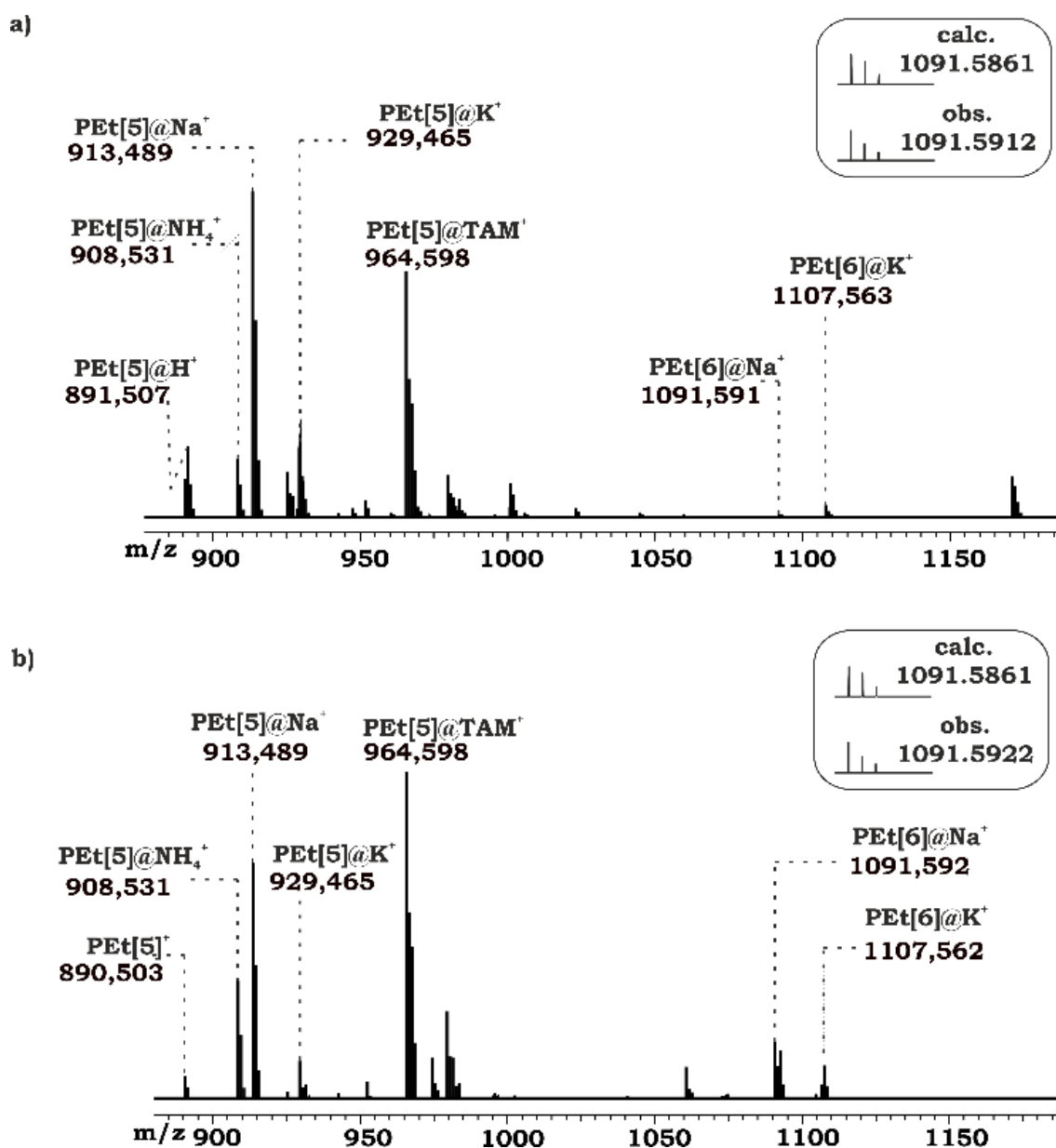
Figure 4.5 ESI-FTICR-MS spectra of *PEt[5]* conversion into *PEt[6]* in the presence of FeCl₃ and *TMAC*, a) after one day, b) after four days of stirring. In both spectra are reported the calculated and experimental isotopic distribution for the complex *PEt[6]@Na⁺*.

Stable adducts with common MS background ions, such as NH_4^+, Na^+ and K^+, could be observed for both pillararenes, as well as other small cations present in the reaction mixture, such as tetramethylammonium (**TAM⁺**) which formed a stable complex with **PEt[5]** detectable at *m/z* 964.59 (Figure 4.5). In the upper spectrum the sum of the intensities of all the **PEt[6]** peaks with respect to all the **PEt[5]** peaks was determined to be around 1%, showing, as already mentioned, that the conversion of the smaller macrocycle into the larger one was already occurring after one day. After four days, the conversion reached equilibrium with

roughly 10% of **PEt[6]**, as determined by the intensities peaks ratio between **PEt[6]** and **PEt[5]**, and subsequently isolated by prep-TLC (8% yield).

Formaldehyde was excluded an active source of methylene for the conversion of the cyclic pentamer **PEt[5]** into the cyclic hexamer **PEt[6]**, in fact the same experiment carried out in the absence of paraformaldehyde led to analogous result in terms of amount of **PEt[6]** (8% isolated yield). On the contrary, the exclusion of **TMAC** or $FeCl_3$ from the experimental conditions affected drastically the reaction with negligible formation of **PEt[6]** in both cases.

Since the reaction occurred in an aqueous-organic media, we considered for our investigations the aqueous behavior of the Lewis acid $FeCl_3$. When solvated in water, in fact, the Fe^{3+} aqueous complex ($[Fe(H_2O)_6]^{3+}$) dissociates releasing 3 equivalents of H_3O^+,[143] that at the molar concentration of our reaction, is equal to work in the presence of 2.1 x 10^{-2} mM HCl(aq). The presence of dissociated species such as $[Fe(H_2O)_5(OH)]^{2+}$, $[Fe(H_2O)_4(OH)_2]^+$ and $[Fe(H_2O)_3(OH)_3]$ was confirmed by the color of the aqueous solution which turned from yellow to red.[144] Therefore, we tested the possible role played by the Brønsted acidity performing the conversion reaction of **PEt[5]** into **PEt[6]** assisted only by the presence of HCl(aq) and **TMAC** (Scheme 4.4a). However, since this experiment did not lead to formation of the cyclic hexamer, we concluded that the **PEt[5]** ring opening and rearrangement into the larger **PEt[6]** was promoted by the interaction of the oxygen atoms on the pillararene rims and the Fe^{3+} aqueous species present in solution excluding any role of the possible Brønsted acids present.

(a)

(b)
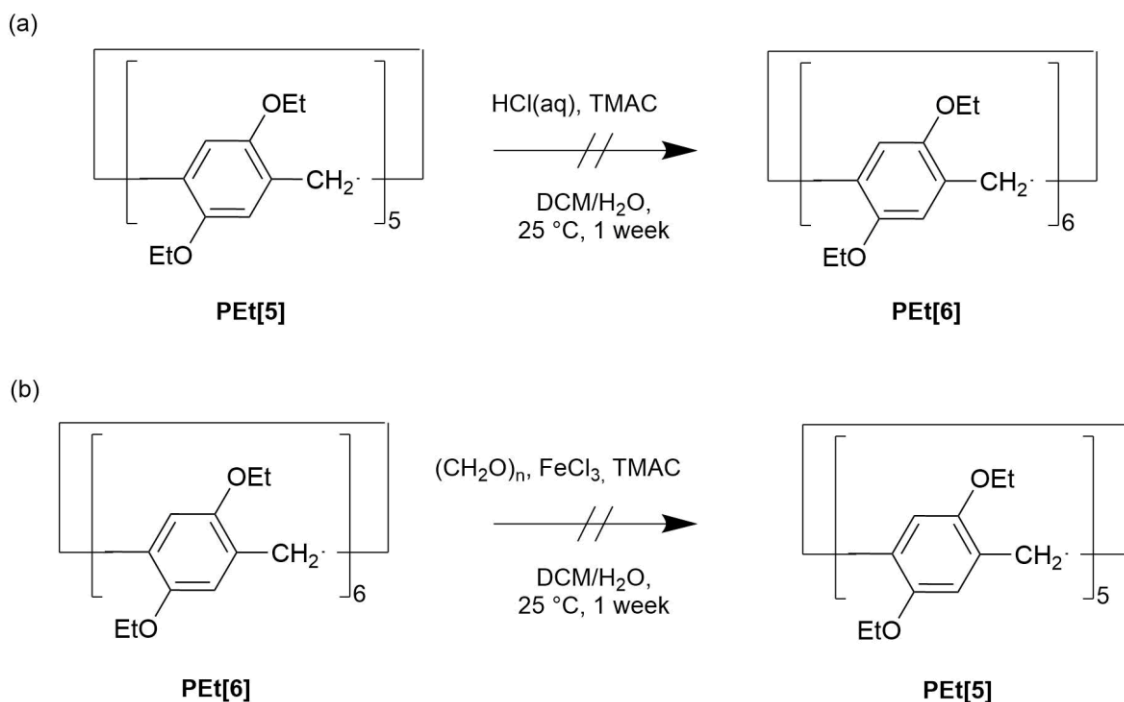
Scheme 4.4 *Conversion experiments from a)* **PEt[5]** *leading to* **PEt[6]** *with HCl(aq) 0.021 mM and* **TMAC***, b)* **PEt[6]** *leading to* **PEt[5]** *with paraformaldehyde, FeCl₃ and* **TMAC***.*

To have a better clue on the reaction under consideration, the reverse reaction, i.e. the conversion of **PEt[6]** into **PEt[5]**, was performed in the presence of all the chemicals actively involved in the reaction (**TMAC** and FeCl₃). The formation of the cyclic pentamer was not observed, highlighting once more the higher observed stability of **PEt[6]** under the reported experimental conditions. These observations are in contrast with morphological considerations arising from crystallographic evidences[106] regarding the average bond angle of the methylene bridge in **PMe[5]**. In fact, it is around 111°, value close to both the ideal 109.51° angle for sp^3 hybridized carbon atoms and the theoretical 108° internal angle for an unstrained pentagon. These observation are also in contrast with previous experiments which generally assess **P[5]s** as the thermodynamic products in **P[n]s** synthesis. Despite these considerations, the selectivity of the reaction could be tuned towards the less favorable macrocyclic products by working under thermodynamic control for **PEt[6]** and therefore using appropriate fitting solvents or templates which form more stable complexes with the cyclic hexamer. As the theory predicted, in our experimental conditions the conversion of **PEt[6]** into **PEt[5]** did not take place since we did not work in the

presence of a template which could steer the selectivity of the reaction toward the smaller macrocycle (Scheme 4.4b).

4.2.3. Scrambling Experiments as New Strategy for the Synthesis of Co-pillar[6]arenes

A couple of experiments were carried out mixing a methoxy- and an ethoxy-substituted **P[5]** with a different dialkoxy benzene derivative, to further demonstrate the existing equilibrium between the cyclic and the linear open form of these **P[5]s** (Scheme 4.5). This procedure was carried out aiming at synthesizing two different co-pillar[6]arenes (**co-P[6]**), **PMe[5]Et[1]** and **PEt[5]Me[1]**.
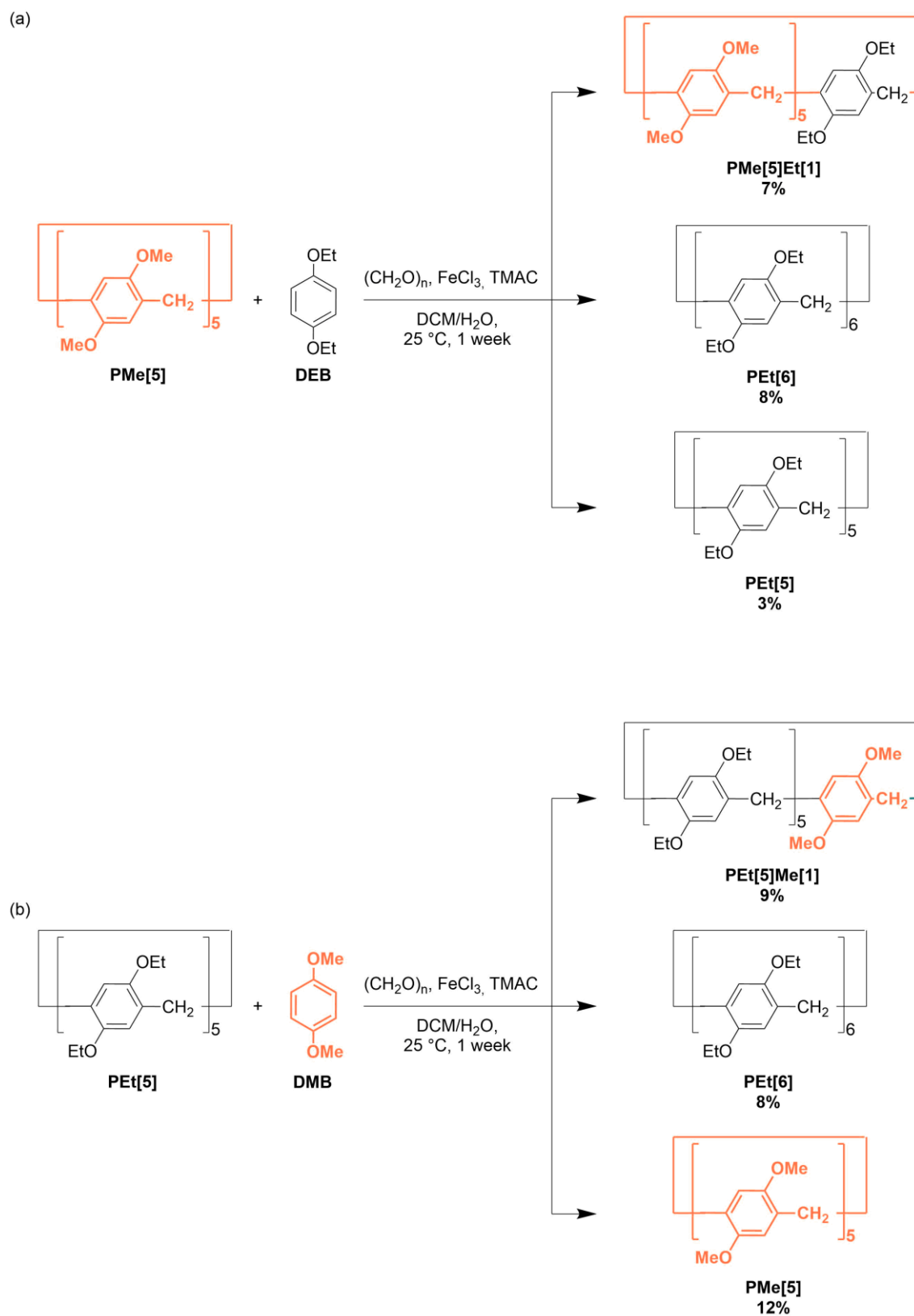
Scheme 4.5 *Scrambling experiments between a)* **DEB** *and* **PMe[5]** *and b)* **DMB** *and* **PEt[5]**.

As expected the reaction between **PMe[5]** and **DEB** in the presence of $FeCl_3$, **TMAC** and paraformaldehyde gave **PMe[5]Et[1]** (Scheme 4.5a) and similarly,

PEt[5] reacted with **DMB** in the presence of the same promoters to give **PEt[5]Me[1]** (Scheme 4.5b). Both reactions were conducted in the biphasic solution DCM/H_2O at room temperature upon one week of stirring and all the products obtained were isolated by prep-TLC. In addition to **PEt[5]Me[1]**, a small amount of **PEt[6]** (8%) was observed as secondary product showing once again the spontaneous tendency of the cyclic pentamer **PEt[5]** to open and eventually rearrange in the hexameric form of **PEt[6]**. On the other hand, as previously underlined in the **PMe[5]** conversion experiment (**Errore. L'origine riferimento non è stata trovata.**), **PMe[6]** was not detected as reaction product. In the scrambling experiment between **PMe[5]** and **DEB** (Scheme 4.5a) a small amount of **PEt[5]** (3%) and a significant amount of **PEt[6]** (8%) were formed, enlightening the high reactivity of the monomer even in the presence of water, which in principle should deactivate the catalyst. In the same way, a quite significant amount of **PMe[5]** (12%) was obtained from the reaction between **PEt[5]** and **DMB** (Scheme 4.5b).

In the ESI mass spectrum of purified **PEt[5]Me[1]** (Figure 4.6 a) we could observe the usual distribution of adducts with common background ions such as NH_4^+, Na^+ and K^+ where the most abundant peak at *m/z* 1058.595 was assigned to the ammonium complex **PEt[5]Me[1]@NH$_4$$^+$**. Analogue interpretation was done for the ESI-MS spectrum of **PMe[5]Et[1]** with the most abundant peak at *m/z* 951.430 (Figure 4.6 b) corresponding to the sodium complex **PMe[5]Et[1]@Na$^+$**. In both spectra, the experimental isotopic distributions of the peaks corresponded to the calculated ones with an error below 1%.

a)

calc.
1058.5988

obs.
1058.5953

PEt[5]Me[1]@NH$_4^+$
1058,595

PEt[5]Me[1]@TEAH$^+$
1142,689

PEt[5]Me[1]@H$^+$
1041,569

PEt[5]Me[1]@Na$^+$
1063,551

PEt[5]Me[1]@K$^+$
1079,525

m/z 950 1000 1050 1100 1150 1200

b)

calc.
951.4290

obs.
951.4308

PMe[5]Et[1]@Na$^+$
951,430

PMe[5]Et[1]@TEAH$^+$
1030,568

PMe[5]Et[1]@NH$_4^+$
946,475

PMe[5]Et[1]@H$^+$
929,448

PMe[5]Et[1]@K$^+$
967,403

m/z 920 960 1000 1040 1080

*Figure 4.6 a) FTICR-MS spectrum of **PEt[5]Me[1]** and comparison with the isotopic distribution for the complex **PMe[5]Et[1]@Na$^+$**; b) FTICR-MS spectrum of **PMe[5]Et[1]** and comparison with the calculated and experimental isotopic distribution for the complex **PEt[5]Me[1]@NH$_4^+$***

These inclusion experiments confirmed the existence of an equilibrium, mediated by the cleavage on a methylene bridge, between a cyclic and open form

of **P[5]s**, where the macrocycles reacted with the dialkoxy benzene derivatives, resulting in a monomer inclusion in the linear pentamers framework which could close in a cyclic hexamer fashion.

4.2.4. Synthesis and Scrambling Experiments of a Deuterium Labeled PEt[5]d$_{10}$

Niertgarten's group described the **PEt[5]** synthetic mechanism [86] on the basis of dynamic covalent chemistry, highlighting how the formation of Ar-CH$_2$ bonds was in equilibrium with the same Ar-CH$_2$ bonds cleavage. With these remarks, we focused our attention on the reasons behind **PEt[5]** Ar-CH$_2$ bond cleavage and formation which led to **PEt[6]**. In order to better understand our observations, we synthesized a deuterium labeled **PEt[5]**, isotopically marked on the ethoxy moieties of just one aromatic unit (**PEt[5]d$_{10}$**), and we studied its ability to convert into larger homologues in the presence of the catalyst FeCl$_3$ and template **TMAC**. The decision to use a labeled **PEt[5]d$_{10}$** as starting material was dictated by the need to investigate the chemical reactivity of the cyclic pentamer with a simple alternative analytical method while maintaining unaltered the chemical structure of the macrocycle itself. The reaction was performed in the same reaction conditions used in all the other experiments described in this chapter (quenched in a biphasic solution DCM/H$_2$O stirred for one week at room temperature) (Scheme 4.6) and the reaction mixture was analyzed by ESI-MS spectroscopy in the *m/z* 800-1300 range.

Scheme 4.6 *Synthesis of PEt[6] and PEt[6]d₁₀ from PEt[5]d₁₀ with FeCl₃ and TMAC in dichloromethane/water.*

Before running the experiment, we speculated on the mechanism behind the conversion (Scheme 4.7).

The suggested pathway involves an initial iron mediated Ar-CH$_2$ bond cleavage leading to the formation of the benzylic linear pentamer **8**.

Assisted by FeCl$_3$ the cyclic pentamer undergoes a selective cleavage on a random CH$_2$ of the bridge, leaving the corresponding linear pentamer bearing a reactive benzylic cation (**8**). To this end, these linear benzylic oligomers **8** react with another **PEt[5]d₁₀** trough an electrophilic aromatic substitution forming the longer oligomers **9**. Eventually, **9** close up in an hexameric fashion, forming **PEt[6]d₁₀** more statistically likely than **PEt[6]d₂₀** (5:1) with the fragment **10** left aside.

The fragment **10** can further react in a similar way with **PEt[5]d₁₀** leaving, after closure into **PEt[6]d₁₀** or **PEt[6]d₂₀** (5:1), another fragment with three aromatic units. The same reaction is repeated until all the fragments react leading to the statistical distribution **PEt[6]d₁₀** : **PEt[6]d₂₀** = 5:1.

Unfortunately, the preliminary results were not consistent with the expected products distribution since we did not observe **PEt[6]s** in an appreciable amount.

However, further investigations will be soon conducted in order to have a better clue on the mechanism behind the pillararenes conversion.

Scheme 4.7 *Conversion mechanism via an initial cleavage which leaves the linear pentamer ready to react with* ***PEt[5]d₁₀*** *and eventually close in* ***PEt[6]d₁₀*** *and* ***PEt[6]d₂₀*** *form.*

Figure 4.7 Statistic of the mechanism explained in Scheme 4.7, showing 1/5 formation probability of $PEt[6]d_{20}$ and 4/5 formation probability for $PEt[6]d_{10}$. The deuterated unit is shown as blue sphere, while the unlabeled are shown as black spheres. The number refers to the position in which the CH2-Ar cleavage occurs.

4.3. Conclusions

In conclusion we proposed two different mechanisms for the conversion of **PEt[5]** into **PEt[6]** evaluating in detail the factors that influenced such reaction. In order to better understand the conversion reaction we first investigated the TMAC templated **P[n]s** synthesis catalyzed by FeCl₃ described in chapter three, characterizing the reaction side products as a mixture of three linear benzylic alcohols that eventually undergo ring closing forming **PEt[5]**, **PEt[6]** and **PEt[7]**. The more abundant **OEt[6]** when dissolved in a biphasic solution of DCM and water and in the presence of both the same catalyst and template could further react to give **PEt[6]** in 55% yields. In the same reaction conditions we successfully converted **PEt[5]** into **PEt[6]** with higher yields (8% yield) compared to the work previously reported by Ogoshi and co-workers.[25] The formation of **PEt[6]** from **PEt[5]** proved the existence of the equilibrium between the macrocycle **PEt[5]** and the linear pentamer. From this knowledge, we successfully synthesized two different **co-P[6]s** (**PMe[5]Et[1]** and **PEt[5]Me[1]**) again in 8% yield, through the inclusion experiment of **DEB** in **PMe[5]** and of **DMB** in **PEt[5]**.

4.4. Experimental Section

4.4.1. General procedures

Solvents used in the study were reagent grade and purchased from commercial sources. Hydroquinone, iodoethane, iodoethane-d$_5$, paraformaldehyde, FeCl$_3$, tetramethylammonium chloride were reagent grade and purchased from Sigma-Aldrich. Deionized water was used in all experiments. ^{1}H and ^{13}C NMR spectra were collected on a Bruker-400 MHz NMR spectrometer. High-resolution ESI mass spectra were measured on an Agilent 6210 ESI-TOF device (Agilent Technologies). HPLC grade solvents were used with a flow rate of 2-4 mL/min.

4.4.2. Synthetic Procedures

4.4.2.1. Overall Synthesis of PEt[6]d$_{10}$

Scheme 4.8 *Complete synthesis of* ***PEt[5]d$_{10}$***.

4.4.2.2. Synthetic Route to DEB

EtI (3.3 mL, 44.1 mmol) and NaOH (1.76 g, 44.1 mmol) were added to a solution of **HQ** (1.6 g, 14.7 mmol) in DMSO (50 mL) under air atmosphere at 25 °C. The mixture was stirred for 2 h and then was poured into ice and water (100 mL). The solid precipitate was filtered and washed with water. Yield: 2.30 g (14.0 mmol, 95%) of **DEB** as white crystals. ^{1}H-NMR spectrum of **DEB** is shown in Figure 4.8. ^{1}H NMR (400 MHz, CDCl$_3$, 298 K), δ 6.82 (s, 1H), 3.98 (q, J = 7.0 Hz, 1H), 1.40 (d, J = 7.0 Hz, 1H).

Figure 4.8 *^{1}H NMR spectrum of **DEB**.*

4.4.2.3. Synthetic Route to PEt[5]

TFA (7.5 mL, 9.8 mmol) and paraformaldehyde (420 mg, 14.00 mmol) were added to a solution of **DEB** (2.30 g, 14.00 mmol) in DCE (150 mL) at 55 °C. The mixture was stirred for 2 h and then was poured into MeOH (100 mL). The solid material was filtered and washed with MeOH. The solid residue was crystallized from boiling EtOH, then filtered and washed with cold EtOH. Yield: 1.12 g (1.26 mmol, 53%) of **PEt[5]** as yellowish powder. NMR spectra of **PEt[5]** are shown in Figure 4.9 and Figure 4.10. ^{1}H NMR (400 MHz, CDCl$_3$, 298 K), δ 6.72 (s, 1H), 3.83 (q, J = 7.0 Hz, 2H), 3.77 (s, 1H), 1.26 (t, J = 7.0 Hz, 3H). ^{13}C NMR (100 MHz, CDCl$_3$, 298 K) δ 149.72, 128.45, 114.74, 63.62, 29.66, 15.14.

Figure 4.9 *^{1}H NMR spectrum of **PEt[5]**.*

Figure 4.10 ^{13}C *NMR spectrum of PEt[5].*

4.4.2.4. Synthetic Route to PEt[4]Q[1]

A solution of CAN (307 mg, 0.56 mmol) in water (5 mL) was added dropwise to a solution of **PEt[5]** (500 mg, 0.56 mmol) in THF (5 mL) under air atmosphere at 25 °C. The mixture was stirred for 24 h and then extracted with DCM (3 x 5 mL), washed with water and brine. The organic layer was dried over $MgSO_4$, filtered and concentrated under vacuum to give a red solid. The crude product was purified by silica gel column chromatography with PET/DCM = 2/1 as eluent. The first fraction was the unreacted **PEt[5]** (175 mg, 0.19 mmol, yield: 35%). The second fraction was **PEt[4]Q[1]** (60 mg, 0.072 mmol, yield: 13%). The third fraction was a pillar[5]arene derivative containing more than one benzoquinone unit (265 mg). NMR and MS spectra of **PEt[5]Q[1]** are shown in Figure 4.11, Figure 4.12 and Figure 4.13. ^1H NMR (400 MHz, $CDCl_3$, 298 K) δ 6.91 – 6.59 (m, 1H), 4.05 – 3.50 (m, 3H), 1.53 – 1.16 (m, 3H). ^{13}C NMR (100 MHz, $CDCl_3$, 298 K) δ 149.51, 149.46, 146.19, 133.10, 129.45, 128.37, 128.24,

114.82, 114.35, 114.19, 114.10, 63.81, 63.54, 63.42, 53.28, 29.36, 29.06, 27.83, 15.23, 15.09. MS (ESI-TOF) m/z 855.402 [M+Na]$^+$, 871,380 [M+K]$^+$.m/z calcd for [M+Na]$^+$ C$_{51}$H$_{60}$NaO$_{10}$: 855.408; found 855.402 (100%).

Figure 4.11 ^{1}H NMR spectrum of *PEt[4]Q[1]*.

Figure 4.12 ^{13}C *NMR spectrum of* **PEt[4]Q[1]**.

Figure 4.13 *ESI-MS spectrum of* **PEt[4]HQ[1]**.

4.4.2.5. *Synthetic Route to PEt[4]HQ[1]*

NaBH$_4$ (12 mg, 0.32 mmol) was added to a solution of **PEt[4]Q[1]** (60 mg, 0.072 mmol) in THF (2 mL) under air atmosphere at 25 °C. The mixture was stirred for 30 min until the color turned from red to colorless. Then 1M aqueous HCl (4 mL) was added and the mixture stirred for 1h. The reaction mixture was extracted with DCM (3 x 5 mL), washed with water and brine. The organic layer was dried over MgSO$_4$, filtered and concentrated under vacuum to give **PEt[4]HQ[1]** (60 mg, 0.071 mmol, yield: 99%) as pinkish powder. NMR and MS spectra are shown in Figure 4.13, Figure 4.14 and Figure 4.15. ^{1}H NMR (400 MHz, CDCl$_3$, 298 K) δ 7.23 (s, 1H), 7.06 - 6.36 (m, 5H), 4.18 - 3.58 (m, 15H), 1.55 - 1.08 (m, 15H). ^{13}C NMR (100 MHz, CDCl$_3$, 298 K) 151.27, 149.82, 149.71, 147.42, 147.30, 129.36, 128.51, 127.61, 127.27, 126.80, 118.04, 115.99, 114.97, 114.70, 113.75, 67.97, 65.23, 63.83, 63.61, 30.87, 30.34, 30.03, 25.59, 15.19, 14.67. MS (ESI-TOF) *m/z* 857.418 [M+Na]$^+$, 873,392 [M+K]$^+$.*m/z* calcd for [M+Na]$^+$ C$_{51}$H$_{62}$NaO$_{10}$: 857.424; found 857.418 (100%).

Figure 4.14 ^{1}*H NMR spectrum of* **PEt[4]HQ[1]**.

Figure 4.15 ^{13}C *NMR spectrum of* **PEt[4]HQ[1]**.

Figure 4.16 *ESI-MS spectrum of* **PEt[4]HQ[1]**.

4.4.2.6. Synthetic Route to PEt[5]d₁₀.

Iodoethane-d$_5$ (100 μl, 1.6 mmol) and NaOH (8.65 mg, 0.22 mmol) were added to a solution of **PEt[4]HQ[1]** (60 mg, 0.072 mmol) in DMSO/THF (6/0.5 mL) under Ar atmosphere at 25 °C. The mixture was stirred for 2 h and then was poured into ice and water (100 mL). The solid precipitate was filtered and washed with water. Yield: 40 mg (0.044 mmol, 63%) of **PEt[5]d₁₀.** as pinkish powder. NMR and ESI-MS spectra of **PEt[5]d₁₀.** are shown Figure 4.17, Figure 4.18, Figure 4.19 and Figure 4.20. ^{1}H NMR (400 MHz, CDCl$_3$, 298 K) δ 6.72 (s, 1H), 3.83 (q, *J* = 7.0 Hz, 2H), 3.77 (s, 1H), 1.26 (t, *J* = 7.0 Hz, 3H). ^{13}C NMR (100 MHz, CDCl$_3$, 298 K) δ 149.96, 128.64, 115.23, 63.92, 29.98, 15.22. ^{2}H NMR (61 MHz, CDCl$_3$, 298 K) δ 3.83 (s, 2H), 1.26 (s, 3H). MS (ESI-TOF) *m/z* 900.560 [M]$^+$, 918.594 [M+NH$_4$]$^+$, 923.549 [M+Na]$^+$, *m/z* calcd for [M]$^+$ C$_{55}$H$_{60}$D$_{10}$O$_{10}$: 900.559; found 900.560 (100%).

Figure 4.17 ^{1}H NMR spectrum of *PEt[5]d₁₀.*

Figure 4.18 ^{13}C NMR spectrum of *PEt[5]d$_{10}$*.

Figure 4.19 ^{2}H NMR spectrum of *PEt[5]d$_{10}$*.

PEt[5]d$_{10}$@NH$_4$$^+$
918.594
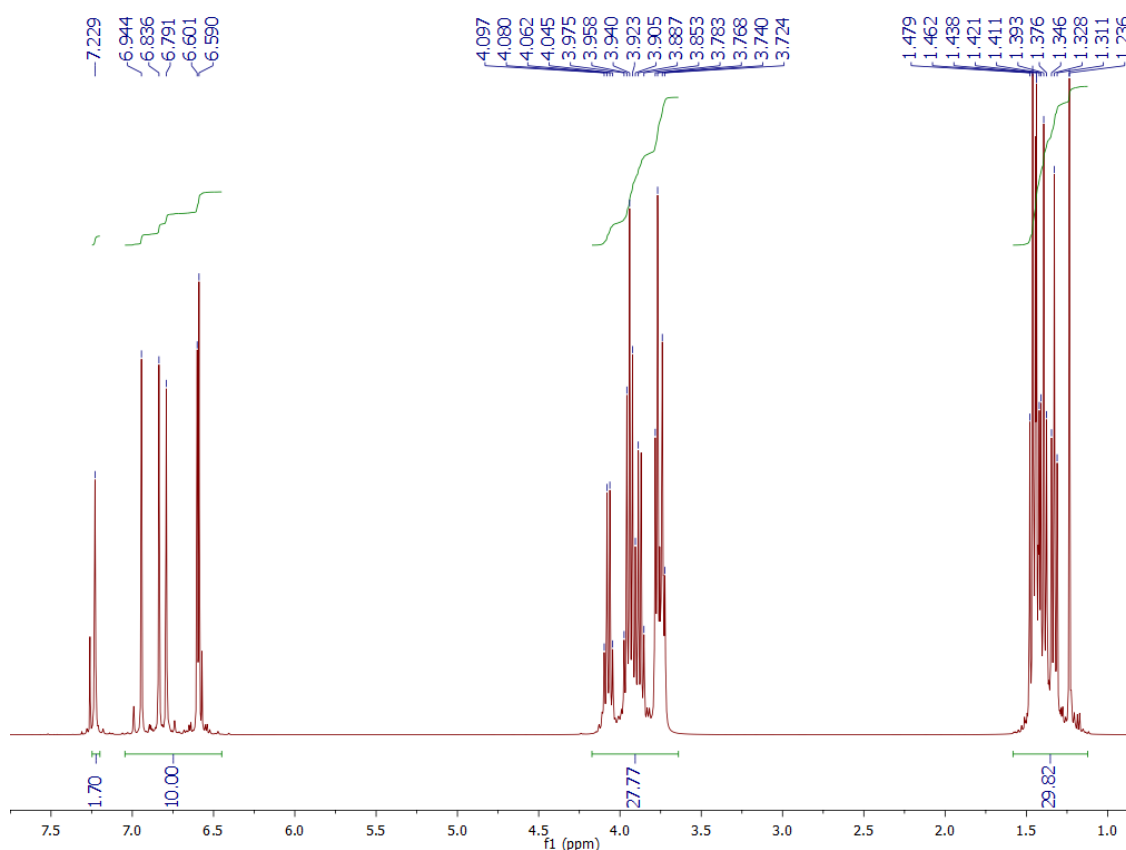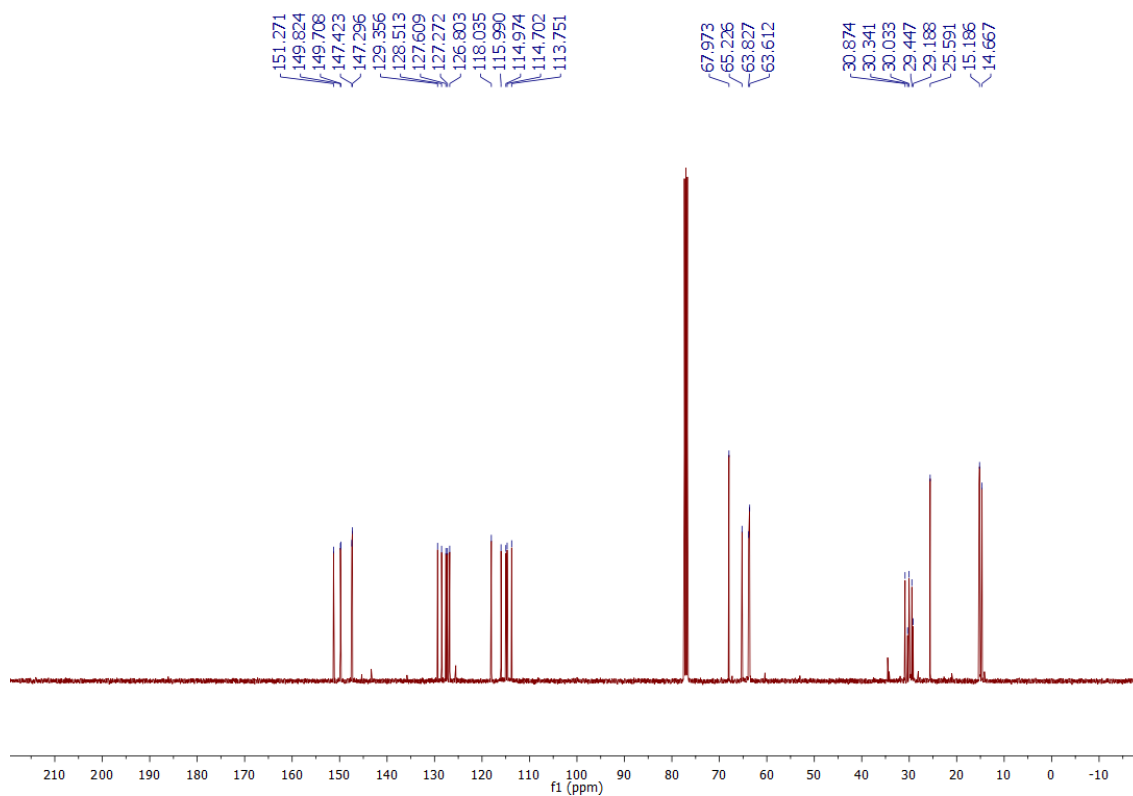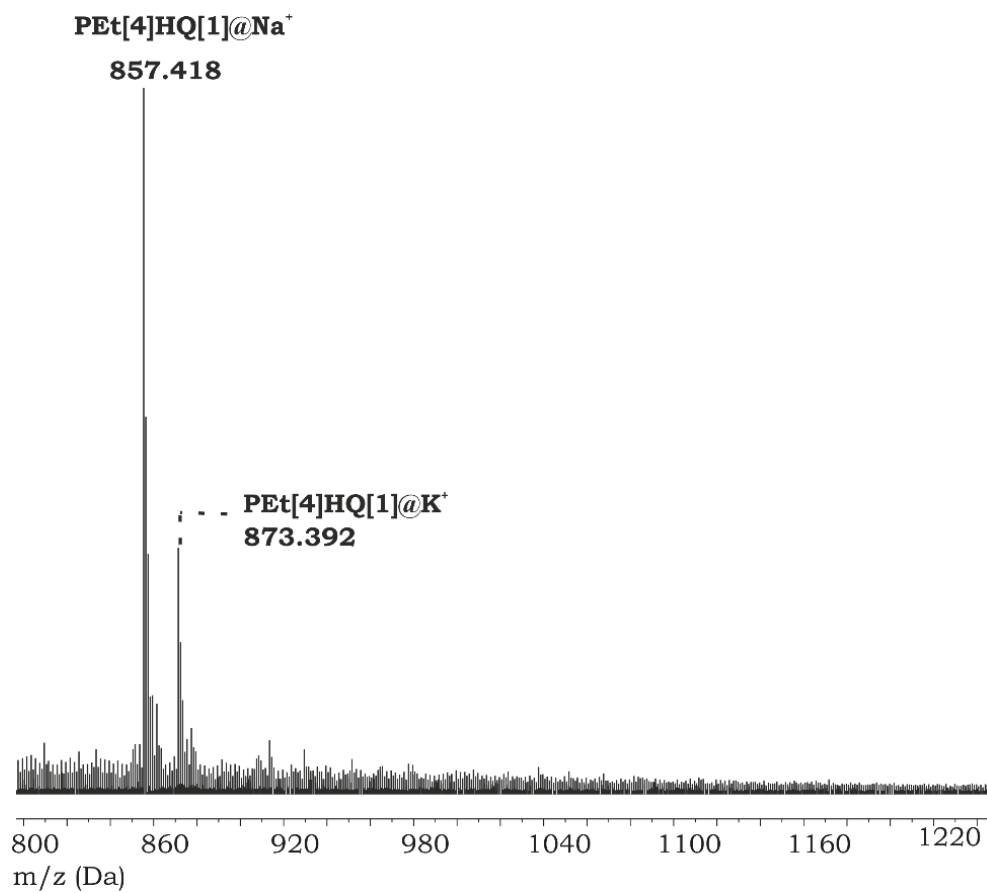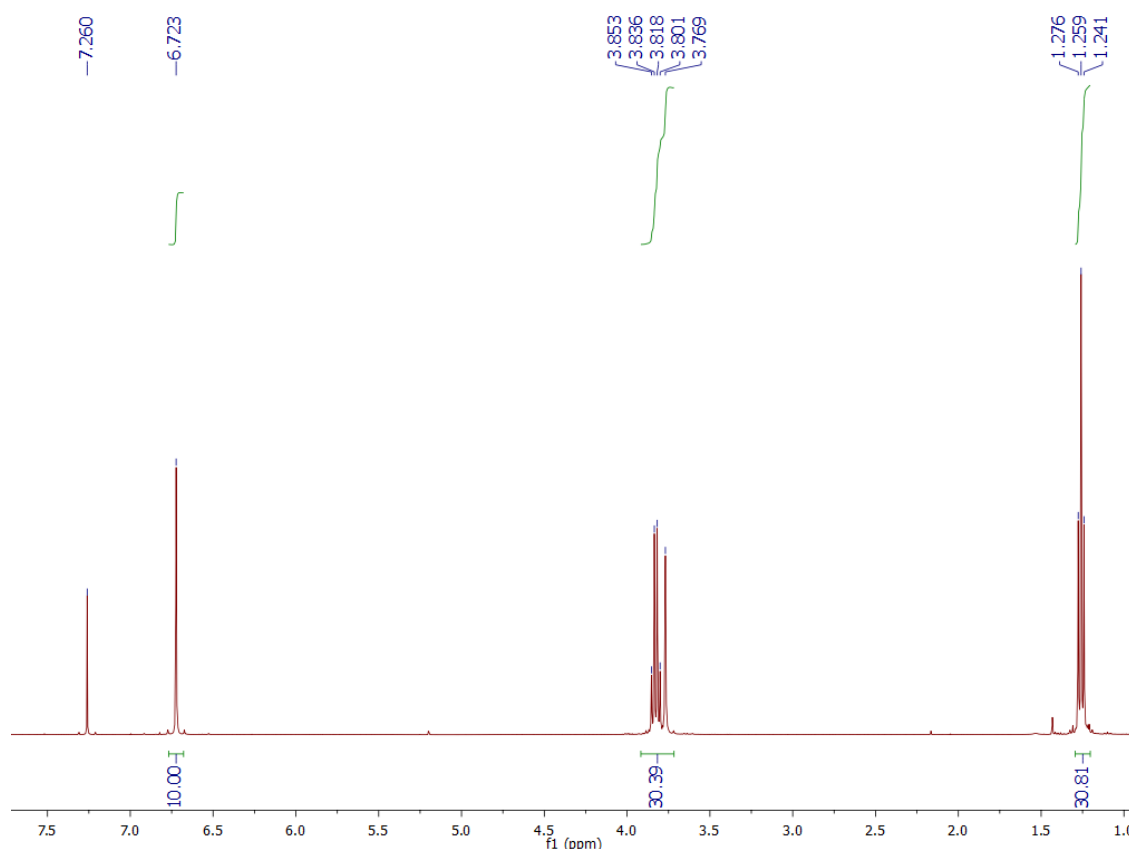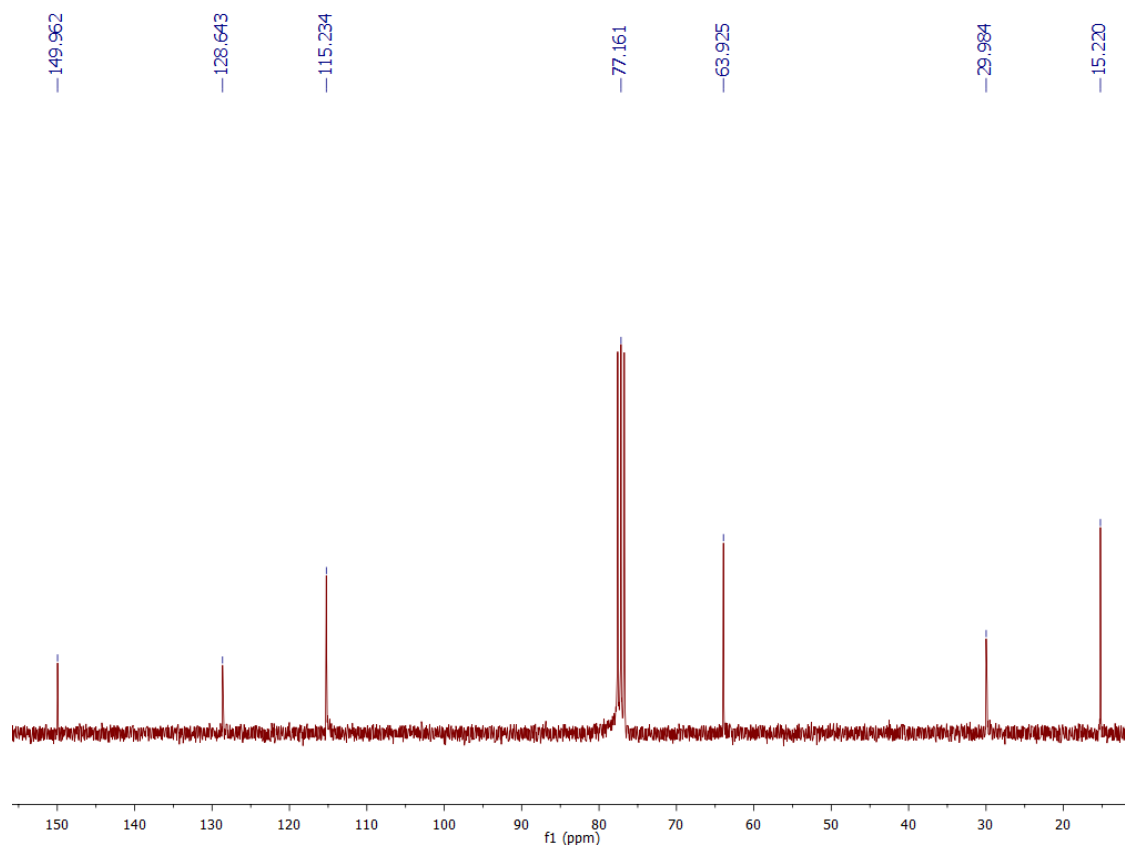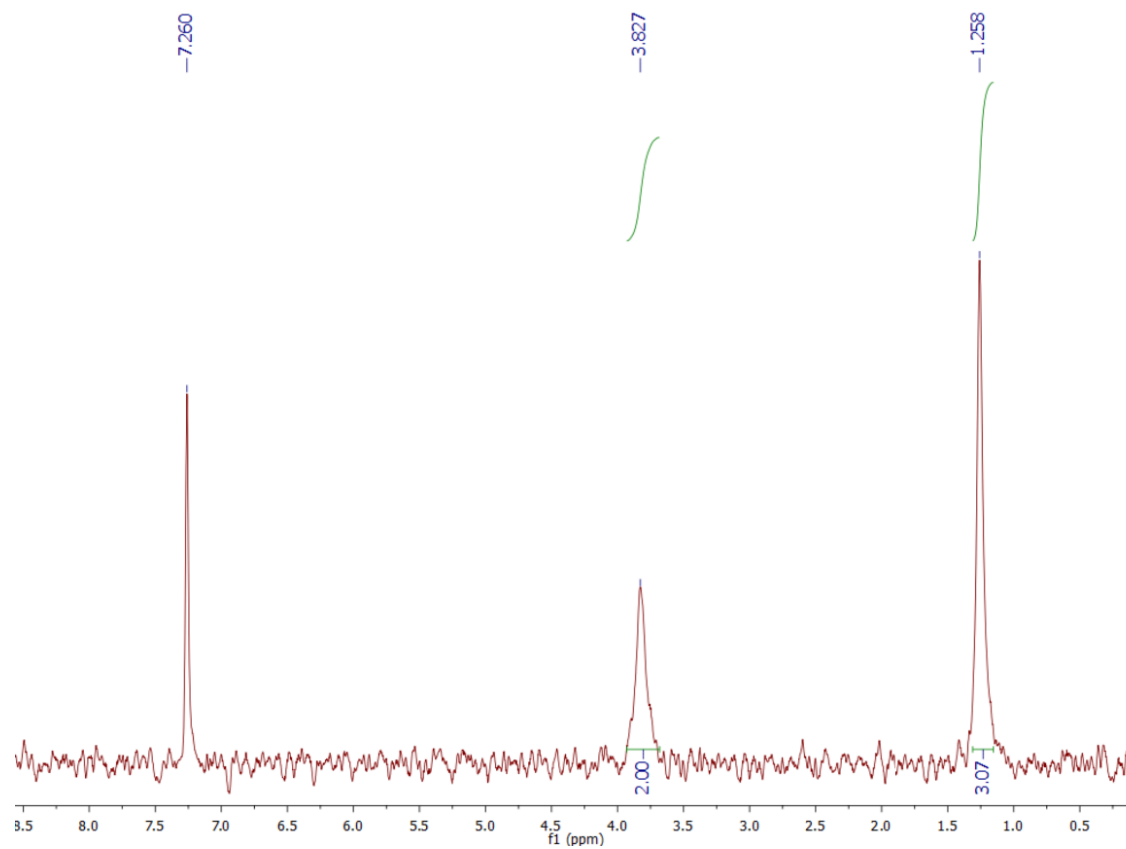
PEt[5]d$_{10}$$^+$
900.560

PEt[5]d$_{10}$@Na$^+$
923.549

900   910   920   930   940   950

m/z (Da)
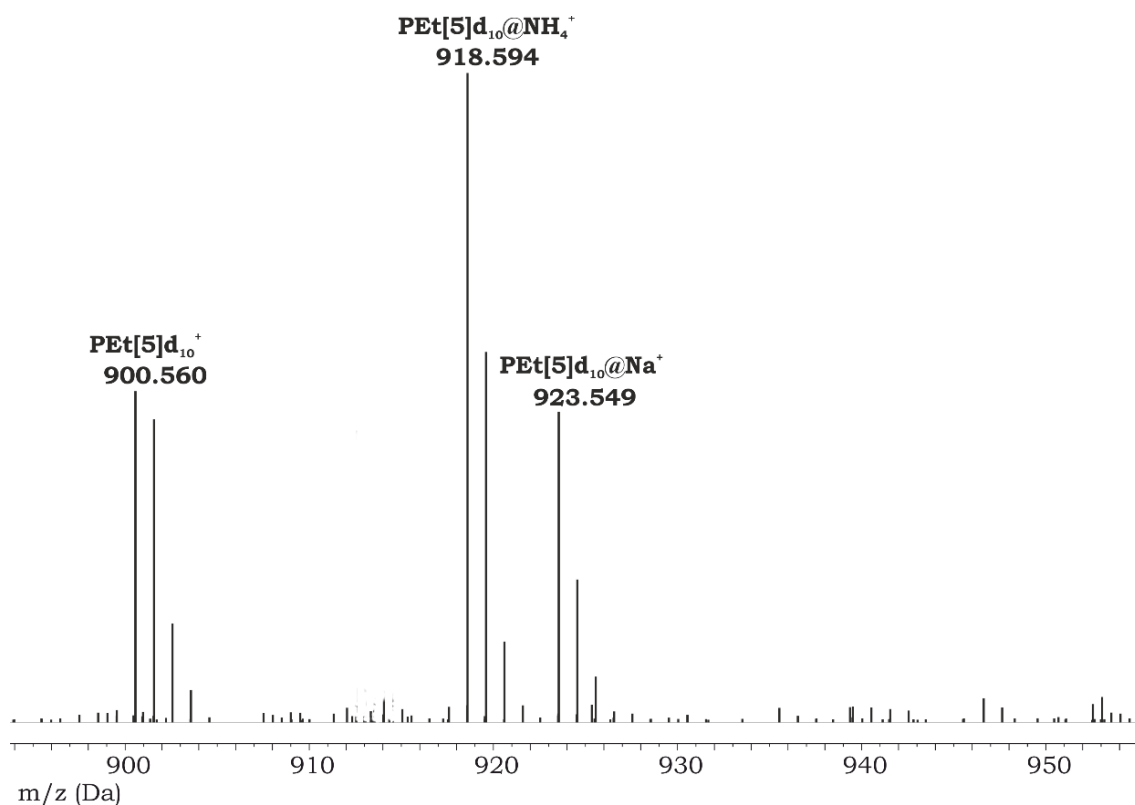
Figure 4.20 ESI-MS spectrum of *PEt[5]d$_{10}$.*

4.4.2.7. OEt[6] Characterization

^{1}H NMR (400 MHz, CDCl$_3$, 298 K) δ 6.75-6.61 (m), 4.06-3.67 (m), 1.43-1.10 (m). MS (EI) *m/z* 534.3 [**OEt[6]**-H$_2$O]$^{2+}$, 890.5 [**OEt[5]**-H$_2$O]$^+$, 1068.5 [**OEt[6]**-H$_2$O]$^+$, 1248.6 [**OEt[6]**-H$_2$O]$^+$, *m/z* calcd for [**OEt[6]**-H$_2$O]$^+$ C$_{66}$H$_{84}$O$_{12}$: 1068.6; found 1068.5 (100%).

4.4.3. General Procedure for PEt[5] Conversion PEt[6] Experiments

All the conversion experiment were performed alternatively with paraformaldehyde, FeCl$_3$ and **TMAC** together and separately. Paraformaldehyde (20 mg, 0.66 mmol), FeCl$_3$ (58 mg, 0.358 mmol) and **TMAC** (28 mg, 0.255 mmol) were heated at 110 °C and gently stirred until a dark brown viscous liquid formed. Then a solution of **PEt[5]** (11 mg, 0.012 mmol) in DCM (25 mL) was added and the mixture was stirred at 25 °C for 2 minutes. Then water (50 mL)

was added and the reaction mixture was stirred at 25 ℃ for 1 week. The reaction was monitored by FTICR-ESI-MS.

4.4.5. *General Procedure for OEt[6] Conversion Experiments*

FeCl$_3$ (58 mg, 0.358 mmol) and **TMAC** (28 mg, 0.255 mmol) were heated at 110 ℃ and gently stirred until a dark brown viscous liquid formed. Then a solution of **OEt[6]** (10 mg, 0.009 mmol) in DCM (25 mL) was added and the mixture was stirred at 25 ℃ for 2 minutes. Then water (50 mL) was added and the reaction mixture was stirred at 25 ℃ for 1 week. The reaction was monitored by FTICR-ESI-MS (Figure S17). The organic layer was then washed with water and brine, dried over MgSO$_4$, filtered and dried over vacuum. The crude product was purified by preparative TLC with PET:Et$_2$O = 8:2 as eluent to give **PEt[6]** between 25% and 55% yield.

4.5. References

1. T. Ogoshi, S. Kanai, S. Fujinami, T.-a. Yamagishi and Y. Nakamoto, *Journal of the American Chemical Society*, 2008, **130**, 5022-5023.

2. T. Ogoshi, T. Aoki, K. Kitajima, S. Fujinami, T.-a. Yamagishi and Y. Nakamoto, *The Journal of Organic Chemistry*, 2011, **76**, 328-331.

3. T. Boinski and A. Szumna, *Tetrahedron*, 2012, **68**, 9419-9422.

4. D. Cao, Y. Kou, J. Liang, Z. Chen, L. Wang and H. Meier, *Angewandte Chemie International Edition*, 2009, **48**, 9721-9723.

5. C. Han, F. Ma, Z. Zhang, B. Xia, Y. Yu and F. Huang, *Organic Letters*, 2010, **12**, 4360-4363.

6. K. Wang, L.-L. Tan, D.-X. Chen, N. Song, G. Xi, S. X.-A. Zhang, C. Li and Y.-W. Yang, *Organic & Biomolecular Chemistry*, 2012, **10**, 9405-9409.

7. Y. Ma, X. Ji, F. Xiang, X. Chi, C. Han, J. He, Z. Abliz, W. Chen and F. Huang, *Chemical Communications*, 2011, **47**, 12340-12342.

8. M. Da Pian, O. De Lucchi, G. Strukul, F. Fabris and A. Scarso, *RSC Advances*, 2016, **6**, 48272-48275.

9. M. Holler, N. Allenbach, J. Sonet and J.-F. Nierengarten, *Chemical Communications*, 2012, **48**, 2576-2578.

10. T. Ogoshi, N. Ueshima, T. Akutsu, D. Yamafuji, T. Furuta, F. Sakakibara and T.-a. Yamagishi, *Chemical Communications*, 2014, **50**, 5774-5777.

11. T. Ogoshi, N. Ueshima, F. Sakakibara, T.-a. Yamagishi and T. Haino, *Organic Letters*, 2014, **16**, 2896-2899.

12. C. Barnes, *Journal of Chemical Education*, 2003, **80**, 747.

13. J. Clark, *Journal*, 2003.

Substrate and Product Selective Supramolecular Catalysis by Pillar[5]arene: Acceleration of the Nucleophilic Substitution of Primary Amines on Allyl Halides
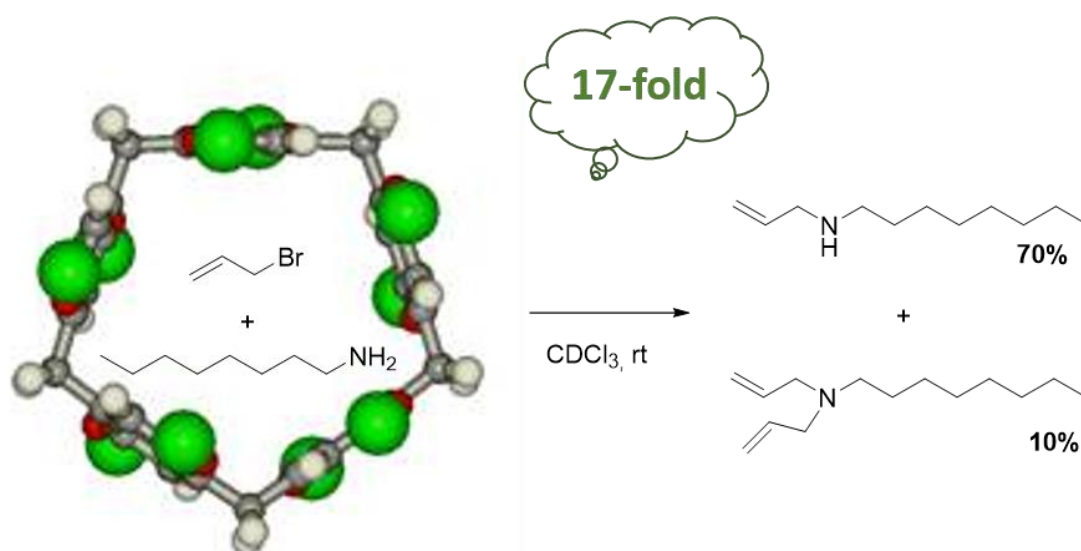
5.1. The Role of Pillar[5]arene in Catalysis

In the last decade, many researchers improved the field of supramolecular catalysis thanks to the rapid development of both supramolecular chemistry and homogeneous catalysis, creating artificial catalysts that through mastering of weak intermolecular forces, mimed some aspects of enzymatic activity in terms of reaction rate acceleration, substrate and product selectivity. Most of the more common host macrocycles such as cyclodextrins, resorcin[4]arenes, calyx[n]arenes and other cyclophanes have been exploited for catalytic applications[145] taking advantage also from their unique self-assembled structures both in water and in organic media[146,52], with impressive catalytic activity like million-fold acceleration of organic transformations[147] or pre-organization of substrates for enhanced substrate and product selectivity.[148]

Among the aromatic macrocyclic hosts suitable for catalytic purposes **P[n]s** represent a new field of research because of their rather narrow and symmetrically accessible cavity that enable the selective recognition of positively charged as well as neutral species in organic media.[79,149,150] So far, **P[n]s** applications in supramolecular chemistry[151] spanned from the development of fluorescent sensors, functional and responsive materials[152] and recently to biomimetic drug delivery systems,[153] but only very few examples of catalytic systems based on **P[n]s** have been yet exploited, all of them concerning the smaller member of the family **P[5]** with different alkoxy substituents (Figure 5.1). In this regard two contributions employed an amphiphilic **P[5]** and a cationic water soluble **P[5]** for the phase transfer catalysis for the oxidation of alkanes (Figure 5.1a)[123] and the phosphate monoester hydrolysis respectively (Figure 5.1b),[124] while in other two **P[5]**-based structures were used as ligand for metal catalysis(Figure 5.1c and d).[127,126] In another example a water soluble **P[5]** was employed as inhibitor of acetylcholine hydrolysis in the presence of the enzyme acetylcholinesterase (Figure 5.1e)[125] and in the last example a **P[5]**-based rotaxane catalyzed a Knovenagel reaction by the presence of an introverted amine group as a stopper (Figure 5.1f).[128]
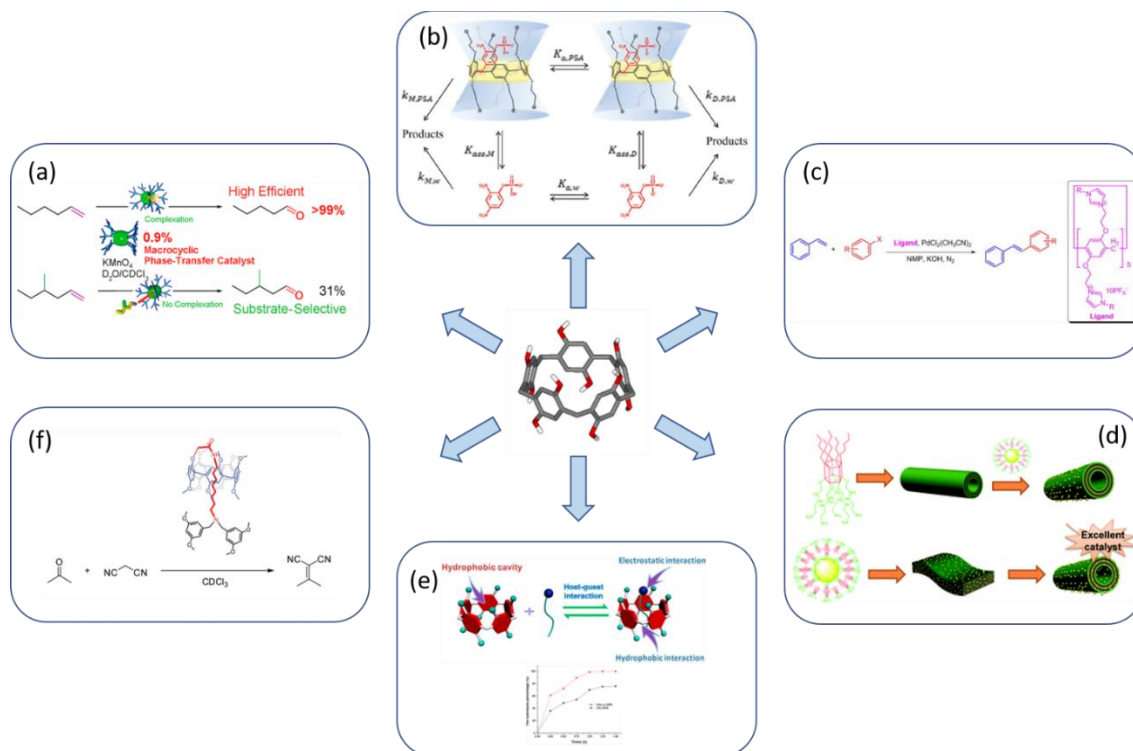
Figure 5.1 Example of catalytic systems based on P[5].

Nevertheless in all these examples **P[5]** is never employed as true organocatalysts where the activation of reactions is a consequence of the substrates binding within the hydrophobic cavity of the **P[5]**. In fact the role of **P[5]** in the above examples is limited to support, bearing sometimes the catalytic moiety itself or assisting the catalyst and the active species responsible for the reaction success.
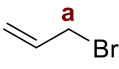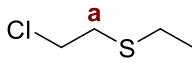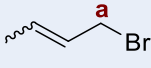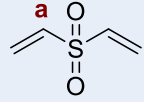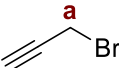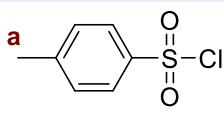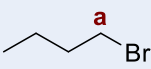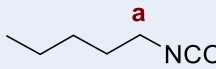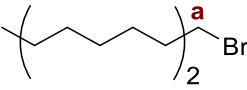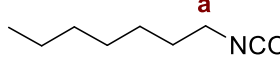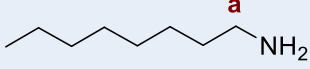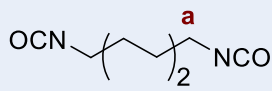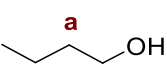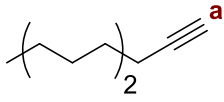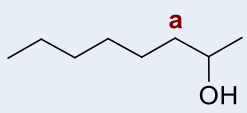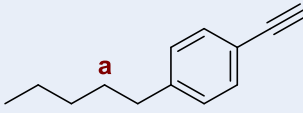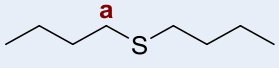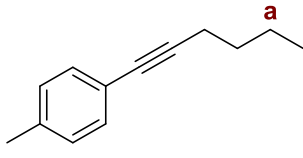
Herein, in the present chapter we present an example of efficient supramolecular catalytic selective synthesis of secondary amines in the nucleophilic substitution reaction between primary amines and allyl halides in the presence of **PEt[5]** as supramolecular recyclable catalyst.

5.2. *Results and Discussion*

5.2.1. *Guests Evaluation*

Since the peculiarity of **P[n]s** relies on the fact that they can efficiently bind neutral narrow guests of small size characterized by bond polarization induced by the presence of terminal electron withdrawing functional groups,[154] we initially investigated through NMR spectroscopy the affinity of **PEt[5]** for model substrates (Table 5.1). The host-guest binding affinity was evaluated in terms of upfield shift of the guest signals upon addition of 0.25 equivalent of **PEt[5]**, in $CDCl_3$, in order to work in excess of substrate with respect to the host.

*Table 5.1 Evaluation of the binding of different electron poor molecules towards **PEt[5]**. Δδ calculated as the difference of the bound guest signal with respect to the free guest. The squared boxes enlighten the best fitting guests. The [Host]/[Guest] ratio was set to 1/5 with [Host]=11 mM and [Guest] =56 mM in CDCl₃*

#	Guest	Guest Δδ (ppm)	#	Guest	Guest Δδ (ppm)
1	allyl bromide	-0.21	10	Cl-CH₂CH₂-S-Et	-0.28
2	crotyl bromide	-0.12	11	divinyl sulfone	-0.12
3	propargyl bromide	-0.03	12	tosyl chloride	-0.12
4	butyl bromide	-0.22	13	pentyl NCO	-1.87
5	alkyl bromide	-0.20	14	hexyl NCO	-1.89
6	octyl NH₂	-0.16	15	OCN-(CH₂)-NCO	-1.89
7	butanol	-0.43	16	alkyne	-0.15
8	octan-2-ol	-0.04	17	aryl alkyne	-0.12
9	dibutyl sulfide	-0.01	18	aryl alkyne	-0.10

As clear from Table 5.1, all the guests evaluated showed upfield shifted signals because of the shielding effect induced by **PEt[5]** cavity after host-guest encapsulation. The best fitting guests, with larger upfield shift up to 1.8 ppm, were those of isocyanates. Even though with smaller $\Delta\delta$ than isocyanates, aliphatic halides, amines, thiols and alcohols turned out to be good guests as well. Therefore, reactions involving all these classes of molecules were evaluated in the presence and in the absence of **PEt[5]**, in order to test the catalytic ability of the cyclic pentamer.

5.2.2. *Synthesis of Carbamate and Urea Derivatives*

The first reactions under study were the synthesis of butyl pentylcarbamate (**3**) and 1-octyl-3-pentylurea (**5**) by reaction of pentyl isocyanate (**1**) with 1-butanol (**2**) or octylamine (**4**) respectively (Scheme 5.1).
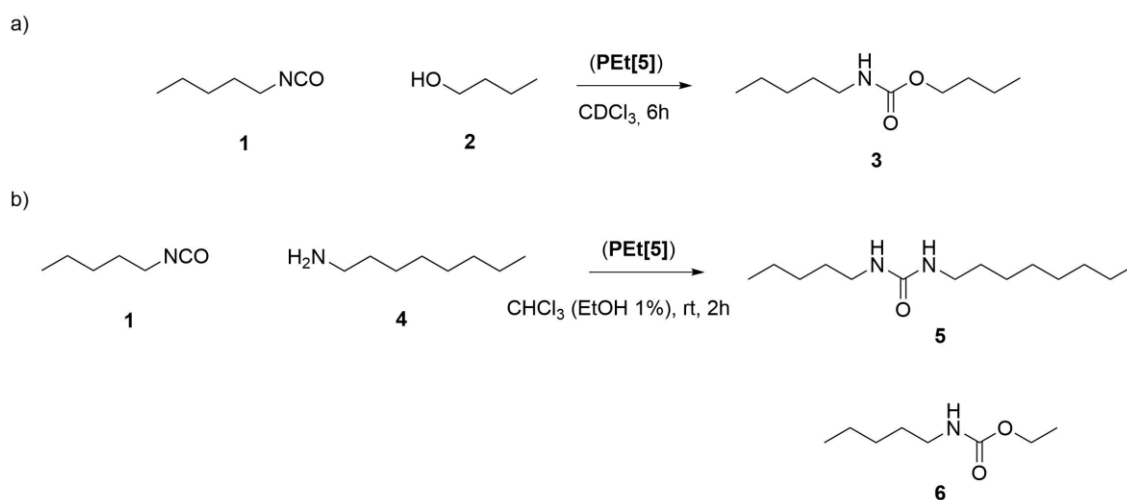
Scheme 5.1 *Synthesis in the presence and in the absence of* ***PEt[5]*** *of (a)* ***3****, (b)* ***5*** *and* ***6***.

All the species involved in the carbamoylation (Scheme 5.1a) were initially present at the equimolar concentration of 56 mM in 800 μl of CDCl$_3$ and the reaction was monitored by ^{1}H NMR. After roughly 4 h product **3** was formed in 61% yield, while in the presence of the equimolar amount of **PEt[5]**, **3** was observed in only 43% yield (Figure 5.2). Indeed, the presence of the cyclic pentamer inhibited the reaction, probably because of the high affinity showed by

the electrophilic substrate for the host cavity that protects the substrate thus reducing its conversion into the corresponding product.
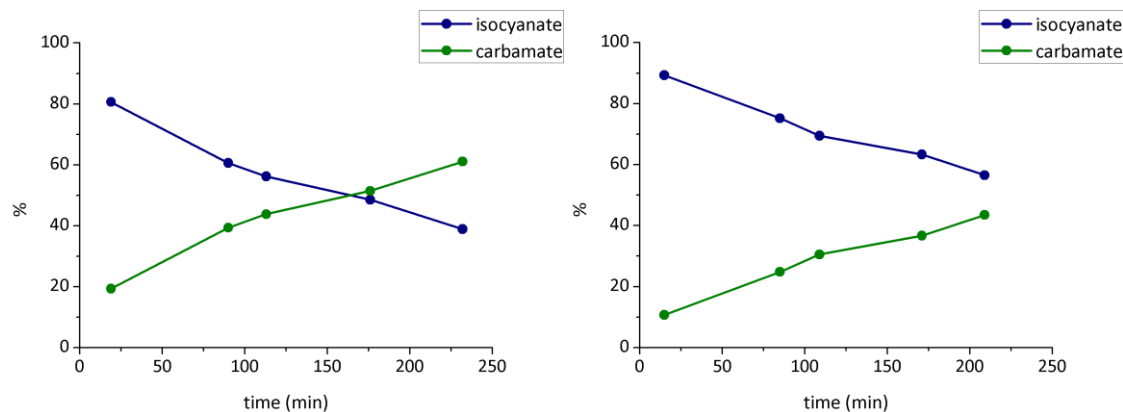

Figure 5.2 *Plot of the product distribution for the reaction between* **1** *and* **2** *in the absence (left) and in the presence (right) of* **PEt[5]**. *[1]=[2]=[PEt[5]]= 56 mM, chloroform-d 0.8 ml, room temperature.*

Similarly, we monitored by ^{1}H NMR the formation of **5** but, due to the complexity of the resulting spectra, any good consideration about **PEt[5]** catalytic activity could not be derived. Therefore, we decided to study the reaction between **1** and **4**, carried out at the equimolar concentration of 56 mM, through GC-MS analysis in 800 µl of CHCl$_3$ stabilized by 1% of EtOH (Scheme 5.1b). After 1h in the absence of **PEt[5]**, **5** was formed in 26% yield and another adduct, deriving from the side reaction of the stabilizer EtOH with **1**, ethyl pentylcarbamate (**6**), was observed in 40% yield (Figure 5.3 left). The reason behind the low conversion of the substrate into **5** relied on the poor stability of the product itself, which decomposed whether into the original **1** and **4** (Scheme 5.2a) or into a secondary octyl isocyanate (**7**) and pentyl amine (**8**) (Scheme 5.2b) for more than 35%. On the contrary, the presence of **PEt[5]** favored the formation of product **5** (79%) compared to **6** (6%), increasing in addition the stability of **5** which decomposed into **1** and **7** for less than 13% (Figure 5.3 right).
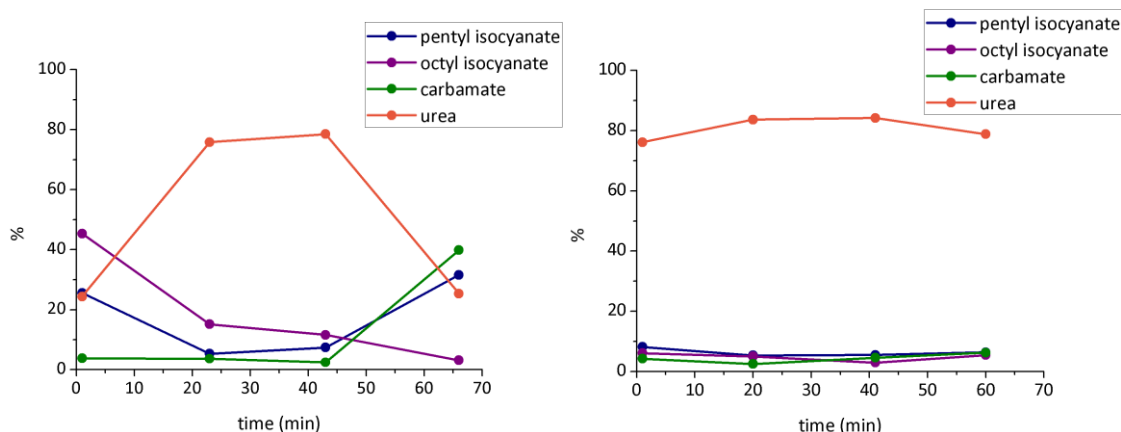
***Figure** 5.3 Plot of the product distribution for the reaction between **1** and **4** in the absence (left) and in the presence (right) of **PEt[5]**. [**1**]=[**4**]=[**PEt[5]**]= 56 mM, chloroform 0.6 ml, room temperature.*
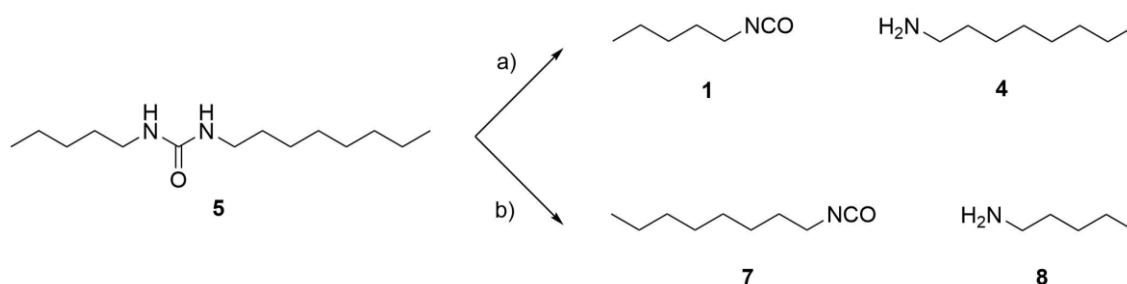
***Scheme** 5.2 Decomposition of **5** into **1** and **4** or **7** and **8**.*

The products instability observed by GC-FID, probably due to the analytical method itself, and the difficult interpretation of the NMR spectra prevented us to study further this class of reactions.

5.2.3. Oxidation of 2-Chloroethyl Ethyl Sulfide

From the NMR investigations 2-chloroethyl ethyl sulfide (**9**), when complexed within **PEt[5]**, showed significant up-field shifted peaks for the protons close to the halide. We therefore decided to investigate its reactivity upon oxidation with a water solution of H_2O_2 (30% w/w) in the presence of the cyclic pentamer as catalyst. Both reactions were performed in a 2 ml vial in $CDCl_3$ under vigorous stirring at room temperature for 2 days, at the equimolar concentration of 56 mM for all the chemical species involved and the reactions were monitored by ^{1}H-NMR. In the absence of **PEt[5]** the oxidation of **9** proceeded slowly with a conversion of 28% into the desired product 2-chloroethyl

ethyl sulfoxide (**10**) after two days. Similarly, in the presence of **PEt[5]**, after 2 days of reaction, **10** was obtained in 35% yield. Such low conversions were justified by the aqueous nature of the oxidant which was not homogeneously dispersed in the organic solutions and–we did not observe any phase transfer effect performed by **PEt[5]** which could help to favor the solubilization of the oxidant in the organic phase through H-bonding. For this reason, we did not try any further similar reactions and we concentrated our attentions on homogeneous systems in organic media.

5.2.4. *Nucleophilic Substitution of Aliphatic Bromides and Octylamine*

The next reactions we investigated was the nucleophilic substitution of aliphatic bromides with octylamine. We firstly evaluated the catalytic activity of **PEt[5]** in the equimolar reactions (concentration set at 56 mM for all species) of bromobutane (**11**) with octylamine and of bromododecane (**12**) with octylamine, both in $CDCl_3$ after 3h heating at 65 °C. In both reactions catalyzed by **PEt[5]** a small amount of the corresponding secondary amines (**13** and **14** respectively) was observed (around 1%), while, in the absence of the catalysts the formation of the products **13** and **14** was negligible.

Since both bromides had similar affinity for **PEt[5]** we decided to investigate the possible substrate selectivity induced by the presence of macrocycle, by performing a competitive reaction with both aliphatic bromides together as substrate and octylamine in the presence of **PEt[5]** (Scheme 5.3). Since the characteristic peaks of the products overlapped in the ^{1}H-NMR spectrum, the reaction was studied by GC-MS, where the retention times of the products were different enough to allow a clear interpretation.
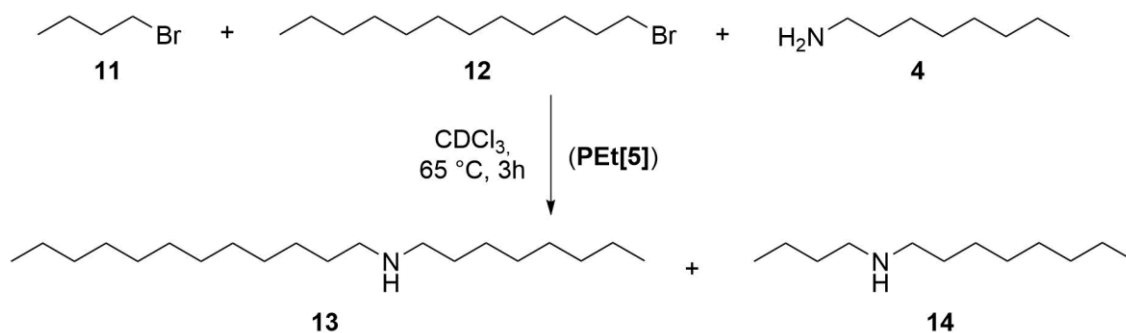
***Scheme* 5.3** *Nucleophilic substitution between aliphatic bromides and octylamine in the presence of **PEt[5]** at room temperature or 65 °C.*
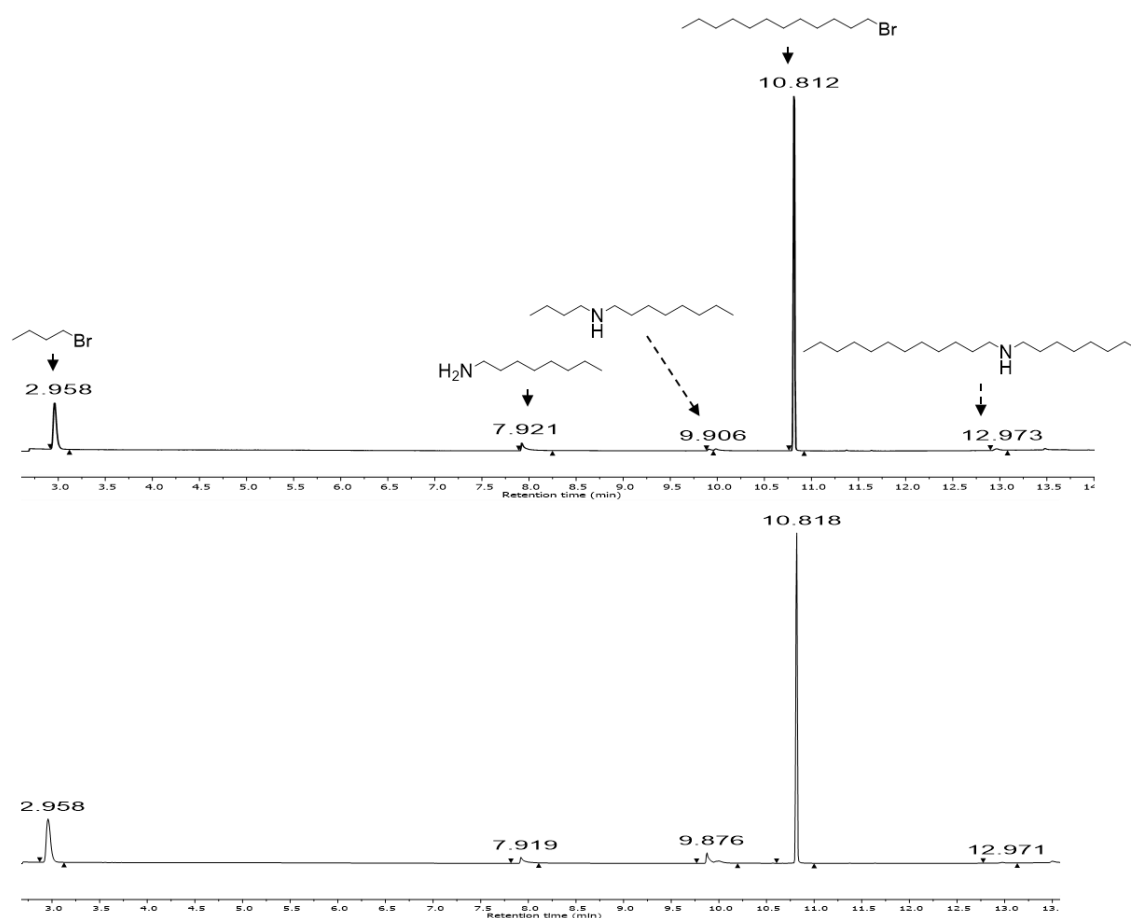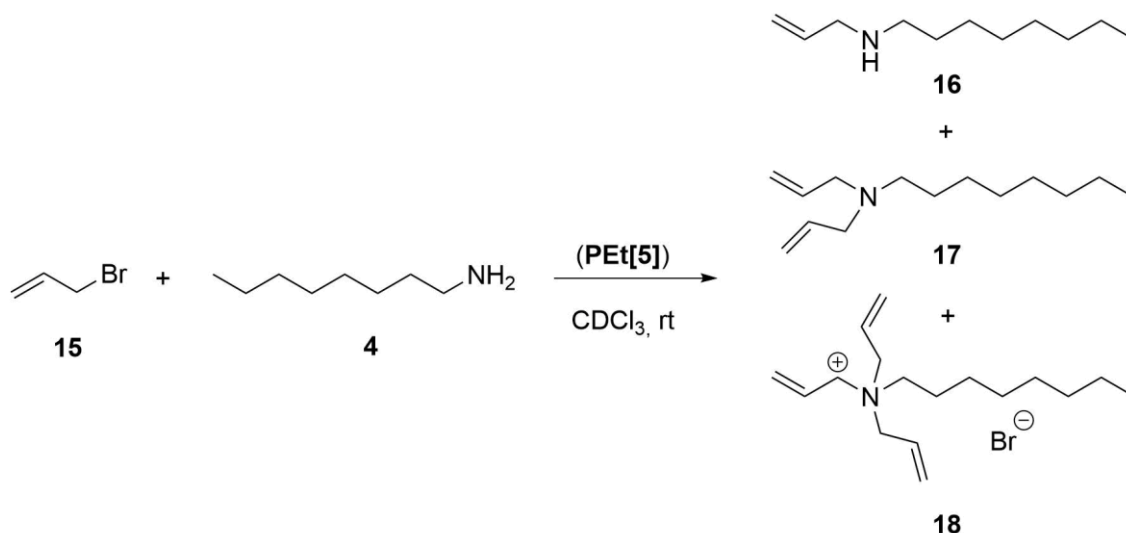

***Figure* 5.4** *GC-FID spectra of the reaction between bromobutane, bromododecane and octylamine in the absence of **PEt[5]** (top) and in the presence of **PEt[5]** after 70 min of reaction (bottom). [octylamine]=[bromobutane]=[bromododecane]=[**PEt[5]**] 56 mM, CDCl₃ 0.8 ml, room temperature.*

After 3h of heating at 65 °C and in the presence of **PEt[5]** the main product was **14** (6%), while **13** was barely detectable (less than 1%). Similarly but with lower conversion, in the absence of **PEt[5]**, **14** was formed in 2% yield while **13** in 1% yield (Figure 5.4). The conversion values here reported were calculated by

integration of the corresponding peak in the GC-FID chromatograms. These results confirmed the acceleration of the reaction imparted by **PEt[5]** whose presence also enhanced the selectivity towards the smaller secondary amine **14** due to the stronger binding observed for the shorter bromide **11** with respect to the longer bromide **12**. Encouraged by these results, we investigated the reactivity of similar but more active substrates, such as those described in the next paragraph.

5.2.5. *Nucleophilic Substitution of Octylamine on Allyl Bromide*

As stated before, octylamine and aliphatic bromides when complexed within **PEt[5]**, displayed upfield shift of the resonances, while the macrocycle showed the corresponding downfield shift of the aromatic peaks. We concentrated our attention on the allyl bromide **15** which has the same binding affinity for **PEt[5]** as the aliphatic bromides already tested. Initial catalytic tests were carried out for the reaction between the same equimolar amounts of octylamine, allyl bromide and **PEt[5]** (56 mM), following the formation of the substitution products (secondary amine **16**, tertiary amine **17** and quaternary ammonium **18**) by ^{1}H-NMR spectroscopy and comparing the reaction outcome with the control experiment in the absence of **PEt[5]** (Scheme 5.4).

Scheme 5.4 *Nucleophilic substitution reaction between allyl bromide and octylamine catalyzed by **PEt[5]** in CDCl₃.*

From the analysis of the NMR spectra (Figure 5.5 and Figure 5.6) of the reactions and the plots showing the variation of the area of the substrate **4** and the products **16**, **17** and **18** over the time (Figure 5.7), it was clear that in the absence of the catalyst **PEt[5]** the reaction in more than 7 h led to the formation of the secondary amine **16** (17%) together with non negligible amounts of tertiary amine **17** (8%). After 20 h the product distribution changed, displaying a complex mixture of 18% secondary amine **16**, 18% of tertiary amine **17** and also the quaternary ammonium bromide **18** in the appreciable amount of 3%. On the contrary, already in roughly 3 h and in the presence of **PEt[5]** we observed the selective formation of the 60% of the secondary amine **16** with only 5% of tertiary amine **17** and no formation at all of the quaternary ammonium **18**. The reaction was complete in about 20 h, the secondary amine **16** was formed in 70% while tertiary amine reached only the 10% and again no appreciable quaternary ammonium **18** was observed.
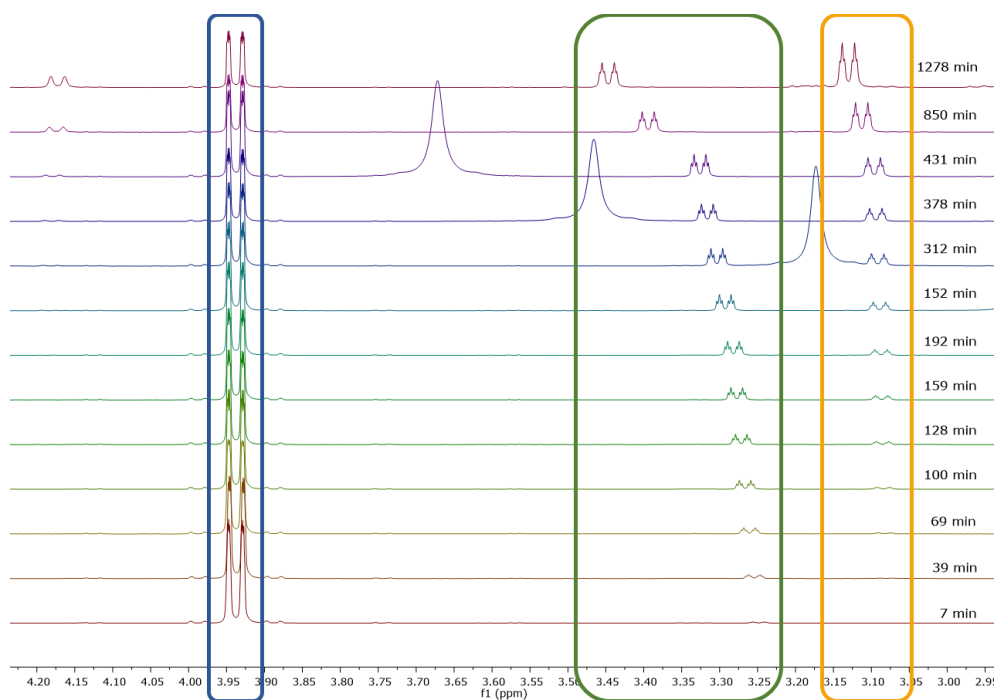
Figure 5.5 ^{1}H NMR (400 MHz, 298K, CDCl₃) Reaction between allyl bromide with octylamine in CDCl₃ in the absence of **PEt[5]** with enlightened in square boxes the peaks corresponding to NCH₂-CH=CH₂ of (blue) allylbromide **16** (green), **17** (yellow) and **18** (red). [allyl bromide]=[octylamine]= 56 mM. The peaks assignation followed literature datas[155,156]
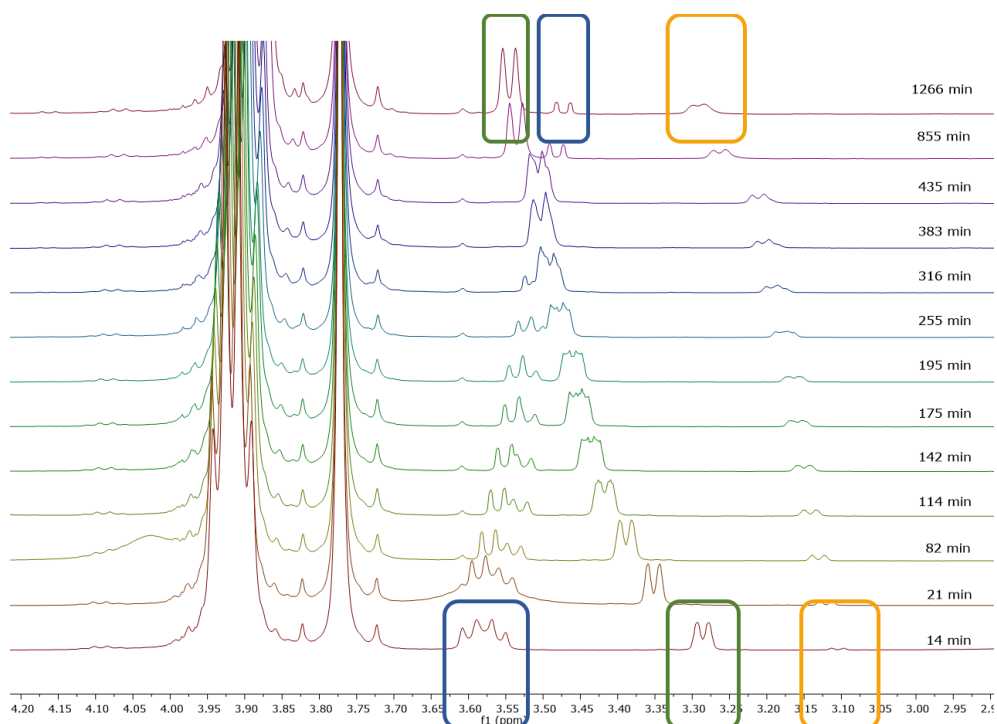
Figure 5.6 ^{1}H NMR (400 MHz, 298K, CDCl₃) Reaction between allyl bromide with octylamine in CDCl₃ in the presence of **PEt[5]** with enlightened in square boxes the peaks corresponding to (blue) octylamine, **16** (green) and **17** (yellow). [allyl bromide]=[octylamine]=[**PEt[5]**]= 56 mM.
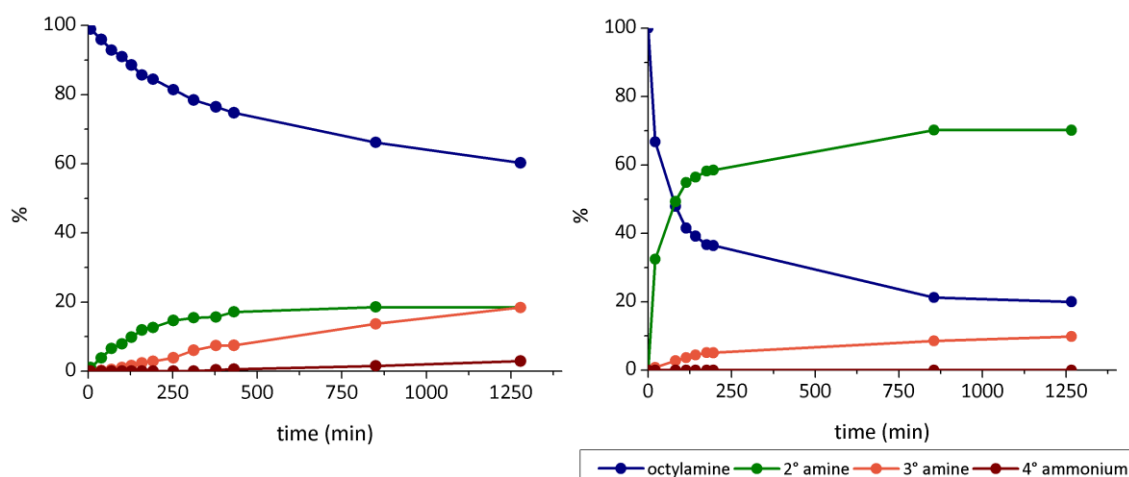
Figure *5.7 Plot of the product distribution for the reaction between octylamine, allyl bromide in the absence (left) and in the presence (right) of **PEt[5]**. [octylamine]=[allyl bromide]=[**PEt[5]**]= 56 mM, chloroform-d 2 mL, room temperature.*

It was clear that the presence of the catalyst not just increased the selectivity of the reaction towards the less substituted amine **16** favoring its formation in higher yields, but also accelerated the reaction over 17 times with respect to the uncatalyzed one. The rate acceleration was calculated in the first 100 minutes of reaction.

5.2.5.1. Different P[5] Homologues as Catalyst

A series of control experiments were carried out to disclose the role played by **PEt[5]** cavity in the reaction under study, ensuring that the activation of the substrates was due to their binding within the cavity.

Table *5.2 Substrate selectivity in the reaction between allyl bromide and octylamine mediated by different macrocycles or **DEB**.*

#	Catalyst	Time (h)	2 amine (%)	3 amine (%)	N+ (%)
1	DEB	18	33	21	0
2	PEt[6]	18	28	16	0
3	PMe[5]	100	34	4	0
4	PBu[5]	100	45	3	0

The reaction was then repeated replacing **PEt[5]** with five equivalents of **DEB**, the constituent monomer of the macrocycle, in order to mimic the presence of the electron rich aromatic surfaces in the reaction system. We observed similar activity and product distribution to the reaction without **PEt[5]** (Table 5.2, entry 1), confirming in this way the importance of the tubular shape of the macrocycle in the reaction.

The same nucleophilic substitution was tested in the presence of the larger homologue **PEt[6]**, observing after 3 h the formation of 17% secondary amine **16** and 3% of tertiary amine **17**, while, after 18 h, the amount of **16** and **17** was 28% and 16%, respectively (Table 5.2, entry 2). This demonstrated how inefficient **PEt[6]** was to catalyze the reaction although with the retention of the selectivity towards the less substituted amine. **PEt[6]**, with a nearly 30% larger internal diameter than that of **PEt[5]**, does not favor the allylic substrate encapsulation as demonstrated by binding experiments performed in solution and displayed in Figure 5.8.
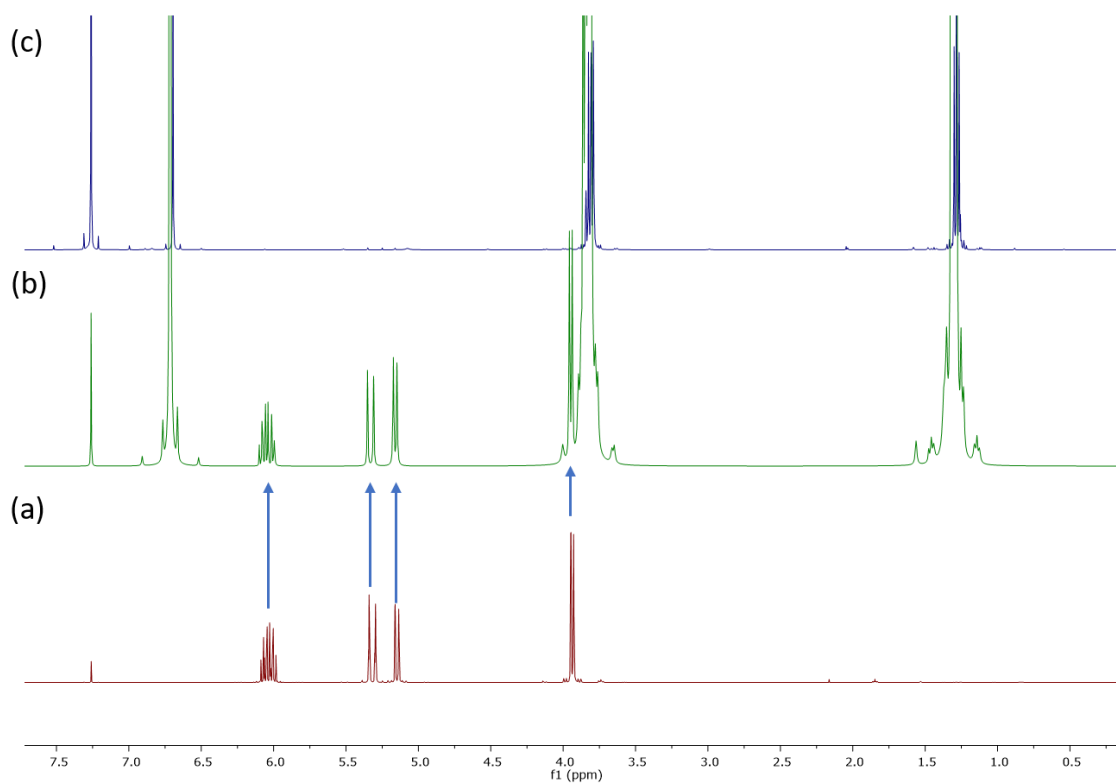
Figure 5.8 *^{1}H NMR (400 MHz, 298K, CDCl₃) spectra of a) allyl bromide (56 mM); b) allyl bromide (56 mM) and **PEt[6]** (11mM); c) **PEt[6]** (11mM).*

Finally, we decided to investigate the effect of the alkoxy groups on the rim of the cyclic pentamer **P[5]** performing the reaction in the presence of the different substituted **PMe[5]**, **PEt[5]** and **PBu[5]**. Initially the model reaction was repeated in the same molar concentration (56 mM) in the presence of the shorter **PMe[5]** leading after 100 min to 34% of the secondary amine **16**, 4% of tertiary amine **17** and 62% of residual primary amine **4** (Table 5.2, entry 3). Slightly better than the previous reaction with the longer **PBu[5]** derivative after 100 min 45% of secondary amine **16**, 3% of tertiary amine **17** and 52% or residual primary amine **4** were observed (Table 5.2, entry 4). As comparison with **PEt[5]** after the same reaction time **16** was obtained in 55%, **17** in 4% and the original substrate left was only 41%. All the products distributions were plotted as function of the time to have a more clear understanding of the differences between each system (Figure 5.9).
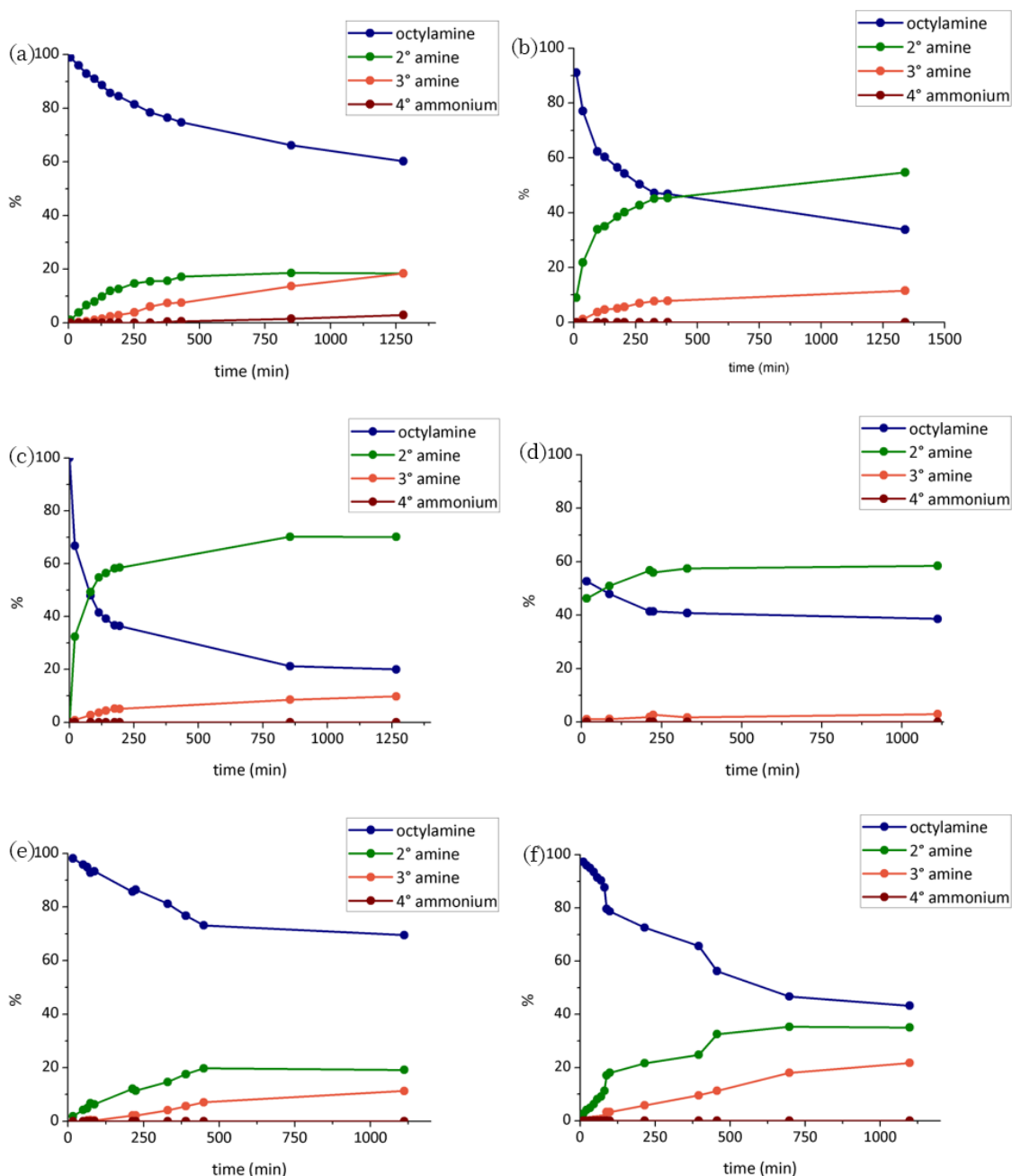
Figure 5.9 *Plot of the product distribution for the reaction between octylamine, allyl bromide (a) in the absence of any catalyst; in the presence of (b) PMe[5]; (c) PEt[5]; (d) PBu[5]; (e) PEt[6]; (f) DEB. [octylamine]=[allyl bromide]=[P[5]]=([PEt[6]]) 56 mM [DEB]=280 mM CDCl₃ 0.8 mL, room temperature.*

NMR titration performed on the allylic substrate **15** together with the different **P[5]s** showed a decreasing binding affinity as the alkoxy chain length on **P[5]** rims increased, evaluated as function of the upfield shift of the guest resonances (**PMe[5]>PEt[5]>PBu[5]**) (Figure 5.10). Nevertheless, comparing

these results with the one obtained with **PEt[5]**, the catalytic activity of the different hosts seemed only in part to be related with the complexation ability observed. Essentially in accord with this trend using **PBu[5]** we observed worse conversions than with **PEt[5]**, as expected by the host-guest affinity. Counter intuitive with respect to the strong binding with **15**, **PMe[5]** displayed lower catalytic effect than **PEt[5]** on the substitution reaction considered.
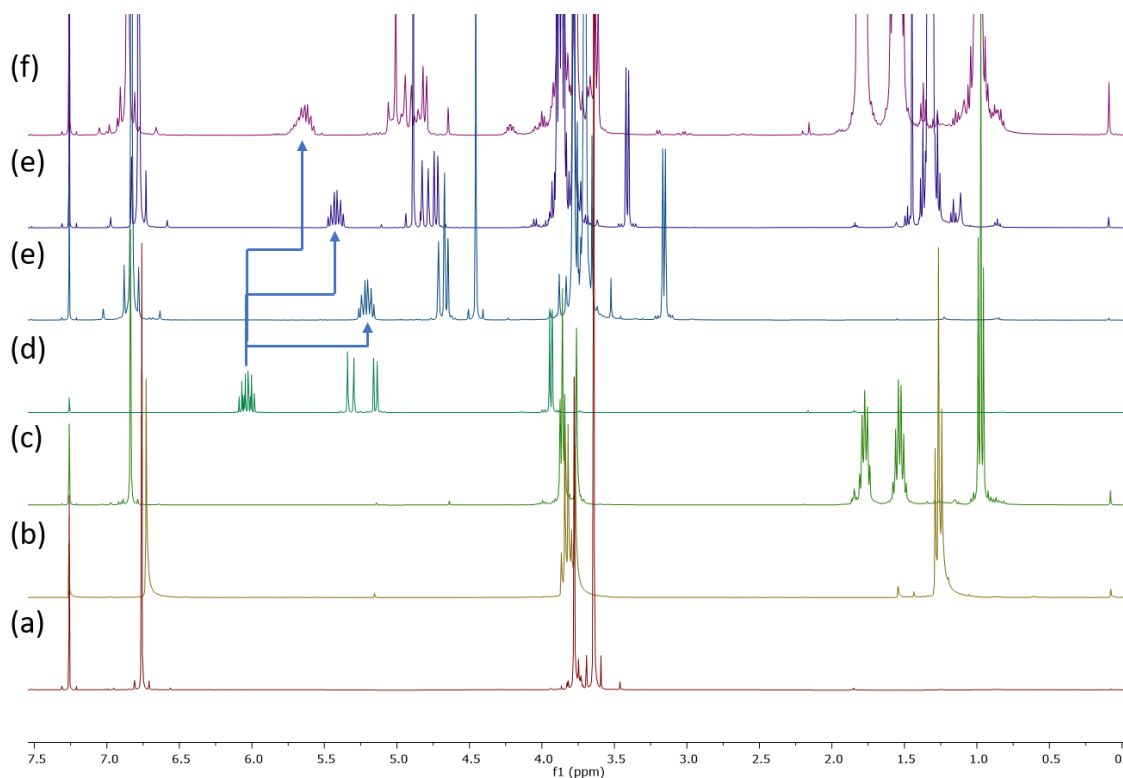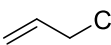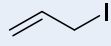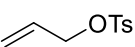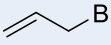
Figure 5.10 ¹H NMR (400 MHz, 298K, CDCl₃) spectra of a) **PMe[5]** (11mM); b) **PEt[5]** (11mM); c) **PBu[5]** (11mM); d) allyl bromide (56 mM) and **PMe[5]** (11mM); a) allyl bromide; e) allyl bromide (56 mM) and **PEt[5]** (11mM); f) allyl bromide (56 mM) and **PBu[5]** (11mM).

Similar to what we observed with other reactions, a strong binding between the macrocycle **PEt[5]** and the main substrate was not enough to efficiently catalyze the reaction and probably a specific combination of binding of all the species involved in the reaction is crucial to promote the reaction itself and, in this particular case among different macrocycles **PEt[5]** represented the best compromise.

5.2.5.2. *Different Allyl Halides as Substrates*

In order to give a general character to the catalysis promoted by **PEt[5]**, other allylic compounds, such as allyl iodide, chloride and tosylate, were tested as substrates together with the primary amine **4** at the equimolar concentration of 56 mM in CDCl$_3$ at room temperature.

Table 5.3 *Substrate selectivity in the reaction between different allylic substrates and octylamine mediated by PEt[5].*

#	Allylic substrate	PEt[5]	Time (h)	2 amine (%)	3 amine (%)	N+ (%)
1	Cl **19**	✓	18	22	0	0
2		-	18	0	0	0
4	I **20**	✓	21	41	13	3
5		-	21	19	14	8
6	OTs **21**	✓	17	55	13	0
7		-	25	18	6	0
8	Br **15**	✓	20	70	10	0
9		-	20	18	18	3

When allyl chloride was used as substrate (**19**) the uncatalyzed reaction did not lead to any conversion into the products **16** or **17**, while in the presence of **PEt[5]** the preferential formation of **16** was observed in 22% (Table 5.3, entries 1 and 2). With allyl iodide (**20**) as substrate, **PEt[5]** promoted the substitution with an observed 41% for the secondary amine **16**, 13% for the tertiary amine **17** and 3% for the quaternary ammonium **18** after 21h of reaction, while, without **PEt[5]**, 19%, 14% and 8% of the products **16**, **17** and **18** were observed respectively (Table 5.3, entries 3 and 4). Due to the lower affinity of **20** for the cavity, confirmed by the lower upfield shift of the allylic resonances compared to allyl bromide, the reaction on **20** showed lower efficiency than the case study with **15** (Table 5.3, entries 8 and 9). Those results were also graphically represented in

Figure 5.11 to better illustrate the products distribution over the time of the reaction.
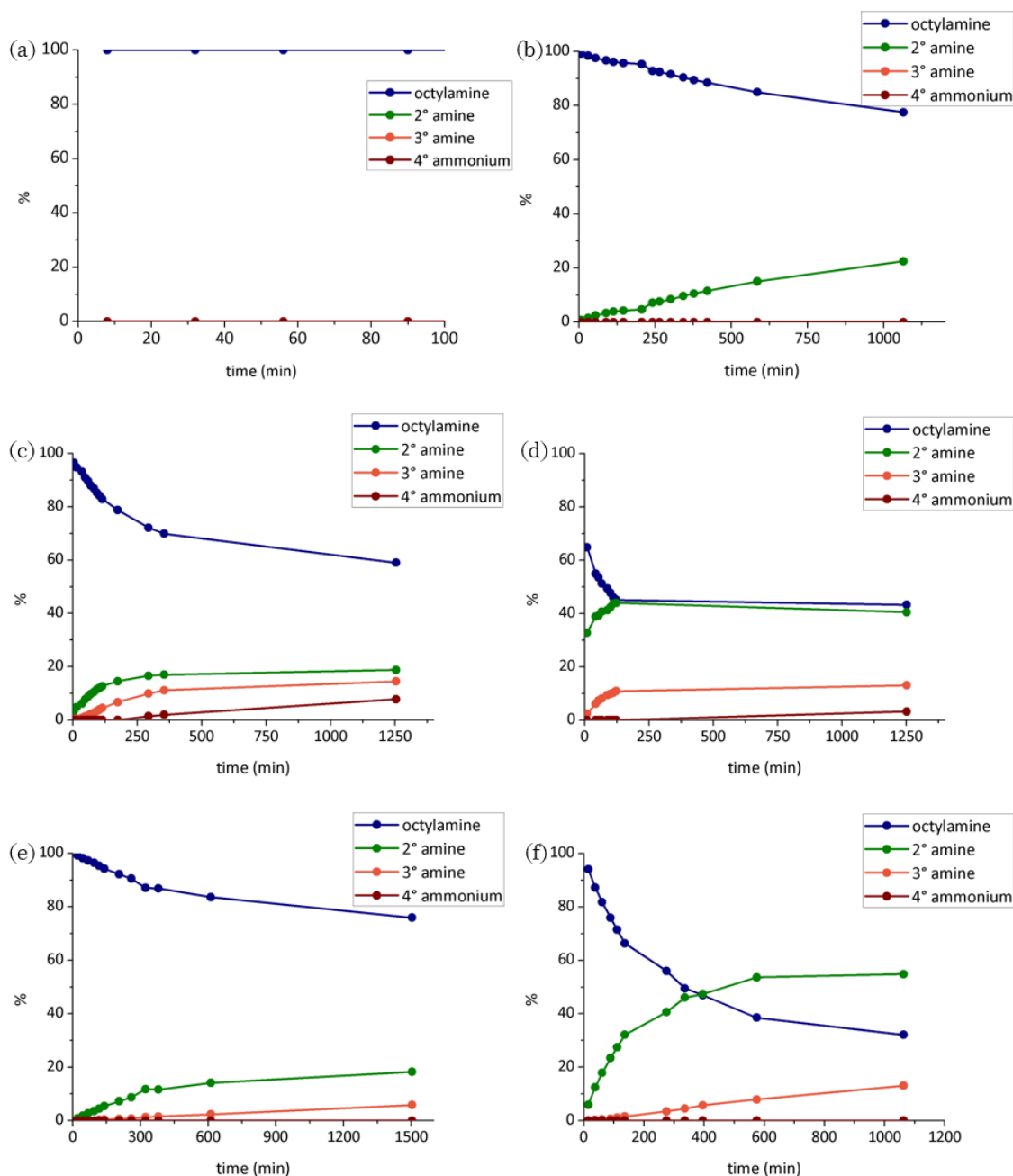
*Figure 5.11 Plot of the product distribution for the reaction between octylamine, (a) allyl chloride in the presence of **PEt[5]**; (b) allyl iodide in the absence of **PEt[5]**; (c) allyl iodide in the presence of **PEt[5]**; (d) allyl tosylate in the absence of **PEt[5]**; (e) allyl tosylate in the presence of **PEt[5]**;. [octylamine]=[allylic substrate]=[**PEt[5]**]= 56 mM, CDCl₃ 0.8 mL, room temperature*

Together with these allyl halides, another allylic substrate, the allyl tosylate **21**, was tried as electrophile in the reaction with octylamine. From the NMR titration it was clear that the interaction between **21** and **PEt[5]** cavity involved

the methyl group of the aromatic ring of **21** rather than the allyl moiety. The activation of the allylic substrate occurred in a different way compared to the allyl halides considered so far, and therefore, this result could not be really compared with the other. Nevertheless, after 17 h the presence of **PEt[5]** in the reaction (Table 5.3, entry 6) led to the formation of 55% of **16** and 13% of **17**, while in its absence after 25 h **16** was formed in 18% and **17** in 6% (Table 5.3, entry 7).
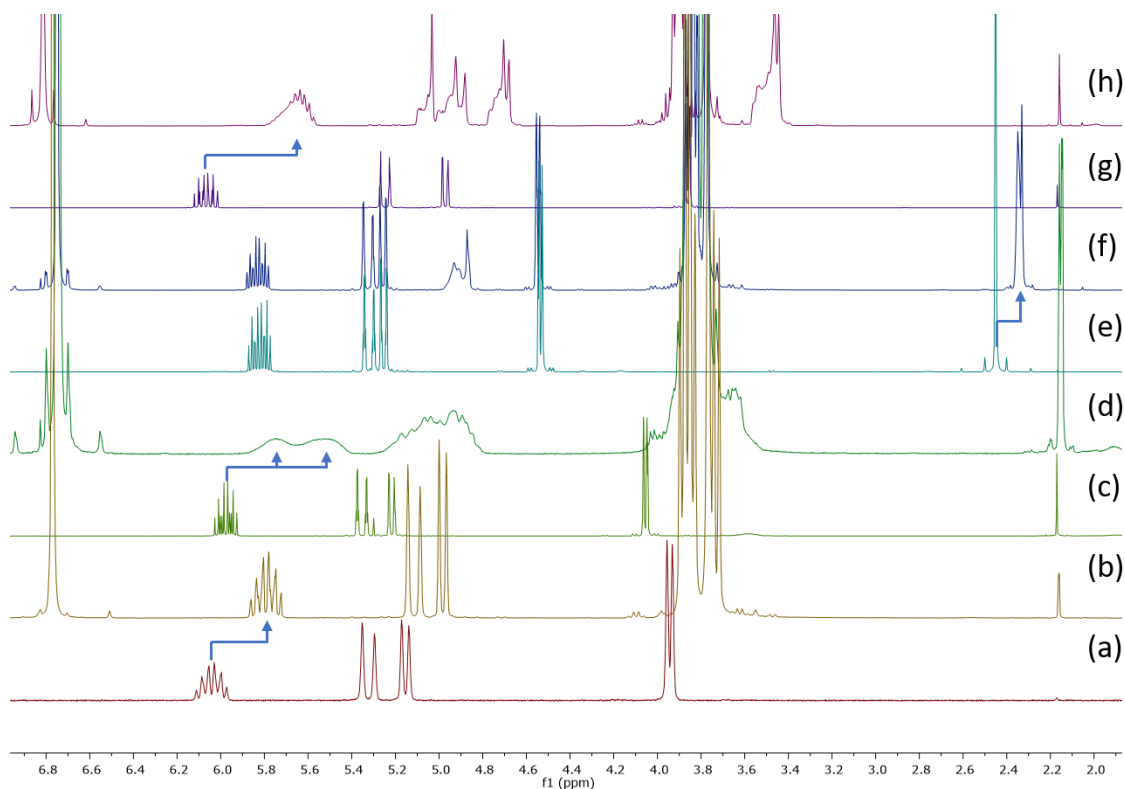
Figure 5.12 *¹H NMR (400 MHz, 298K, CDCl₃) spectra of a) allyl bromide (56 mM); b) allyl bromide and **PEt[5]** (14 mM); c) allyl chloride (56 mM); d) allyl chloride and **PEt[5]** (14 mM); e) allyl tosylate (56 mM); f) allyl tosylate and **PEt[5]** (14 mM); g) allyl iodide (56 mM); h) allyl iodide and **PEt[5]** (14 mM)*

General considerations on the results obtained could be derived on the basis of the reactivity of the substrates together with their steric hindrance rather than their binding affinity toward **PEt[5]** (Figure 5.12). In fact, from the NMR spectra the most promising substrates were the allyl iodide and chloride. However, even though **20** led to a doubled amount of the secondary amine **16** compared to **19**, their conversion was lower than the one of **15** in the same experimental conditions.

The leaving group ability, and therefore the intrinsic reactivity of these allylic compounds (OTs>I>Br>Cl), was partially in agreement with our experimental observations explaining the reason why **19** was less reactive than **15** in the reaction under study. Although **20** was supposed to be more intrinsically reactive, it was too large to fit into **PEt[5]** cavity together with the octylamine as nicely as **15**, displaying lower upfield shift of the resonances in the presence of the amine **4** and the macrocycle (Figure 5.13f) with respect to the complexation experiment between only the allylic substrates and **PEt[5]** (Figure 5.13e).
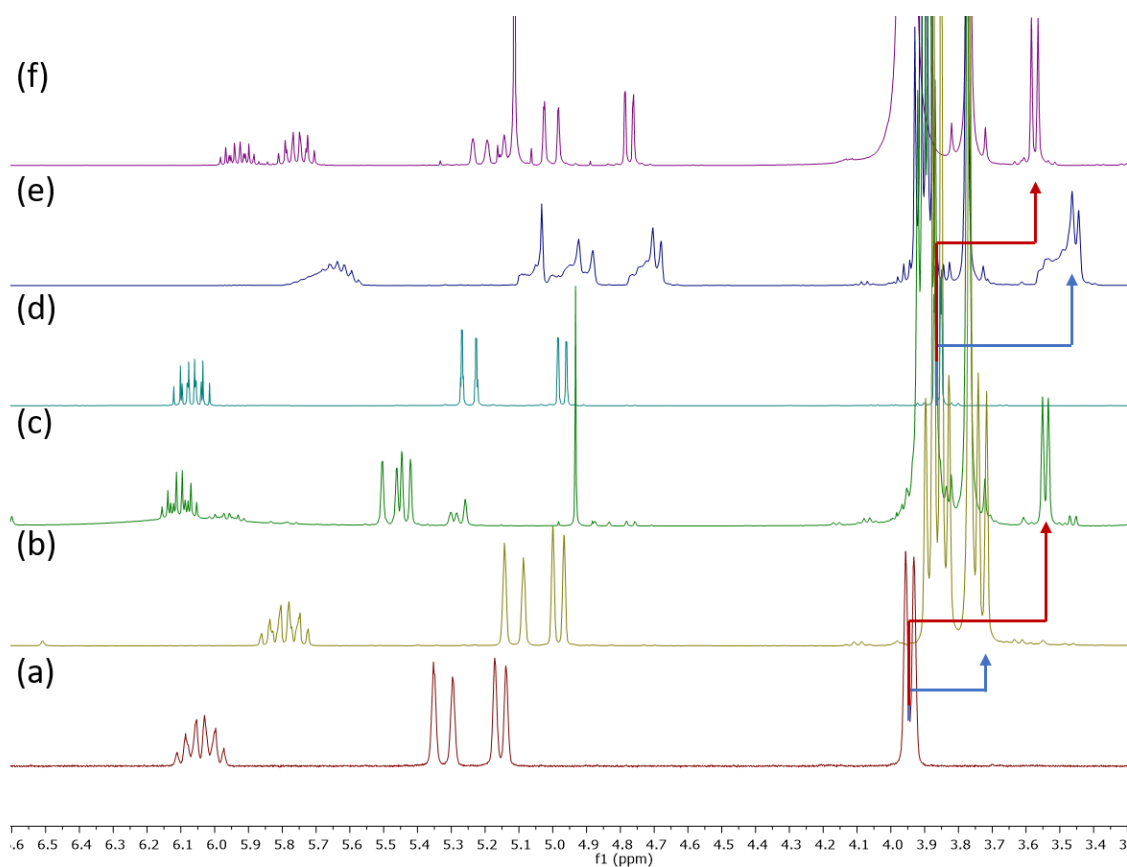
Figure 5.13 *¹H NMR (400 MHz, 298K, CDCl₃) spectra of a) allyl bromide (56 mM); b) allyl bromide and **PEt[5]** (14 mM); c) allyl bromide with octylamine and **PEt[5]**; d) allyl iodide (56 mM); e) allyl iodide and **PEt[5]** (14 mM); f) allyl iodide with octylamine and **PEt[5]**. Up-field shift on the allylic resonance upon complexation with **PEt[5]** enlightened in blue, upfield shift on the allylic resonance upon complexation with **PEt[5]** and octylamine enlightened in red.*

Once again a combination of factors explained such a high reactivity we observed for the allyl bromide **15** with the octylamine **4** in the presence of **PEt[5]**.

5.2.5.3. *Broadening the Range of Substrates with Propargyl Bromide*

A similar reaction was carried out on a substrate bearing the same leaving group and number of carbon atoms with a different unsaturation grade. The reaction between propargyl bromide **22** and **4** in the presence of **PEt[5]** (Scheme 5.5) was studied through ^{1}H-NMR and GC-MS analysis and the results plotted in Figure 5.14.
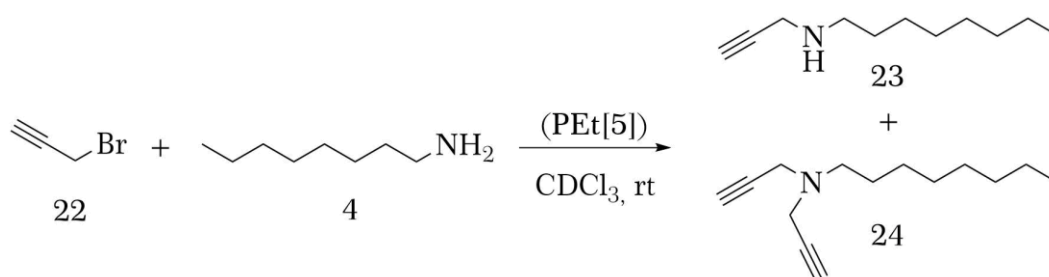
Scheme 5.5 *Nucleophilic substitution between propargyl bromide and octylamine in the presence of **PEt[5]***

After more than 20 h the reaction conducted within **PEt[5]** cavity led to the formation of 30% of the secondary amine **23** and 23% of the tertiary amine **24**, while in the same time and in the absence of the macrocycle 32% of **23** and 3% of **24** were observed, showing how the presence of the cyclic pentamer increased the overall conversion of the substrate into the substitution products. The reaction performed with **PEt[5]** had worse selectivity with respect to the reaction without **PEt[5]**, since in the first case the amount of **24** formed was closer to the amount of **23** (Figure 5.14 right) than in the latter case (Figure 5.14 left). Nevertheless, the reaction in the presence of the cyclic pentamer in the first 200 minutes led to 23 faster than the uncatalyzed reaction, losing the selectivity achieved at the beginning only over the time.
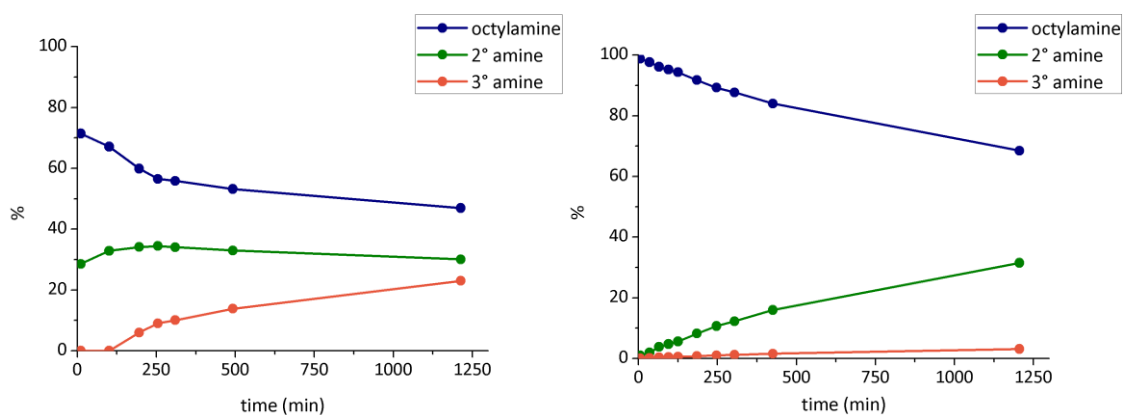
***Figure* 5.14** *Plot of the product distribution for the reaction between octylamine and propargyl bromide in the presence (left) and in the absence (right) of **PEt[5]**. [octylamine]=[propargyl bromide]=[**PEt[5]**] 56 mM, CDCl$_3$ 0.8 mL, room temperature.*

5.2.5.4. Different Amines as Nucleophiles
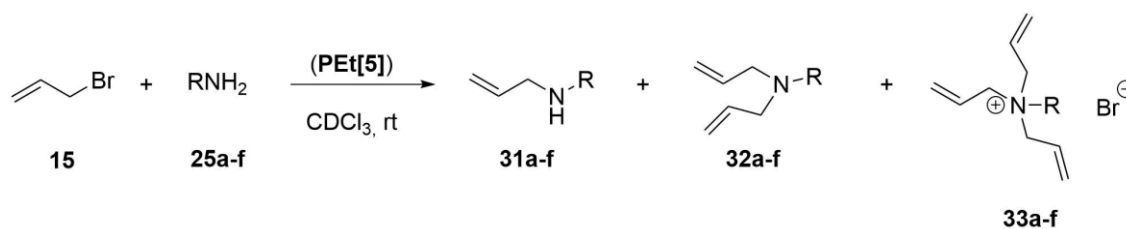
***Scheme* 5.6** *Nucleophilic substitution between allyl bromide and various amines in the presence of **PEt[5]**.*

Once we had established the best electrophile in the reaction we investigated the effect of the size and shape of the nucleophile performing the model reaction on various primary amines (**25a-f**), listed in Table 5.4, which led to the formation of the common substitution products **31** (**a-f**), **32** (**a-f**) and **33** (**a-f**) (Scheme 5.6).

Table 5.4 *Substrate selectivity in the reaction between different primary amines and allyl bromide mediated by* **PEt[5]**.

#	Amine	PEt[5]	Time (h)	2 amine (%)	3 amine (%)	N+ (%)
1	**25a**	✓	6	52	6	0
2		-	18	14	8	0
3	**25b**	✓	18	61	0	0
4		-	18	18	0	0
5	**25c**	✓	18	35	7	0
6		-	18	29	13	1
7	**25d**	✓	18	14	0	0
8		-	18	16	0	0
9	**25e**	✓	19	42	23	0
10		-	19	20	23	2

As it was clear from the observed product distribution linear narrow primary amines such as the long hexadecylamine **25a** and the shorter 2-methoxy-ethylamine **25b** both showed enhanced product formation in the presence of **PEt[5]** leading in the first case to 52% of **31a** and 6% of **32a** and to 61% of **31b** respectively (Table 5.4, entries 1-4). Without **PEt[5]** the amine conversion was definitely smaller with only 14% of **31a**, 8% of **32a** and 18% of **31b** formed. A similar behavior was showed by the linear hexylamine **25e** where in the presence of **PEt[5]** led after 18 h to the formation of 42% of **31e** and 20% of **32e** and without the catalyst the same amines **31e** and **32e** were observed in 20% and 23% respectively(Table 5.4, entries 9-10). No formation at all of the quaternary ammonium salt was observed in the presence of **PEt[5]**, while in its absence **25e** led to a small amount of the respective quaternary ammonium. As observed all

over this chapter, **PEt[5]** increased the selectivity of all these reaction favoring the secondary amine rather than the tertiary amine products. On the contrary, larger amines like cyclohexylamine (**25c**) and 1-phenyl-ethylamine (**25d**) did not show substantial acceleration of the product formation and their activity was substantially equivalent to the reaction in the absence of **PEt[5]** (Table 5.4, entries 5-8). We explained the inactivity of the amines **25c** and **25d** in the reaction under study on the basis of the poor binding showed towards the macrocycle **PEt[5]**, due to the steric hindrance of the branched part of **25c** and **25d** which barely fitted inside the cavity. From all these experiment it was clear that, together with products selectivity for secondary amines and reaction rate acceleration, **PEt[5]** showed also substrate selectivity for linear amines.
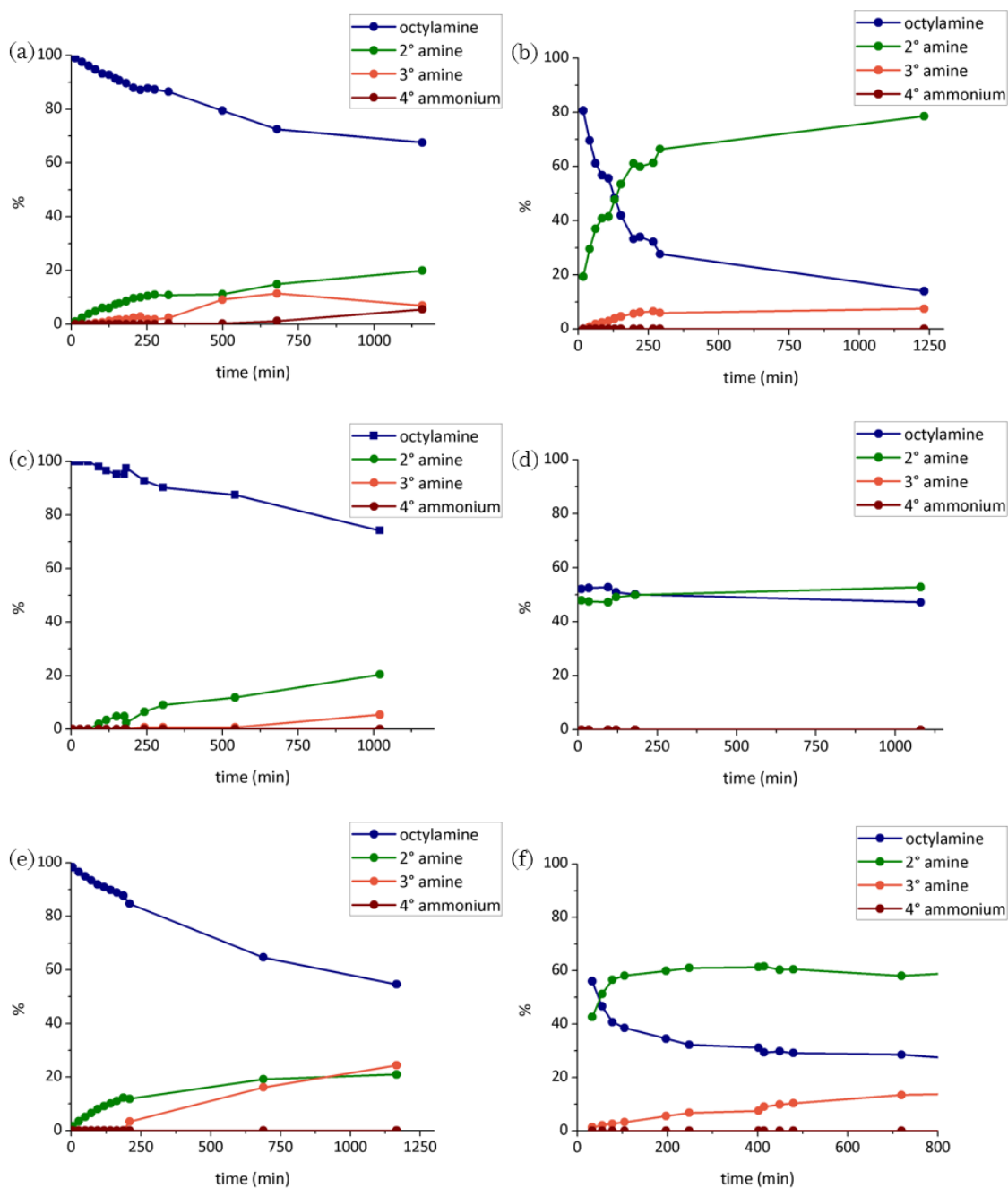
*Figure 5.15 Plot of the product distribution for the reaction between allyl bromide and a) hexadecylamine in the absence of **PEt[5]**; b) hexadecylamine in the presence of **PEt[5]** c) 2-metossi-ethylamine in the absence of **PEt[5]**; d) 2-metossi-ethylamine in the presence of **PEt[5]** e) hexylamine in the absence of **PEt[5]**; f) hexylamine in the presence of **PEt[5]**. [amine]=[allyl bromide]=56 mM, CDCl₃ 0.8 mL, room temperature.*

The products distributions were plotted as function of the time for the linear amines **25a**, **25b**, **25e** in order to better appreciate the differences between the catalyzed and the uncatalyzed reactions (Figure 5.15).

5.2.5.5. *Improving the Efficiency of the Reaction*

During the reactions studied so far, we observed the formation of HBr, an undesired side-product which is likely to inactivate the nucleophilic amines forming the corresponding ammonium cation and to hamper in this way the reactivity of the substrates. The problem could be avoided by adding to the reaction mixture a compound able to interact with HBr leaving all the other chemical species untouched. We therefore repeated the model reaction between the octylamine and allyl bromide in the presence of di-isopropylethylamine (**DIEA**) as a scavenger for the Brønsted acid in equimolar amount with respect to the reagents (Figure 5.16). The nucleophilic substitution was studied in the presence of the cyclic pentamer and compared to the same reaction in its absence. The same reactions were also performed with the shorter butylamine (**34**), to prove the possible general improvement given by **DIEA** (Scheme 5.7).
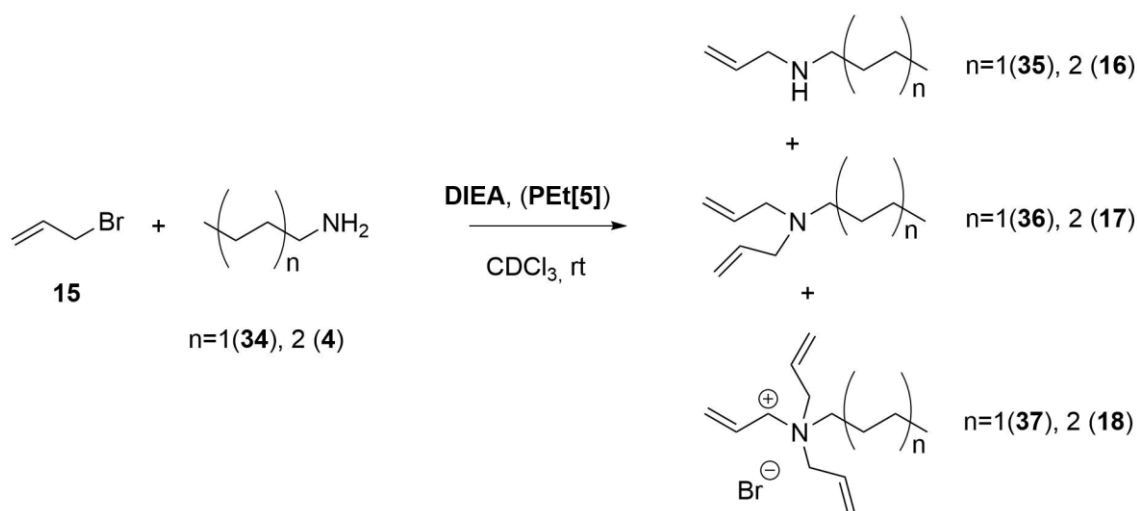
Scheme 5.7 *Nucleophilic substitution between allyl bromide and octylamine or butylamine with DIEA in the presence of PEt[5].*

The addition of **DIEA** improved both the reactions in terms of overall conversion, leading to 24% of **16** and 23% of **17** without **PEt[5]** and to 72% of **16** and 14% of **17** with **PEt[5]** (Figure 5.16a and Figure 5.16b). In the presence of **PEt[5]**, the conversion of **34** was even higher than the model substrate **4**, with the formation of the secondary amine **35** over 79% and 10% of the tertiary amine **36** (Figure 5.16d). The shorter butylamine **34** reacted even better than the longer octylamine **4** because of its smaller dimensions which favored the inclusion

within **PEt[5]** cavity together with allyl bromide. In both the reaction the addition of **DIEA** turned out to be a good strategy to increase the overall substrates conversion leaving intact the selectivity of the reaction.
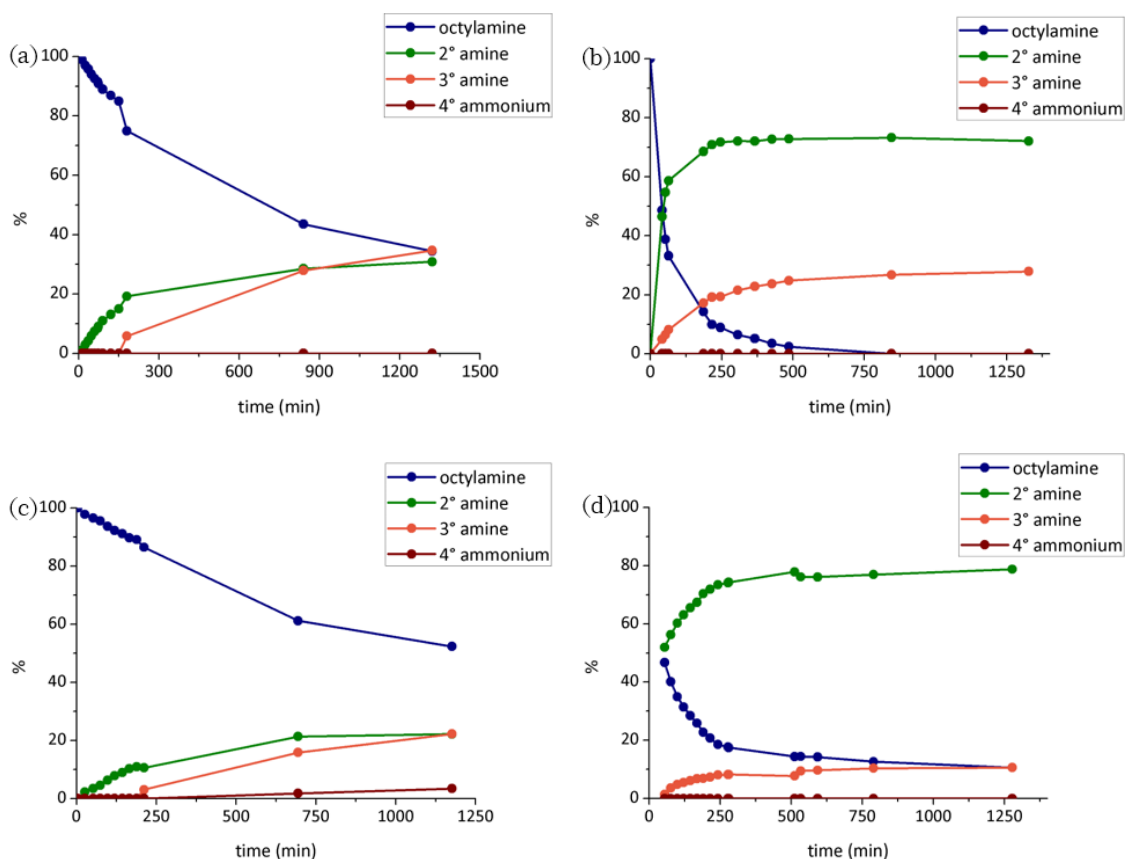
*Figure 5.16 Plot of the reaction between octylamine and allyl bromide with **DIEA** (a) in the absence of **PEt[5]** and (b) in presence of **PEt[5]**. Plot of the reaction between butylamine and allyl bromide with **DIEA** (a) in the absence of **PEt[5]** and (b) in presence of **PEt[5]**. [amine]=[allyl bromide]=[**PEt[5]**]=[**DIEA**] 56 mM, CDCl₃ 0.8 ml, room temperature.*

Furthermore, the model reaction between octylamine and allyl bromide was tested with a sub-stoichiometric amount of **PEt[5]**, observing that with 50 mol% of supramolecular catalyst with respect to the substrates, the reaction led after 20 h to the formation of 66% of **16** and 4% of **17**, with no substantial change in the products distribution compared to the reaction with stoichiometric amount of **PEt[5]**. In addition, the macrocyclic catalyst was recycled by recovered by precipitation with methanol and after drying under vacuum was re-used for the same reaction observing formation of **16** and **17** in 67% and 4%, respectively, confirming the possible reuse of the supramolecular catalyst.

5.2.5.6. S_N1 or S_N2 Mechanism: Nucleophilic Substitution of Crotyl Bromide and Octylamine

The allylic nucleophilic substitution, due to resonance stabilization, could in principle occur through a carbocation intermediate (S_N1) or through a highly stabilized transition state with the two substrates together (S_N2) (Scheme 5.8).
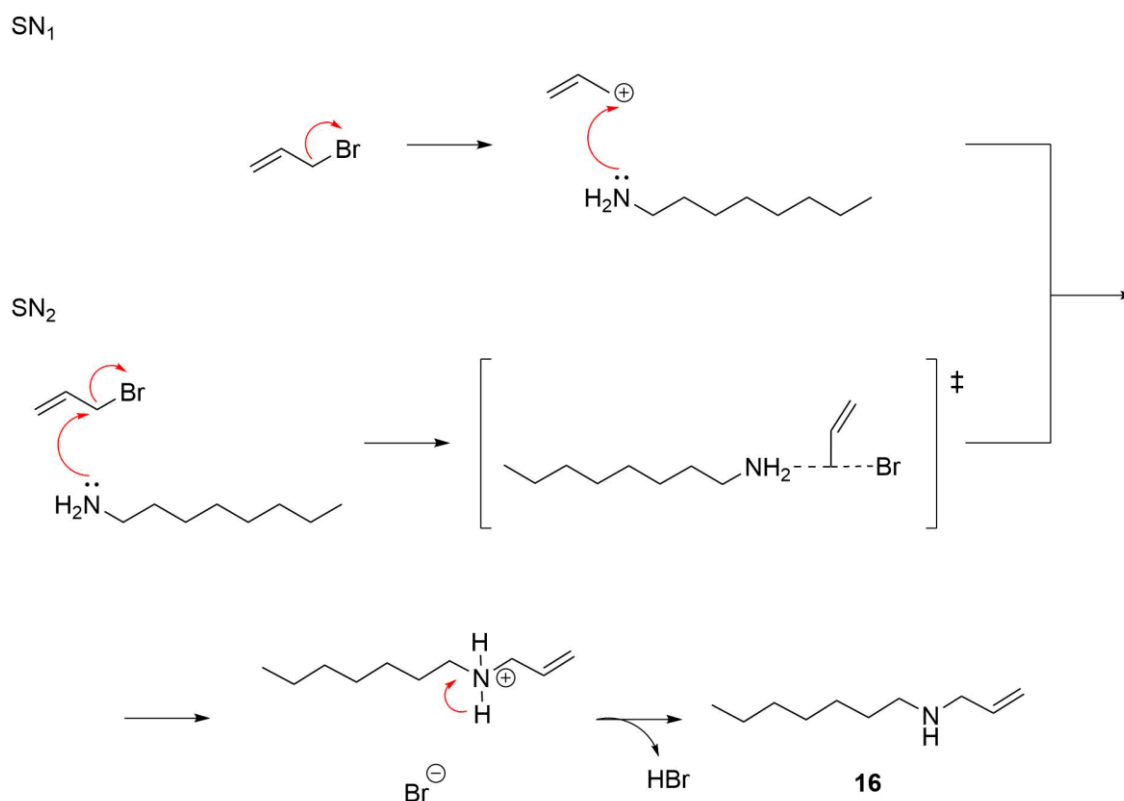
Scheme *5.8 S_N1 or S_N2 mechanisms for the reaction between allyl bromide and octylamine*

In the S_N1 mechanism, the cationic intermediate formed by the bromide separation could be attacked by the lone pair present on the nitrogen of the octylamine, while in the S_N2 mechanism, the attack performed by the octylamine is concerted to the separation of the bromide, leading to a transition state in which the nucleophile was not completely attached and the leaving group was not yet detached. In both cases, after deprotonation, the secondary amine **16** could be obtained.

Allyl halides are known to undergo both mechanisms depending of the reaction conditions, and, in order to discriminate which pathway was predominant in our system, we decided to perform this model reaction with the

commercially available crotyl bromide **38** as substrate (mixture of cis- and trans isomers 1:5) (Scheme 5.9) in CDCl$_3$ at room temperature.
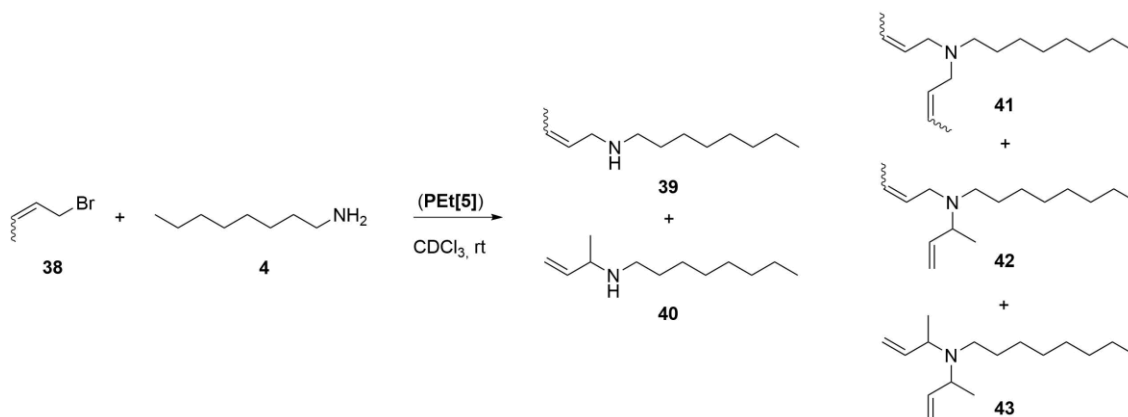
Scheme 5.9 *Nucleophilic substitution between crotyl bromide and octylamine*

Due to the nature of the substrate the rearrangement of the carbocation in the S$_N$1 mechanism could lead more probably to the branched secondary amine **40** than to the linear secondary amine **39**. In the case of a pure S$_N$2 mechanism instead, the linear **39** should be formed, or considering another possible attack of the amine from the back of the crotyl system the branched amine **40** should be formed as preferential products. The so formed secondary amine could further react with the allylic substrate again with S$_N$1 or S$_N$2 mechanism, leading in the first case to all the substitution products, while the latter pathway would only to **41** or only to **43**. The reaction was performed in the presence of **PEt[5]** and compared with the model reaction without the catalyst.
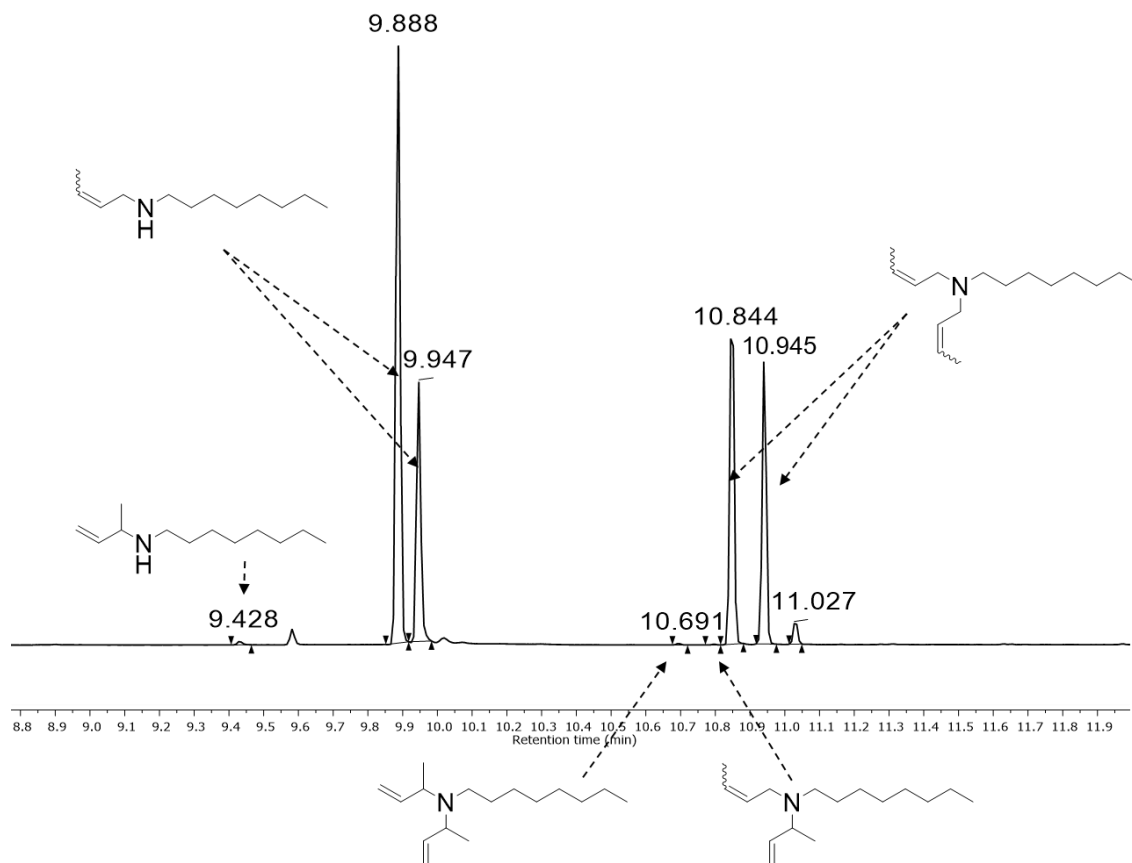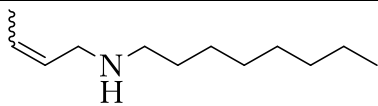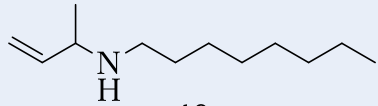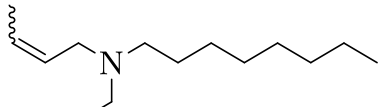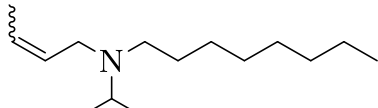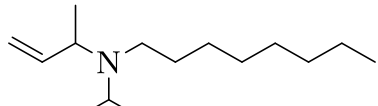
***Figure* 5.17** *GC-FID spectrum zoomed between retention time = 9 min and retention time = 11.6 min of the reaction between crotyl bromide and octylamine in the presence of **PEt[5]** after 30 min of reaction. [octylamine]=[crotyl bromide]=[**PEt[5]**] 56 mM, CDCl₃ 0.8 mL, room temperature.*

From the ¹H-NMR the discrimination between the different amines was not clear and therefore the correct distribution was evaluated by GC-MS analysis, resulting, after 30 min of reaction in the presence of **PEt[5]**, in 23% of **39** and 16% of **41** (Table 5.5, entries 1 and 5) while the branched amines **40**, **42** and **43** were barely observed (Table 5.5, entries 3, 7 and 9). Without the catalyst, the reaction showed the same product distribution but with less efficiency, leading only to 13% of **39** and 7% of **41** (Table 5.5, entries 2 and 6).

Table 5.5 *Substrate selectivity in the reaction between octylamine and crotyl bromide (isomeric mixture) mediated by* **PEt[5]**.

Entry	Products	PEt[5]	Time(min)	%
1		✓	30	23
2	**39**	-	30	13
3		✓	30	<1
4	**40**	-	30	<1
5		✓	30	17
6	**41**	-	30	7
7		✓	30	<1
8	**42**	-	30	<1
9		✓	30	<1
10	**43**	-	30	<1

It is worth to mention that in the reactions so far studied the catalytic effect of **PEt[5]** was strongly dependent to the host-guest affinity of all the substrates involved in the reaction, modulated by the whole steric hindrance of the electrophile and the nucleophile. These considerations, together to the product distribution we observed in the latter experiment, led us to believe that the nucleophilic substitution occurred through S_N2 mechanism.

Nevertheless, the results obtained with crotyl bromine did not perfectly match with the model reaction of allyl bromide and the mechanistic consideration we derived were only partially fitting the model system. In fact, the presence of the catalysts did not considerably accelerate the reaction rate and

similar products distribution between the catalyzed and uncatalyzed reaction was observed.

To finally determine the substitution mechanism, future investigations are needed, involving for example a ^{13}C isotopically marked allyl bromide as substrate, which products distribution depending on the position of the marked carbon will discriminate between S_N1 and S_N2.

5.3. Conclusions

In summary, in this chapter we reported some example of true catalytic applications of **PEt[5]** as a supramolecular catalyst, in particular promoting the nucleophilic substitution of primary amines on allyl halides which led selectively to secondary amines and limited the over-alkylation of the nucleophile. Different primary amines and allyl halides were investigated confirming the importance of a simultaneous binding into the macrocycle cavity modulated by intrinsic reactivity and steric reasons. Overall, the reaction was carried out also with a sub-stoichiometric amount of **PEt[5]** with respect to the substrates with good accelerations up to 17 times compared to the uncatalyzed reaction and with possible catalyst recycle after pouring the mixture into MeOH. Finally, further investigations with an appropriate substrate suggested the nature of the nucleophilic substitution as S_N2 reaction.

5.4. Experimental Section

5.4.1. General

^{1}H NMR were recorded at 298 K, unless otherwise stated, on a Bruker AVANCE 400 spectrometer operating at 400.15 MHz. δ values in ppm are relative to $SiMe_4$. GC analysis were performed on HP SERIES II 5890 equipped with a HP5 column (30 m, I. D. 0.25 m, film 0.25 μm) using He as gas carrier and FID. GC-MS analyses were performed on a GC Trace GC 2000 equipped with a HP5-MS column (30 m, I.D. 0.25 mm, film 0.25 μm) using He gas carrier and coupled with a quadrupole MS Thermo Finnigan Trace MS with *Full Scan* method.

Solvents and reactants were used as received, otherwise they were purified as reported in the literature.[157] TLC analysis were performed on TLC Polygram ® Sil G/UV254 of 0.25 mm thickness and flash-chromatography separations were performed on silica gel Merk 60, 230-400 mesh.[158]

All reagents octylamine, hexadecylamine, 2-methoxy-ethylamine, cyclohexylamine, 1-phenylethylamine, allyl bromide, allyl chloride, allyl iodide, 1,4-diethoxy-benzene, were all commercially available products (Aldrich, Alfa Aesar) and were used as received without any further purification. Allyl tosylate was prepared according to literature procedure.[159] The pillararenes investigated in the work were prepared following reported procedures: **PEt[5]**, **PEt[6]**, **PMe[5]** and **PBu[5]**.[142] All the products of the reaction were identified by GC-MS and ^{1}H-NMR analysis.

5.4.2. Catalytic Studies

5.4.2.1. Synthesis of Carbamate and Urea Derivatives in the Presence of PEt[5]

In a 2 ml vial **PEt[5]** (8 mg, 0.045 mmol), pentyl isocyanate (5 mg, 0.045 mmol) and 1-butanol (4.11 µl, 0.045 mmol) or octylamine (7.4 µl, 0.045 mmol) were added to CDCl$_3$ (0.8 ml). The solution was then stirred at room temperature and the reaction progress was monitored by ^{1}H NMR ad GC analysis by periodically sampling directly from the reaction mixtures. Conversion, product assignment and product distribution were determined by direct GC-FID, GC-MS and ^{1}H NMR analysis of the reaction mixture as the average of three experiments.
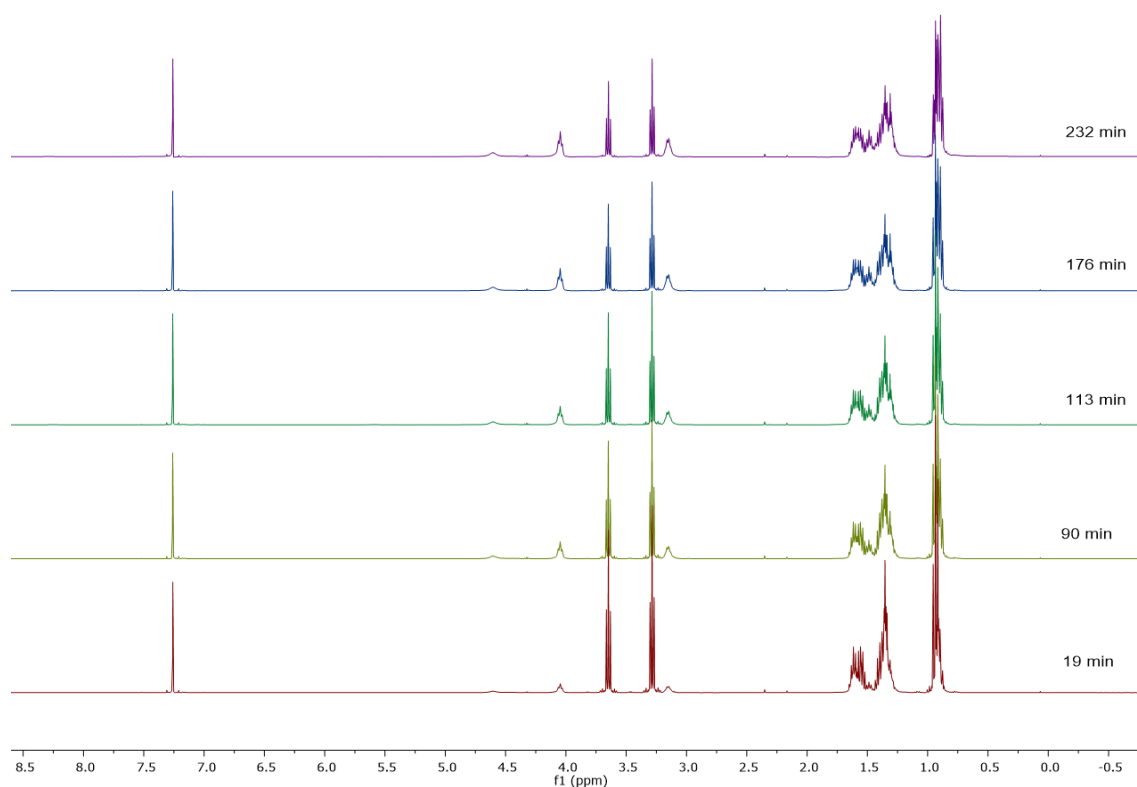
*Figure 5.18 ^{1}H NMR (400 MHz, 298K, CDCl$_3$) Reaction between pentyl isocyanate with 1-butanol in CDCl$_3$ in the absence of **PEt[5]**. [pentyl isocyanate]=[1-butanol]= 56 mM.*
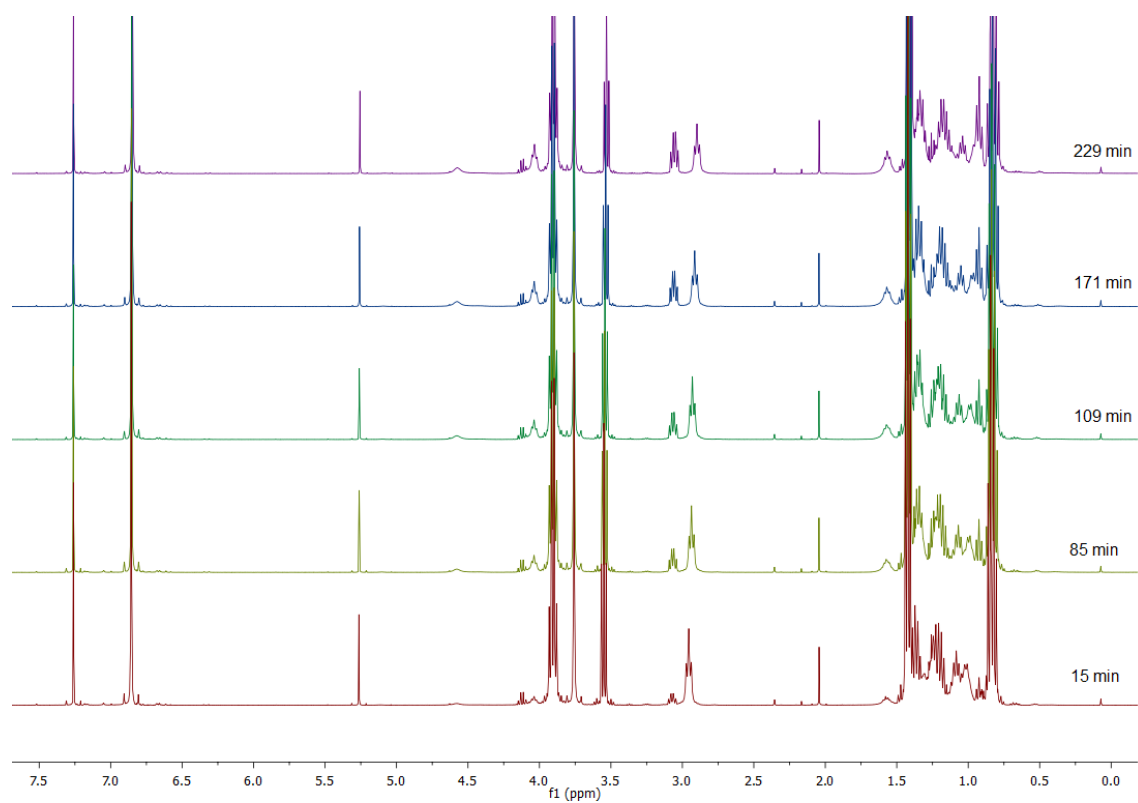
Figure 5.19 ¹*H NMR (400 MHz, 298K, CDCl₃) Reaction between pentyl isocyanate with 1-butanol in CDCl₃ in the presence of* **PEt[5]***. [pentyl isocyanate]=[1-butanol]= 56 mM, [***PEt[5]***]= 56 mM.*
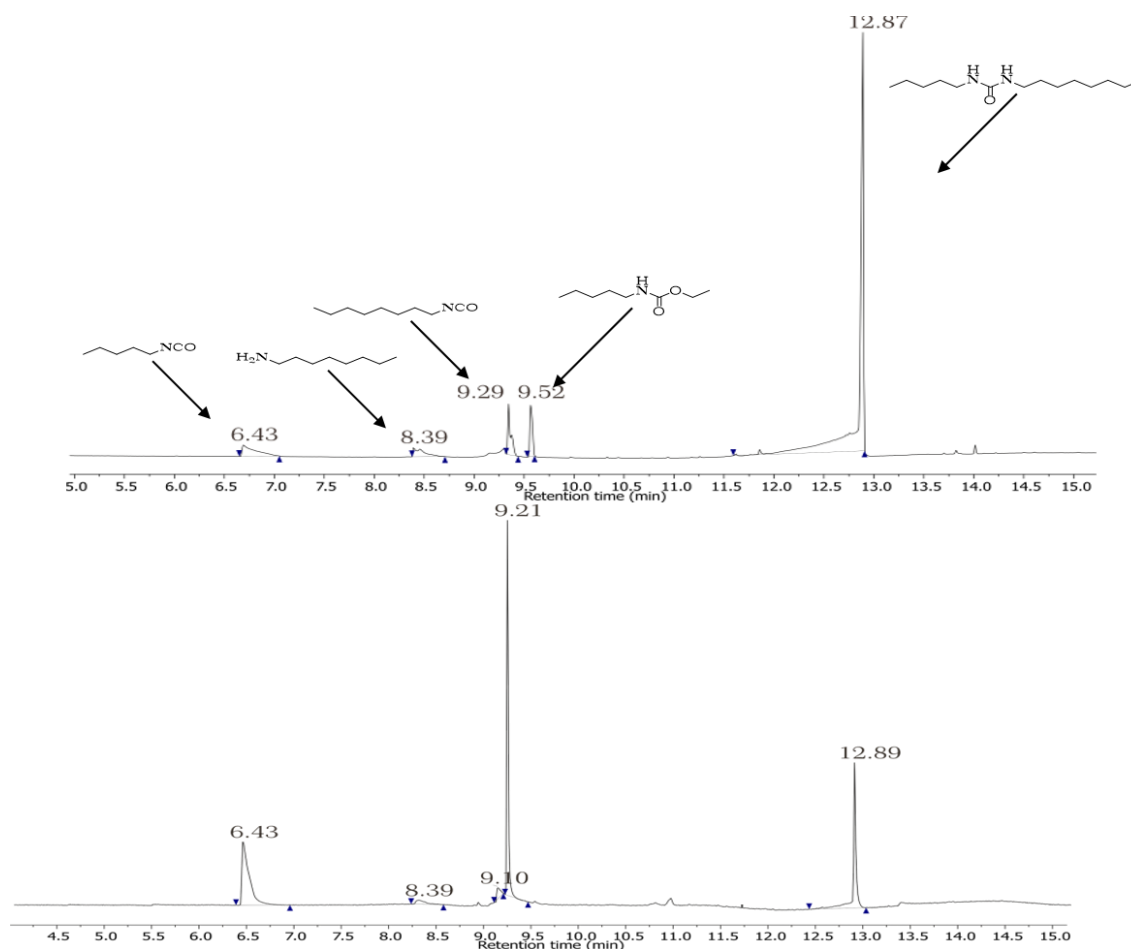
Figure *5.20 GC-FID spectra of the reaction between pentyl isocyanate and octylamine in the absence of* ***PEt[5]*** *(bottom) and in the presence of* ***PEt[5]*** *after 70 min of reaction (top). [octylamine]=[pentyl isocyanate]=[**PEt[5]**] 56 mM, CDCl₃ 0.8 ml, room temperature.*

5.4.2.2. Oxidation of 2-Chloroethyl Ethyl Sulfide

In a 2 ml vial **PEt[5]** (8 mg, 0.045 mmol), 2-chloroethyl ethyl sulfide (5.2 μl, 0.045 mmol) and H₂O₂ 30% v/v (4.6 μl, 0.045 mmol) were added to CDCl₃ (0.8 ml). The solution was then stirred vigorously at room temperature and the reaction progress was monitored by ¹H NMR by periodically sampling directly from the reaction mixtures. Conversion, product assignment and product distribution were determined by ¹H NMR analysis of the reaction mixture.
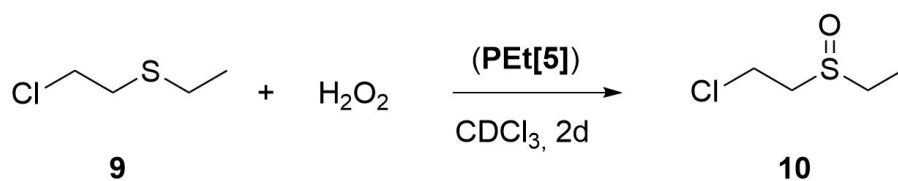
Scheme 5.10 *Oxidation of 2-chloroethyl ethyl sulfide to 2-chloroethyl ethyl sulfoxide with* H_2O_2 *catalyzed by* **PEt[5]** *in CDCl₃.*
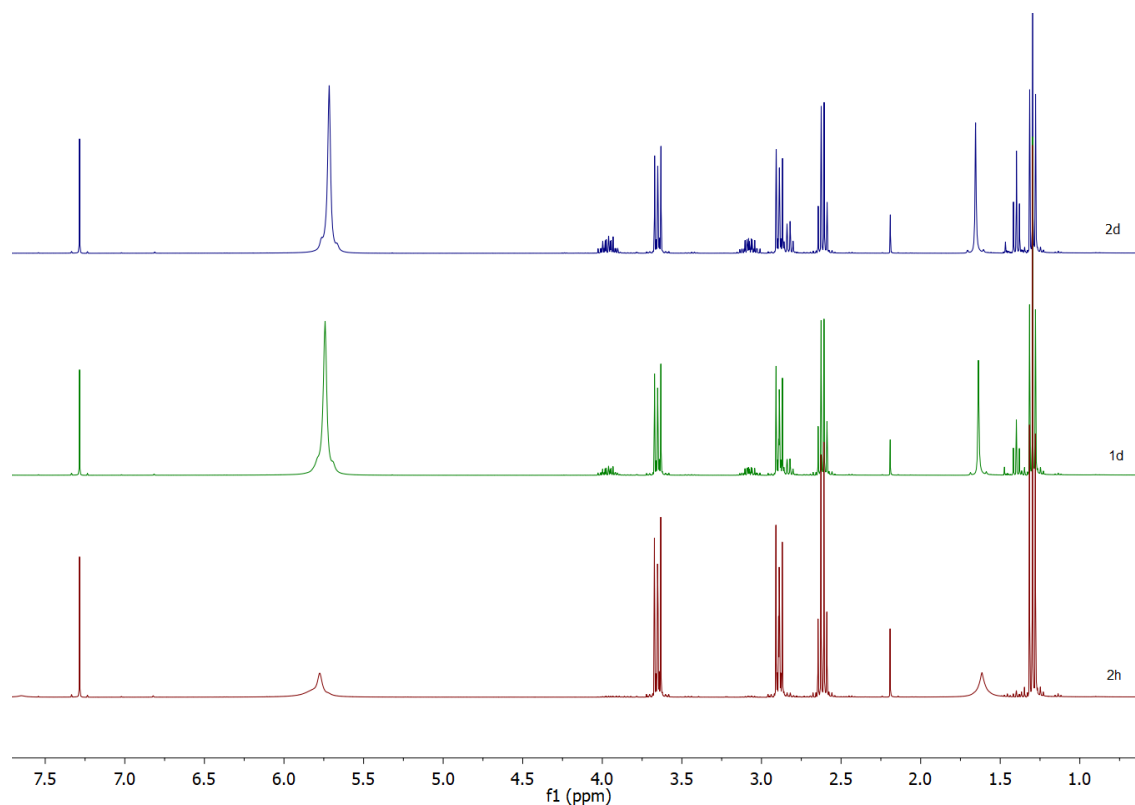
Figure 5.21 *¹H NMR (400 MHz, 298K, CDCl₃) Oxidation of 2-chloroethyl ethyl sulfide with* H_2O_2 *in CDCl₃ in the absence of* **PEt[5]**. *[2-chloroethyl ethyl sulfide]=[H_2O_2]= 56 mM.*
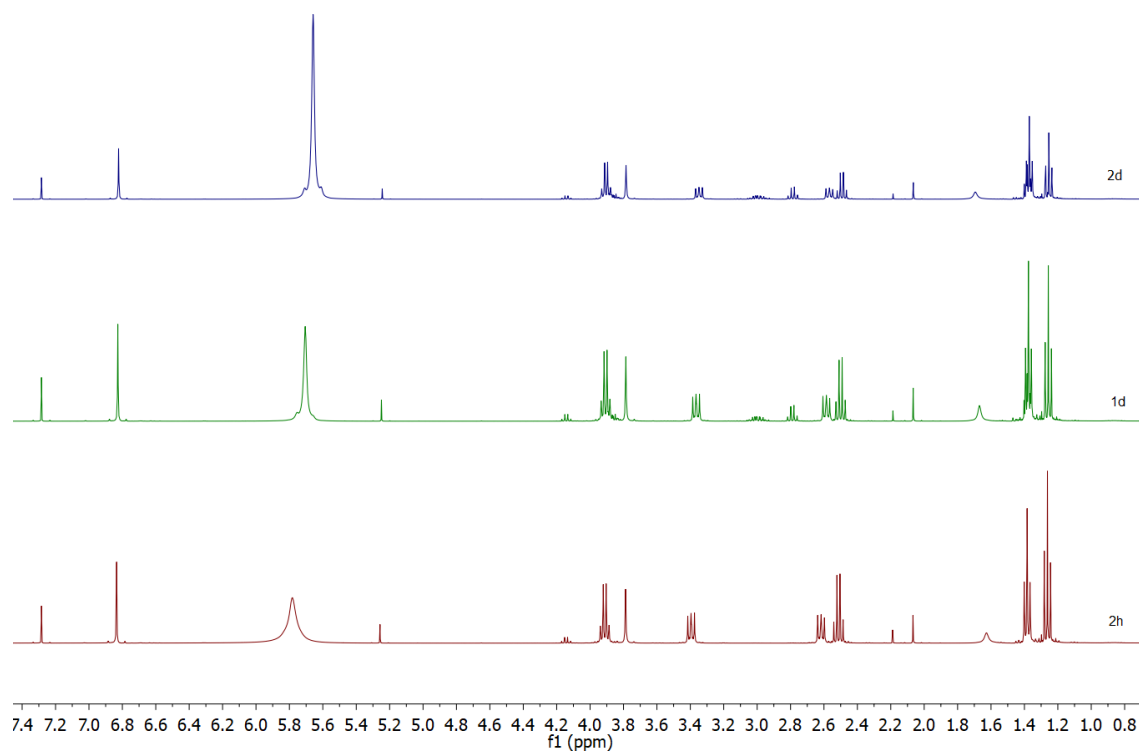
Figure 5.22 *¹H NMR (400 MHz, 298K, CDCl₃) Oxidation of 2-chloroethyl ethyl sulfide with H₂O₂ in CDCl₃ in the presence of **PEt[5]**. [2-chloroethyl ethyl sulfide]=[H₂O₂]=[**PEt[5]**]=56 mM.*

5.4.2.3. Nucleophilic Substitution Reaction of Octylamine on Allyl Bromide in the Presence of DEB, P[5] or PEt[6]

In a 2 ml vial **P[5]** (Me, Et, Bu) (0.045 mmol), allyl bromide (3.9 μl, 0.045 mmol) and octylamine (7.4 μl, 0.045 mmol) were added to CDCl₃ (0.8 ml). The solution was then stirred at room temperature and the reaction progress was monitored by ¹H NMR ad GC analysis by periodically sampling directly from the reaction mixtures. Conversion, product assignment and product distribution were determined by direct GC, GC-MS and ¹H NMR analysis of the reaction mixture as the average of three experiments.

All the performed catalytic studies have been conducted with the same substrates concentration (56 mM).

The same procedure was applied to **PEt[6]** (48 mg, 0.045 mmol) while **DEB** concentration was set 5 times higher (37 mg, 0.225 mmol).
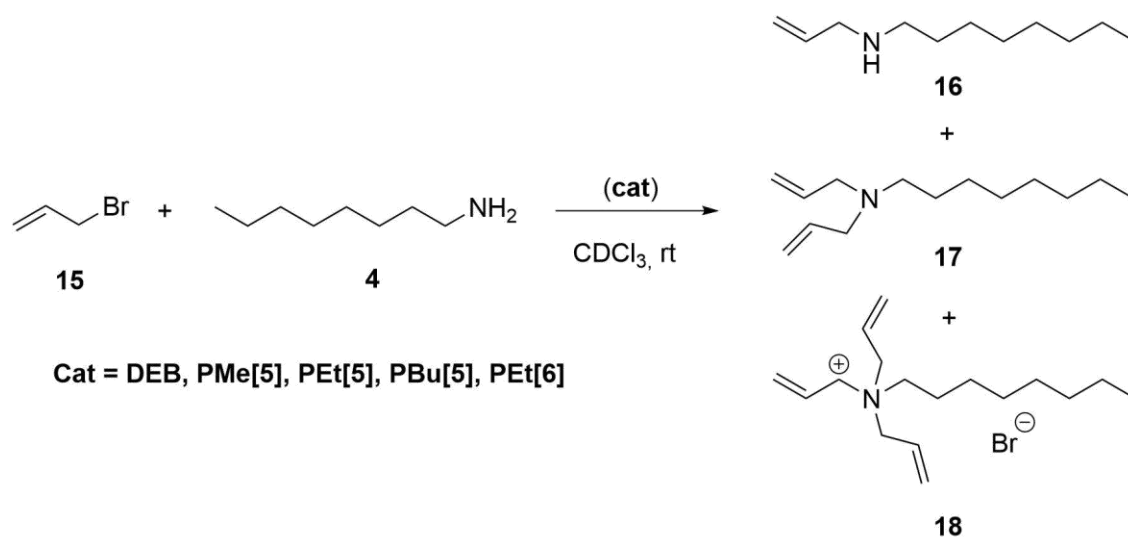
***Scheme* 5.11** *Nucleophilic substitution reaction between allyl bromide and octylamine catalyzed by the presence of **DEB**, **P[5]** or **PEt[6]** in CDCl₃.*
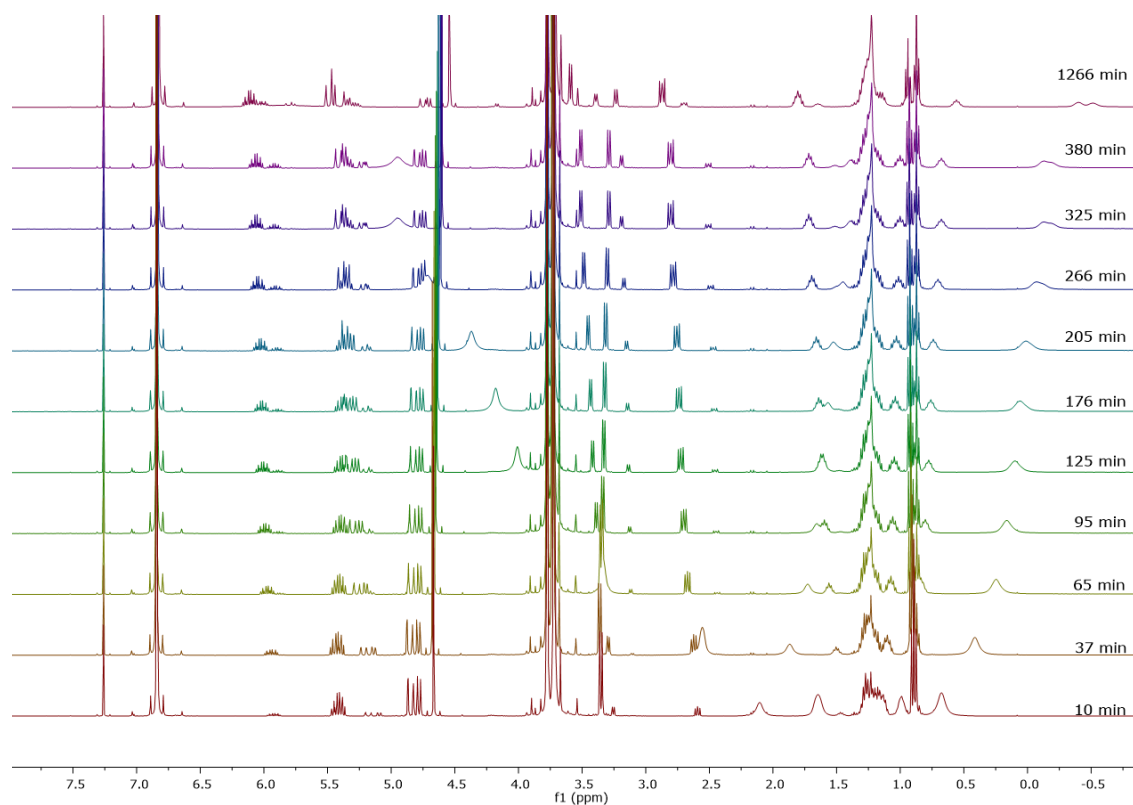
***Figure* 5.23** *¹H NMR (400 MHz, 298K, CDCl₃) Reaction between allyl bromide with octylamine in CDCl₃ in the presence of **PMe[5]**. [allyl bromide]=[octylamine]= 56 mM, [**PMe[5]**]= 56 mM.*
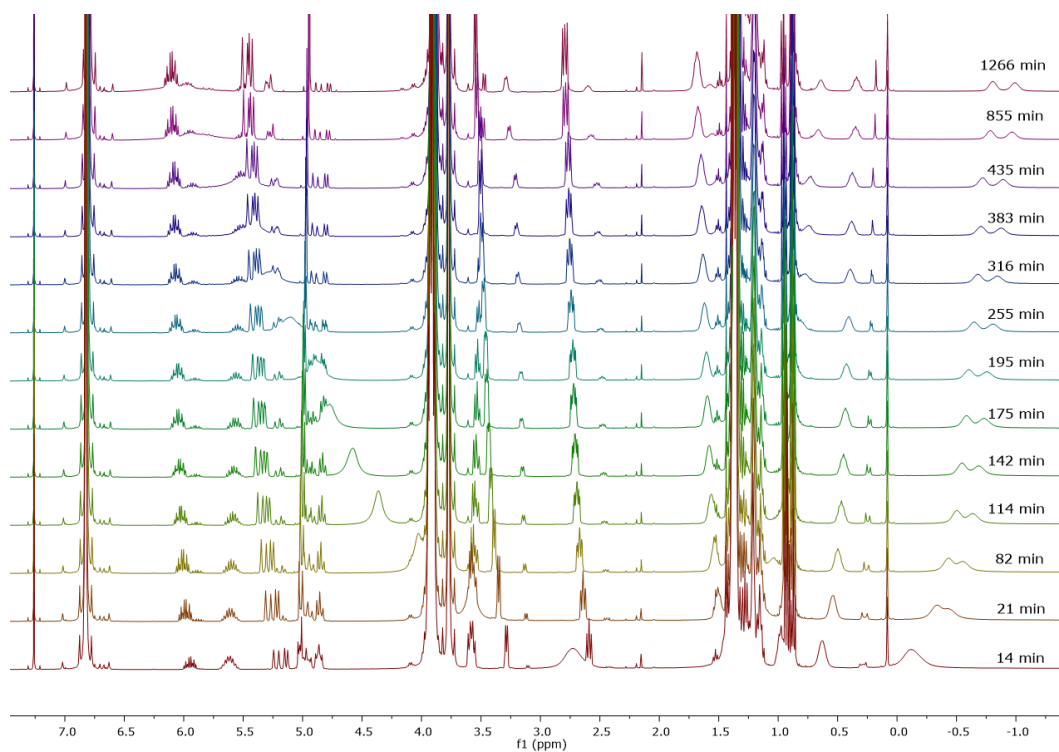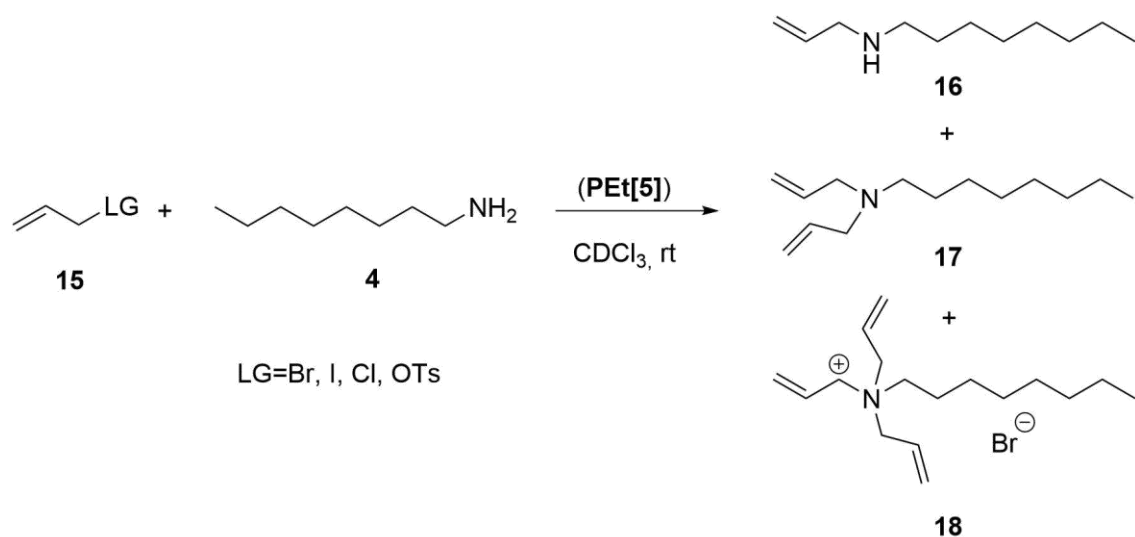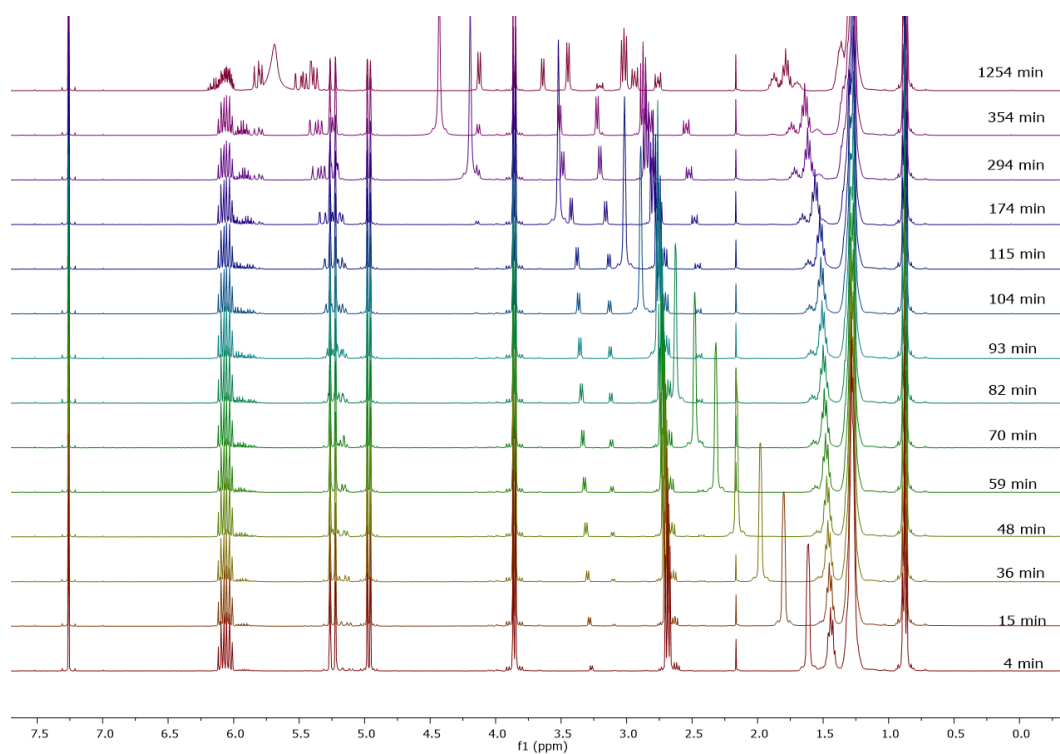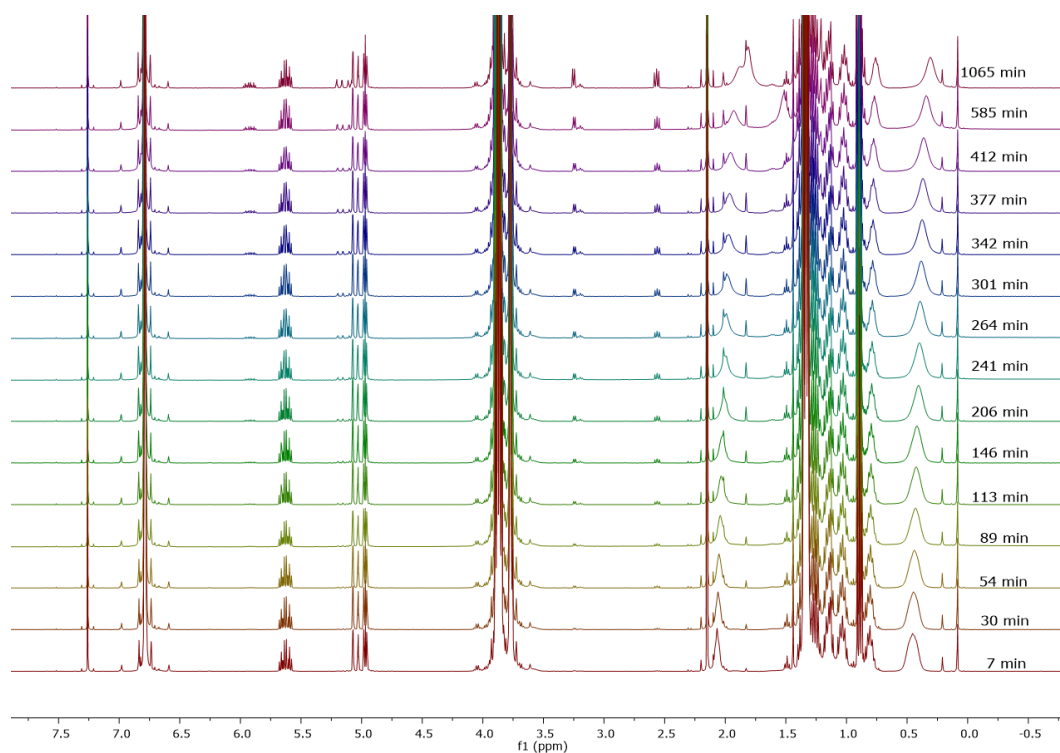
Figure 5.24 ¹H NMR (400 MHz, 298K, CDCl₃) Reaction between allyl bromide with octylamine in CDCl₃ in the presence of **PEt[5]**. [allyl bromide]=[octylamine]= 56 mM, [**PEt[5]**]= 56 mM.
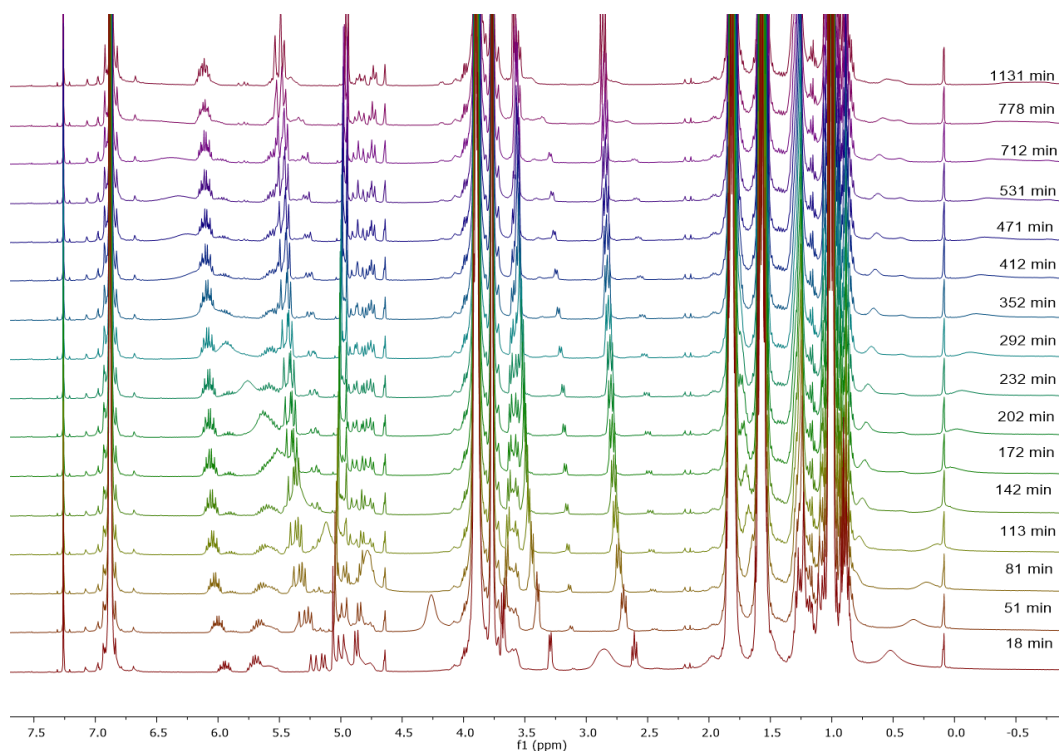
Figure 5.25 ¹H NMR (400 MHz, 298K, CDCl₃) Reaction between allyl bromide with octylamine in CDCl₃ in the presence of **PBu[5]**. [allyl bromide]=[octylamine]= 56 mM, [**PBu[5]**]= 56 mM.
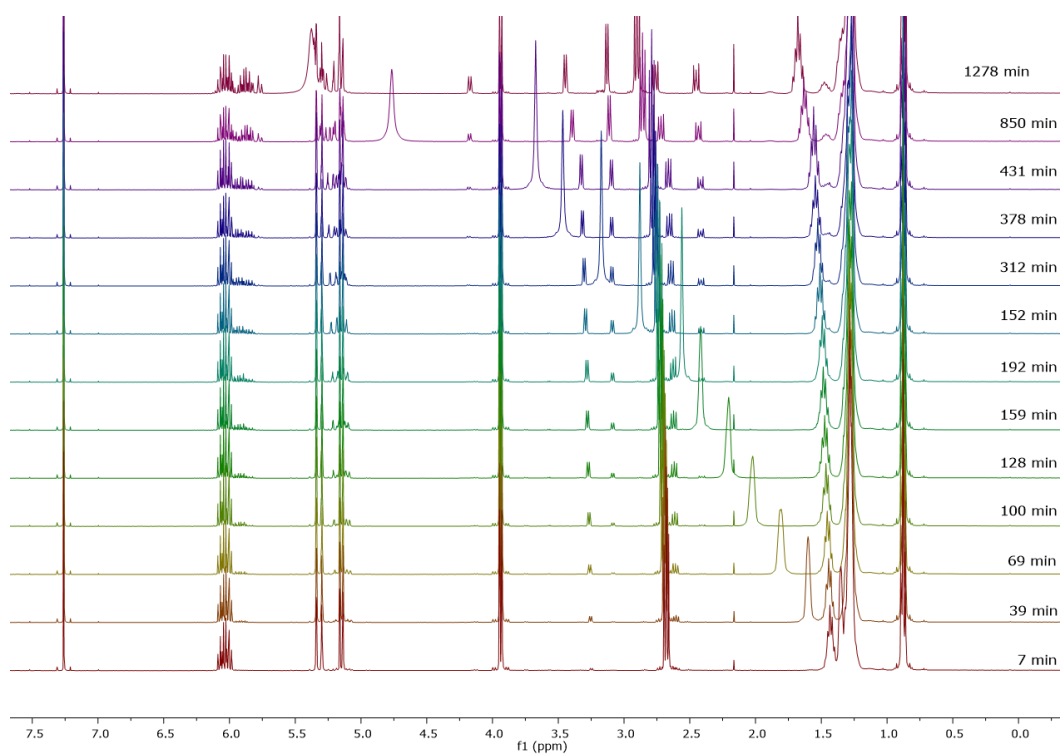
Figure 5.26 ^1H NMR (400 MHz, 298K, CDCl$_3$) Reaction between allyl bromide with octylamine in CDCl$_3$ in the absence of **P[5]** (R = Me, Et, Bu). [allyl bromide]=[octylamine]= 56 mM.
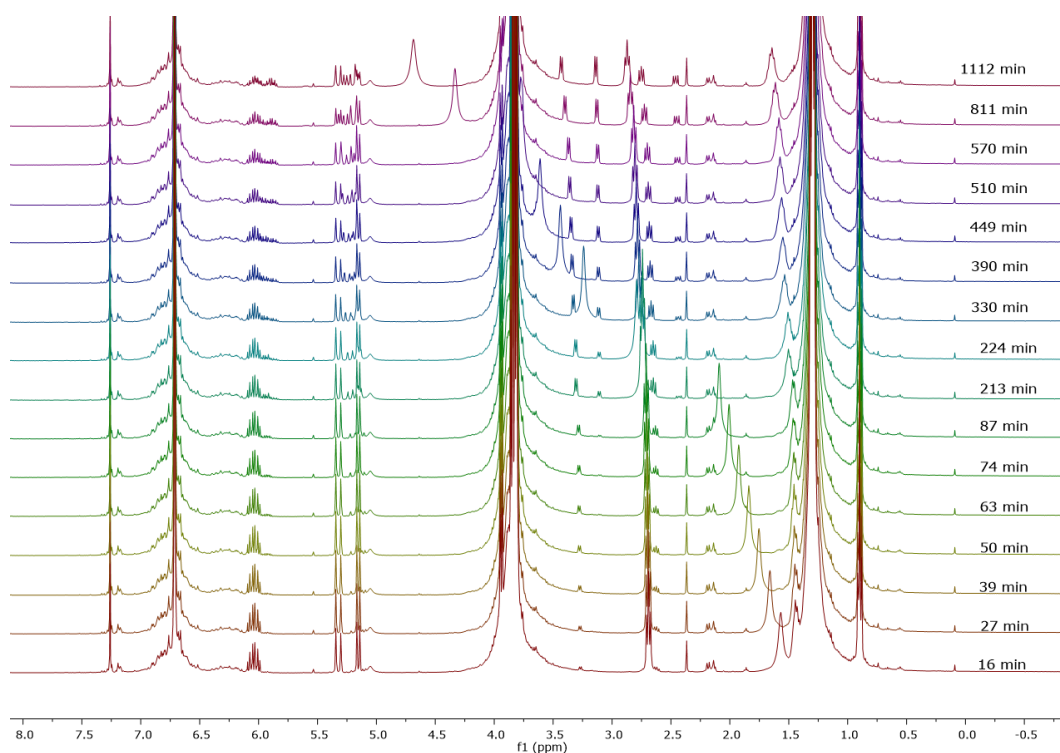
Figure 5.27 ^1H NMR (400 MHz, 298K, CDCl$_3$) Reaction between allyl bromide with octylamine in CDCl$_3$ in the presence of **PEt[6]**. [allyl bromide]=[octylamine]= 56 mM, [**PEt[6]**]= 56 mM.
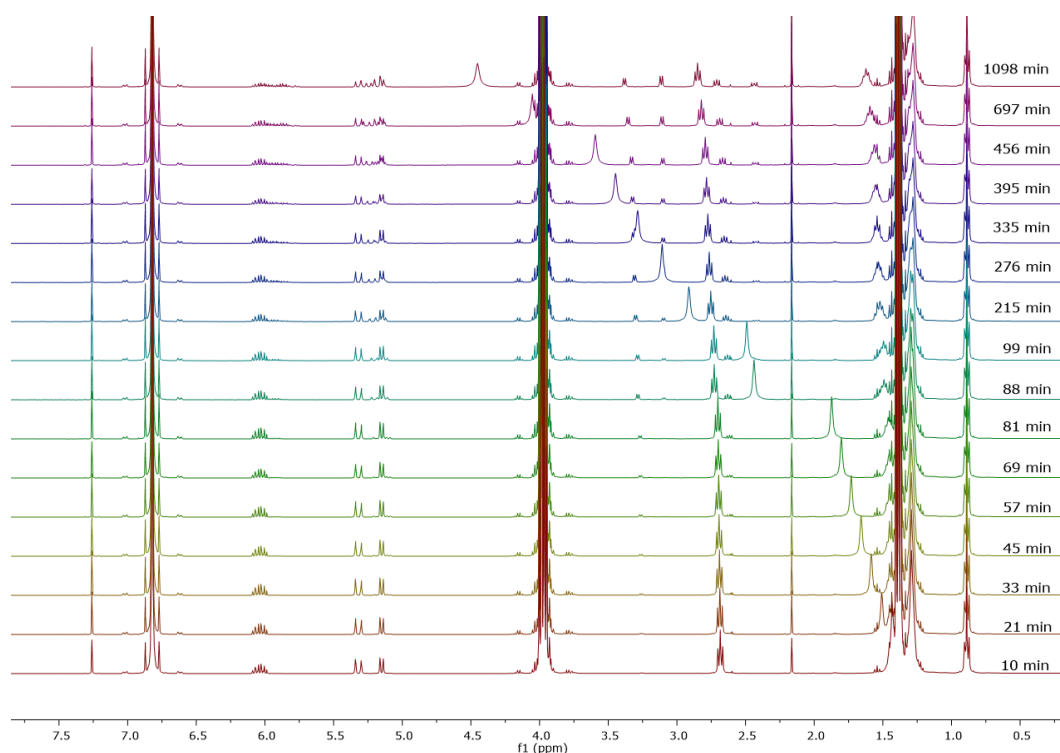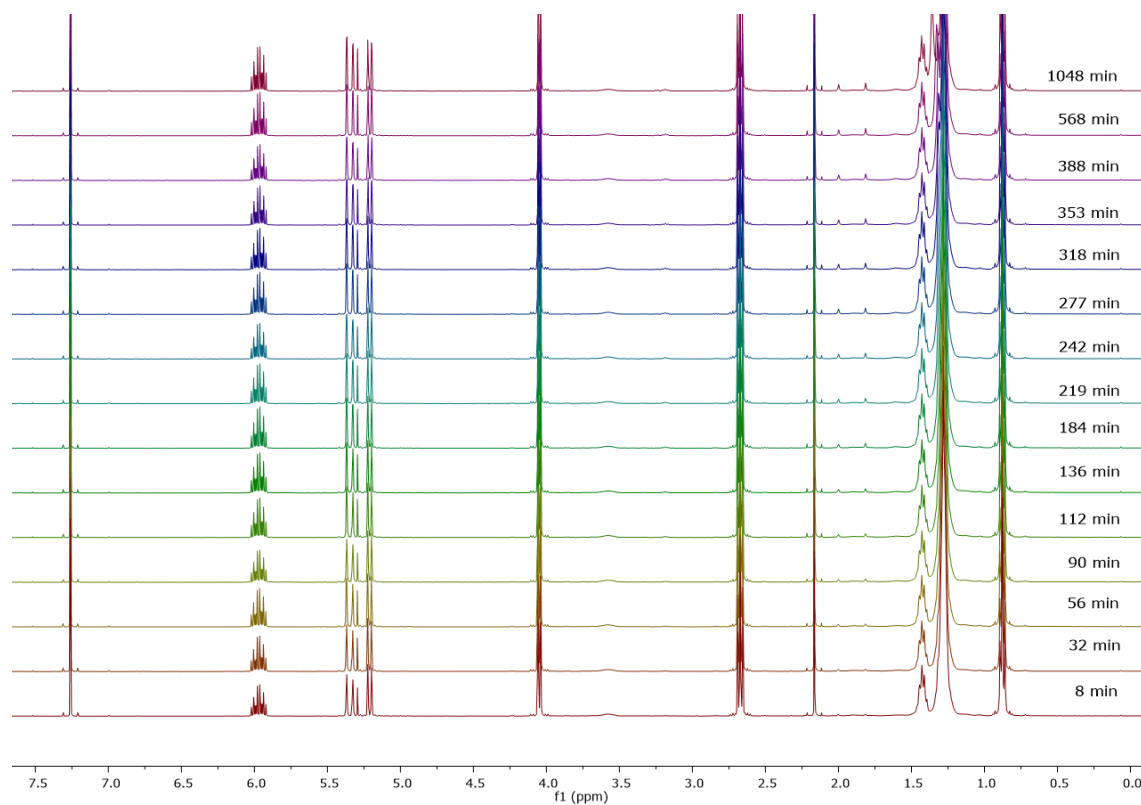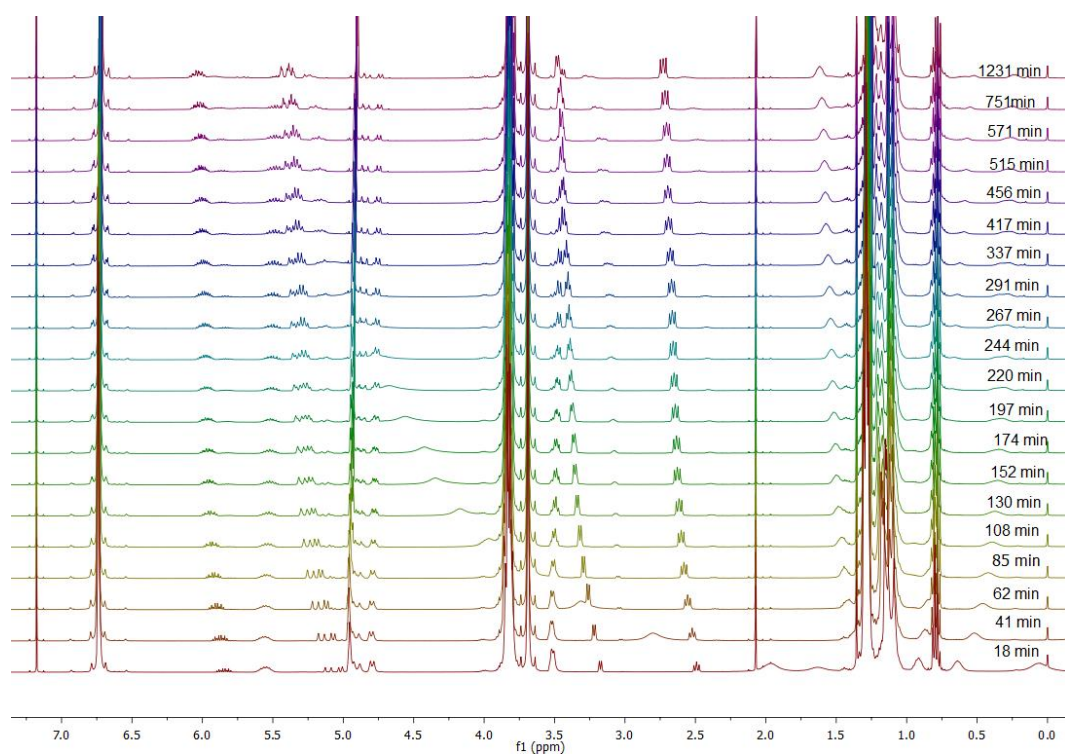
Figure 5.28 *¹H NMR (400 MHz, 298K, CDCl₃) Reaction between allyl bromide with octylamine in CDCl₃ in the presence of **DEB**. [allyl bromide]=[octylamine]= 56 mM, [**DEB**]= 0.28 M.*

5.4.2.4. Nucleophilic Substitution on Different Allyl Halides

In a 2 ml vial **PEt[5]** (40 mg, 0.045 mmol), allyl halides (I, Cl) (0.045 mmol) and octylamine (7.4 μl, 0.045 mmol) were added to CDCl₃ (0.8 ml). The solution was then stirred at room temperature and the reaction progress was monitored by ¹H NMR ad GC analysis by periodically sampling directly from the reaction mixtures. Conversion, product assignment and product distribution were determined by direct GC, GC-MS and ¹H NMR analysis of the reaction mixture as the average of three experiments.

All the performed catalytic studies have been conducted with the same substrates concentration (56 mM).

169

Scheme *5.12* *Nucleophilic substitution reaction between allyl halides (iodide, chloride) and octylamine catalyzed by* ***PEt[5]*** *in CDCl₃.*
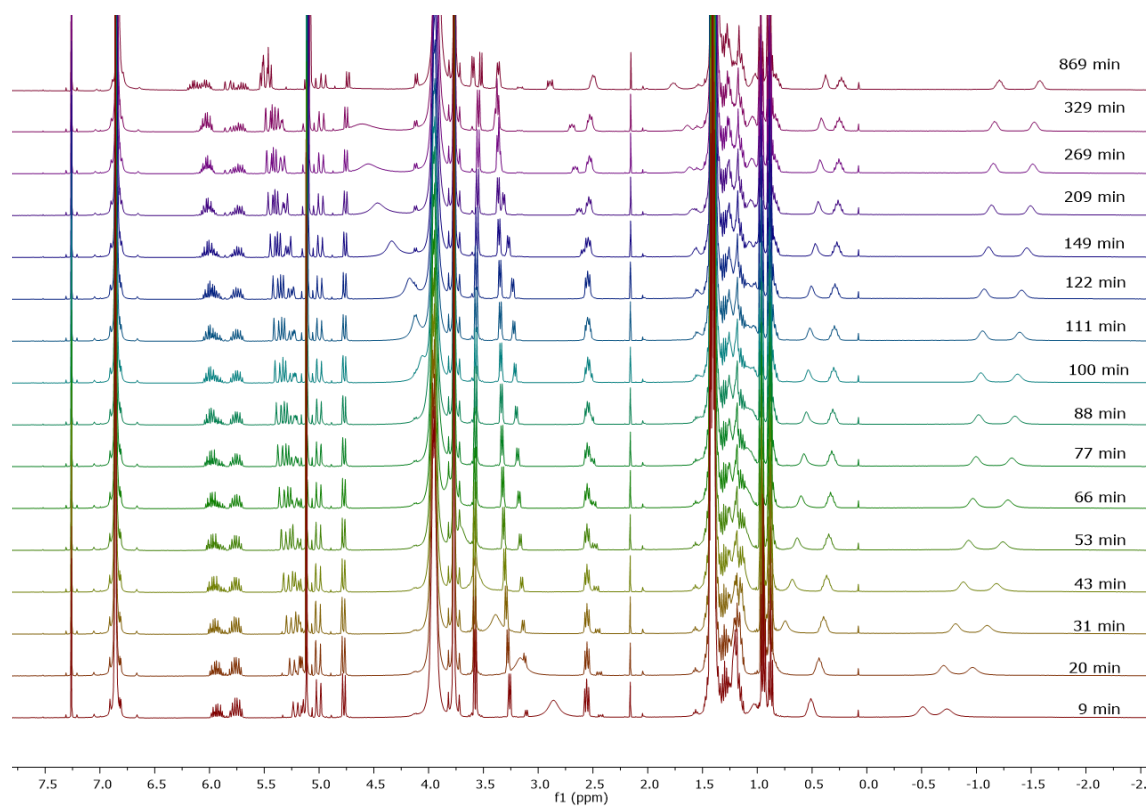
Figure *5.29 ¹H NMR (400 MHz, 298K, CDCl₃) Reaction between allyl iodide with octylamine in CDCl₃ in the presence of* ***PEt[5]***. *[allyl iodide]=[octylamine]= 56 mM,* ***PEt[5]****= 56 mM.*

Figure 5.30 *¹H NMR (400 MHz, 298K, CDCl₃) Reaction between allyl iodide with octylamine in CDCl₃ in the absence of **PEt[5]**. [allyl iodide]=[octylamine]= 56 mM.*

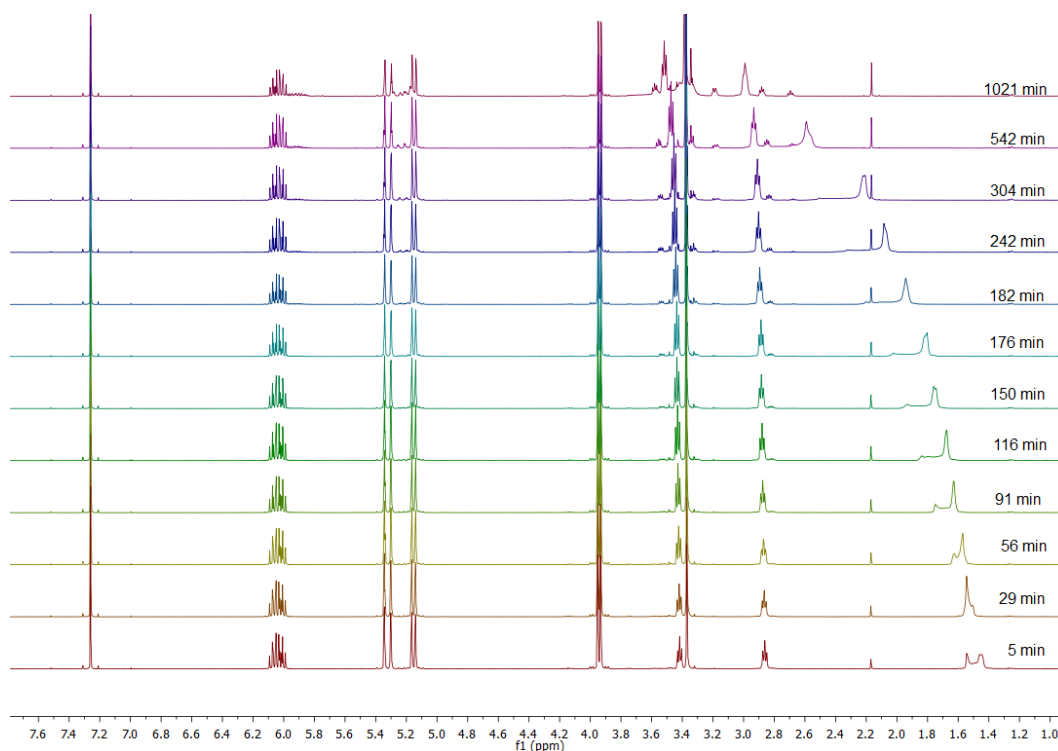
Figure 5.31 *¹H NMR (400 MHz, 298K, CDCl₃) Reaction between allyl chloride with octylamine in CDCl₃ in the presence of **PEt[5]**. [allyl chloride]=[octylamine]= 56 mM, **PEt[5]**= 56 mM.*

171

Figure 5.32 *^{1}H NMR (400 MHz, 298K, CDCl$_3$) Reaction between allyl chloride with octylamine in CDCl$_3$ in the absence of **PEt[5]**. [allyl chloride]=[octylamine]= 56 mM.*

5.4.2.5. Nucleophilic Substitution with Different Amines

In a 2 ml vial **PEt[5]** (10 mg, 0.045 mmol), allyl bromide (3.9 μl, 0.045 mmol) and primary amines (0.045 mmol) were added to CDCl$_3$ (0.8 ml). The solution was then stirred at room temperature and the reaction progress was monitored by ^{1}H NMR ad GC analysis by periodically sampling directly from the reaction mixtures. Conversion, product assignment and product distribution were determined by direct GC, GC-MS and ^{1}H NMR analysis of the reaction mixture as the average of three experiments.

All the performed catalytic studies have been conducted with the same substrates concentration (56 mM).

Figure 5.33 ^{1}H NMR (400 MHz, 298K, CDCl$_3$) Reaction between allyl bromide with hexadecylamine in CDCl$_3$ in the presence of **PEt[5]**. [allyl bromide]=[hexadecylamine]= 56 mM, [**PEt[5]**]= 56 mM.
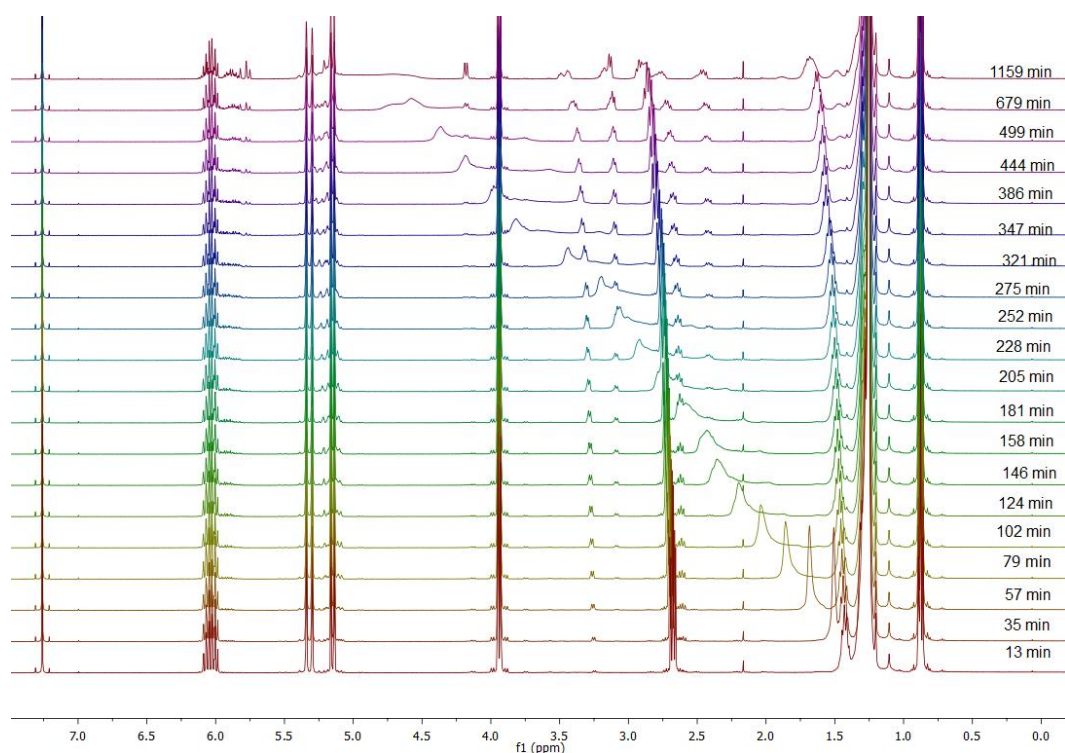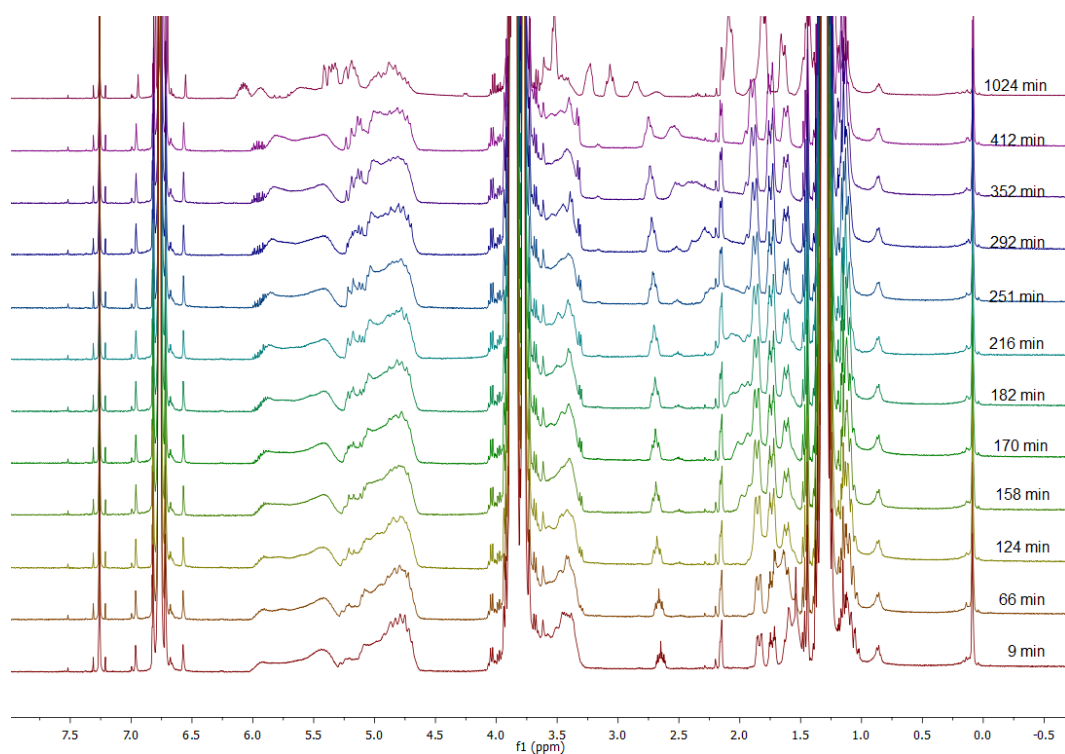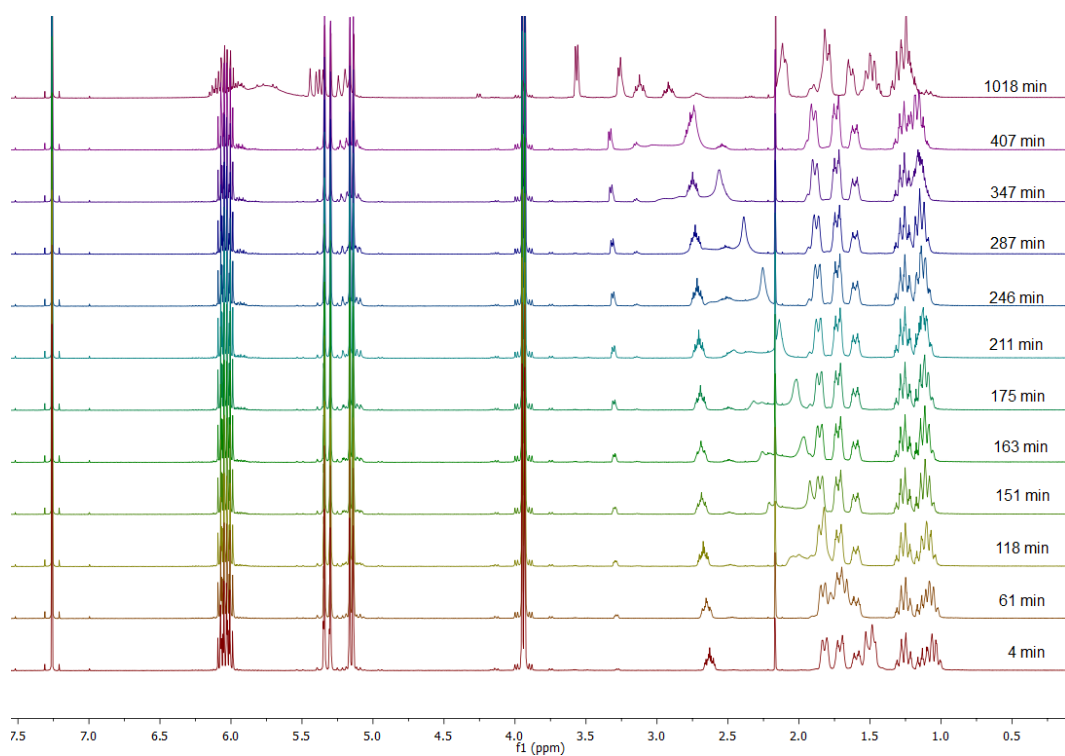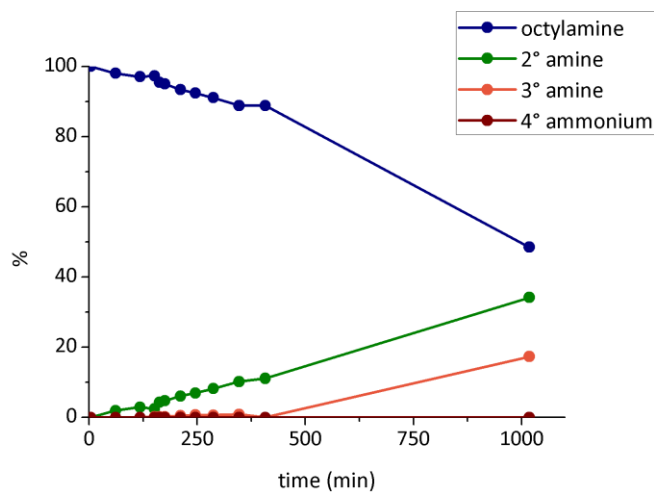

Figure 5.34 ^{1}H NMR (400 MHz, 298K, CDCl$_3$) Reaction between allyl bromide with hexadecylamine in CDCl$_3$ in the absence of **PEt[5]**. [allyl bromide]=[hexadecylamine]= 56 mM.

173
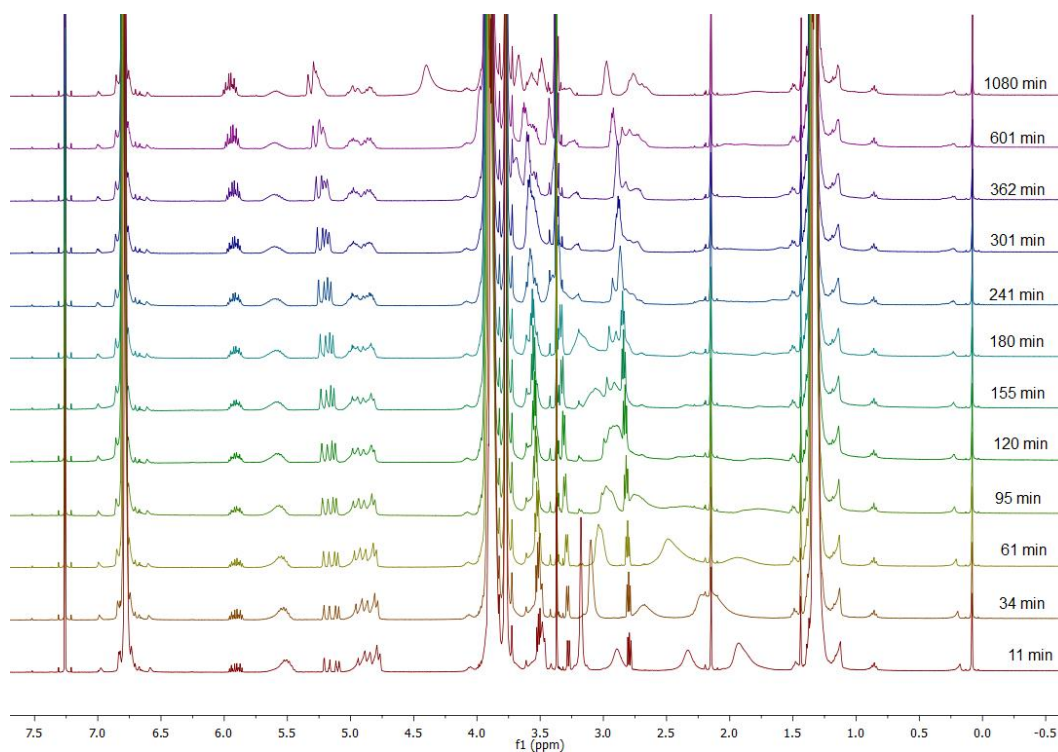
Figure 5.35 *^{1}H NMR (400 MHz, 298K, CDCl$_3$) Reaction between allyl bromide with 2-methoxyethylamine in CDCl$_3$ in the presence of **PEt[5]**. [allyl bromide]=[2-methoxyethylamine]= 56 mM, [**PEt[5]**]= 56 mM.*
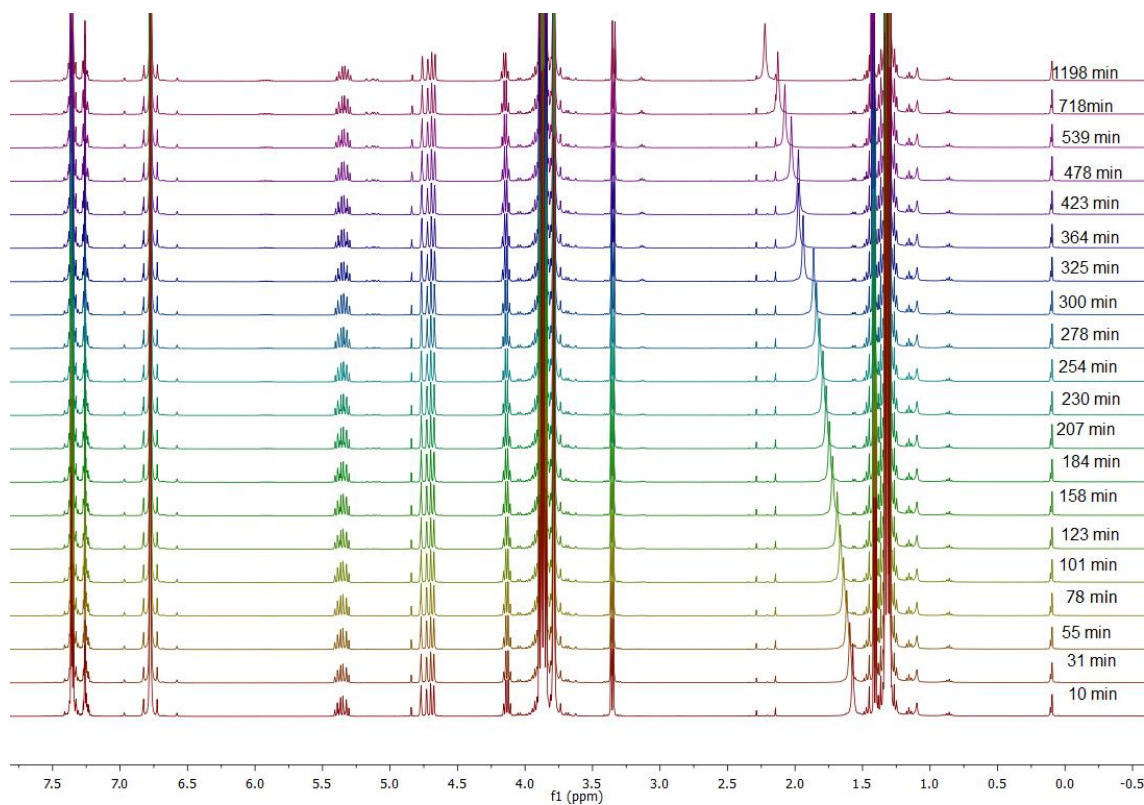

Figure 5.36 *^{1}H NMR (400 MHz, 298K, CDCl$_3$) Reaction between allyl bromide with 2-methoxyethylamine in CDCl$_3$ in the absence of **PEt[5]**. [allyl bromide]=[2-methoxyethylamine]= 56 mM.*

Figure 5.37 ^{1}H NMR (400 MHz, 298K, CDCl$_3$) Reaction between allyl bromide with cyclohexylamine in CDCl$_3$ in the presence of **PEt[5]**. [allyl bromide]=[cyclohexylamine]= 56 mM, [**PEt[5]**]= 56 mM.
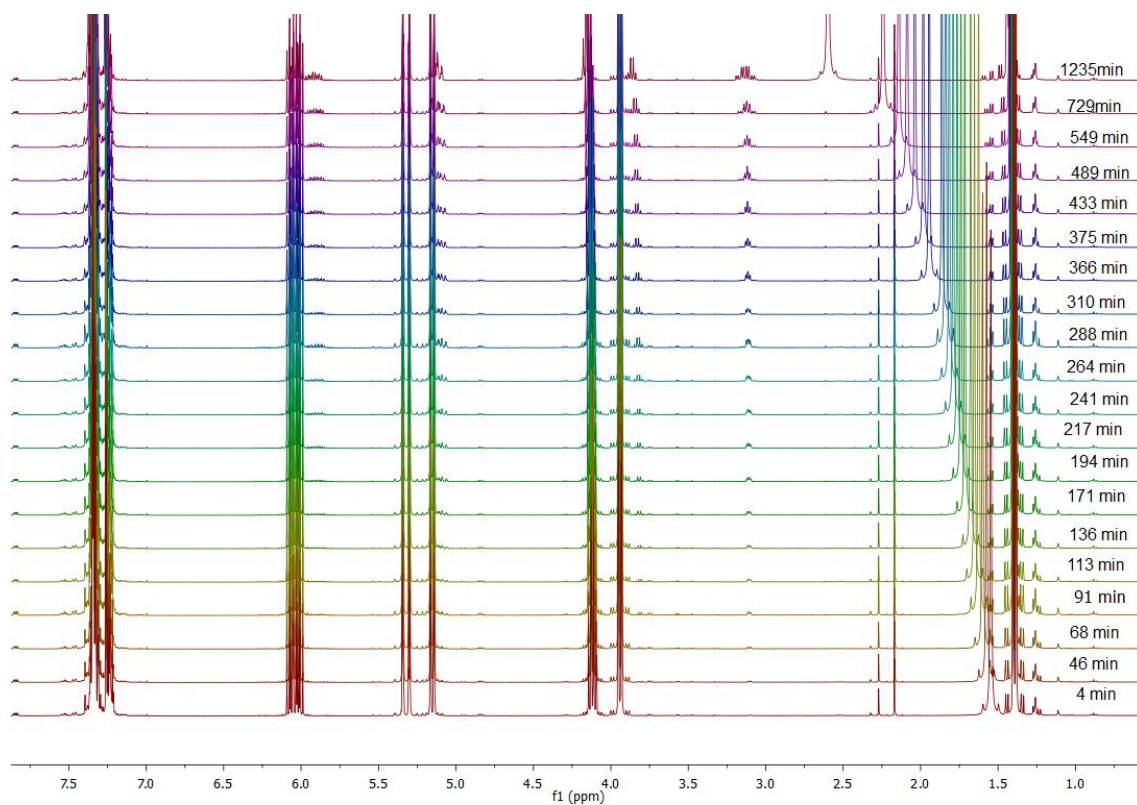

Figure 5.38 ^{1}H NMR (400 MHz, 298K, CDCl$_3$) Reaction between allyl bromide with cyclohexylamine in CDCl$_3$ in the absence of **PEt[5]**. [allyl bromide]=[cyclohexylamine]= 56 mM.

*Figure 5.39 Plot of the product distribution for the reaction between cyclohexylamine, allyl chloride in the absence of **PEt[5]**. [cyclohexylamine]=[allyl chloride]=[**PEt[5]**]= 56 mM, CDCl₃ 0.8 mL, room temperature.*

*Figure 5.40 ¹H NMR (400 MHz, 298K, CDCl₃) Reaction between allyl bromide with 1-phenylethylamine in CDCl₃ in the presence of **PEt[5]**. [allyl bromide]=[1-phenylethylamine]= 56 mM, [**PEt[5]**]= 56 mM.*

176

***Figure* 5.41** *^{1}H NMR (400 MHz, 298K, CDCl3) Reaction between allyl bromide with 1-phenylethylamine in CDCl3 in the absence of **PEt[5]**. [allyl bromide]=[1-phenylethylamine]= 56 mM.*
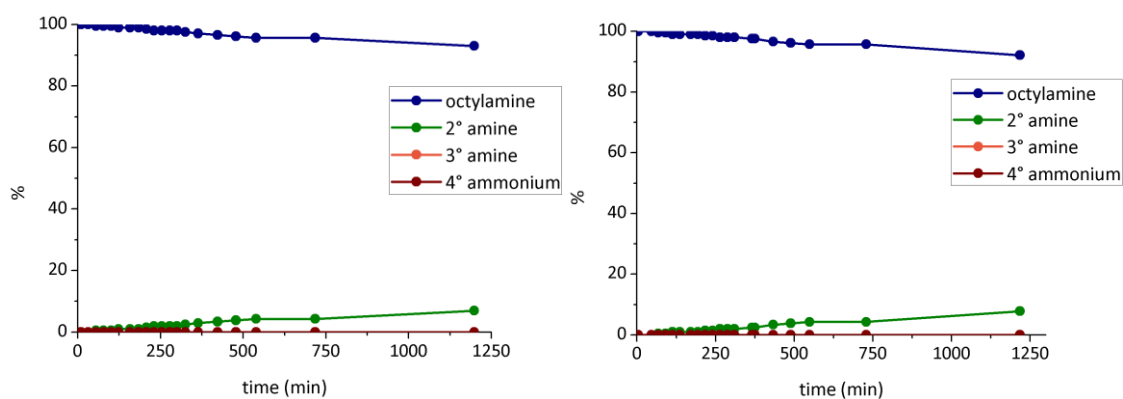

***Figure* S5.42** *Plot of the product distribution for the reaction between 1-phenylethylamine, allyl iodide in the presence (left) and in the absence (right) of **PEt[5]**. [1-phenylethylamine]=[allyl iodide]=[**PEt[5]**]= 56 mM, CDCl3 0.8 mL, room temperature.*

5.4.2.6. Nucleophilic Substitution with Different Amines in the Presence of DIEA

In a 2 ml vial **PEt[5]** (10 mg, 0.045 mmol), allyl bromide (3.9 µl, 0.045 mmol), DIEA (7.8 µl, 0.045mmol) and primary amines (0.045 mmol) were added to CDCl$_3$ (0.8 ml). The solution was then stirred at room temperature and the reaction progress was monitored by ^{1}H NMR ad GC analysis by periodically sampling directly from the reaction mixtures. Conversion, product assignment and product distribution were determined by direct GC, GC-MS and ^{1}H NMR analysis of the reaction mixture as the average of three experiments.

All the performed catalytic studies have been conducted with the same substrates concentration (56 mM).
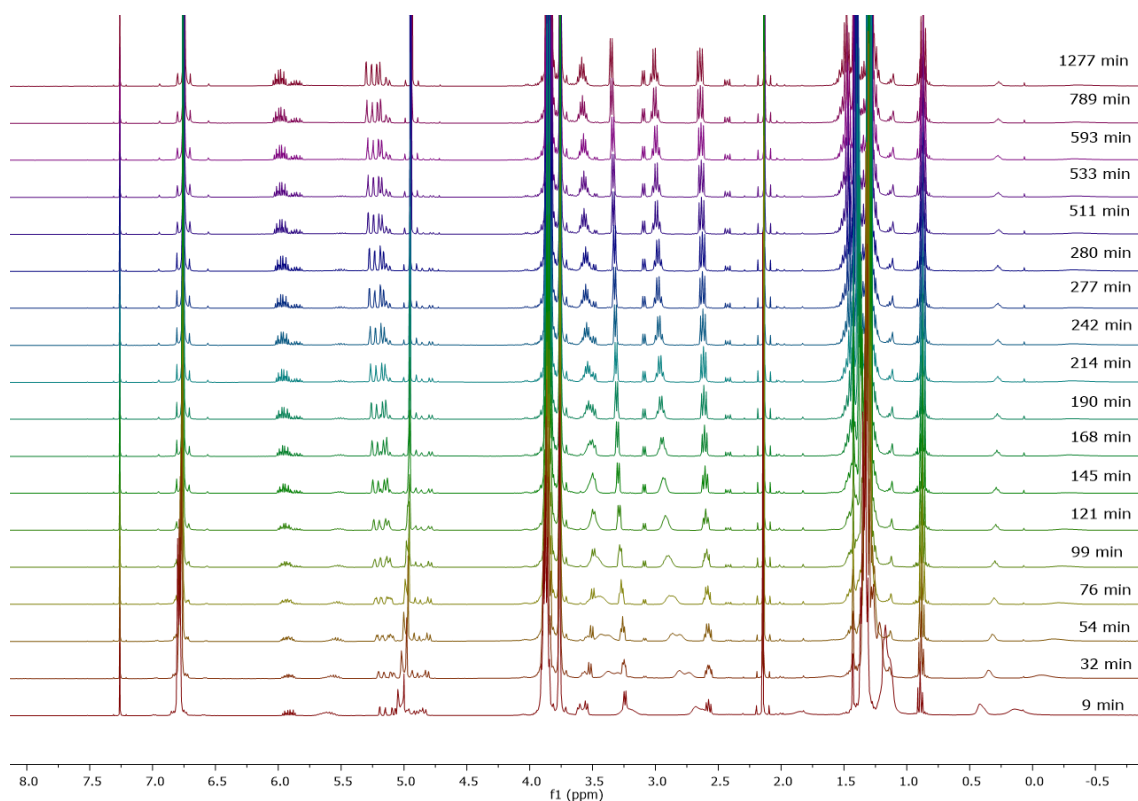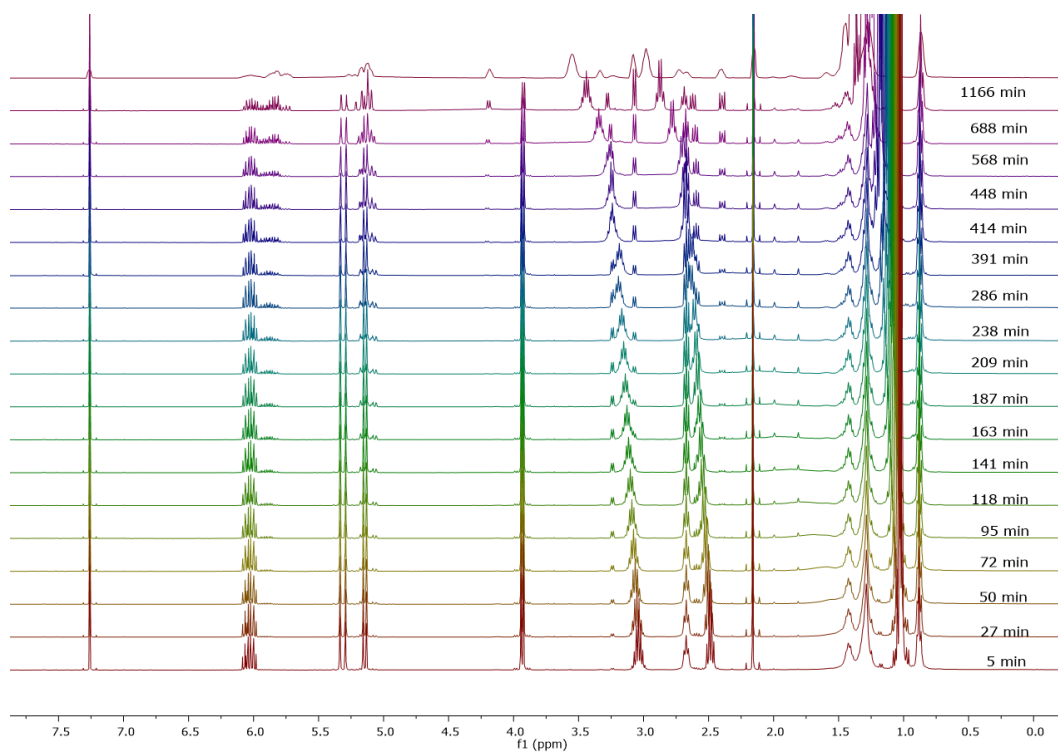

Figure 5.43 ^{1}H NMR (400 MHz, 298K, CDCl$_3$) Reaction between allyl bromide with butylamine in CDCl$_3$ in the presence of **PEt[5]** and DIEA. [allyl bromide]=[butylamine]= 56 mM, [**PEt[5]**]=[DIEA] 56 mM.
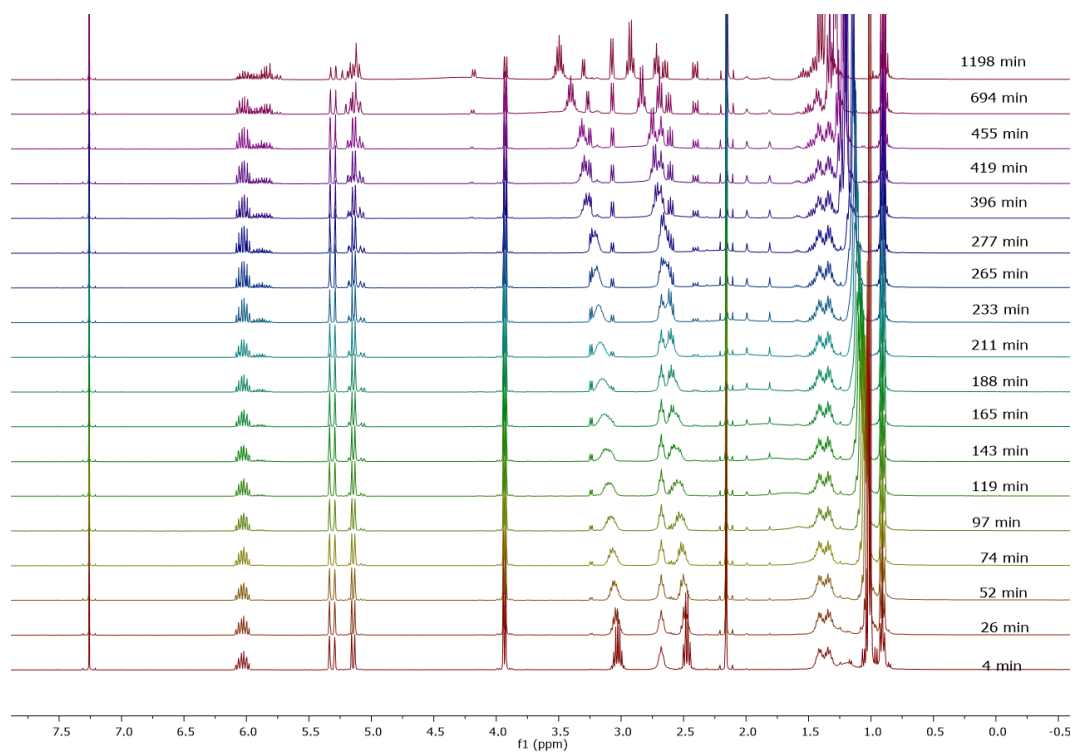
***Figure* 5.44** *¹H NMR (400 MHz, 298K, CDCl₃) Reaction between allyl bromide with butylamine in CDCl₃ in the presence of DIEA and in the absence of **PEt[5]**. [allyl bromide]=[butylamine]= 56 mM, [DIEA] 56 mM*
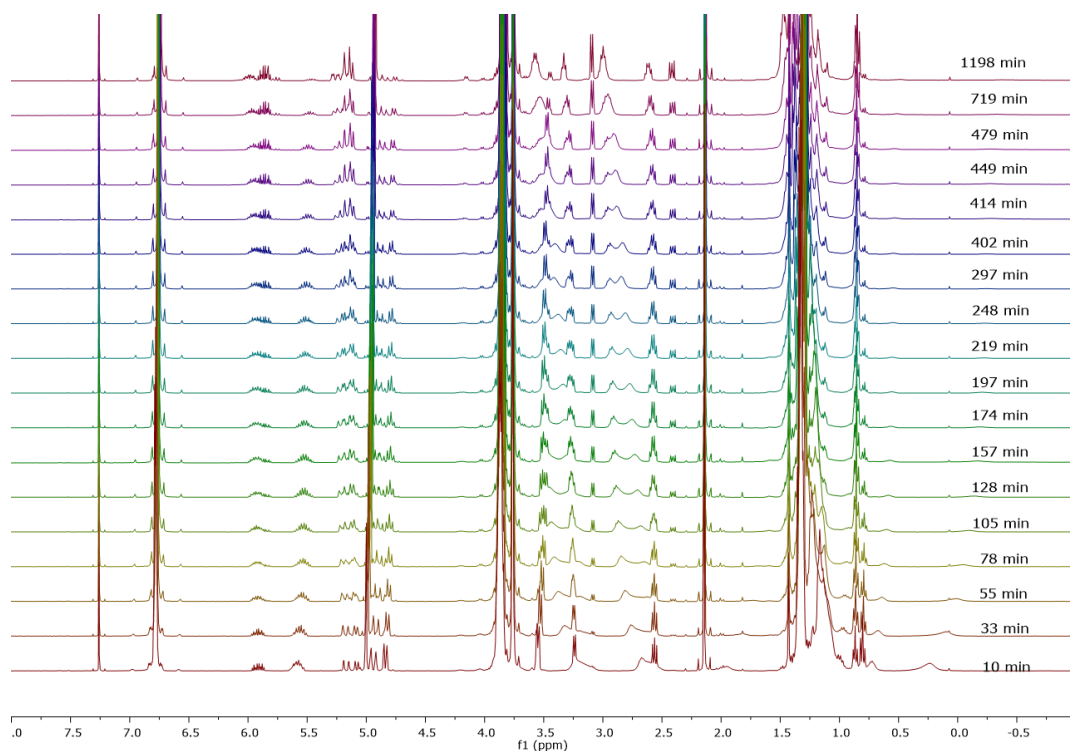
***Figure* 5.45** *¹H NMR (400 MHz, 298K, CDCl₃) Reaction between allyl bromide with hexylamine in CDCl₃ in the presence of **PEt[5]** and DIEA. [allyl bromide]=[hexylamine]= 56 mM, [**PEt[5]**]=[DIEA] 56 mM*
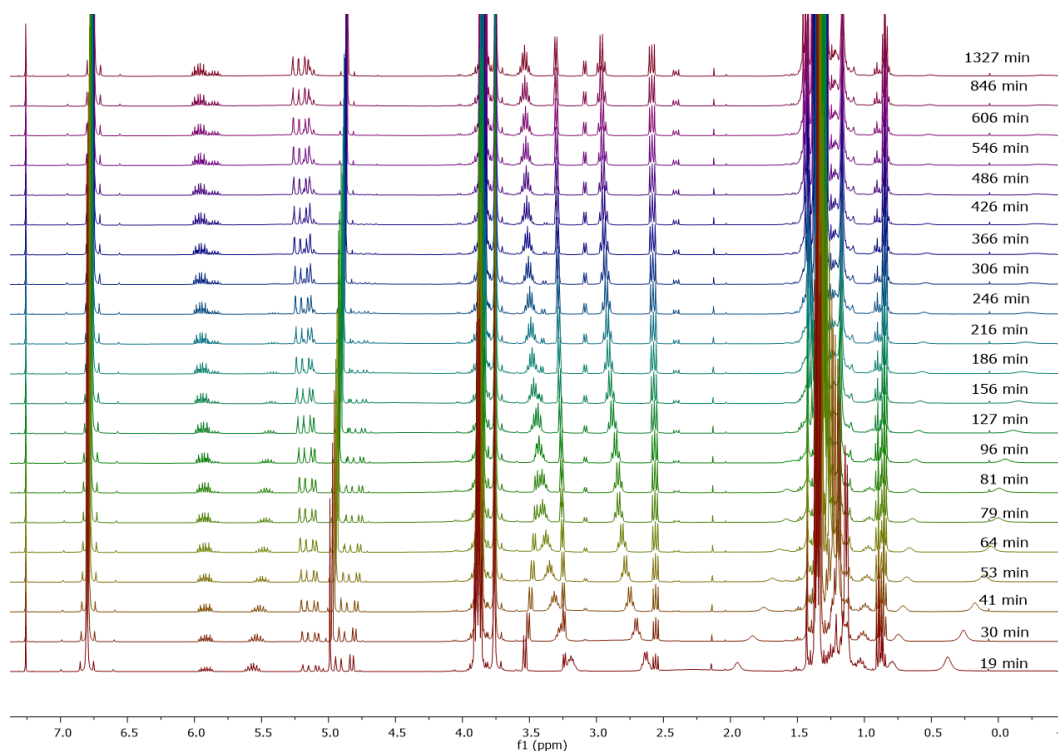
Figure 5.46 *¹H NMR (400 MHz, 298K, CDCl₃) Reaction between allyl bromide with butylamine in CDCl₃ in the presence of DIEA and in the absence of **PEt[5]**. [allyl bromide]=[butylamine]= 56 mM.*

Figure 5.47 *¹H NMR (400 MHz, 298K, CDCl₃) Reaction between allyl bromide with octylamine in CDCl₃ in the presence of **PEt[5]** and DIEA. [allyl bromide]=[octylamine]= 56 mM, [**PEt[5]**]=[DIEA] 56 mM.*
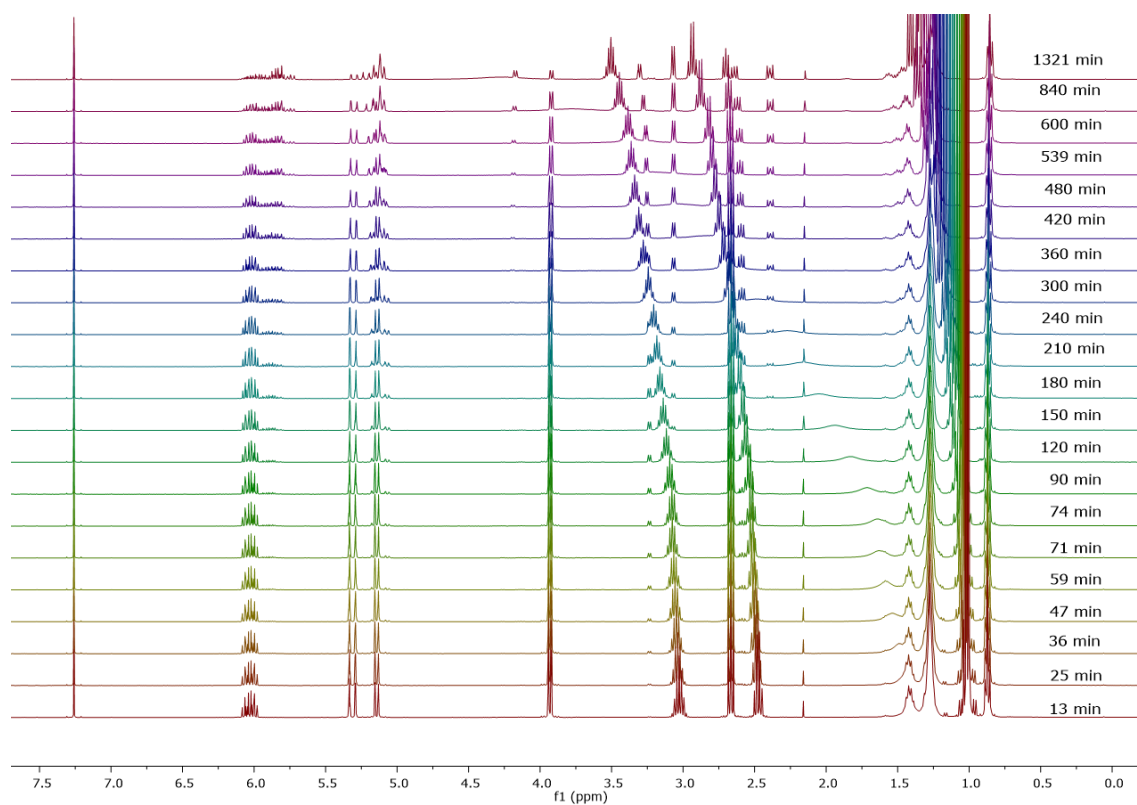
***Figure* 5.48** *¹H NMR (400 MHz, 298K, CDCl₃) Reaction between allyl bromide with octylamine in CDCl₃ in the presence of DIEA and the absence of **PEt[5]**. [allyl bromide]=[octylamine]= 56 mM, [DIEA] 56 mM.*
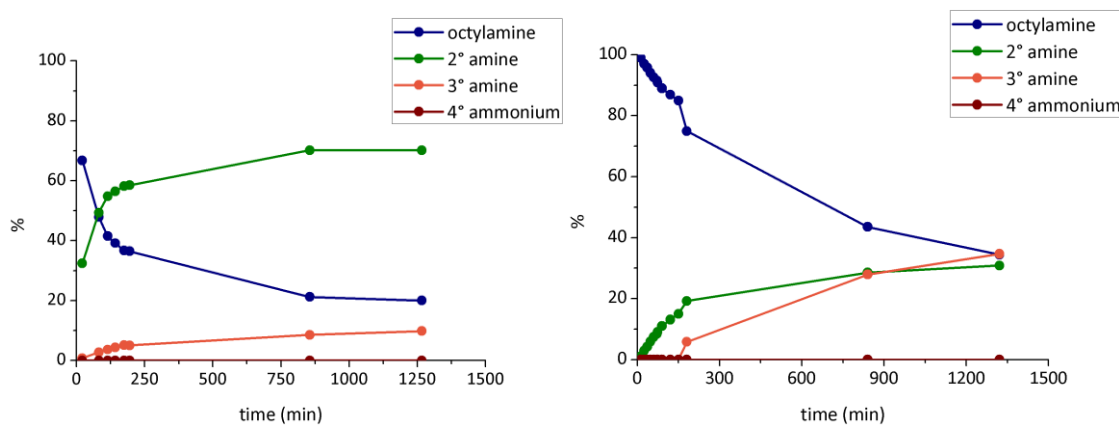

***Figure* 5.49** *Plot of the product distribution for the reaction between octylamine, allyl bromide in the presence (left) and in the absence (right) of **PEt[5]**. [octylamine]=[allyl bromide]=[**PEt[5]**]=[DIEA] 56 mM, CDCl₃ 0.8 mL, room temperature.*

5.4.2.7. Stability Study of Allyl Bromide in the Presence of PEt[5]

In a 2 ml vial **PEt[5]**(40 mg, 0.045 mmol), allyl bromide (μl, 0.045 mmol) were added to CDCl$_3$ (0.8 ml). The solution was then stirred at room temperature and the reaction progress was monitored by ^{1}H NMR analysis by periodically sampling directly from the reaction mixtures. Conversion, product assignment and product distribution were determined by direct ^{1}H NMR analysis of the reaction mixture as the average of three experiments.
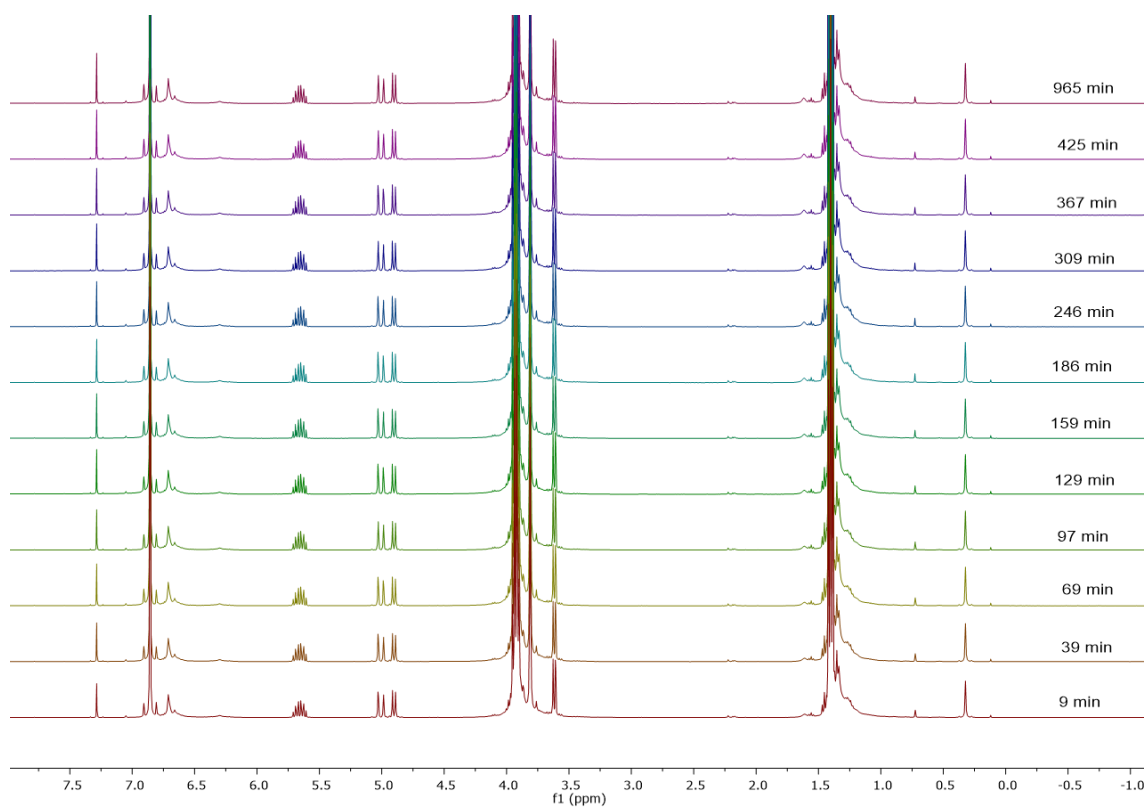
Figure 5.50 ^{1}H NMR (400 MHz, 298K, CDCl$_3$) Stability study of allyl bromide in CDCl$_3$ in the presence of **PEt[5]**. [allyl bromide]=[**PEt[5]**]= 56 mM.

5.4.2.8. *Nucleophilic Substitution Reaction of Octylamine on Propargyl Bromide in the Presence of PEt[5].*

In a 2 ml vial **PEt[5]**(40 mg, 0.045 mmol), propargyl bromide (3.9 μl, 0.045 mmol) and octylamine (5 μl, 0.045 mmol) were added to CDCl$_3$ (0.8 ml). The solution was then stirred at room temperature and the reaction progress was monitored by ^{1}H NMR ad GC analysis by periodically sampling directly from the reaction mixtures. Conversion, product assignment and product distribution were determined by direct GC, GC-MS and ^{1}H NMR analysis of the reaction mixture as the average of three experiments.
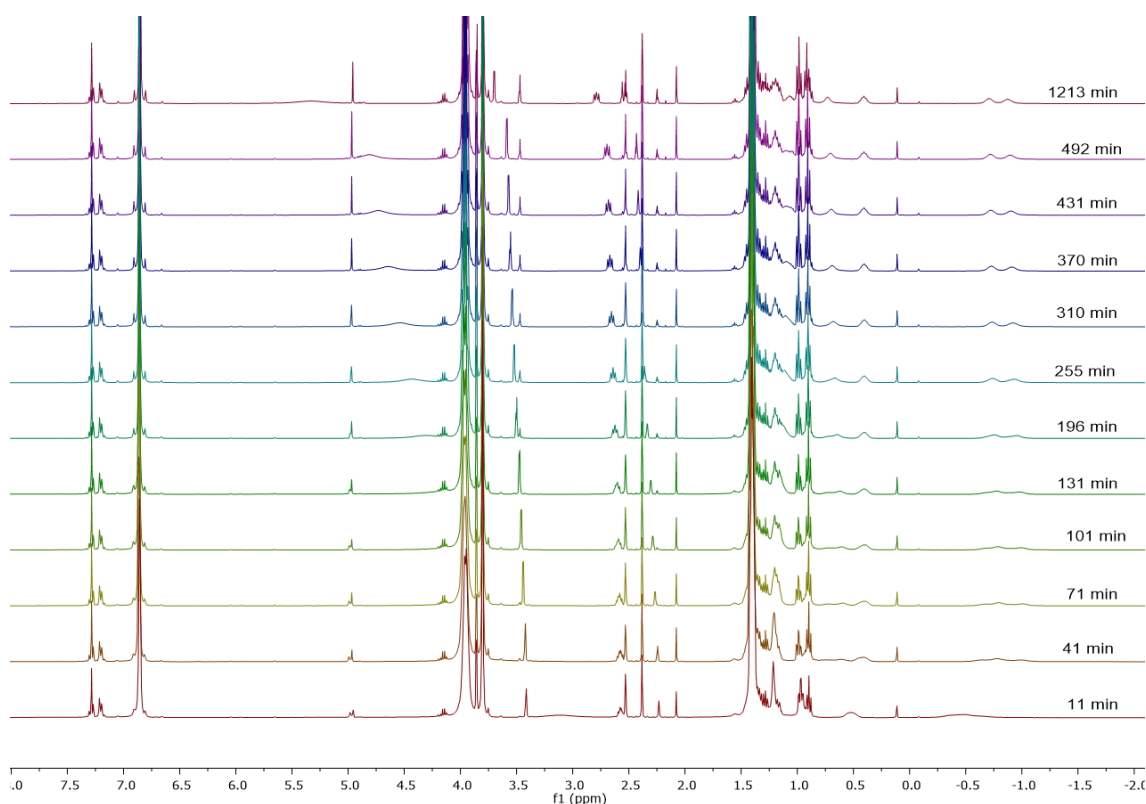
Figure 5.51 *^{1}H NMR (400 MHz, 298K, CDCl$_3$) Reaction between propargyl bromide with octylamine in CDCl$_3$ in the presence of **PEt[5]**. [propargyl bromide]=[octylamine]= 56 mM, [**PEt[5]**]= 56 mM.*
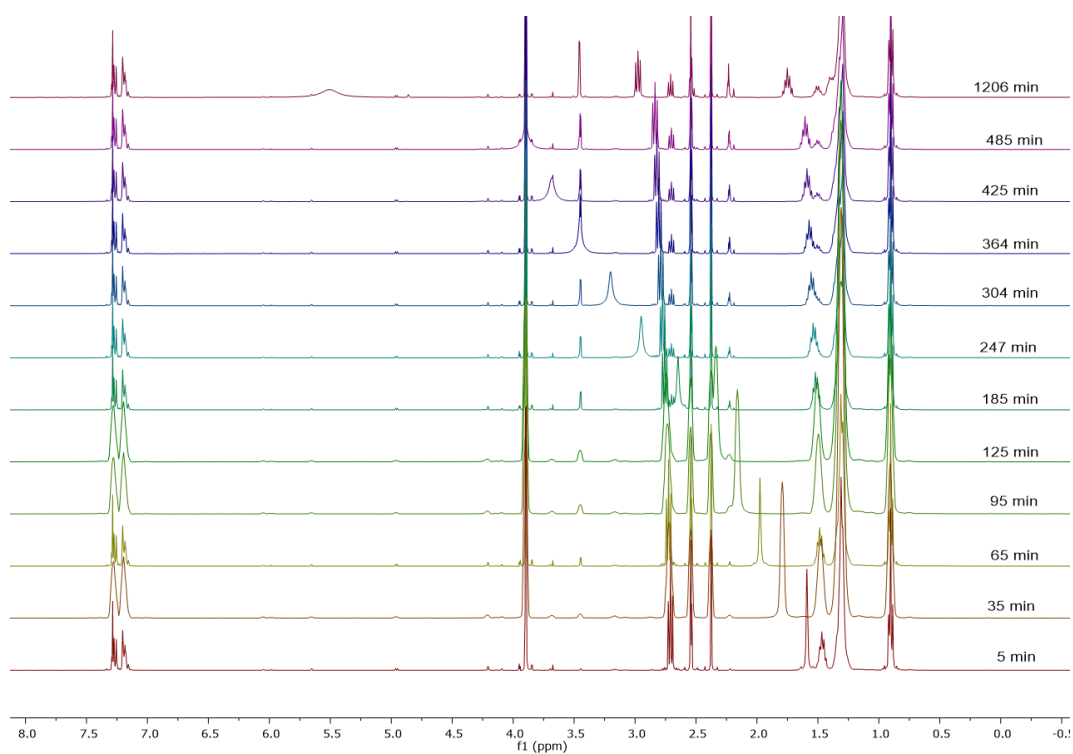
Figure 5.52 *¹H NMR (400 MHz, 298K, CDCl₃) Reaction between propargyl bromide with octylamine in CDCl₃ in the absence of **PEt[5]**. [propargyl bromide]=[octylamine]= 56 mM.*

Figure S5.53 *GC-MS spectra of the reaction between propargyl bromide and octylamine a) in the absence of **PEt[5]** and b) in the presence of **PEt[5]**. [octylamine]=[propargyl bromide]=[**PEt[5]**] 56 mM, CDCl₃ 0.8 mL, room temperature.*

5.4.2.9. Nucleophilic Substitution Reaction of Octylamine on Crotyl Bromide in the Presence of PEt[5]
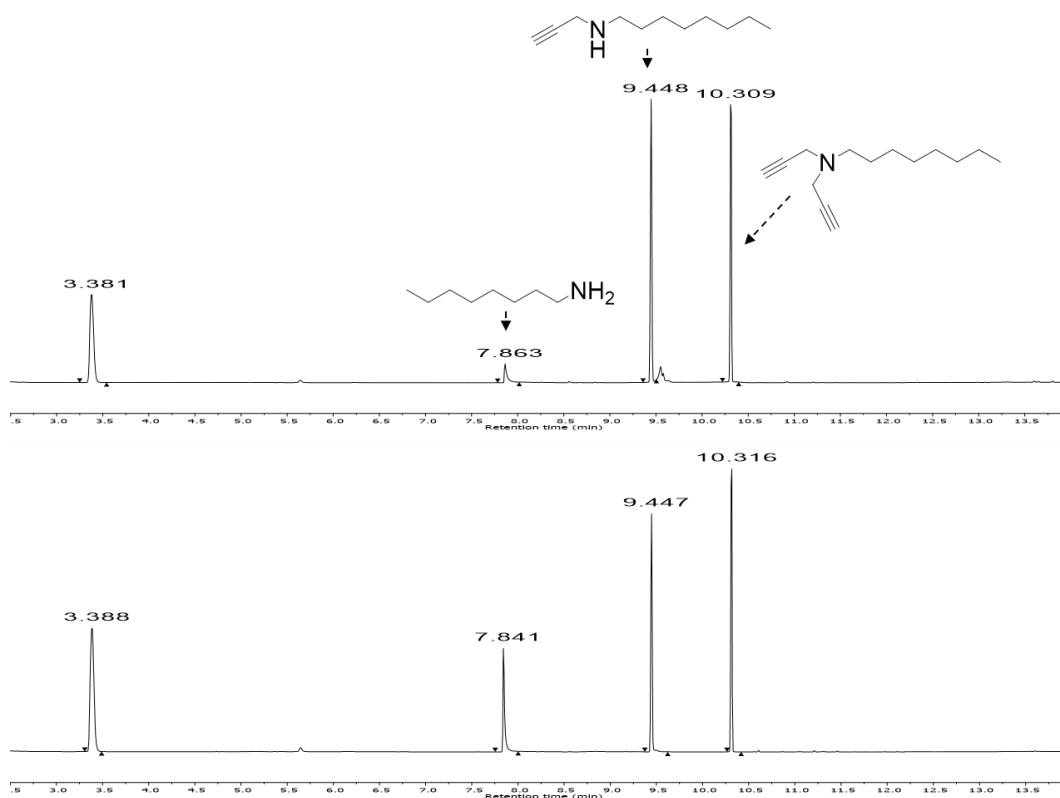
In a 2 ml vial **PEt[5]**(40 mg, 0.045 mmol), crotyl bromide (4.6 μl, 0.045 mmol) and octylamine (5 μl, 0.045 mmol) were added to CDCl$_3$ (0.8 ml). The solution was then stirred at room temperature and the reaction progress was monitored by ^{1}H NMR ad GC analysis by periodically sampling directly from the reaction mixtures. Conversion, product assignment and product distribution were determined by direct GC, GC-MS and ^{1}H NMR analysis of the reaction mixture as the average of three experiments.
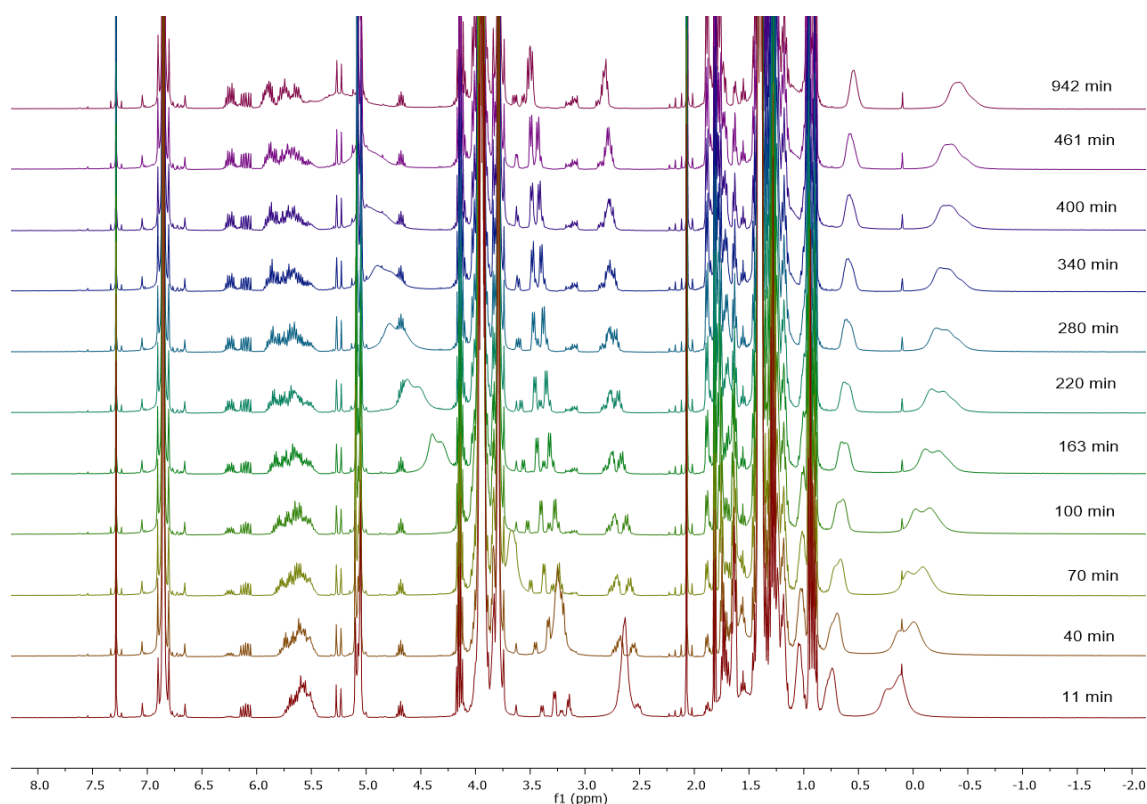
Figure 5.54 ^{1}H NMR (400 MHz, 298K, CDCl$_3$) Reaction between crotyl bromide with octylamine in CDCl$_3$ in the presence of **PEt[5]**. [crotyl bromide]=[octylamine]= 56 mM, [**PEt[5]**]= 56 mM.

185

Figure 5.55 *¹H NMR (400 MHz, 298K, CDCl₃) Reaction between crotyl bromide with octylamine in CDCl₃ in the absence of **PEt[5]**. [crotyl bromide]=[octylamine]= 56 mM.*
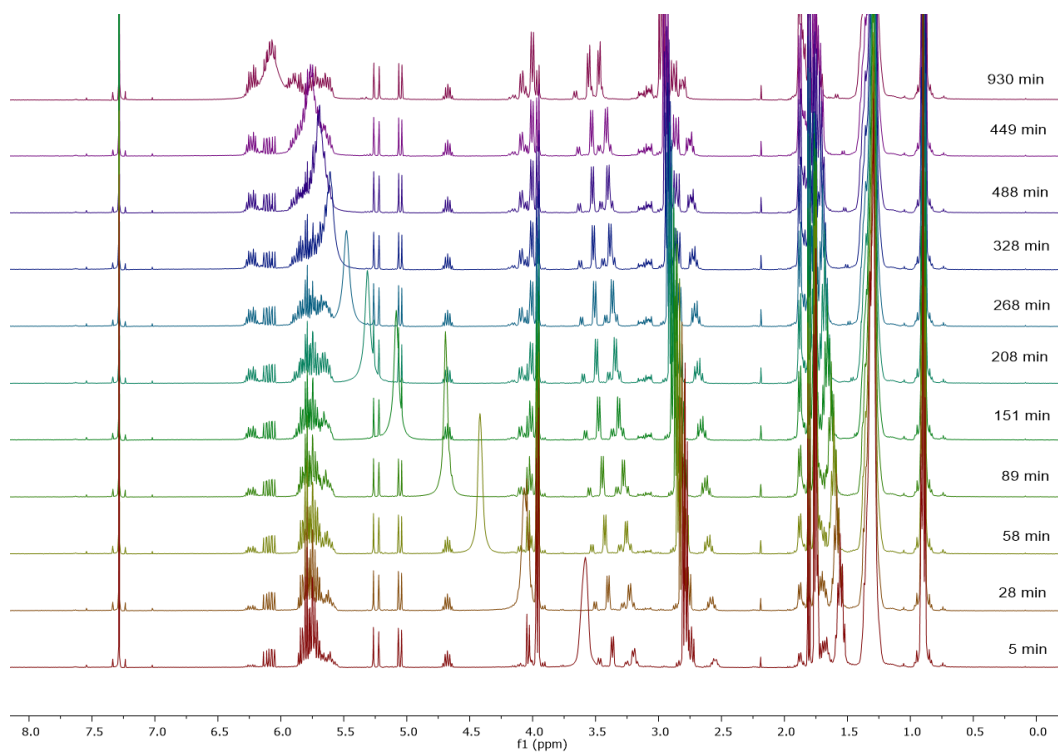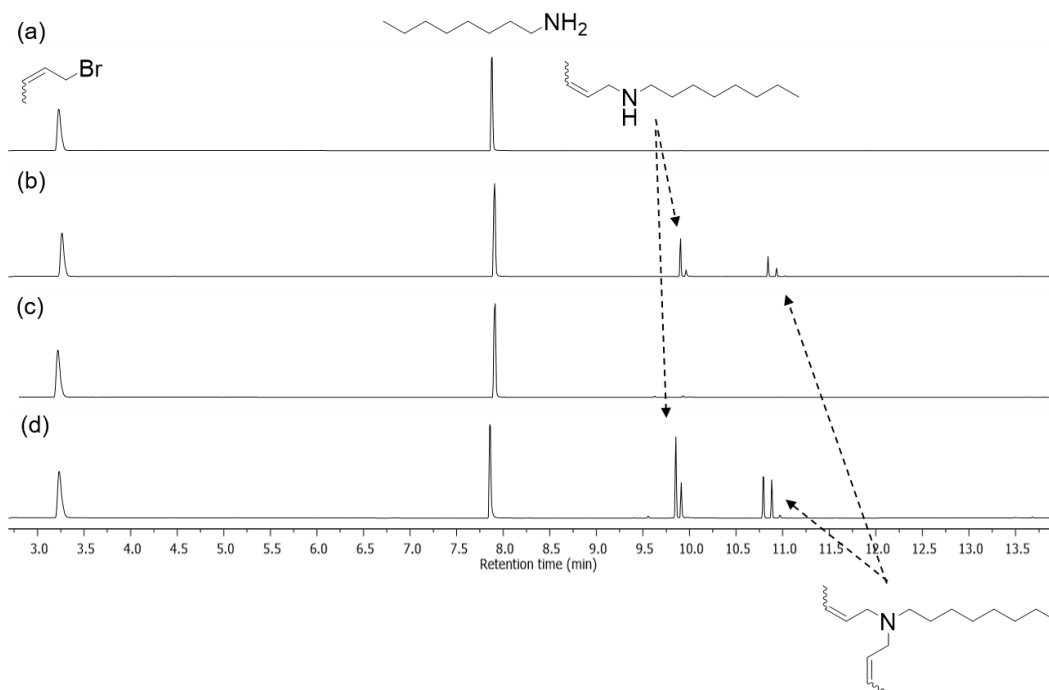

Figure 5.56 *GC-FID spectra of the reaction between crotyl bromide and octylamine a) in the absence of **PEt[5]** and b) in the presence of **PEt[5]** after 1 min of reaction, c) in the absence of **PEt[5]** and d) in the presence of **PEt[5]** after 30 min of reaction. [octylamine]=[crotyl bromide]=[**PEt[5]**] 56 mM, CDCl₃ 0.8 mL, room temperature.*

5.5. References

1. C. Deraedt and D. Astruc, *Coordination Chemistry Reviews*, 2016, **324**, 106-122.

2. M. Raynal, P. Ballester, A. Vidal-Ferran and P. W. N. M. van Leeuwen, *Chemical Society Reviews*, 2014, **43**, 1660-1733.

3. M. Raynal, P. Ballester, A. Vidal-Ferran and P. W. N. M. van Leeuwen, *Chemical Society Reviews*, 2014, **43**, 1734-1787.

4. G. Xue, R. De Hont, E. Münck and L. Que Jr, 2010, **2**, 400.

5. P. Dydio and J. N. H. Reek, *Chemical Science*, 2014, **5**, 2135-2145.

6. N. L. Strutt, R. S. Forgan, J. M. Spruell, Y. Y. Botros and J. F. Stoddart, *Journal of the American Chemical Society*, 2011, **133**, 5668-5671.

7. X. Shu, J. Fan, J. Li, X. Wang, W. Chen, X. Jia and C. Li, *Organic & Biomolecular Chemistry*, 2012, **10**, 3393-3397.

8. X.-S. Hu, H.-M. Deng, J. Li, X.-S. Jia and C.-J. Li, *Chinese Chemical Letters*, 2013, **24**, 707-709.

9. T. Ogoshi, T.-a. Yamagishi and Y. Nakamoto, *Chemical Reviews*, 2016, **116**, 7937-8002.

10. L.-L. Tan and Y.-W. Yang, *Journal of Inclusion Phenomena and Macrocyclic Chemistry*, 2015, **81**, 13-33.

11. Q. Duan, Y. Cao, Y. Li, X. Hu, T. Xiao, C. Lin, Y. Pan and L. Wang, *Journal of the American Chemical Society*, 2013, **135**, 10542-10549.

12. T. Ogoshi, N. Ueshima and T.-a. Yamagishi, *Organic Letters*, 2013, **15**, 3742-3745.

13. D. G. Liz, A. M. Manfredi, M. Medeiros, R. Montecinos, B. Gomez-Gonzalez, L. Garcia-Rio and F. Nome, *Chemical Communications*, 2016, **52**, 3167-3170.

14. X.-D. Xiao, Y.-L. Bai, J.-Q. Liu and J.-W. Wang, *Tetrahedron Letters*, 2016, **57**, 3385-3388.

15. Y. Yao, M. Xue, Z. Zhang, M. Zhang, Y. Wang and F. Huang, *Chemical Science*, 2013, **4**, 3667-3672.

16. B. Hua, J. Zhou and G. Yu, *Tetrahedron Letters*, 2015, **56**, 986-989.

17. X.-S. Du, C.-Y. Wang, Q. Jia, R. Deng, H.-S. Tian, H.-Y. Zhang, K. Meguellati and Y.-W. Yang, *Chemical Communications*, 2017, **53**, 5326-5329.

18. R. R. Kothur, J. Hall, B. A. Patel, C. L. Leong, M. G. Boutelle and P. J. Cragg, *Chemical Communications*, 2014, **50**, 852-854.

19. N. A. Bongartz and J. W. Goodby, *Chemical Communications*, 2010, **46**, 6452-6454.

20. S. Nakanishi, K. Okamoto, H. Yamaguchi and T. Takata, *Synthesis*, 1998, **1998**, 1735-1741.

21. D. D. Perrin and W. L. F. Armarego, *Purification of laboratory chemicals*, Pergamon press, Oxford, 3rd edition edn., 1993.

22. W. C. Still, M. Kahn and A. Mitra, *The Journal of Organic Chemistry*, 1978, **43**, 2923-2925.

23. M. Rössle, D. J. Del Valle and M. J. Krische, *Organic Letters*, 2011, **13**, 1482-1485.

24. M. Da Pian, O. De Lucchi, G. Strukul, F. Fabris and A. Scarso, *RSC Advances*, 2016, **6**, 48272-48275.

Chapter 6

General Conclusions

In summary this work provided a high yield synthesis of the cyclic hexamer **P[6]**, a detailed study of the mechanism behind its formation and the first example of **P[5]** as true organocatalyst.

In more detail, in Chapter 3 we reported four template syntheses of the hexameric pillararenes **P[6]**, starting from three different para-dialkoxy benzene derivatives **DMB**, **DEB** and **DBB**. The reactions occurred with paraformaldehyde as methylene source and $FeCl_3$ as Lewis acid. The small cationic molecules investigated as templates, **TMAC**, **COCP**, **FECP** and **BmimPF₆**, where selected in accord with the binding affinities observed for **PEt[5]** and **PEt[6]**. These templating units were employed in substoichiometric amount (25% mol), making the reaction more economically convenient and environmentally friendly. In the presence of the templates **BmimPF₆** and **FECP**, despite their preferential affinity for **P[5]** and **P[6]** respectively, the **P[6]**/**P[5]** yields ratio was even. In the reaction templated by **BmimPF₆** we evaluated the role of the counter anion observing a negative templating effect as the anionic radius increased. The best **P[6]**/**P[5]** yields ratio was observed after full conversion of the monomer **DEB** in the presence of 25 mol% of **COCP** as template. The amount of required template was set after the reaction was repeated with 30% mol and 20% mol of **COCP** leading to a lower selectivity. Finally, the reaction was seven-fold scaled up, obtaining in an overall 38% yield **PEt[6]** in two steps, starting from hydroquinone.

In the fourth Chapter we observed the conversion of **PEt[5]** into **PEt[6]** in the cyclization of the monomer **DEB** templated by **TMAC** and in the presence of $FeCl_3$ as catalyst. We first characterized the reaction by-products identifying them as a mixture of three linear oligomers bearing a terminal benzyl alcohol moiety which, depending on the number of their constituent units, were addressed as **OEt[5]**, **OEt[6]** and **OEt[7]**. The mixture resulted to be composed of more than 90% from **OEt[6]** while the other two were barely detectable. **OEt[6]** when dissolved in a biphasic solution of DCM and water in the presence of $FeCl_3$ and **TMAC**, cyclized giving **PEt[6]** in 55% yields. The same reaction in the presence of either the catalyst or the template gave the closed product in 24% and 32% respectively. Similarly, we observed the conversion of **PEt[5]** into 8%

PEt[6], after one week of stirring in a DCM/water solution in the presence of FeCl$_3$ and **TMAC.** The equilibrium between the macrocycle **PEt[5]** and its linear open pentamer was hypothesized as mechanism at the basis of the pillar[n]arene conversion. This study inspired our novel approach for the synthesis of two different **co-P[6]s** (**PMe[5]Et[1]** and **PEt[5]Me[1]**) in 8% yield, through the scrambling experiments of **DEB** in **PMe[5]** and of **DMB** in **PEt[5]**.

Finally in Chapter 5 we reported some examples of catalytic applications involving **PEt[5]** as true organocatalyst in reaction occurring between neutral substrates. The cyclic pentamer promoted the nucleophilic substitution between allyl bromide and octylamine leading selectively to the mono-substituted product, limiting the amine over-alkylation and accelerating over 17-fold the reaction rate. The catalytic effect of **PEt[5]** was tested on narrow and steric alkyl hindered primary amines and different allylic and propargylic substrates, showing a strong dependence on the simultaneous binding with **PEt[5]** cavity, modulated by the intrinsic reactivity of the substrates themselves. In fact, it turned out that the better guest were not always the better substrates in the nucleophilic substitutions under study. The reaction was successfully carried out with a sub-stoichiometric amount of **PEt[5]** (50 % mol) with respect to the substrates, showing the same selectivity and similar acceleration rate compared to the equimolar reaction. The catalyst was further recycled after precipitation from MeOH and reused with the same efficiency. Finally, the outcome of the reaction performed on crotyl bromide as electrophile suggested a S$_N$2 mechanism for the **PEt[5]** mediated reaction. Further studies involving a ^{13}C labeled allylic substrate will be considered for the confirmation of the mechanistic hypothesis.